

Sheffield Hallam University

The relationship between surface heat transfer and stress generation in components.

NASSERI, Mahnaz.

Available from the Sheffield Hallam University Research Archive (SHURA) at:

<http://shura.shu.ac.uk/20111/>

A Sheffield Hallam University thesis

This thesis is protected by copyright which belongs to the author.

The content must not be changed in any way or sold commercially in any format or medium without the formal permission of the author.

When referring to this work, full bibliographic details including the author, title, awarding institution and date of the thesis must be given.

Please visit <http://shura.shu.ac.uk/20111/> and <http://shura.shu.ac.uk/information.html> for further details about copyright and re-use permissions.

101 380 983 1



Sheffield Hallam University

REFERENCE ONLY

ProQuest Number: 10697418

All rights reserved

INFORMATION TO ALL USERS

The quality of this reproduction is dependent upon the quality of the copy submitted.

In the unlikely event that the author did not send a complete manuscript and there are missing pages, these will be noted. Also, if material had to be removed, a note will indicate the deletion.



ProQuest 10697418

Published by ProQuest LLC (2017). Copyright of the Dissertation is held by the Author.

All rights reserved.

This work is protected against unauthorized copying under Title 17, United States Code
Microform Edition © ProQuest LLC.

ProQuest LLC.
789 East Eisenhower Parkway
P.O. Box 1346
Ann Arbor, MI 48106 – 1346

**THE RELATIONSHIP BETWEEN SURFACE HEAT TRANSFER
AND STRESS GENERATION IN COMPONENTS**

**BY
MAHNAZ NASSERI**

**A THESIS SUBMITTED IN PARTIAL
FULFILMENT OF THE REQUIREMENTS OF
SHEFFIELD HALLAM UNIVERSITY
FOR THE DEGREE OF
DOCTOR OF PHILOSOPHY**

COLLABORATING ESTABLISHMENT;

**British Steel Technical,
Swinden Labs.,
Rotherham,
United Kingdom.**

Date: January 1993

PREFACE

The work represented in this thesis was carried out in the Department of Metals and Materials Engineering at Sheffield Hallam University.

The candidate was registered with the Council for National Academic Awards for a higher degree, in which she has not been registered for any other CNAA award or University degree.

The research here is, as far as can be ascertained, original except where due reference has been made to previous work.

In accordance with the requirements of the work, training course on finite element analysis was taken.

ACKNOWLEDGEMENTS

The author wishes to thank Dr. A. J. Fletcher for his continuous support, guidance, encouragement and advice throughout this project and would also like to thank Mr. W. T. Cook for his external supervision. Further appreciation is extended to the Technical staff of the School of Engineering whose services were invaluable. Gratitude is also given to John Stanley and Amir, finite element specialists for their considerable help and assistance.

The author would also like to express her sincere gratitude to Prof. A.W.D. Hills for his initial encouragement to undertake the work. Additional thanks are given to North East Corrosion Ltd., for support in the final preparation of this thesis.

Lastly, the author wishes to give her everlasting gratitude to her family.

ABSTRACT

The heat transfer coefficients in even relatively simple components varies significantly at different points on the surface. Although this has been known for some time the amount of work which has been done is limited to the relationship between these variable thermal conditions and the generation of stress and strain during the quench. The object of the work was to investigate the relationship between the variables using standard quenchant.

The variation in the surface heat transfer coefficients has been determined at points along the horizontal and vertical axes of a stainless steel plate and upper and lower surface of a plate held vertically and horizontally in water.

Photographic studies of the appearance of the quenchant in contact with the surface of the plate have been carried out in conjunction with the horizontal and vertical quenches which are mentioned above.

The data obtained have been used in the determination of the variation in stress and strain generated in the plate during the quench by involving a 2-D finite element analysis using the PAFEC package.

LIST OF SYMBOLS

The symbols given below are those used in the text except where locally redefined.

h	surface heat transfer coefficient W/m^2K
λ	thermal conductivity $W/m^{\circ}C$
ρ	density Kg/m^3
θ	temperature $^{\circ}C$
C_p	specific heat capacity $J/Kg^{\circ}C$
q	rate of heat transfer W
A	surface area of specimen in contact with the fluid, m^2
M	mass of specimen, Kg
t	time, s
Δt	time interval, s
ΔX	distance between nodes, m
ρ	number of times intervals before $(q_n^{TC})_E$ and q_n^{TC} are compared
E	suffix E refers to experimental values
α	thermal diffusivity, m^2s^{-1}
θ^a	temperature of quenchant, $^{\circ}C$
θ_n^{TC}	temperature at thermocouple hot junction after n time intervals,
$^{\circ}C$	
θ_t	temperature at thermocouple hot junction after n time intervals,
$^{\circ}C$	

θ_0	temperature of specimen at time t, °C
θ_1	surface temperature
θ_2	bulk liquid temperature
ν	poisson's ratio
E	Young's modulus, MNm ⁻²
Δ	finite difference
ϵ	strain
σ	normal stress, MNm ⁻²
X, Y, Z	principal directions; double subscripts repeat same letters for normal stress, but use different letters for shear stress.
ϵ_{tp}	transformation plasticity
U	displacement
V	displacement
W	displacement
G	shear modulus N/mm ²
α_{ex}	coefficient of linear thermal expansion, °C ⁻¹
$\Delta V / \sigma_y$	transformational strain / yield strength
σ_2	applied stress
Bi	Biot number
F ₀	Fourier number
Y _s	distance between reference points on edges of plate in softened condition
Y _h	distance between reference points on edges of plate in quenched condition
J	position of node

K number of nodes in plate half section
L number of time intervals
N position of node

CONTENT

	Page
1.0 INTRODUCTION	13
2.0 LITERATURE SURVEY	16
2.1 General description of steel hardening	16
2.1.1 Mechanism of heat removal during quenching	17
2.1.2 Quenching stresses and quench cracking	19
2.2 Heat transfer at the surface during quenching	212
2.2.1 Influence of experimental variables on the surface heat transfer coefficient	26
2.2.2 Determination of the surface heat transfer coefficient during quenching	30
2.3 The prediction and calculation of thermal stresses during quenching	35
2.3.1 Calculation of thermal stresses during quenching	36
2.3.2 Experimental methods for determining residual stress	44
2.3.3 Transformation plasticity	46
2.3.4 Effect of specimen size	51

3.0 EXPERIMENTAL PROCEDURES	54
3.1 Experimental measurements of surface heat transfer coefficient	54
3.2 Photographic examination of the plate surface during quenching	56
3.3 Calculation of the surface heat transfer coefficient and the prediction of the generation of the thermal stress and strain of a stainless steel plate during quenching	57
3.4 Calculations of the surface heat transfer coefficient from relationships between temperature and time	58
3.5 Finite element method	60
3.5.1 Theory of finite element technique	60
3.5.2 Finite element techniques	60
3.5.3 PAFEC finite element package	61
3.5.4 Development of finite element model	61
3.6 Experimental determination of residual stress and strain in quenched plates	65
3.6.1 Quenching the plate	65
3.6.2 Measurements of residual strain	66
3.6.3 Residual stress measurements	68

4.0 RESULTS	70
4.1 Cooling curves and surface heat transfer coefficients	70
4.1.1 Observation of cooling curves in plates held vertically during quenching	70
4.1.2 The relationship between time and temperature in plates quenched in a horizontal position	71
4.1.3 Surface heat transfer coefficients and temperature distributions produced during quenching with the plate held in various positions in the bath	72
4.1.4 Vertical plate	72
4.1.5 Horizontal plate	74
4.2 Calculation of temperature distributions in the plates during quenching	76
4.3 Photographic observations of the cooling of the plate in a water quench	78
4.4 Generation of stress and strain during quenching by using constant and variable surface heat transfer coefficients	82
4.4.1 Using constant surface heat transfer coefficient around the surface of the plate	82
4.4.2 Using variable surface heat transfer coefficient around the periphery of the plate	85

4.5	The calculated and experimental residual strains in plates held in vertical and horizontal positions during quenching	88
4.6	Experimental measurements of residual stress in horizontal plate	89
4.7	Calculated stresses in plates held horizontally during quenching	90
4.7.1	Using constant surface heat transfer coefficient around the periphery of the plate	90
4.7.2	Using variable surface heat transfer coefficient around the periphery of the plate	91
5.0	DISCUSSION	93
5.1	Photographic observations of the plate in a water quench and the mechanism of cooling around the periphery of the plate	93
5.1.1	Introduction	93
5.1.2	Photographic observations - Vertical Plate	93
5.1.3	Photographic observations - Horizontal Plate	94
5.1.4	Relationships between photographic data and the cooling curves during quenching	97
5.2	Comparison of constant 'h' and variable 'h' during quenching	99
5.2.1	Vertical plate	99

5.2.2	Horizontal plate	100
5.2.3	Comparison of cooling rates in the vertical and horizontal positions	101
5.3	Thermal stress and strain generation during quenching	103
5.3.1	Horizontal plate	106
6.0	CONCLUSIONS AND RECOMMENDATIONS FOR FURTHER WORK	109
7.0	REFERENCES	112
	TABLES	122
	FIGURES	128
	APPENDIX A	206

1.0 INTRODUCTION

The heat transfer coefficients in even relatively simple component vary significantly from point to point on the surface. Although this has been known for some time the amount of work which has been done is very limited in the case of relationships between these variable thermal conditions and the generation of stress and strain during the quench. The object of the work will be to investigate the relationships between these variables using standard quenchants particularly water when, cooling stainless steel plates.

The variation in the surface heat transfer coefficients has been determined at points along the horizontal and vertical axes of a stainless steel plate held vertically. Similar information has also been obtained in the case of the upper and lower surface of a plate held horizontally during water quenching.

Photographic studies of the appearance of the quenchant in contact with the plate vertical face have been carried out in conjunction with both horizontal and vertical quenching in order to relate the quenching mechanism with the surface heat transfer coefficients. The data obtained above have been used in the determination of the variations in stress and strain generated in the plate during the quench. Thus, this thermal data has been used as the boundary condition in a two dimensional finite element analysis using the PAFEC package.

The first objective of the present work has been to investigate the effect of geometry on quenching characteristics of a standard quenchant (i.e. water).

The information obtained on the quenching process has then been used to determine the variation in thermal stress and strain in the specimens specified as the quenching process continues.

The development of thermal stresses and strains in steel components is of great importance since it can cause distortion and cracking, and the problem has been subjected to a great deal of both experimental and theoretical evaluation. The experimental investigation of residual stresses and strains after quenching is laborious and it is impossible to follow the generation of the stress during quenching by an experimental procedure. The finite element technique produced a particularly powerful tool to follow the quenching and distortion of thermal stresses introduced during quenching by applying variable heat transfer coefficients to the surface of the material. The analysis was performed on a Prime computer system using two types of software; (a) PAFEC (Programme for Automatic Finite Element Calculation) and (b) PAFEC INTERACTIVE GRAPHICS SYSTEM (PIGS).

In principle, the control of complex phenomena involved during quenching can be achieved by using the PAFEC finite element programme, which is an extremely powerful software package and has been one of the most notable advances in engineering practice in the last twenty years. It can perform many types of analysis such as stresses, creep, thermal, vibration and electromagnetics in both two and three dimensions.

At the present moment the work on the vertical and horizontal plate has been completed except that some instability was obtained during the finite element calculation at certain points in the structure. The mesh has been further refined and smaller time steps has been used to overcome this problem although the computing capacity available limits the amount of refinement that will be possible.

As far as the work on the horizontal plate is concerned the surface heat transfer coefficients have been determined on the upper and lower faces.

When this data was obtained the finite element calculations were carried out for the complete plate section.

The results of the finite element strain calculation have been compared with measurements of residual strain made on quenched vertical and horizontal plates.

2.0 LITERATURE SURVEY

2.1 GENERAL DESCRIPTION OF STEEL HARDENING

It is well known that the internal structure of steel can be of several different kinds, dependent upon the composition, temperature and heat treatment of the material.

Above a certain critical temperature, steels form the austenite phase which is a face-centred cubic structure. At lower temperatures, this is replaced by a mixture of ferrite, which is a practically carbon-free body centred cubic structure, and cementite (Fe_3C , containing 6.7% carbon). In a 0.8%C the mixture is so arranged that a lamellar structure of ferrite and cementite plates called pearlite is produced. At other compositions, regions of pure ferrite or cementite intermix with these pearlite regions.

The above description of the low temperature equilibrium structure is, however, only valid for components that have been cooled very slowly. The rearrangement in structure necessary to form pearlite from the austenite involves carbon diffusion in the material, which means that the process is controlled by a finite carbon diffusion velocity that decreases with temperature. The process would thus, in fact require that the temperature was kept for some time at a relatively high level to allow for this diffusion. If, however, the component is cooled rapidly the carbon atoms will not have sufficient time to diffuse to form the pearlite structure but will instead, form a ferrite/cementite mixture with a different morphology; this is bainite. The finer carbon particles in this case allow sufficient diffusion to occur even at the relatively low temperatures involved. If, however, the cooling is so fast that even bainite formation is not

possible the structure remains supersaturated with carbon. The carbon atoms thus get trapped at interstitial positions in the crystal structure. The resulting structure is called martensite and only the fast cooling rates produced in quenching permits this structure to form. This martensite is extremely strong, hard, and wear-resistant and its formation is the main purpose of a quenching heat treatment.

2.1.1 MECHANISM OF HEAT REMOVAL DURING QUENCHING

The structure, hardness and strength resulting from a heat-treating operation are determined by the actual cooling rate obtained by the quenching process. If the actual cooling rate exceeds the critical cooling rates, only martensite will result. If the actual cooling rate is less than the critical cooling rate, the part will not completely harden. The greater the difference between the two cooling rates, the softer will be the transformation products and the lower the hardness.

A cooling curve illustrates the three stages of heat transfer from the hot metal piece to the cold quench liquid. These three cooling zones have been discussed in section 2.2.

Many factors determine the actual cooling rate. The most important of which are the type of quenching medium, the temperature of the quenching medium, the surface condition of the part, the size and mass of the part.

QUENCHING MEDIUM

The following industrial quenching medias are listed in order of decreasing quenching severity;

- (1) brine

- (2) water
- (3) fused or liquid salts
- (4) polymer
- (5) soluble oil and water solutions
- (6) oil
- (7) air

According to Thelning⁽¹⁾ water is not very suitable because of its greatest cooling rate which occurs close to the M_s temperature of the component resulting in cracking and distortion.

TEMPERATURE OF QUENCHING MEDIUM

Generally, as the temperature of the medium rises, the cooling rate decreases. This is due to an increase in the persistence of the vapour-blanket stage. Since the medium is closer to its boiling point, less heat is required to form the vapour film. This is particularly true of water and brine. Monroe and Bates⁽²⁾ reported that an oil is sensitive to temperature changes due to a reduction in viscosity as the temperature increases but that water and polymers are less sensitive in this respect.

SURFACE CONDITION

When steel is exposed to an oxidising atmosphere at elevated temperature, a layer of iron oxide is formed. Berenson⁽³⁾ showed that a rougher surface increases heat transfer during nucleate boiling and also it was increased in all the recognised stages of boiling or cooling curves. Allen and Fletcher⁽⁴⁾ stated that the degree of surface roughness affected both the duration of the vapour

blanket stage and the maximum surface heat transfer coefficient obtained during nucleate boiling in a water quench. The former was at a minimum when specimens of intermediate (400 grade) roughness were used, while the latter increased progressively as the surface became smoother.

SIZE AND MASS

Since it is only the surface of a component which is in contact with the quenching medium, the ratio of surface area to mass is an important factor in determining the actual cooling rate. This ratio is a function of the geometric shape of the component and is largest for a spherical shape. Thin plates and small-diameter wires have a large ratio of surface area to mass and therefore have rapid cooling rates.

2.1.2 QUENCHING STRESSES AND QUENCH CRACKING

The act of quenching from the austenite region to room temperature is a drastic treatment which all too often leads to distortion in the part and even serious cracking. These defects arise from internal stresses which develop during quenching from two sources;

- (1) thermal stresses arising directly from the different cooling rates experienced by the surface and the interior of the steel,
- (2) transformation stresses due to the volume changes that occur when austenite transforms to other phases.

Scott⁽⁵⁾ has investigated the generation of thermal stresses for various cooling conditions and specimen sizes. He found that if the section size or quenching power of the bath were increased then stresses at the surface became more

tensile, until a maximum was reached. Further increase in either section size or the quenching power of the bath reduced the magnitude of these tensile stresses, which then became compressive.

Bodson et al⁽⁶⁾ used an acoustic method to study the effects of different media on the quench cracking of 8 to 24 mm diameter cylinders. Two casts of a 0.56% C, 0.75% Mn steel were used: one cast had high residual (0.35% Cr, 0.25% Ni and 0.24% Cu) contents whilst the other contained much lower quantities of these elements (0.09% Cr, 0.07% Ni and 0.105% Cu). They found that for a particular quenchant there was a critical diameter at which cracking was most probable. This diameter was larger in the case of the steel with high impurity levels, which was attributed to the greater hardenability of this material.

They also found that an increase in water temperature reduced the severity of the quench by an extension of the vapour blanket stage to lower temperatures and also by a reduction in the severity of the nucleate boiling rate. Beck⁽⁷⁾ has reported that cracking might be the result of a thermal shock associated with the breakdown of the vapour blanket stage. However, Bodson et al⁽⁶⁾ estimated that when specimens were quenched into water at 70°C, the breakdown of the vapour blanket occurred at a time when the core temperature was still around 550-600°C; at these temperatures the core was still austenitic and able to withstand such a thermal shock. They proposed that the occurrence of a critical diameter, at which quench cracking was most pronounced, was due to a complex interaction between thermal and transformation strains which they were unable to interpret.

2.2 HEAT TRANSFER AT THE SURFACE DURING QUENCHING

Heat transfer is the transfer of energy occurring as a result of a driving force related to the temperature difference, and the study of heat transfer deals with the rate at which such energy is transferred. The actual mechanism is complicated. The heat transferred through the surface of a body represents the boundary conditions, which in the case of quenching are complex.

It is necessary to understand the mechanism of the heat removal during quenching. It is apparent that the cooling rate is constantly changing during cooling⁽⁸⁾. The simplest classification of a typical cooling curve involves the following stages⁽⁸⁾;

Stage A- vapour blanket cooling stage, in this first stage, the temperature of the metal is so high that the quenching medium is vapourized at the surface of the metal and a thin stable film of vapour surrounds the hot solid. Cooling is by conduction and radiation through the gaseous film, and since vapour films are poor heat conductors, the cooling rate is relatively slow through this stage.

Film boiling heat transfer has been of interest to workers in many fields of Heat Engineering. Many studies have been performed since the first by Bromley⁽⁹⁾. As mentioned above, the first model of film boiling heat transfer was due to Bromley⁽⁹⁾ who modified an analysis of film condensation by Nusselt to calculate the heat transfer coefficient from horizontal and vertical tubes and plates in a saturated liquid. Bromley⁽⁹⁾ assumed that the vapour interface was smooth and continuous and that heat transfer occurs by conduction from the hot surface through the vapour layers, with a very short period of radiation.

Film boiling has been treated with considerable success from a theoretical point of view(10). According to Jordon(10), who reviewed the literature on film boiling, interest was first directed toward the problem of film boiling in the late 1940s, with respect to the nuclear industry. Jordon reviewed film boiling on horizontal cylinders and surfaces, vertical surfaces and also with respect to forced convection and subcooling.

An approach to evaluate the film boiling heat transfer from the upper surface of a horizontal plate has usually been based on the Taylor instability theory. Originally, Berenson(11) predicted the theoretical film boiling heat transfer on an infinite horizontal plate facing upward by adopting the Taylor's theory under the assumptions of an infinite vapour film thickness and a two dimensional analysis using a derivation of interfacial wavelength. His prediction gives a reasonably good agreement with experimental results at the minimum heat flux. Taylor(12) studied an accelerated interface between two fluids and, supported by experimental work, Lewis (13), concluded that when an interface containing an initial disturbance was accelerated perpendicularly from the direction of the lighter fluid to the heavier one then the disturbance would grow exponentially to become unstable. This was precisely the case in film boiling on a horizontal surface where the lighter fluid, (vapour), lay beneath the heavier fluid, and the interface was accelerated perpendicularly by gravity. It was accepted that heat transfer from horizontal surfaces was controlled by bubble release as the vapour at a particular point in the interface formed a bubble which then departed. The pattern and periodicity of this bubble release was regular and Berenson(11) proposed that it was governed by hydrodynamic instability. While the interface would contain oscillations of many different wavelengths, all with greater or

lesser potentials for growth, the instability which controlled the rate of bubble release was assumed to be governed by one wavelength which gave the maximum rate of interface growth.

Ishigai, et al⁽¹⁴⁾ conducted pool boiling experiments on the upper surface of two kinds of circular plate of 25 mm and 50 mm in diameter, with saturated water as liquid. They concluded that the burn-out point for the downward facing surface would occur at a much lower heat flux than that on the upward facing surface. Farahat, et al⁽¹⁵⁾ used an explicit finite difference technique to model saturated film boiling heat transfer on downward facing surfaces and compared their predictions based on the laminated boundary layer theory with the experimental results by Ishigai, et al⁽¹⁴⁾ with saturated water. Their data for the plate of 50 mm diameter were four or five times smaller than those obtained by Ishigai, et al⁽¹⁴⁾. Finally, it was made clear that the heat transfer characteristics of film boiling depend drastically on the orientation of the heating surface, namely, facing downward or facing upward⁽¹⁶⁾. Fukusako et al⁽¹⁶⁾ found that the average convective heat transfer coefficient for the facing upward surfaces is several times larger than that of those facing downward.

It has been suggested⁽¹⁷⁾ that the frequency with which the film reforms is reduced to zero when the point of maximum heat transfer is reached. This maximum is described as the critical heat flux. After this point heat transfer rates fall with decreasing surface temperature in what is termed the nucleate boiling stage.

Stage B- vapour transport cooling stage

Heat transfer in the vapour transport stage is dependent on many factors including the latent heat of vaporisation, extracted as a bubble is formed, and a "microconvection" term which has been used⁽¹⁸⁾ to describe the bringing of cold liquid to the hot surface as a bubble is released. Heat transfer is therefore dependent on factors which govern the nucleation and growth of bubbles such as surface condition and the contact angle and surface tension of the liquid. When the surface temperature has fallen below the boiling point of the liquid then boiling is halted and cooling occurs by convection in the liquid. This stage is important in quenchants. Mitsutaka and Fukuda⁽¹⁹⁾ observed that when a hot steel plate was immersed vertically in still water vapour films cover the entire plate after immersion, but they are soon broken locally along the edges and at projections where the temperature falls more quickly than in other parts of the plate. Then nucleate boiling begins near edges and projections where the temperature falls more rapidly.

According to Tong⁽²⁰⁾ heat is transferred during nucleate boiling, from the hot surface to the liquid through several mechanisms:

- (a) Heat transfer by single phase forced convection on the wetted bare surface, between patches of bubbles.
- (b) Heat transport by continuous evaporation from a liquid microlayer at the root of the bubble and the corresponding condensation at the top of the bubble, while the bubble is still attached to the surface.
- (c) Heat transfer by liquid-vapour exchange during bubble detachment from the surface.
- (d) Heat transport by the latent heat carried by the detached bubbles.

Westwater(21) describes the characteristic feature of nucleate boiling as the rapid repeated formation of small bubbles at a randomly located specific nuclei, and positions on the component where quenchant is in contact with the component but no bubbles form. During nucleate boiling bubbles forming at point sources grow to a maximum size before becoming detached. As soon as a bubble breaks free a new one is formed in its place. This rapid emission of bubbles results in good agitation and heat is removed by the latent heat of vaporisation required to form the vapour bubbles in the quenchant, thus causing rapid heat removal during this stage.

Stage C- liquid cooling stage, this stage starts when the surface temperature of the metal reaches the boiling point of the quenching liquid. Vapour no longer forms, so cooling is by convection through the liquid. The rate of cooling is slowest in this stage.

The characterisation of the quenchant behaviour from cooling curves obtained by temperature measurements within the specimen are of limited value, although this technique has been widely used to compare and analyse the behaviours of different quenchants(22-23).

Quench data presented in the form of cooling curves can not be used directly in the solution to the differential heat conduction equation. This data must be used first to determine the surface heat transfer coefficient. Furthermore, the heat transfer mechanisms operating during the quench are dependent on the temperature at the surface. Hence the surface thermal condition must reflect this temperature dependence. Most of the published cooling curves refer to temperature at the centre of specimen(22-23) which means that such data will

not give very accurate information about the surface thermal condition.

Knowledge of the variation of the surface heat transfer coefficient 'h' with surface temperature is required for the correct analysis of quenchant behaviour since this information can be used in the calculation of the time- temperature distribution(24).

2.2.1 INFLUENCE OF EXPERIMENTAL VARIABLES ON THE SURFACE HEAT TRANSFER COEFFICIENT

Many factors have an effect on the shape of the cooling curve showing the relationship between time and temperature. The most important are the type of quenchant, component size and shape, material, surface condition, initial temperature of specimen, quenchant temperature. Also quenchant agitation accelerates the overall cooling rate. Price and Fletcher(25) showed the effect of quenchant type on the heat transfer coefficient. As would be expected the greater values of 'h' were obtained with water quenched at 20°C, while the values of 'h' produced during the polymer quench were lower than those in water, and the lowest values were produced during the oil quench. The values of 'h' obtained by Price and Fletcher(25) were in general higher than those obtained by Mitsutsuka(26). Also the oxidation of the specimen surface during a water quench increased the rate of heat transfer(25).

Mixtures of water with polymers or oils are capable of cooling rates intermediate between those of water and oil alone(27,28). Quenching oils are usually fast, intermediate and slow. The significant differences between such oils are due to the temperature at which the vapour blanket breaks down(29).

Beck and Chevrier(30) have used cooling curves measured at the centres of the

cylinder of 10 to 30 mm diameter to determine surface heat fluxes. Radial heat flow only was considered, despite a diameter to height ratio of merely 1:3. The use of an explicit finite difference method to analyse the cooling curve data required small time intervals in order to meet the relevant stability criteria.

Beck and Chevrier⁽³⁰⁾ have reported a dependence of 'h' on specimen size during experiments that involved the quenching of nickel cylinders in boiling water. Figure 1 reports their results, which showed there is a variation of surface heat flux with surface temperature (calculated from thermocouple measurements made at the centres of the cylinders). However it was observed that boiling started at the bottom of the cylinders and moved upwards as a front (shown schematically in figure 2).

The dependence of 'h' on the diameter of the cylinders was attributed to an anomaly caused by the narrow width of the nucleate boiling front. Thus the sharp increase in cooling rate experienced at the centre of the cylinder as the nucleate boiling front moved up past it, was reduced by the vapour blanket and convection stages above and below it respectively. Beck and Chevrier⁽³⁰⁾ proposed that this effect was accentuated as the cylinder diameter was increased, so that 'h' appeared to be influenced by the specimen diameters.

Lambert and Economopoulos⁽³¹⁾ used an implicit finite difference solution to the transient heat conduction equation in conjunction with temperature measurements made at a point 1 mm below the surface of the specimen. Temperatures were subsequently extrapolated to the surface and 'h' values quoted in terms of the actual surface temperatures. In this case surface heat transfer coefficients were found to vary markedly during the course of the quench.

Nucleate boiling occurs first at edges and corners^(8,32,33) and vapour may be trapped in any recess. The direction in which the specimen is quenched also has an effect.

However, some researchers have used plates⁽²⁶⁾ which showed that the heat transfer coefficient was dependent on the water temperature, see figure 3. It was also found to be dependent on the specimen orientation, (i.e. either vertical or horizontal) and specimen temperature.

Mitsutsuka and Fukuda⁽³⁴⁾ found that the value of h obtained on the underneath surface of a plate, quenched in a horizontal position, was substantially different from that obtained at the upper surface. This was due to the entrapment of vapour underneath the plate.

In the case of very thin specimens and moderate heat fluxes the temperature gradient can be assumed to be negligible and the easiest solution to the problem was the "lumped parameter" approach⁽³²⁾ obtained by a simple heat balance on the whole specimen. This approach was considered accurate provided that the Biot number was less than 0.2. Bergles and Thompson⁽³²⁾ used this with a maximum Biot number of 0.24, their results were accurate to within $\pm 3^{\circ}\text{C}$.

Mitsutsuka and Fukuda⁽³³⁾ used an explicit finite difference method to obtain h from the cooling curves data measured at the centres of quenched plates of 28 mm thickness. For each value of experimental time and temperature they made an initial estimation of h , which was used to obtain a calculated time and temperature at the end of the step. The estimate of h was then successively iterated until an adequate agreement was reached between the calculated and experimental time/temperature data.

Differences between the surface heat transfer coefficients of specimens made

from different materials were due to the different nature of the oxide films present⁽²⁷⁾.

Although, values of 'h' were compared using nickel and mild steel specimens in a water quench, provided that specimens were oxide free, there was little difference in behaviour⁽³¹⁾.

It has been reported⁽³⁵⁾ that due to the formation of oxide layers, the quenching medium used and the mode of quenching, there was a wide variety of values which were obtained.

The effect of surface condition was also investigated by Hessling⁽³⁶⁾, Allen et al⁽⁴⁾ and Jawson⁽³⁷⁾ in which the maximum surface heat transfer coefficient was achieved as the surface became smoother.

Mitsutsuka and Fukuda⁽²⁶⁾ showed that 'h' was dependent on the water temperature and specimen temperature. The stability of the vapour blanket stage was increased as the initial temperature of the quenchant was increased and the vapour blanket persisted to lower temperatures^(38,27,30,39).

Paschkis and Stolz⁽²⁷⁾ and Lambert and Economopoulos⁽³¹⁾ found the greatest effect of agitation occurred in the vapour blanket stage, where it reduced the stability of the vapour blanket. However, the control of agitation is a long established principle in quenching operations⁽⁸⁾.

The surface condition of a specimen on quenching has a great deal of effect on its cooling rate. The principal effect of the surface topography of a specimen is on the number of nucleation sites for vapour production during nucleate boiling. Hessling⁽³⁶⁾ observed that the surface finish of a plate strongly affected the maximum observed surface heat transfer coefficient during quenching.

The effect of surface roughness on the surface heat transfer coefficient produced

during the quench was obtained experimentally⁽⁴⁰⁾. The surface heat transfer coefficients were represented as a function of the actual surface temperature and not the thermocouple temperature which was obtained 1.5 mm below the surface. All the three stages of the quenching process were present in the relationship between temperature and time during the cooling process. The duration of the vapour blanket stage was shortest with the specimen of roughness (400 grade), and also the rate of cooling during nucleate boiling was greatest as the surface became smoother (600 grade finish). The most significant effect of a smoother surface was an increase in the maximum surface heat transfer coefficient. The overall level of the surface heat transfer coefficients during the complete nucleate boiling stage also increased as the surface roughness was reduced.

2.2.2 DETERMINATION OF THE SURFACE HEAT TRANSFER COEFFICIENT DURING QUENCHING

Transient or unsteady-state heat transfer problems are characterised by time-dependent heat fluxes and temperature fields.

The heat transferred from the surface of a quenched specimen represents one of the boundary conditions which is required to solve the transient heat conduction equation, which must be used to obtain the temperature distribution.

The effect of time on the temperature distribution in a quenched specimen is given by the differential heat conduction equation, see Carslaw and Jaeger⁽⁴¹⁾.

$$\begin{aligned}
 & \left[\frac{\partial}{\partial X} \left[(\lambda \frac{\partial \theta}{\partial X}) \right] + \left[\frac{\partial}{\partial Y} \right] \left[(\lambda \frac{\partial \theta}{\partial Y}) \right] + \left[\frac{\partial}{\partial Z} \right] \left[(\lambda \frac{\partial \theta}{\partial Z}) \right] + Q \right. \\
 & \left. = [(\rho C_p)] \left[\frac{\partial \theta}{\partial t} \right] \dots \dots \dots (1) \right.
 \end{aligned}$$

Where;

λ = Thermal conductivity W/m°C

ρ = Density Kg/m³

θ = Temperature °C

C_p = Specific heat capacity J/Kg°C

This equation is a three dimensional representation of the conduction of heat and can be solved by numerical methods such as finite elements or finite differences. Suitable numerical solutions have been used in various investigations, examples being in references⁽⁴²⁻⁴⁴⁾.

Numerical solutions to the transient heat conduction equation can be achieved by the replacement of the partial differentials by finite difference terms. In this case the component was divided into small finite regions and the temperature at a point within this region was calculated and taken to be representative of the region as a whole. The calculation of the temperature at each point involved the solution of partial quotients involving the temperature in adjacent regions and a heat balance on the region in question. Soomro⁽⁴⁵⁾ cited the work of Rogers and Adams⁽⁴⁶⁾ and Ames⁽⁴⁷⁾ for the derivation of an explicit form of the finite difference equation for uniaxial heat flow.

Heat transfer at the surface of a quenched specimen can be written in the form of Newton's law of cooling by convection which was a function of the temperature difference between the solid and the fluid (convective flow is assumed at the surface).

$$\text{Heat flow } q = hA (\theta_1 - \theta_2) \dots \dots \dots (2)$$

$$h = q / A(\theta_1 - \theta_2)$$

Where;

q = rate of heat transfer

A = surface area of specimen in contact with the fluid

θ_1 = surface temperature

θ_2 = bulk liquid temperature

h = surface heat transfer coefficient

The heat transfer coefficient 'h' can be defined in terms of specimen surface area, specimen and quenchant temperature difference, and the rate at which heat is transferred in unit time. This is a physical property that defines the boundary condition required in the solution of the unsteady heat conduction equation 1. Its determination is an essential step in the solution of equation 1.

In the case of thin specimens and moderate heat fluxes the temperature gradient can be assumed to be negligible and the magnitude of h can be obtained by a simple heat balance on the whole specimen⁽²⁸⁾ in conjunction with the experimental cooling curves, in which case the surface heat transfer coefficient may be obtained at any time during the quench from;

$$h = (MCp / At) \ln\{(\theta_2 - \theta_t) / (\theta_2 - \theta_0)\} \dots \dots \dots (3)$$

However, the specific heat is temperature dependent⁽⁴⁸⁾.

Due to the high errors found in the measurement of actual temperature at the liquid-solid interface using a thermocouple attached to the specimen surface, work on surface heat transfer coefficients always involves temperature measurements at a point just below the surface⁽⁴⁹⁾.

The investigation by Davis⁽⁵⁰⁾ was to determine the temperature distribution

and cooling rates in steel plates on quenching in water. A constant value of 'h' was used and reported results were said to be in good agreement with experimental data.

Lambert and Economopoulos⁽³¹⁾ suggested that temperature measurement should be at a distance of less than 1 mm below the surface of the specimen. They used an implicit finite difference solution to the transient heat conduction equation in conjunction with temperature measurements made at a point 1 mm below the surface of specimen. Surface heat transfer coefficients were found to vary markedly during the quench. The accuracy of the results was related to the depth below the surface at which the temperature was measured. The method depended on the measurement of temperature changes in a certain time interval, at some point in the specimen. Therefore, the reduction in the surface heat flux became more attenuated as the distance of the point of temperature measurement from the surface was increased.

Paschkis and Stolz⁽²⁷⁾ have also pointed out that the thermocouple should be located as close to the surface as possible. It was found that during investigation with 25 mm and 50 mm diameter spheres, the temperature gradients could be ignored when the values of 'h' were low (e.g., in vapour blanket and convection stages). At higher values of 'h', when significant temperature gradients occurred within the specimens (e.g., in nucleate boiling stages), they developed two methods of solution⁽²⁷⁾ based on an electrical analogue and a numerical step-wise solution to the inverse heat conduction problem. Both methods of solution were liable to become unstable with very high heat transfer rates.

An explicit finite difference method was used^(33,25) in conjunction with the experimentally determined relationship between temperature and time in

quenched steel plates to obtain 'h'. For each value of time an initial estimation of 'h' was used to calculate an approximation of time and temperature. This estimate of 'h' was varied during an iteration sequence until an adequate agreement between calculated and experimental temperature was obtained⁽³³⁾.

This calculation was carried out using successive estimates of h by the use of the explicit finite difference solution to equation 1. This method of determining h is feasible, provided that the temperature at one point at the new time is known. In principle, this temperature at the new time may be obtained from the experimental cooling curves. However, the explicit finite-difference method is subjected to the restriction on the size of the time step. This gives such a small value of time interval that, in practice, it is not possible to obtain accurate experimental data about the change in temperature by thermocouples during a single time interval. Therefore, an iterative technique has been used which involves the determination of an initial approximate value of 'h' over a large time interval. The use of the approximate method for the determination of surface heat transfer coefficients produced values that were significantly lower at any specific temperature than those produced by explicit finite difference methods.

2.3 THE PREDICTION AND CALCULATION OF THERMAL STRESSES DURING QUENCHING

A considerable amount of work has been done towards the prediction of thermal stresses during the quenching process. The earliest attempts to calculate quench stresses have been made by Maurer⁽⁵¹⁻⁵²⁾ when the residual stresses in a circular disk are calculated from a known temperature history, assuming linearly elastic material. However Buhler⁽⁵³⁾ in 1952, strongly underlined the point that plastic flow plays a significant role in the problem and has to be considered in such calculations. Mura⁽⁵⁴⁾ managed to get a solution in closed form using very simplified assumptions such as;

- (i) Linear elastic material at temperatures below the phase transformation temperature and
- (ii) perfectly plastic material with zero yield stress at temperature above the phase transformation temperature.

Russell⁽⁵⁵⁾ published the results of calculations of stresses in quenched steel cylinders, in which he assumed the material behaviour was elastic. Nevertheless, he proposed that before calculation of thermal stresses could be calculated, there were certain problems which should be considered. These are;

- (i) The calculation of the temperature distribution throughout the body, allowing for the heat generated during the decomposition of the austenite.
- (ii) The progress of the decomposition of austenite at different positions in the specimen.
- (iii) The determination of the flow stress and plastic behaviour over the temperature range involved.
- (iv) The determination of the elastic constants over the temperature range

involved.

(v) The influence of the pressure set up during partial transformation on the remainder.

Solutions of thermal stress problems for simple shapes and simple temperature distributions are available in many texts when plastic flow does not occur ref.(56-57). Only in recent years has the use of digital computers increased the number of solutions to problem of stress generated in quenched specimens. This has involved particularly the introduction of finite element analysis in the case of components of complex shapes(58-62).

The accuracy of the finite element and finite difference techniques has been reported by determining a numerical solution to the inverse heat conduction problem(58-60). It was found that of the three basic numerical solutions to the transient heat conduction equations, i.e. the Crank-Nicholson recurrence formula, the Galerkin process and quadratic interpolation method, the Galerkin process was significantly better in terms of short time step accuracy(58).

2.3.1 CALCULATION OF THERMAL STRESS DURING QUENCHING

Benham and Hoyle(63) have given solutions to steady-state and transient thermoelastic problems, and also a method of solution when plastic flow is present in some parts of the material. Boley and Weiner(57) have defined the complete problem when a thermal gradient generates elastic stresses, providing that the temperature distribution is known.

Thus, the problem involves;

6 stress components: $\sigma_{XX}, \sigma_{YY}, \sigma_{ZZ}, \sigma_{XY}, \sigma_{YZ}, \sigma_{ZX}$

6 strains components: $\epsilon_{XX}, \epsilon_{YY}, \epsilon_{ZZ}, \epsilon_{XY}, \epsilon_{YZ}, \epsilon_{ZX}$

3 displacement components: U V W

The values of these functions must be such that the boundary conditions are satisfied, which can be divided into two types.

1 - Traction boundary conditions;

$$X = \sigma_{XX}n_X + \sigma_{XY}n_Y + \sigma_{XZ}n_Z$$

$$Y = \sigma_{YY}n_Y + \sigma_{YX}n_X + \sigma_{YZ}n_Z$$

$$Z = \sigma_{ZZ}n_Z + \sigma_{ZX}n_X + \sigma_{ZY}n_Y$$

Where X, Y, Z are the components of the prescribed surface traction in the X, Y, Z directions and n_X , n_Y , n_Z are the direction cosines of the outward drawn surface.

2- Displacement boundary conditions;

$$u = f(p)$$

$$v = g(p)$$

$$w = h(p)$$

where f, g and h are prescribed functions.

The values of following fifteen equations representing the functions must also be fulfilled throughout the specimens (plate).

6 stress-strain relations;

$$\epsilon_{XX} = 1/E [\sigma_{XX} - \nu(\sigma_{YY} + \sigma_{ZZ}) + \alpha e_x \theta], \epsilon_{XY} = (1/2G)\sigma_{XY}$$

$$\epsilon_{YY} = 1/E [\sigma_{YY} - \nu(\sigma_{ZZ} + \sigma_{XX}) + \alpha e_x \theta], \epsilon_{YZ} = (1/2G)\sigma_{YZ}$$

$$\epsilon_{ZZ} = 1/E [\sigma_{ZZ} - \nu(\sigma_{XX} + \sigma_{YY}) + \alpha e_x \theta], \epsilon_{ZX} = (1/2G)\sigma_{ZX}$$

3 equilibrium relations;

$$\partial\sigma_{XX}/\partial X + \partial\sigma_{XY}/\partial Y + \partial\sigma_{XZ}/\partial Z + X = 0$$

$$\partial\sigma_{XY}/\partial X + \partial\sigma_{YY}/\partial Y + \partial\sigma_{YZ}/\partial Z + Y = 0$$

$$\partial\sigma_{XZ}/\partial X + \partial\sigma_{YZ}/\partial Y + \partial\sigma_{ZZ}/\partial Z + Z = 0$$

and 6 strain displacement relation;

$$\begin{aligned}\epsilon_{XY} &= [1 / 2\nu_{XY}] = 1 / 2 [(\partial_U / \partial_Y) + (\partial_V / \partial_X)], \epsilon_{XX} = \partial_U / \partial_X \\ \epsilon_{YZ} &= [1 / 2\nu_{YZ}] = 1 / 2 [(\partial_V / \partial_Z) + (\partial_W / \partial_Y)], \epsilon_{YY} = \partial_V / \partial_Y \\ \epsilon_{ZX} &= [1 / 2\nu_{ZX}] = 1 / 2 [(\partial_W / \partial_X) + (\partial_U / \partial_Z)], \epsilon_{ZZ} = \partial_W / \partial_Z\end{aligned}$$

The solutions to the equations, according to Price⁽⁶⁴⁾ could only be obtained by classical techniques in a small number of cases where the above equations could be simplified. Price⁽⁶⁴⁾ pointed out that plates and cylinders allow simplifications to the stress system (plane stress and plane strain respectively). This greatly reduces the number of unknowns to be determined. Solutions which involve plastic flow, i.e. when one of the co-ordinates in the 3-dimensional system lies on or beyond the yield surface of the specimen, require the use of Prandtl-Reuss stress-strain relations;

$$(\partial \epsilon_{P_X}) / \partial_X = (\partial \epsilon_{P_Y}) / \partial_Y = (\partial \epsilon_{P_Z}) / \partial_Z = 3/2 \partial \beta$$

where $\partial \beta$ = proportionality factor dependent on temperature. Also required when considering plasticity is the Von Mises yield criterion which is used to determine whether flow will occur;

$$(\sigma_X - \sigma_Y)^2 + (\sigma_Y - \sigma_X)^2 + (\sigma_Z - \sigma_X)^2 = C\sigma^2$$

where σ is a parameter called the effective stress and σ_X , σ_Y and σ_Z are principal stresses. The former variable determines whether flow will occur.

In order to obtain a solution, Weiner⁽⁶⁵⁾ assumed constant thermal and

mechanical properties and simplified the temperature distribution, but the method of solution did not incorporate the effect of strain due to transformation. When this technique was taken a stage further by Boley⁽⁶⁶⁾, who assumed both a temperature dependent flow stress and the possibility of time dependent stress-strain behaviour, a complete analytical solution was no longer possible and numerical methods were employed to achieve an approximate but nevertheless acceptable solution.

The results of the calculation of the stresses which developed during the quenching of plates⁽⁶⁷⁾ showed that the stresses at the surface of the plate became initially tensile, then compressive during transformation of the surface region to martensite and finally tensile after the transformation of the centre region of the plate.

Fletcher⁽⁶⁸⁾ proposed a numerical method for the determination of the stresses in plates of low alloy steel which transformed completely to martensite on quenching. The type of residual stress distribution on quenching was dependent upon the cooling rate. A residual tensile stress at surface was associated with a high quenching rate. The reverse residual stress pattern was produced by the slowest quench. A small amount of plastic deformation was produced by the initial tensile stress at the surface, throughout the range of quenching media.

Later, the experimental results from a series of water, polymer and oil quenches were compared with calculated values⁽⁶⁹⁾. Good agreement has been found in the case of stresses generated during the polymer quench.

Jeanmart and Bouvaist⁽⁷⁰⁾ carried out finite element calculations of thermal stresses on high strength aluminium alloy plates. The results showed that residual stresses produced during a hot water quench were lower than those

obtained during a cold water quench. This method gave good agreement between theoretical predictions and the experimental values of residual stresses, as measured by the layer removal method. It was suggested that the control of complex phenomena involved during quenching could be achieved by determining the temperature distribution, thermal strains, and residual stresses using the MARC finite element programme.

Chevrier⁽⁷¹⁾ has calculated the stresses produced during quenching of aluminium alloy cylinders in which the material did not exhibit any transformation effect and all the physical data obtained during the calculation was derived experimentally. Chevrier⁽⁷¹⁾ applied the Von Mises yield criterion and modified the initial elastic stress estimates. However, he did not adjust the stresses to take into account the necessary rebalancing. Therefore, Archambault⁽⁷²⁾ modified the method which had been used by Chevrier by the addition of an extra stage after the application of the plasticity, so that during this stage the internal stresses were rebalanced to produce zero force on the section.

In the absence of the transformation strains, tensile plastic flow at the surface resulted in compressive residual surface stresses at the end of the quench.

Schroder⁽⁷³⁾ determined the stress distribution in steel cylinders of different diameters, quenched with and without the inclusion of transformation effects from different temperatures. This involved the use of a finite element programme. Schroder also used a classical analytical technique to determine stresses in very thin plates or very long cylinders at points well away from the ends. In the thin plate, there was no component of stress acting in the axial direction, and the axial strain varied with the radius. In the regions of long

cylinders that were far from the frontal surfaces, the radial variation of the axial strains was suppressed and axial components of stress appeared. The radial and tangential stresses in cylinders were distributed as in the plates. All cylinders showed the same distribution of stress, but the stresses themselves increase continuously with increasing diameter. Only the tangential stress component acting near the inner surface depended on diameter in a continuous manner (with transformation).

Quenching and residual stresses were evaluated in carburized steel cylinders⁽⁷⁴⁾. A variety of experimentally generated data including dilation strains, temperature-dependent elastic-plastic properties, and thermal profiles from oil and water which were used as input data for a finite element programme.

Residual stresses were evaluated by x-ray diffraction methods and results compared favourably with those found from the finite element programme. Comparison of stress patterns by other investigators⁽⁷⁵⁾ also supported the results. Also it was found that the tangential residual compressive stress at the surface increased to a maximum at about the 1.5% carbon level and then reversed to a tensile state in the core. Furthermore, the type of quench changed the rate of formation of plastic strain and the final residual stress.

Hidenwall⁽⁷⁵⁾ predicted thermal stresses using a formulation developed by Sjoström⁽⁷⁶⁾, which could cope with simple geometric shapes such as cylinders and plates. The physical property data was related to temperature, except for the thermal expansion coefficient of austenite, which for carbon and low alloy steel, was independent of temperature in the range of $20-25 \times 10^{-6} \text{C}^{-1}$. The values of heat transfer coefficients used were lower than those obtained by other

authors⁽²⁵⁾. Surprisingly the quench condition was similar in the cases of both water and oil.

Experimental measurement of the residual stresses were made using x-ray diffraction which was probably more accurate than the mechanical methods. The measured and calculated compressive stresses agreed in value and position through the specimen. However, the residual stresses were less accurate nearer the centre of the specimen. The maximum value of compressive stress was found to be dependent on the carbon profile and this value was also influenced by the dimensions of the specimen.

Recent analyses have been developed in parallel with the development of computers and numerical methods. Several recent studies have been carried out⁽⁷⁶⁻⁷⁸⁾ all based on a thermo-elastic-plastic theory and finite element analysis. The major difference between these studies is the manner of taking into account the induced volume changes due to phase transformation in steel alloys. Sjostrom⁽⁷⁶⁾ took a long cylinder and used water or oil quenches to cool the specimen from the austenite range to room temperature. The temperature history was analysed with a finite difference method. The phase transformation process was modelled using the time-temperature-transformation diagrams. The stresses were calculated with a finite element programme, in which it was assumed that all the elastic and plastic properties were temperature dependent and phase composition was taken into account. Transformation plasticity covered the heterogeneous deformation of austenite at relatively low applied stresses, the strain remaining after the removal of the load even though the yield stress of the material would not have been exceeded.

A finite element method has been used to investigate the effect of the edge⁽⁷⁷⁾

on the generation of thermal stress in a water-quenched circular plate of a steel of high hardenability. Both the temperature distribution and the produced thermal stresses were obtained by the use of the Bersafe finite element programme. The calculation of the temperature distribution during the quench involved a Crank- Nicholson solution to the transient heat conduction equation. The diameter of the disc was 60 mm and the thickness 10 mm and only a single quadrant of a radial section was necessary to be considered. The study of stress distribution based on an elastic analysis was made by Horvay⁽⁷⁹⁾ who showed that stresses produced would be perpendicular to the radial direction. In the recent work plasticity was included in the thermal stress calculation⁽⁷⁷⁾.

The results indicated that an average correction factor considerably higher than that used by Fletcher and Price⁽⁸⁰⁾, and slightly higher than that obtained by the use of Saint Venant's principle⁽⁸¹⁾, which explained the effect of edge on the stress distribution in a component.

Choi, Bi et al⁽⁸²⁾ have used the FEM codes ADINA and ADINAT to predict the distributions of temperature, internal stress, and residual stress in a 0.4% carbon steel (20 mm diameter*50 mm long) during water quenching from 850°C. The effect of phase transformation was not considered. However, the magnitude of residual stress appeared to be smaller than other results that considered phase transformation, indicating the crucial effect of the phase transformation. It was also found that the entire cylinder reached the cooling water temperature after 2 minutes. The surface of steel cylinder was found to be under tension at the beginning and under compression at a latter stage of cooling, whereas, the centre showed the opposite tendency.

2.3.2 EXPERIMENTAL METHODS FOR DETERMINING RESIDUAL STRESS

Fletcher, Allen, Soomro, Abbasi^(40,45,64,80,83-87) have all used a mechanical method involving the surface layer removal techniques which were described by Fletcher and Price⁽⁸⁰⁾ to calculate the residual stresses. The method used for flat plates was described by Andrews⁽⁸⁸⁾ and involves the grinding away of surface layers of a plate whilst a strain gauge rosette affixed to the back of the plate measures surface distortion. Abbasi⁽⁸⁹⁾ used the technique in order to assess the accuracy of the method on a strain free plate and found that stresses induced by the process were negligible. It is thought then that the suitability of mechanical techniques for discerning residual stresses is dependent on the yield strength of the as-quenched material.

The results obtained from this method have been used in order to compare them with predicted stresses using a finite element calculation technique with varying degrees of correlation. Jeanmart and Bouvaist⁽⁴⁴⁾ reported that good correlation was obtained between stresses calculated using finite element analysis and those experimentally determined using experimental techniques involving a layer removal technique for quenched plates of high strength aluminium alloy.

Buhler and Buckhdz⁽⁹⁰⁻⁹¹⁾ describe the use of the Sachs boring technique to measure residual stress in plain carbon steel cylinders quenched in water and air cooled. Their results indicated that radial stress varied with radial depth in a complex manner and also that water quenching gave a higher maximum residual stress than air cooling. This method was also used by Buhler and Rose⁽⁹²⁾ to determine the residual stresses in steel cylinders of differing diameters and

compositions. The results indicated that increasing the cylinder diameter or the severity of the quench used altered the stress at the surface to a compressive from a tensile value.

Fujio et al⁽⁹³⁾ also utilised 0.45%C steel cylinders 50 mm in diameter to calculate quench stresses. They assumed the physical data was not temperature dependent, but remained constant throughout the quench. Dilatometric tests were carried out to deduce the amount of martensite formed at different radial depths. Strain hardening was not taken into account and experimental results were determined using the Sach's boring method, a comparison being made with the calculated stresses. The results indicated that the calculated stresses were influenced greatly by the amount of austenite and martensite present at any one time.

Denis et al⁽⁹⁴⁾ compared their results obtained by finite element analysis using a Sachs method and found good agreement between calculated and predicted stress patterns in cylinders.

Kral et al⁽⁹⁵⁾ reported that the hole drilling strain gauge method was used in the measurement of residual stress. This method is based on the measurement of the strains produced by the stress relaxation during the introduction of a hole into a residually stressed body. The main aims were to increase the production reliability and to shorten the cooling down period of the casting in the mould.

The x-ray technique was used in the measurement of residual stress distribution in carburised gear wheels of differing chemical composition by Inoue et al⁽⁹⁶⁾. Their results stated good agreement between those obtained from x-ray diffraction and calculated using a finite element method.

Residual stress measurements using ultrasonic and x-ray diffraction techniques were made on cylindrical cross sections of low alloy steel that had been cut from the larger cylinder at least one foot from the nearest end⁽⁹⁷⁾.

The preliminary results of the x-ray diffraction analysis showed qualitative agreement with the ultrasonic results. The ultrasonic technique uses a wave that travels through the thickness of the specimen, but x-ray radiation only penetrates the specimen to a depth of about 10um.

2.3.3 TRANSFORMATION PLASTICITY

It has been shown that when a phase transformation takes place under an applied stress, a permanent strain occurs even for stresses lower than the yield stress of the material.

This phenomenon is called transformation plasticity⁽⁹⁸⁾. A complete review for the phenomenon of transformation plasticity for steels is given in ⁽⁹⁴⁾. When transformation takes place under an applied stress transformation plasticity occurs which is related to the applied stress and to the progress of transformation. This phenomenon is observed in numerous alloys with different types of transformation (with or without diffusion)⁽⁹⁴⁾. Investigations have taken place into the metallurgical and mechanical analysis of the effect of stresses on phase transformation. Low stress transformation interactions can be introduced into a model which calculates internal stresses by two methods.

In the first, a simplified model of transformation plasticity can be used in the calculation of internal stresses, which allows for the possibility of the metal undergoing plastic deformation by introducing as input data in the calculation a very low yield stress at the beginning of the martensitic transformation interval.

This simplified approach has been used by other authors⁽⁹⁹⁻¹⁰¹⁾.

However, two problems were produced by the use of this model. Firstly, the plastic strain resulting from the transformation had a finite value which depended on the progress of the transformation, whereas, the resulting plastic strain obtained by using a decrease in the metal yield stress was not limited in the same way. Secondly, transformation plasticity also depended on the stress state. This led to the second, more accurate model of transformation plasticity, viz;

The effect of the stress-phase interaction on the development of internal stresses during quenching have been included in the calculation and transformation plasticity has been considered as an additional strain related to the progress of transformation and to the stress state.

The total strain is then given by the following equation,

$$\varepsilon_{\text{Total}} = [E / (1 - \nu)]\sigma + \varepsilon_p + \varepsilon_{\text{Trans}} + \varepsilon_r$$

In addition the effect of stress on the kinetics of the transformation should be introduced into the calculation of stress as coupling between the stress and quantity of transformation product. This has been investigated by Denis⁽¹⁰²⁾, who suggested relatively little effect on the stress generation process.

Abbasi and Fletcher⁽⁸³⁾ have reviewed the effect of stress on the characteristics of the martensite transformation. Two methods have been used, one is the concept of a reduction in yield stress and the other is an additional transformation strain. The use of either method improved the correlation between experimental and calculated stresses..

The introduction of the reduced yield stresses into the calculation of thermal stress caused significant changes to the relationship between thermal stress and strain produced during the later stages of a quench in either water or oil. In the case of water, compressive flow occurred at the surface as soon as M_s was reached and continued until, at 256°C , the yield stress rose rapidly. In the case of oil, plastic flow occurred at the surface as soon as M_s was reached. Hence, there was no build-up of stress at this stage. Unloading occurred in both cases at 274°C , but the final surface stress was more tensile when transformation plasticity was present. Additional strain was included in elastic calculations at temperatures below M_s and the relationships between stress and strain were identical to those without transformation plasticity. Once transformation began the additional strain generated by the formation of martensite was added to that produced by the thermal gradient, as though it was an elastic stress. The change which transformation plasticity had introduced caused no change to the residual stress distribution. There was a small change in the residual stresses which were obtained after either an oil or water quench by introducing additional strain as a plastic instead of an elastic component and there was good agreement with experimental and theoretical work. The residual strains were different from those obtained when the additional strain was considered to be elastic and were instead slightly lower than the values obtained when transformation plasticity was introduced by a reduction in yield stress. There was a threshold of about 40MNm^{-2} below which the absolute applied stress does not affect the amount of transformation strain.

Denis⁽¹⁰²⁾ has also tried to simulate the effect of transformation plasticity by introducing a yield stress drop at temperatures below M_s , figure 4 curve 4. It

affected the residual stress after the oil quenching only marginally but had a pronounced effect on the water quenched specimens, see figure 5. Considerable plastic deformation resulted in the zone undergoing martensitic transformation. When the stresses were low as in the oil quench case the yield drop was not enough to produce plasticity. Denis⁽¹⁰²⁾ also studied the effect of a +15°C rise in M_s but found very little effect.

It has been suggested⁽¹⁰³⁾ that the thermo-mechanical behaviour of steel during the martensitic transformation should be established by experiment and this data introduced in a finite element programme for the calculation of internal stresses during quenching from the austenite temperature.

The modification of the kinetics of the martensitic transformation by the stress state are shown to have little effect on either the generation of internal stresses during cooling or on the residual stress state. However in the case of steel which undergoes not only martensitic transformation but also pearlitic and bainitic transformations the effect of internal stresses on the transformation kinetics has important consequences on the hardenability of steel and further calculations must be carried out in order to show if these modifications of the transformation kinetics have a great effect on the onset of internal stresses during quenching.

Li and Chen⁽¹⁰⁴⁾ developed a mathematical model for calculating the temperature, stress and strain fields and their interaction in a metallic material undergoing phase transformation during quenching. An experiment by Todaro et al⁽¹⁰⁵⁾ was chosen for comparison of the calculated results. Residual stress measurements were made on cylindrical specimens cut from long hollow cylinders of ASTM A723 steel with an outer diameter 23.9 cm and inner diameter of 9.4 cm. The entire cylinder was austenitised at 1116K and

quenched from outer surface to 366K in 12 minutes. A 7.5 cm thick cylindrical section was cut at a section 30.43 cm from the end. The model used in computation was given the same inner and outer diameters and temperature drop as the specimen. It was observed that near the surface instead of the measured compressive stress, the calculation predicted tensile stress. One possible explanation was that in the calculation the bainite transformation was omitted for simplicity. Therefore, the volumetric expansion, associated with this transformation which would cause compressive stress, was not introduced.

Huang et al⁽¹⁰⁶⁾ compared calculated results with residual stresses measured by x-ray diffraction. The results showed that the surface residual stresses in all samples quenched in water or oil, are compressive to a depth of several microns. The calculated results demonstrated qualitative agreement with experiments.

Greenwood and Johnson⁽¹⁰⁷⁾ developed the use of an additional strain increment due to transformation plasticity. It was suggested that this additional strain could be calculated for the complete transformation in the presence of an uniaxial stress state. The quantity of strain due to transformation plasticity was considered to be governed by the equation;

$$\epsilon_{tp} \sim 5 / 6 [(\Delta V / V) Y] \sigma_Z$$

where ϵ_{tp} = transformation plasticity strain

$\Delta V / V$ = transformation strain

Y = Yield strength

σ_Z = Applied stress

Sattler and Wasserman⁽¹⁰⁸⁾ considered a reduction of yield stress in the material during the transformation of austenite to martensite as a means of introducing transformation plasticity.

Also Fletcher and Abbasi⁽⁸³⁾ considered models with transformation plasticity calculated using both yield stress reduction and enhanced strain methods, although experimental justification for the reduction in the yield stress could not be obtained. Both methods of introduction of transformation plasticity affected significantly the predicted stress and strain pattern, although the modelling used over-estimated the stresses produced at the end of the water quench in comparison with experimentally determined residual stresses.

Good agreement with experimentally determined residual stresses after an oil quench was obtained when transformation plasticity was modelled as a reduction in yield strength, but not by the addition of an increment into the elastic strain calculation. On the other hand the addition of an extra increment to plastic strain gave good agreement with both the experimental results and those obtained when transformation plasticity was represented by a drop in yield stress.

2.3.4 EFFECT OF SPECIMEN SIZE

Schroder⁽¹⁰⁹⁾ has carried out calculations of thermal and transformations stresses related to infinite plates or cylinders as well as the investigation of stress distributions in steel cylinders of different diameters, quenched with and without transformation effects from different temperatures. When it was assumed that no transformation occurred on quenching, the method of quenching did not influence the qualitative distribution of stress. The difference between the stresses were in fact, modest and there was no difference at all in the middle of

the cylinder of diameter 30 mm. The residual stresses were constant only over about one-third of the cylinder length, and also all cylinders showed the same type of distribution of stress, but that the stresses themselves increased continuously with increasing diameter. The highest tensile stresses occurred on the axis of the cylinder, which also showed a continuous reduction in the normal stresses in the radial direction, so that the surface was subjected to compression stresses.

Considering quenching of a steel that has undergone transformation, the curved surface was also subjected to compressive residual stresses, but the magnitude of the stresses were higher. Great differences have been seen to occur near the frontal surfaces. The quenching of the frontal surfaces had a large influence on the residual state of stress. The maximum tensile stresses appeared in areas away from surfaces or axes. Compressive stresses appeared both in the centre and at the surface, balanced by the tensile stress in between. The influence of cylinder diameter showed that only the tangential stress component acting near the frontal surface depended on diameter. It has been found that in the middle of the cylinder the stresses are nearly identical for diameters 20, 30 and 40 mm. Results of computations have been compared with x-ray measurements, which showed good qualitative and fair quantitative agreement⁽¹¹⁰⁾. Yu⁽¹¹¹⁾ has applied his computer programme⁽¹¹²⁾ to study the effect of cylinder diameter (100, 50, 30 and 10 mm) and cooling medium (oil and water) for a 1045 type steel. In case of oil quenched specimens ferrite/pearlite was formed and after a water quench martensite and bainite as well. The 10 mm cylinder started to transform to martensite at the surface and the front moved gradually inwards resulting in a typical tensile stress at the surface. The large diameter

cylinders first transform to ferrite/pearlite at intermediate radii and then to martensite at the surface. The final residual stress was compressive at the surface and tensile in the core.

Good agreement was obtained with x-ray stress measurements in several cases, as well as with other mechanically measured data.

3.0 EXPERIMENTAL PROCEDURES

3.1 EXPERIMENTAL MEASUREMENT OF THE SURFACE HEAT TRANSFER COEFFICIENT

The determination of the surface heat transfer coefficient during quenching in water which involved the use of the method developed by Price and Fletcher⁽²⁵⁾ is outlined below.

The plates of grade 316 stainless steel which have dimensions of 120 mm*120 mm*20 mm were heat treated in a stream of argon at the temperature of 860°C before being quenched in water at 20°C. During the quench the plate was held vertically in a glass tank of dimensions 856 mm*490 mm*430 mm, filled with water to a depth of 300 mm as illustrated in figure 6. The temperature of the plates were measured by thermocouples whose hot junctions were placed at positions 1.5 mm below the face surface and along one face diagonal or from top to centre (straight line) or on the side edge. These positions were 60 mm, 45 mm, 30 mm and 25 mm from the top edge of the plate face as seen in figures 7-9. Alternatively, the thermocouples were placed at the corresponding distances from the lower edge.

In the case of the vertical quench a rod of a (T) bar construction of diameter 12 mm was used to suspend the plate from the centre of the top edge (figure 7). The chromel-alumel thermocouples emerged from the plate at a point adjacent to the rod and were secured to it.

Figures 10a, 10b, 11a and 11b show the top and bottom face of the plate when the plate was quenched horizontally.

The plate was cleaned by shot blasting the surface to remove the oxide scale

after which the surface was hand polished with silicon carbide paper to a 400 finish. Then the plate was cleaned with acetone to remove any grease before being placed in the furnace. Four thermocouples were attached to the logging system which was programmed to record the temperature at each thermocouple position every 0.3s. This maximised the efficiency with which the data was collected and enabled this data to be used to determine the surface heat transfer coefficient directly.

Immersion of the plate into the water took place as soon as the temperature reached 860°C, the position of the plate in the tank being determined by the (T) bar attachment on the top of the suspending rod. The position and depth of immersion was controlled by the presence of guide rails with slots within which the plate handle rested.

Five positions at the surface of the plate were considered in each vertical quench, viz; points along the upper half of the diagonal face of the plate; corresponding positions along the lower half of the same diagonal; points on the upper half of a vertical section through the face centre; the corresponding positions along the lower half of the same vertical face; and finally one half of a horizontal section through the face centre.

Also two positions were examined on the top and bottom face of the plate when quenched horizontally. This involved, points along half of the diagonal face of the plate.

All the above has been carried out with the plate held either vertically or horizontally in the centre of the quenching tank.

Three experiments were carried out for each set of the quenching conditions outlined above.

3.2 PHOTOGRAPHIC EXAMINATION OF THE PLATE SURFACE

DURING QUENCHING

Photographic studies have been carried out by using high speed photographic techniques to observe the appearance of the face of the plate during quenching, and to relate the phenomena observed to surface heat transfer coefficients and the cooling curves at different positions on the plate face.

In all cases the plate surface was positioned in the centre of the tank.

The photography was carried out using a 35 mm Nikon camera with motor drive and a 55 mm micro-Nikon lens. Lighting was provided by two flash guns positioned to the left and right of the visible face of the plate and at the same level and at an angle of approximately 45° to an axis between the camera and the centre of the plate face. The flashes were controlled by a computer setting on 200 ASA at f8.

**3.3 CALCULATION OF THE SURFACE HEAT TRANSFER
COEFFICIENT AND THE PREDICTION OF THE GENERATION OF
THE THERMAL STRESS AND STRAIN OF A STAINLESS STEEL
PLATE DURING QUENCHING**

The surface heat transfer coefficient during quenching was obtained from the sub-surface time/temperature relationships and a successive approximations solution to the finite difference equation for unidirectional heat flow. This allowed the surface heat transfer coefficient to be calculated without resource to a direct inverse solution of the differential heat flux equation, which tends to involve stability problems. This information was then used as the boundary condition in the subsequent finite element calculation of the temperature distributions considering two dimensional heat flow in the plate during vertical and horizontal quenching.

Ultimately the temperature data was used in the finite element calculation of the thermal stress and strain generated during the quench.

3.4 CALCULATION OF SURFACE HEAT TRANSFER COEFFICIENT FROM RELATIONSHIPS BETWEEN TEMPERATURE AND TIME

The surface heat transfer coefficient was determined from the time and temperature relationships obtained during quenching by the use of an inverse solution to the explicit finite difference formation of the transient heat conduction equation, as detailed by Price and Fletcher⁽²⁵⁾. This procedure which used a method of successive approximations, is shown in figure 12. The temperature distribution and heat transfer was assumed to be symmetrical about the centre-line of the plate so that the 20 mm plate was split into two half- plate sections each 10 mm thick. The surface heat transfer coefficient was calculated for each half of the plate separately from the data obtained from each of the thermocouples placed just below the surface at the approximate centre of each face. The half section was divided into fifteen elements. This required knowledge of the physical properties such as thermal conductivity, thermal diffusivity and specific heat capacity of the material, (grade 316 stainless steel), and their relationships with temperature. The chemical composition and physical properties of the material are given in table 1.

The data used in the calculation was a series of pairs of time and temperature values, obtained by the thermocouples referred to above.

The time step was calculated from the following stability criterion,

$$\Delta F_0 < 1 / (2 + \Delta Bi)$$

$$\text{where } \Delta F_0 = \alpha \Delta t / (\Delta X)^2$$

$$\Delta Bi = h \Delta X / \lambda$$

Δt = time intervals, seconds

ΔX = distance between nodes, m

Bi = Biot number

F_0 = Fourier number

α = Thermal diffusivity m^2s^{-1}

For each time step it was necessary to make an initial estimate of h using;

$$h = [(MCp) / (\rho A \Delta t)] \ln [(\theta^a - (\theta_n^{TC})_E) / (\theta^a - \theta_{n+p}^{TC})_E]$$

where, Δt , θ^a , and θ_n^{TC} are time intervals, s, temperature of the quenchant, °C and temperature at the thermocouple hot junction after n time intervals, °C respectively. The limited accuracy of this approach produced an error in the calculated temperature at the end of the interval. Therefore h was modified by a quantity given by;

$$\Delta h = [(MCp) / (\rho A \Delta t)] \ln [(\theta^a - (\theta_n^{TC})_E) / (\theta^a - \theta_n^{TC})]$$

and a new final temperature calculated. The iteration procedure was continued until the calculated and experimentally determined temperatures were to within 1k of each other. The current value of h was assumed to be correct for the time interval in question.

This procedure produced not only values for the surface heat transfer coefficient but also the temperature distribution throughout the plate and therefore, the surface-temperature to which the surface heat transfer coefficient was related.

3.5 FINITE ELEMENT METHOD

The finite element method was evolved from the matrix framework method in which natural structural elements occur. The number of elements into which the structure is divided is a matter of engineering judgment and skill, although the solution accuracy increases with the number of elements. The elements are considered to be correlated at a discrete number of nodal points at their boundaries. The state of displacement in each element is defined by functions in terms of the nodal displacement. The state of stress throughout each element is defined in terms of strains and the elastic properties of the material. This very powerful technique is usually applied to the calculation of elastic stresses and strains, although the method can also be applied to non-linear situations, such as are encountered in quenched components(117,118,57,119).

3.5.1. THEORY OF FINITE ELEMENT TECHNIQUE

The finite element method can be used to evaluate the stress distribution at nodes in a variety of differently shaped components. These stresses are usually based on elastic theory, although the PAFEC commercial package includes facilities for plasticity, creep, fracture mechanics and buckling.

3.5.2 FINITE ELEMENT TECHNIQUES

The body or system under study is divided into a set of small elements within which the properties vary in some previously defined way. The unknowns are determined at specified points termed nodes.

The shapes used are frequently single geometrical bodies such as triangles or rectangles, although these shapes are not exclusive.

There are usually limitations on the shape of a particular type of element. Thus

a rectangular element should have an aspect ratio $< 1/6$.

3.5.3 PAFEC FINITE ELEMENT PACKAGE

A two dimensional finite element analysis has been undertaken to determine the temperature and the stress- strain distribution in the component. These calculations were undertaken using the PAFEC finite element package . Comparison of results using two different mesh configurations have confirmed the accuracy and suitability of this approach.

Also three dimensional thermal analysis has been done in order to compare the results with two dimensional thermal analysis.

3.5.4 DEVELOPMENT OF FINITE ELEMENT MODEL

The finite element package PAFEC (programme for automatic finite element calculation) level 6 is used in conjunction with the PRIME 9750 computer together with PIGS (PAFEC INTERACTIVE GRAPHICS SUITE). The boundary co-ordinates of the body were introduced and the space within was filled with 160 and 320 individual elements for the vertical and horizontal quenches respectively. Eight noded isoparametric quadrilateral standard elements are considered by the deployment of the general coded elements such as 36210 and 39210 for stress and thermal analysis respectively.

Also twenty noded standard elements such as 39710 are considered for thermal analysis only.

To ensure the accuracy of the solution it was necessary to model the sections of the component that contained high stress gradients by progressively finer meshes. However, a compromise between the accuracy, the time as well as the

storage requirements for the calculations has to be reached.

The determinite of the variation of the temperature field, with respect to time which is an essential preliminary to the stress calculation is carried out in the PAFEC system by a finite difference technique.

The explicit finite-difference method is subject to the restriction that

$$\alpha\Delta t/(\Delta X)^2 < 0.5$$

This gives such a small value of Δt that it is, in practice, not possible to obtain accurate experimental data about the change $(\theta^T_n)_E$ during a single time interval. Then an iterative technique must be used involving use of an average value of h and a longer time.

An alternative method of calculation of temperature distribution in a quenched component is by use of the implicit finite difference solution. This method is usually referred to as the Crank Nicholson method and it is this technique which has been used in the present work.

Donea⁽⁵⁸⁾ shows that the accuracy of the Crank Nicholson method decreases when small time increments are used. The convergence of both explicit and implicit forms of the series depends on (ΔX) and (Δt) intervals between two nodes and time interval respectively which represent the number of additive expressions in the series. In both the series, the truncation error is of the order $(\Delta X)^2$, but the truncation error induced instability will not grow in the case of the explicit method providing the changes in the Fourier number does not exceed $1/2$ ⁽⁴⁷⁾.

This is the maximum value that has been used in the present work.

Some data i.e. work hardening rates from ref. (85) have been used in the thermal analysis. Then these data have been used in Yielding- Elements module of the thermal analysis which incorporates three consecutive sections namely;

- the plate material properties
- number of elements which are allowed to yield
- the load increments to be applied as a percentage of the total load. In the present case, the loading is solely due to thermal gradients (no mechanical loading). The temperature history is computed independently of the stress calculation. The thermal loading is divided into 85 increments (i.e time) steps. Thus this involves the use of STEP.LIST values for plastic material in the SLOP.AND.YIELD.TABLES module. This data has been taken from the known relationship between stress and strain⁽⁸³⁾ illustrated in figure 13. Furthermore, it can be seen that the intersection of the plastic line at 125 and 250 MPa with that representing the elastic relationship gave the yield stress relevant to the temperature consideration.

The properties which have been used in the calculations of the thermal and stress analysis are given in table.2.

The values of the work hardening coefficients used in the calculations of thermal stress suggest that variations in this property are much less important than the effect of temperature on yield stress even though high work hardening rates have been suggested for quenched components at room temperature⁽⁸⁵⁾. Figure 14 shows the relationship between work hardening coefficients and temperature in the case of 835M30 specimens cooled from 850°C.

The values of surface heat transfer coefficients are within the range of 0.00005-0.018W/mm²C which vary with temperature in the range of 0-850°C

respectively.

The current version of PAFEC relates temperature to a datum of 0°C. This prevents the direct use of temperatures to provide temperature differences for use in the thermal stress calculations. Therefore it was necessary to post-process the temperatures to convert actual temperature to temperature differences relevant to each time step in turn. These temperature differences are then introduced at the corresponding stage of the thermal stress calculation.

Considerable discussions took place with the suppliers of the PAFEC package and certain suggestions were made that were usable in the case of material that underwent no transformation change. However it could not be applied to a situation where the coefficient of expansion varied markedly during a phase transformation. Promises were made that the new version of PAFEC that appeared 2 years after the start of the project would allow this facility were not kept by the PAFEC support team. Therefore all the results obtained relate to a material that does not undergo a phase transformation.

Post-processing can go some way to removing this difficulty but to allow the extreme variation associated with the formation of martensite and introducing plastic transformation, a new version of PAFEC is required. A full description of the theory of finite elements is given in references (113-116).

3.6 EXPERIMENTAL DETERMINATION OF RESIDUAL STRESS AND STRAIN IN QUENCHED PLATES

The stainless steel plate used was of the same dimensions as the plate used for the determination of the surface heat transfer coefficients. The composition and physical properties of the material used are given in table 1.

The residual stress and strain in the quenched plates was determined after quenching in water horizontally but residual strain was obtained only in the case of the vertical quench. This allowed a comparison with the corresponding calculated results obtained by the use of finite element analysis. Therefore this would give an indication of the level of agreement between the two sets of results and also the accuracy of the theoretical calculations.

The experimental procedure involved quenching, residual strain and stress measurements.

3.6.1 QUENCHING THE PLATE

Before quenching the plate was austenised for 1.5 hours at 850°C under an atmosphere of argon supplied to the furnace at a pressure of 0.1 bar. In order to ensure adequate soaking time, a thermocouple was held in contact with the plate inside the furnace. Quenching was carried out in the same tank that had previously been used for the determination of surface heat transfer coefficients, and care was taken to ensure the minimum disturbance of the quenchant when the specimen was transferred from the furnace to the quenching tank. Once the specimen had cooled to the temperature of the quenchant, it was removed and its new dimensions and residual stress distributions measured.

3.6.2 MEASUREMENTS OF RESIDUAL STRAIN

To allow the stress relieved plate to acclimatise it was allowed to stand in the metrology laboratory, a temperature and humidity controlled room, for 24 hours. The breadth, length and thickness of the plate were then measured at the points indicated in figure 15 using a Ferranti Merlin 750 measuring system. The accuracy of this apparatus was estimated at ± 5 microns.

After quenching the plate was again allowed to acclimatise for 24 hours in the laboratory before it was remeasured at the same points. This provided a measure of the longitudinal residual strain at depths of 1 mm, 4.5 mm, 10 mm, 14.5 mm and 19 mm below the plate surface and also the lateral residual strain at the centre of the plate face.

As was mentioned above, to achieve maximum accuracy a Ferranti Merlin 750 measuring system was used. The specimen was divided up into the zones shown in figure 15. The X, Y, Z coordinates were fed into the computer which controlled movement of the measuring probe (which had previously been calibrated) over the points indicated in figure 15. These points were measured automatically and recorded on a printer connected to the computer. It was necessary to use a datum point on one corner of the plate as a reference for the readings by the probe. This datum point was kept constant for both sets of measurements taken before and after the quench.

The plate was placed on a supporting plate in the centre of the granite work surface. The probe, controlled by the computer, moved on air bearings and measured all the points in one complete action; after the datum point had been input into the computer.

The results before and after the austenisation and quenching treatments were used to calculate the percentage strain in the longitudinal direction using the expression:

$$\Delta Y\% = [(Y_h - Y_s) / Y_s] * 100$$

The Ferranti Merlin 750 measuring system was also used to measure the change in thickness of the plate. These measurements were necessary because measurements in the longitudinal direction were subject to edge effects⁽¹²⁰⁾.

Again the datum point was kept constant for the before and after quench measurements. The plates were placed on edge and measurements were carried out at the points indicated in figure 16. The thickness measured, prior to (T_s) and after (T_h) quenching were then used to determine the strain produced in the thickness direction using:

$$(\Delta \epsilon_{zz})\% = [(T_h - T_s) / T_s] * 100$$

The results obtained from this equation gave experimental evidence of the edge effect, which influenced the final shape of the plate.

All measurements of the change in plate length and breadth made across points of the specimen included positions that were affected by the edge (figure 17). Therefore, the strain resulted from these measurements were also influenced by this effect (in-plane strains) either directly or theoretically. As no stress existed in a direction perpendicular to the plane of the plate (plane-stress condition), the measurement of the change in thickness at the points not influenced by the edge,

were directly related to the main change in length and breadth across the thickness at positions away from the edge affected regions. Therefore changes in thickness at the centre could be used to obtain values of the strain in the plane of the plate at points where the edge exerted no influence. However, only an average strain for the whole thickness was obtained by this method, although it was useful to compare the values so obtained with the average of the directly measured in plane- strains, which were affected by the edge.

3.6.3 RESIDUAL STRESS MEASUREMENTS

In order to determine the residual stress in a quenched plate a layer removal method was employed as detailed by Fletcher and Price⁽⁶⁹⁾. After the residual strain was determined a strain gauge rosette, (type FRA-6-11 manufactured by Tokyo Sokki Kenkyujo Co.Ltd), was attached to the centre of the plate while another was attached within the recess of a cast iron supporting plate.

The two plates then insulated with a layer of wax so as to be protected from the coolant present during the grinding operation. The purpose of the second set of gauges was to detect any spurious strain introduced into the supporting plate. This assembly was then allowed to acclimatise in the laboratory for 12 hours. A diagram showing the arrangement of the stainless steel plate and the cast iron supporting plate is given in figure 18. The layer removal process used was that given by Treuting and Read⁽¹²¹⁾ as modified by Andrews⁽⁸⁸⁾ and Price⁽⁶⁴⁾;

1 mm layers were removed by a precision grinder in 15 passes of 50 microns thickness and 10 passes of 25 microns thickness each. This reduced grinding stresses to negligible amounts⁽⁶⁴⁾. After a 1 mm layer had been removed the plate was allowed to rest for 15 minutes before each gauge was read three times

by the Orion Datalogger. The gauges were connected up in a 1/4 bridge configuration. After every reading the grinding wheel was dressed before the grinding off of the next layer commenced. Another gauge was affixed to a strip of the same material and placed along side the work plate (figure 19). This gauge was needed to provide information on the condition of temperature on the bed plate of the grinding machine. Also it provided information about the amount of stress in the work plate during the grinding operation as this 'compensating plate' was in an unstressed condition, figure 20.

The readings obtained from each of the rosette arms were relatively independent of the orientation of the device, so the mean of the results obtained from the three arms was used in the subsequent calculation of stress. The strain recorded by the gauge affixed to the supporting plate was deducted from the above mean value.

It was not possible to measure the stresses throughout the whole thickness of the plates, since grinding became dangerous when the thickness fell below a critical minimum value⁽⁶⁴⁾. Therefore stress measurements were made only over half the thickness of the plates and the results in the remaining part of the plates were obtained by interpolation and the use of the assumption of symmetry of stress and strain about the centre of the plate.

The experimental results indicated that the residual stresses found in the plate were insignificant, so it was concluded that no stresses were induced into the plate as a consequence of the grinding operation. Comparison with the calculated residual stresses was then possible.

4.0 RESULTS

4.1 COOLING CURVES AND SURFACE HEAT TRANSFER

COEFFICIENTS

The relationships between time and temperature during cooling from 850°C were obtained at five positions just below the face of the stainless steel plate as mentioned in the experimental procedure and illustrated further in figure 26. In addition the thermocouple positions relative to the plate face are shown in each of the figures 21-25. The information obtained was used to calculate the surface heat transfer coefficient and its relationship with surface temperature during the quench. The surface heat transfer coefficients were in turn used to calculate the thermal stress and strain generated during quenching in stainless steel plates using a finite element method.

The relationships between temperature and time in figures 21-25 obtained from specimens quenched in water from 850°C showed the classical characteristics of a slow initial stage, a fast intermediate stage and a final slower cooling period. These stages can be identified as the vapour blanket, nucleate boiling and convective stages respectively.

4.1.1 OBSERVATION OF COOLING CURVES IN PLATES HELD

VERTICALLY DURING QUENCHING

When measurements were made along the plate face diagonal (figures 23-24), the duration of the vapour blanket was greatest at a point below the centre of the plate face and shortest at the point closest to the corners. This result was unaffected by the position of the point of measurement in the upper and lower

halves of the plate. This shows that the retreat of the vapour blanket from the corners towards the centre occurred in a relatively symmetrical manner about the plate centre.

In the case of the thermocouples arranged on the upper half of the vertical line through the centre of the face (figure 21), the relationships between time and temperature were relatively unaffected by position along this line, although the vapour blanket remained for a slightly longer time at the intermediate positions. This suggests that the vapour blanket is retained along this line to a relatively late stage in the quench and the last point where vapour remains is at a point midway between the centre and the top edge of the plate.

The result in figure 22 indicates that the vapour blanket retreats at a constant rate from the lower edge, whereas at the upper edge it gives rise to the results shown in figure 21. These effects are shown in tables 3 and 4. Figure 25, obtained along a horizontal line through the face centre is very similar to figure 23, which suggests that the constant rate of retreat of the vapour blanket holds everywhere except along the upper half of the vertical line through the plate centre (figure 22). During the fast nucleate boiling stage the slope of the cooling curves were very similar in all cases except at the corners of the plate. Thus figures 23 and 24 show particularly fast cooling towards these points.

4.1.2 THE RELATIONSHIP BETWEEN TIME AND TEMPERATURE IN PLATES QUENCHED IN A HORIZONTAL POSITION

The relationship between time and temperature during quenching in water is depicted in figures 27-28, at the top and bottom of the plate held horizontally during the quench (figures 27-28). Both sets of results were similar to one

another, with only the duration of the vapour blanket stage at the centre of the bottom face of the plate longer than that obtained on the top face.

In addition, the duration of the vapour blanket fell as the position of measurement moves outwards along a diagonal from the centre of the face. Tables 5 and 6 show the temperature and time at which the vapour blanket dispersed at the top and bottom face of the plate. In both cases the vapour blanket stage dispersed first at the plate periphery, after which it retreated steadily to the centre. However, in the case of the face centres, the vapour blanket lasted longer on the lower than the upper face. The results from the upper face were similar to those from the lower half of the plate when it was held in a vertical position. It is of interest that the change in slope is not as sharp in the case of the upper horizontal face as is the case of the other positions (figures 21 and 25).

4.1.3 SURFACE HEAT TRANSFER COEFFICIENTS AND TEMPERATURE DISTRIBUTIONS PRODUCED DURING QUENCHING WITH THE PLATE HELD IN VARIOUS POSITIONS IN THE BATH

4.1.4 VERTICAL PLATE

The relationships between heat transfer coefficient and surface temperature were calculated from the data obtained from quenching which involved the use of the method explained in section 3.4. This method required the use of the experimentally determined relationships between time and temperature as well as an accurate knowledge of the depth below the surface at which the temperature was measured. As mentioned in section 3.1, three experiments were carried out for each set of the quenching conditions outlined above.

Each of the figures 29-32 shows the effect on surface heat transfer coefficient of changes in the position of measurement from the face centre towards the periphery along an upper vertical line, a lower vertical line, an upper diagonal, a lower diagonal and a horizontal line respectively. The corresponding cooling curves from which this data was obtained are shown in figures 21-35 respectively. Each curve followed the same general pattern with the surface heat transfer coefficient at a lower value initially, during the vapour blanket stage, rising to a maximum during nucleate boiling, before falling towards the end of the quench. However, the orientation of the line on the plate face along which each set of data was obtained showed some interesting variations. The maxima obtained at the upper corners of the face (figure 31) and the mid point of the vertical edge were (figure 33) were particularly high, although these results were not reproduced at the lower corners of the face (figure 32). The remainder of the relationships between surface heat transfer coefficient and temperature were very similar although it should be noted that all the results obtained along the lower vertical line (figure 30) showed a higher than average maximum surface heat transfer coefficient. However, these results were not comparable to the very high maxima recorded at the upper corner position (figure 31).

Overall, the surface heat transfer coefficients vary in the range 5000-13000 $\text{Wm}^{-2}\text{K}^{-1}$ with the maximum values at the corner of the plate. Figure 34 represents the effect of temperatures on the mean of the surface heat transfer coefficients obtained from each set of results at the face centre, the face corner and the two intermediate positions respectively. Hence these results do not consider the effect of plate orientation, (i.e. diagonal, vertical line, horizontal

line). However they do show the effect of change of position outwards from centre of the face to the periphery. The average maximum value of the surface heat transfer coefficient in the vapour blanket stage was of the order of 500-650 $\text{Wm}^{-2}\text{K}^{-1}$ at a mean surface temperature of 800°C shown in figure 34. The same figure illustrates that during the nucleate boiling stage the surface heat transfer coefficient rose to a maximum and then fell very rapidly with decreasing surface temperature and quickly reached values of the order of those associated with the film boiling stage shown in figure 34. The mean maximum surface heat transfer coefficients during nucleate boiling were 13000 and 6426 $\text{Wm}^{-2}\text{K}^{-1}$ at the corner and centre of the plate respectively. These maxima occurred at the mean temperatures of 180°C and 350°C respectively. The corner high maximum surface heat transfer coefficient was a characteristic of the edge position and was not found elsewhere, where very similar results were obtained at all points. Tables 3 and 4 show the variation in surface temperature and surface heat transfer coefficient at points between the top and bottom of the face of the plate.

4.1.5 HORIZONTAL PLATE

The same procedure of determining the surface heat transfer coefficient has been carried out in the case of plates held in the horizontal position. Figures 35 and 36 show the values of surface heat transfer coefficient against surface temperature on the top and the bottom face of the plate respectively. The relationship between time and temperature in figures 27 and 28 show that on the top surface the temperature at which the maximum value of surface heat transfer coefficient occurred varied irregularly within the temperature range 276°C and

217°C at positions along the diagonal line. The maximum surface heat transfer coefficient at these same temperatures were 5000 and 10832 $\text{Wm}^{-2}\text{K}^{-1}$ from centre towards the corner of the plate respectively.

On the bottom face of the plate, the surface temperature at which the maximum value of surface heat transfer coefficient occurred varied from 6000 to 13000 $\text{Wm}^{-2}\text{K}^{-1}$ from centre towards the corner of the plate. The corresponding surface temperatures at which these maxima occurred were 171°C and 213°C respectively. Comparing the top and bottom face results, the maxima were about the same in both cases but were displaced to lower temperatures in the case of bottom face, although the lower face gave slightly higher values of the surface heat transfer coefficient.

4.2 CALCULATION OF TEMPERATURE DISTRIBUTIONS IN THE PLATES DURING QUENCHING

The surface heat transfer coefficients described above were obtained from the relationship between time and temperature at selected points in the plate, using a technique that assumed uniaxial heat flow and related the set of 'h' values to one set of relationships between time and temperature.

However, the latter are experimental points obtained during the cooling of a plate that was in reality subject to multi-dimensional heat flow. It is therefore of interest to use the surface heat transfer coefficients obtained above as boundary values in a multi-dimensional calculation of the temperature distribution in the cooling plate and to compare the predicted temperatures with the experimental data obtained in the cooling curves (figures 21-25). A high level of agreement may indicate that the method of determining the surface heat transfer coefficient and its associated assumption of unidirectional heat flow is satisfactory. To this end a two dimensional calculation has been carried out using vertical and horizontal quenched plates. Furthermore, to investigate the significance of the observed variation in the surface heat transfer coefficient at a fixed temperature at different points on the plate surface the following situations have been considered.

- (i) constant surface heat transfer coefficient values at all points at a fixed time but surface heat transfer coefficient variable with time.
- (ii) variable surface heat transfer coefficient with respect to both position on the surface and to time.

Both situations have been considered with the plate quenched in both vertical and horizontal positions.

Figures 37 and 38 show the results obtained in a vertical quench using constant 'h' values and variable 'h' values respectively at constant time during the quench. The faster overall cooling rates at the edge clearly showed the effect of multi-dimensional cooling at this point, although change in position on the plate face did not appear to have increased the overall cooling rate relative to that at the face centre. The use of the variable 'h' values at different positions and constant times has, as might be expected produced greater variation in the overall cooling rates at different positions, with higher values at both the edge centre and the nearest point on the face to the edge. A comparison of these results with the experimental results described above is given in the discussion. Also figures 39 and 40 represent the two sets of data which were obtained in order to apply the corresponding constant and variable surface heat transfer coefficient around the surface of the plate which were obtained experimentally during a horizontal quench. The main difference is at the initial stage of the quench where the duration of the calculated vapour blanket stage is shorter than that obtained by experiment.

4.3 PHOTOGRAPHIC OBSERVATIONS OF THE COOLING OF THE PLATE IN A WATER QUENCH

Figures 41-46 show the appearance of the face of the plate while quenched in the vertical position in still water with the suspending rod at the top of the photographs.

Figure 41 shows the front face of the plate after only one third of a second from the start of the quench and as can be seen the vapour blanket covers almost the entire face with broken patches of vapour at the edges. Also this photographs show a number of large bubbles which contain air displaced by the plate as it entered the bath.

Figures 42-44 show the Taylor waves on the front surface of the plate. These are the discontinuous horizontal wedges of vapour which are thicker than the rest of the blanket. They, like all the vapour layer are transparent to light. These waves rise continuously and do not discharge any vapour until they reach the top edge of the plate. These waves are an indication of turbulence.

Figure 44 shows the disappearance of the Taylor waves and the appearance of bubbles around the edge of the vapour blanket which has already disappeared from the position of the thermocouples closest to the corner. Nucleate boiling is already in progress after 1.3 of a second at positions close to the plate corners, as seen in figure 43. As the quench proceeds in figures 45 and 46, the vapour blanket continues to decrease in size, until individual bubbles are seen to be forming on the periphery of the plate.

Figures 41-46 show the gradual reduction of the vapour blanket and the presence of the bubbles on the face of the plate. Figure 44 indicates that the

Taylor waves have reappeared but are restricted to the upper part of the plate surface.

Figure 45 shows the point where the vapour blanket disappears and nucleate boiling still predominates, although only convective cooling now occurs at the edges of the plate, where no bubbles are formed.

In figure 46 the last portions of the vapour blanket are about to disappear. It is interesting that these occur in a thin line between the midpoint of the top edge of the face down to the face centre.

The whole series of photographs indicate the position of the hot junctions of the thermocouples and allow the physical phenomena shown in the photographs to be correlated with the time/temperature relationships obtained from the thermocouples. They also show the influence of the edges of the plate on the duration of the vapour blanket stage, as well as the more rapid contraction and more regular shape of the blanket from the lower half of the vertical section compared to the corresponding bubble in the upper section.

Figures 47-69 are the photographic representation of the top and bottom face of the plate when it is quenched in a horizontal position. These experiments were carried out simultaneously with the determination of the surface heat transfer coefficients around the surface of the plate at top and bottom face of the plate, so that a direct correlation of this data with the photographic results was possible.

The results obtained from the photographic data followed essentially a similar sequence to those reported in section 4.2 in the case of the corresponding surface heat transfer coefficients. Figures 47 and 53, obtained at top and bottom of the plate respectively, show that the vapour blanket has already contracted

away from the positions at which the outermost thermocouple hot junctions were located; after times of 1.3s and 1.5s respectively. Although the photograph is distorted by the surface of the bath it is possible to see that the vapour blanket appearance is similar to that on a vertical face, except possibly Taylor waves may be absent.

Tables 5 and 6 show the times and temperatures of start and finish of the vapour blanket stage at centre and corner of the plate. Figures 27 and 28 and tables 5 and 6 show that at the thermocouple position closest to the centre of the plate, the rate of cooling began to increase rapidly after 10s and 19.3s respectively. The photographs taken after this length of time (figures 51 and 63), clearly show that the innermost thermocouple hot junctions lay below the vapour blanket, and therefore should be expected to show a slow rate of cooling at this time. Figures 64-69 indicate that there are explosion of bubbles underneath the plate after completion of the vapour blanket stage which allow the vapour generated on the lower face to escape and travel to the top surface of the bath.

The whole sequence of photographs from figures 64-69 show the appearance and dispersion of two consecutive bubbles on the bottom face during the nucleate boiling stage. Figure 64 shows that the vapour blanket stage is complete and the surface show only a few bubbles of moderate size. The very fine bubbles normally associated with the nucleate boiling stage are not observed. In figure 65 one of the moderately sized bubbles has suddenly begun to grow much more rapidly than the others, while at a slightly later stage it has grown to such a size that it covers the greater path of the face (figure 66). It has also absorbed on the way the smaller bubbles in its path. In figure 67 the edges of the bubble have reached the edge of the face and the vapour contained therein

has escaped in a large mass upwards to the surface of the bath. This is followed by the disappearances of the whole feature (figure 69). Then, the repetition of the whole sequence is repeated with a second bubble. The wall like edge of these bubbles should be noted as well as their rapid growth and disappearance. The effect is almost explosive with the buoyancy created by the bubble pushing the whole plate upwards with a resultant violent vibration.

4.4 GENERATION OF STRESS AND STRAIN DURING QUENCHING BY USING CONSTANT AND VARIABLE SURFACE HEAT TRANSFER COEFFICIENTS

4.4.1 USING CONSTANT SURFACE HEAT TRANSFER COEFFICIENT AROUND THE SURFACE OF THE PLATE

The predicted relationships between time and temperature shown in figures 37-38 were calculated using either the constant or variable heat transfer coefficients along the surface of the plate as thermal boundary conditions at the positions indicated in figure 26. This data was used to determine the relationships between stress and strain produced during quenching of the stainless steel plate. This involved the use of the finite element method, as described in the procedure. The results shown in figures 70-74 refer to predicted stress components in the plate after quenching for 1 second with no spatial variation in the surface heat transfer coefficient around the periphery of the plate. In figure 70 it is evident that the radial and hoop stresses coincide at points along the axis of the plate (positions 1 to 2) with negative values towards the centre and positive values where the axis reaches the surface. The axial stresses are zero at all points along the axis. Along the surface of the plate the latter stress conditions prevail from point 2 until a position very close to the corner (4) is reached (figure 71). Here the radial stress falls to zero at the corner while the hoop component rises to a much higher positive value. The axial component, as would be expected remains zero at all points between positions 2 and 4. Thus at the corner only the hoop component is not zero, so that a comparatively large value is required to accommodate the relatively large contraction at this position.

Along the central plane of the plate (between points 1 and 3) the stress components remain constant until a point close to the edge (3) is reached (figure 72). This is in accordance with the surface results referred to above. However, in this case the axial stress becomes negative 15 mm from the edge before reversing to give a comparatively high positive value at point 3 on the edge. During the last 7 mm of this transverse the hoop stress, whose value also changes from negative to positive, coincides with the axial stress. Simultaneously with these changes in stress the radial stress becomes less negative until it becomes zero at the edge.

Figure 73, which refers to the state of stress along the edge, shows that the positive axial stress at position 3 falls to zero as the corner (position 4) is approached. The hoop stress, on the other hand simultaneously becomes more positive as the corner is approached, until it is the only non-zero stress component at position 4.

The state of stress after one second of the quench, represents the conditions at an early stage in the cooling process when the periphery of the plate is cooling more rapidly than the centre. Later, the centre cools more quickly, as the periphery approaches ambient, so that reversal of the stress components are produced. This situation is obtained 7.8 seconds into the quench (figure 74). The temperatures at the points where the axis reaches the surface (point 2), the central plane reaches the edge (point 3) and the corner (point 4) are 775°C , 510°C and 295°C respectively.

Figure 75 shows that along the axis (positions 1 to 2) the radial and hoop stresses coincide with positive values at the surface (position 2) but show wide variations in stress at the centre (position 1). However, the axial stress towards

position 2 is not zero, which is unexpected. All three stress components follow the same trend with change in distance along the axis. These results are almost certainly affected by instabilities in the calculation method. The same instabilities are shown close to position 1 in figure 76, which refers to the central plane. However at a distance of 7.5 mm from the centre figure 76 shows the instabilities disappear and approximately constant values are obtained for all stresses until a point close to the edge is reached. These constant values probably represent the true position at position 1, with negative values of about -80MPa for both hoop and radial stresses. Figure 76 also shows that towards the edge (point 3) the radial stress again decays to zero at point 3 while the hoop stress first becomes more compressive then positive, before becoming negative again at point 3. The axial component is effectively zero until a point 10 mm from the edge is reached, when it becomes positive with values very similar to the hoop stress, before becoming negative at position 3.

Along the edge between positions 3 and 4 the axial stress remains constant until the corner is approached, where it falls steadily to zero. Simultaneously the hoop stress becomes more negative, reaching it's most compressive value at the corner (figure 77).

Figure 78 shows a moderate instability on the axis (point 2) but along the greater length of the surface the radial and hoop components have constant positive values that coincide, while the axial stress is zero. Close to the corner the radial stress reverses before becoming zero at point 4 (corner). The hoop stress follows a similar pattern but remains at a high negative value at the corner. The results obtained after 7.8 seconds are more complex than these obtained after 1 second. The increased complexity is due to the initiation of the

stress reversal referred to above at points along the edge (between 3 and 4). This reversal has not progressed along the surface, despite the comparatively low temperature at point 2.

At the end of the quench the state of stress resembles the pattern obtained after 40 seconds (figures 79, 80, 81 and 82). The maximum tensile stress at the surface has fallen (compare figures 78 and 82) and the points at which the stress reversals occur have been displaced a little further away from the edge (point 4) likewise the negative stress formed along the greater part of the central plane has decayed. The pattern of stress reversal as the edge is approached remain the same. (Compare figures 80 and 76 and also figures 82 and 78). However, along the edge the hoop stress has generally become more negative and is relatively constant at points between positions 3 and 4 (figure 81). In contrast, the hoop stress has remained relatively unchanged (compare figures 81 and 77).

4.4.2 USING VARIABLE SURFACE HEAT TRANSFER

COEFFICIENTS AROUND THE PERIPHERY OF THE PLATE

Figure 83 is the predicted temperature distribution used to determine the stress profile shown in figures 84-95.

Figures 84 to 87 are representative of the situation 1.0 second after the start of the quench when the surface heat transfer coefficient varies around the periphery of the plate at any given instant. 1 second represents a stage when all points on the surface are covered by a vapour blanket, so that the rate of cooling is low everywhere. This is the same as the position after the same length of time in the case when the heat transfer coefficient does not vary around the surface of the component, (section 4.4.1). Hence similarities are to be expected between the

corresponding stress distributions (compare figures 70-74 with the corresponding results in figures 84-87). Both sets of results show low levels of stress, as would be expected from the slow cooling rates and there are considerable similarities between the corresponding results. However, the following should be noted. In figure 84 the instability is more marked than in figure 70, with a non-zero axial stress towards the centre. Despite this both figures 84 and 70 show equality of radial and hoop components with tensile values at the surface and negative values at the centre. The main differences in the two sets of results are unexpectedly large values of both radial and hoop stress at the surface at positions intermediate between axis and corner (figure 87). Further, the axial stress at points on the edge does not rise towards the corner (point 4 in figure 86), but in fact falls significantly. The high stresses at surface positions intermediate between corner and axis suggests significantly higher surface heat transfer coefficients here than elsewhere on the surface.

Figures 88 to 91 represent the variation in stress in the plate 7.8 seconds after the start of the quench. This represents the situation where the corner has cooled to about 450°C at thermocouple temperature, so that nucleate boiling is finished, whereas on the surface at the axial point the nucleate boiling is just beginning (at a temperature of 720°C). Thus the differences in temperature are even more extreme than was the case at this time when constant thermal conditions were used around the boundary. However, if the unstable results along the axis is ignored (figure 88) the variations in stress are not very different from the corresponding results obtained using surface heat transfer coefficients that do not vary with position (compare figures 88-91 with figures 75-78). The most significant differences occur along the edge (figure 90) where the hoop

stress is now tensile at the central plane and compressive at the corner, whereas in figure 77 the hoop stresses are negative at all points on the edge.

In addition the axial stress in figure 90 is at a minimum at an intermediate position, although it is always negative along the edge of the plate.

At the end of the quench (40 seconds) the residual stress distribution (figures 93 to 95) are similar to these obtained after 7.8 seconds. The most significant difference is the increased hoop stress along the edge particularly towards the centre plane and a more limited increase in the axial compressive stress at the same positions.

On the surface away from the corner the stress is tensile (both components) (figure 95), which is opposite to the situation along the edge (figure 94).

4.5 THE CALCULATED AND EXPERIMENTAL RESIDUAL STRAINS IN PLATES HELD IN VERTICAL AND HORIZONTAL POSITIONS DURING QUENCHING

The experimental and theoretical residual strains are shown in figures 96-97 for vertical and horizontal quenches respectively. The points shown on these curves indicate the positions of each measurement. The predicted residual strains in plates held in either a vertical or horizontal position quenched in water followed the same trend, which was compressive at all points between the surface and centre.

The calculated strain distribution was symmetrical about the centre of the plate. This symmetry was a consequence of the assumption that temperature distributions and therefore, calculated stress and strain, were symmetrical about the centre line of the plate.

In contrast, the experimental determinations of residual strain were tensile in all parts of the plate for which calculation were performed. In the case of the vertical quench, the measured residual strains at 10 mm, 30 mm, 90 mm and 110 mm through the length of the plate were a maximum at the surface and a minimum at the centre whereas, the residual strains measured at 60 mm midway through the length of the plate is a minimum at the surface and rose to a maximum at the centre. On the other hand in the horizontal quench, the residual strains were a maximum at one surface and decline as the centre and the opposite face (surface) were approached.

Only one result was anomalous in the measured residual strains at 60 mm through the length of the plate while all the others were consistent.

4.6 EXPERIMENTAL MEASUREMENTS OF RESIDUAL STRESS IN HORIZONTAL PLATE

The experimental determination of residual stress was carried out on the lower half of the plate quenched horizontally. The result is given in figure 98. The experimental values of residual stress obtained from the plate showed that the surface stress was tensile and the centre stress compressive. Experimental measurement was carried out only for half of the plate, due to the practical limitations of the technique as the section becomes very thin.

4.7 CALCULATED STRESSES IN PLATES HELD HORIZONTALLY DURING QUENCHING

4.7.1 USING CONSTANT SURFACE HEAT TRANSFER COEFFICIENT AROUND THE PERIPHERY OF THE PLATE

In this example average surface heat transfer coefficients have been used at each instant in time during the quench. Therefore, the results on the upper and lower surfaces should be the same. The small differences are due to inaccuracies inherent in the method, which are related to the distribution of nodes. Figures 100-103 which refer to the situation after 1 second of the quench show very similar results to the those obtained in the vertical quench. Thus along the surfaces the tensile hoop and radial stresses are tensile and identical except close to the corner where the hoop stress rises to a maximum value and the radial stress falls to zero. Some instability was present close to the corner on one surface, as shown by the erratic variation in the axial stress, which should always be zero at the surface.

The stress on the axis varies from tensile at the surface to compressive at the centre and the two non-zero stress components are identical.

The axial stress at the edge varies from zero at the corner to a maximum value at the central plane intersection with the edge, while simultaneously the hoop stress falls to a minimum value. All stress components on the edge are positive, (figure 101).

Figures 104-107 show the residual stresses at 40 seconds through the quench. The level of the predicted residual stress increased to a maximum tensile of 140MPa towards the corner edge (figure 104). It can be observed that the stress

variations followed the same pattern as at 1.0 seconds with the exception that the absolute values tend to be higher at equivalent points.

4.7.2 USING VARIABLE SURFACE HEAT TRANSFER

COEFFICIENTS AROUND THE PERIPHERY OF THE PLATE

The purpose of the work is to look at the effect of introducing variable 'h' at positions around the periphery of the plate. By considering the use of variable surface heat transfer coefficient, it followed the same trend as with surface heat transfer coefficient constant with position, with the exception of instability at some points.

Figures 108-115, which refer to the situation after 1.0 and 40.0 seconds of the quench, show very similar results to those obtained in the vertical quench. After 40.0 seconds, the tensile hoop and radial stresses rise to higher values along the surface while the axial component is zero, but each follows the same trends as were obtained when constant surface heat transfer coefficient and were used at this point in the quench (figures 112-115).

The radial component is zero along the edge and axial and hoop components are tensile at the surface and compressive at the centre while the hoop remains in compression at the other face (figure 113).

Figure 115 represents the residual stresses at the end of the quench. The overall view of residual stresses are similar to those obtained after 1.0 seconds except that the values tend to be higher and there are few instabilities.

At the end of the quench the state of stress resembles the pattern obtained after 40.0 seconds (figures 114-115). It can be observed that the stress variations

followed the same pattern at 40.0 seconds using constant 'h' except that there are instabilities only in figure 114.

5.0 DISCUSSION

5.1 PHOTOGRAPHIC OBSERVATIONS OF THE PLATE IN A WATER QUENCH AND THE MECHANISM OF COOLING AROUND THE PERIPHERY OF THE PLATE

5.1.1 INTRODUCTION

The observations of the appearance of the vapour in contact with the vertical plate have been well documented in earlier investigations ⁽¹²²⁾⁽²⁵⁾. The purpose of their inclusion here is to provide a comparison with the form of the vapour on the faces of the plate when in a horizontal position.

5.1.2 PHOTOGRAPHIC OBSERVATIONS - VERTICAL PLATE

The main features of the results from the vertical faces are:-

- (i) contraction of the vapour blanket from the side edges and bottom edge, leading to the disappearance of the last traces of the blanket at a point just below the centre of the top edge (figures 45 and 46),
- (ii) very fine bubbles during the height of nucleate boiling, followed by the evolution of smaller quantities of rather larger bubbles as the temperature fell further (figures 41-44),
- (iii) the appearance of Taylor waves and other instabilities on the vapour blanket surface (figures 42 and 43).

*Footnote: In this context "constant" and "variable" refers to spatial effects at a constant time. In both cases, of course 'h' varies during the course of the quench.

5.1.3 PHOTOGRAPHIC OBSERVATIONS - HORIZONTAL PLATE

The photographic data obtained in the case of the horizontal plate shows marked variations between those results and those obtained on the vertical faces. Thus the vapour blankets lingered at the centre of the horizontal faces. In the case of the lower face, evidence of extreme vapour instabilities was observed.

Figures 47-48 show the upper face of the plate after only 13 and 2 seconds from the start of the quench and as indicated in figure 47, the vapour blanket covers almost the whole face with broken patches of vapour at the edges. Figure 48, shows the gradual reduction of the vapour blanket at the centre and the presence of the bubbles on the face of the plate. As can be observed the vapour escapes directly upwards from the upper face⁽¹⁰⁾.

Tables 5 and 6 show the time and temperature at the start and the finish of the vapour blanket stage at centre, intermediates and corner of the plate, which corresponds well to the figures 47-51.

After 13 seconds, figure 47, 'blisters' of vapour can be seen at the edges of the vapour blanket: a similar phenomenon is apparent to a greater extent in figure 48. After 2 seconds similar large masses of vapour may also occur towards the centre of the vapour blanket (figures 49-51).

Observations of the top face were difficult since the lens of the camera was separated from the plate by the surface of the bath, which distorted the appearance of objects below it. However, figures 47-51 show that contraction of the vapour blanket occurred uniformly from the edge of the plate, and bursts of bubbles occurred during nucleate boiling. The surface of the blanket appeared to be, as far as could be observed, smooth. However, observations of the vapour rising from the top face of the horizontal plate when viewed from the

side suggested that the release of bubbles was not always as regular as was the case in the vertical plate. This is surprising since there is no hindrance to the release of vapour from the top face of the horizontal plate. In other respects the results are very similar to those from the vertical face, except of course that the contraction of the blanket was symmetrical about the face centre.

The most interesting effects were observed on the lower face of the horizontal plate. Figures 52-69 show the start and finish of the vapour blanket at the corner and the centre of the plate facing downwards in the horizontal quench. When the plate face is downward, vapour flows out in a direction along the heated surface, in contrast to the case of an upwards facing surface the vapour escapes by simply rising to the bath surface after becoming detached from the solid specimen. Thus in the case of a downwards facing surface there was a complete absence of vapour bubbles so that the vapour blanket could be clearly seen. The absence of the air/water interface also made the observations particularly clear. The blanket contracted slowly from all four edges, with the occasional burst of vapour, particularly from the corners (figure 60). The movement of the vapour in this way was quite unlike that which occurred on the upper surface or on the faces of the vertical plate. It reflected the difficulty of vapour removal from the underside of the plate, where the buoyancy of the bubbles forces it against the face, so that it must travel along the face to the edge, before being ejected upwards. Although not as violent as the processes that come later in the quench, this occurs in an irregular manner, with the sudden ejection of a large quantity of vapour.

The vapour blanket finally disappears leaving isolated bubbles that lie on the face as shown in figure 64. This should represent the point of greatest heat

removal, with the evolution of a very large number of small bubbles. However, on the bottom face this process is prevented by the presence of the plate face, which stops the escape of the vapour. The solid is in contact with water at a temperature well above the boiling point of the latter, so that the creation of vapour must continue even though the vapour blanket has dispersed. This does not involve the formation of a mist of fine bubbles, as is the case with the face in the vertical position, otherwise the surface in figure 64 would not be clearly visible.

The sequence of figures 64-69 are characteristic of the removal of heat and vapour from the underside of the plate after the disappearance of the vapour blanket. A sequence of very large bubbles grow very rapidly leading to vapour ejection at the face edge, after which it can rise freely from the bath surface. Any smaller bubbles in the vicinity are absorbed during the process into the large one. The ejection process is violent with a relatively large buoyancy stress created on the lower face of the plate, causing considerable upwards movement and tilting of the specimen. This of course aids the escape of the vapour. The large bubbles are created in quick succession and when viewed by eye have the appearance of a series of waves moving rapidly outwards from the face centre. There is insufficient information to provide a detailed model of this vapour removal process on the underside of the plate, but it can be said that the normal evolution of small bubbles requires their detachment from the solid specimen and subsequent movement through the liquid. This is prevented in this case by the buoyancy force on the bubble which holds it against the solid. The creation of more vapour does not lead to a succession of small individual bubbles under these circumstances. Instead the build-up of vapour leads to a lateral movement

of steam along the face, as the periphery of the "packet" of vapour moves towards the edge of the specimen. The quantity of vapour in any one such packet is considerable (see figures 67-69) and the buoyancy force so created is sufficient to produce the violent movement of the plate. This lateral movement is not continuous but cyclic with periodic quiet stages (e.g. figure 69) between the ejection of one large bubble and the formation of the next. Figure 68 shows that the thickness of the vapour layer is considerable, particularly towards the periphery. It appears considerably thicker at this point than the vapour blanket formed earlier in the quench.

5.1.4 RELATIONSHIPS BETWEEN PHOTOGRAPHIC DATA AND COOLING CURVES DURING QUENCHING

The photographic evidence described above shows clearly the existence of three stages in the cooling of the plate during quenching, involving a vapour blanket stage, a rapid middle stage and a convective cooling stage after the disappearance of boiling. The nature of the second stage depended on the orientation of the plate during the quench. Despite these photographic differences the relationships between time and temperature during cooling (figures 21-25 and 27-28) show very similar results. The most important difference between the various cooling curves was the duration of the vapour blanket stage lasts longer at the centre of the bottom face than at any other position on the surface (figures 21-25). In contrast, the rates of cooling after the completion of the vapour blanket stage were surprisingly similar in all cases despite the very different mechanism of heat transfer from the bottom face at

this stage. This is, however best shown by the relationship between surface heat transfer coefficient and temperature (see below).

A further interesting aspect of the vapour blanket stage is the constant of this stage at points on a vertical line from the centre of the vertical face to the centre of the top edge (figure 21). In all other cases the vapour blanket stage is longer at the edge of the face. The explanation for this is shown in figure 46, where the last remnant of the vapour blanket forms a vertical line between the centre and the top edge. This aspect of the results is not indicated by the calculated relationships between time and temperature (figures 37-38). It would appear that the buoyancy of the vapour blanket and the thickness of the vapour blanket at different positions on the face are obvious additional factors that are not included in the calculated relationships between time and temperature.

5.2 COMPARISON OF CONSTANT 'h' AND VARIABLE 'h' DURING QUENCHING

5.2.1 VERTICAL PLATE

Figures 37-38 represent the relationships between temperature and time obtained from finite element analysis using both constant* and variable* surface heat transfer coefficients.

Despite the good agreement in the case of the magnitude of the surface heat transfer coefficients, the predicted duration of the vapour blanket stage using variable* surface heat transfer coefficient was significantly shorter than that actually observed. When using a constant* heat transfer coefficient, the duration of the vapour blanket were similar at the various positions under consideration. This discrepancy probably is due to three dimensional heat flow which occurs in the experiment, whereas, this phenomenon is not included in the two dimensional finite element analysis.

The low stability of the vapour blanket has important practical implications. Following the work of Stolz et alia (29), it has been widely thought that during water quenching the nucleate boiling peak occurs at around 150^o to 200^oC. The present work clearly shows that it is possible for this nucleate boiling peak to occur at much higher temperatures, e.g. in the range of 180^oC to 390^oC from the corner edge to the centre face of the plate respectively, see tables 3 and 4.

During the quench of a vertical plate a vertical convection current is established with the hot liquid rising up the face of the specimen to be replaced by cold fluid flowing in horizontally from the bulk of the liquid.

Surface heat transfer coefficient at its maximum were 13000 and 12500 W/m²°C at 180^oC in which the thermocouples placed at top and bottom corner

edge of the plate face respectively. The corners show 3 dimensional heat flow in which the rate of cooling is faster than other thermocouple positions. Although the surface area at the top and bottom corner are the same, there is still a small difference between the surface heat transfer coefficients values. Tables 3 and 4 show that the 'h' at the top position along the diagonal face of the plate is higher than top section. It can be concluded that 'h' values are highest at the intermediate and corner thermocouple positions.

5.2.2 HORIZONTAL PLATE

Again the calculated cooling curves are intermediate between the experimental extremes. This is to be expected since the 'h' values are a compromise. The introduction of 2D heat flow has not produced an obvious source of error. It has however failed to predict the unusually long duration of the vapour blanket stage on the upper face (compare figure 39 with figure 28). The introduction of the variable 'h' at positions around the surface of the plate do introduce some variation in the cooling curves at the centre and the edge (figure 40). However this is much smaller than that indicated by experiment (figures 27 and 28). The calculated results do now show a variation between the upper and lower faces (figure 40). However this difference is relatively modest in comparison to the actual differences obtained by experiment (figures 27 and 28). In particular they do not predict either the relatively long vapour blanket stage or the differences in the length of this stage on the upper and underside faces. In fact, if the cooling curves beyond the vapour blanket stage are considered the differences between experiment and calculation are quite small. Again, as in the case of the plate held vertically there is a need to introduce into the model the

variation in the vapour blanket stability at different positions on the plate surface.

The surface heat transfer coefficients during the evolution of the large bubbles on the bottom face of the horizontal face are markedly different from that obtained during normal nucleate boiling (compare figures 34, 35 and 36). The maximum value obtained from the lower face is a little higher than that from the upper face but the differences are small. This is surprising in view of the markedly different mechanism of heat removal in the two positions. Although large quantities of vapour are removed in each case and the total latent heat removal is related to this the latent heat on its own is insufficient to account for the amount of heat produced in nucleate boiling ⁽²¹⁾. There is an additional factor, usually ascribed to enhanced convection associated with the evolution of the fine bubbles. In view of the absence of such bubbles in the case of the lower face of the plate in a horizontal position it is surprising that a larger difference in the surface heat transfer coefficients was not observed.

5.2.3 COMPARISON OF COOLING RATES IN THE VERTICAL AND HORIZONTAL POSITIONS

The results which have been obtained by calculation using the surface heat transfer coefficient as a function of both time and position on the surface are almost identical to those obtained by experiment in vertical and horizontal positions. However, significant differences can be observed between experimental cooling curves and the calculated temperatures obtained when the surface heat transfer coefficient is a function of time only in which the 'h' values are obtained from the experimental time-temperature curves with an

assumption of uni-directional heat flow perpendicular to the face. The experimental time-temperature curves are dependant on multi-directional heat flow, while the 'h' values used to calculate the same relationship, are based on 'h' values possibly affected by the incorrect assumption of uni-directional flow. The calculated cooling curves with variable * h values show more rapid cooling overall when the plate is vertical than when it is horizontal. This applies to both the upper and lower surfaces in the latter case, Table 7. The predictions of the calculations referred to above do not agree well with the experimental results except for the vapour blanket stage. The predicted vapour blanket stage is shorter than when obtained experimentally. The factors that are involved experimentally to determine longer vapour blanket may not have been considered in the case of the calculated predictions.

The results obtained from the upper surface of the horizontal plate are similar to those along a diagonal of the vertical plate (figures 23, 24 and 27). That is vapour release is equally easy in both these positions, so similar phenomena are obtained in these cases. In the case of the lower surface of the horizontal plate the experimental cooling curves show a much more persistent vapour blanket than either that found at the centre of the vertical face or that predicted by the appropriate calculation. The difficulty of release of the vapour from the underneath of the plate would account for this, since the calculation takes no account of this aspect of the process.

5.3 THERMAL STRESS AND STRAIN GENERATION DURING QUENCHING

All previous work on the calculation of thermal stress during quenching has involved the use of constant thermal conditions around the surface of the component at a specific moment during the quench. However, the determination of surface heat transfer coefficients at various points of the surfaces of the plates considered during the present work suggest that this is not a valid assumption (figures 29-36) and the calculated temperature distributions obtained with this data also vary significantly from those obtained with the use of constant values of the surface heat transfer coefficient. These differences can be expected to produce variations in the associated thermal stresses, but it is not clear whether these differences are significant. Hence a detailed analysis has been carried out of the stress generation process to determine whether the introduction of 'h' values that vary around the periphery of the plate are significant.

The difference between states of stress using constant and variable surface heat transfer coefficient values after 1.0 sec of quenching are shown by comparing figures 70-73 and 84-87. In general the pattern of stress distributions are very similar, the main differences being one of magnitude.

Along the plate axis the central stresses are both compressive whilst those at the surface are both tensile.

The constant surface heat transfer coefficient values give slightly higher stresses at the surface, figures 70 and 84.

Along the central plane, the radial and hoop stresses are also very similar and are compressive except very close to the plate edge where the hoop stress

becomes tensile and the radial stress becomes zero. The axial stresses are zero in both cases except within 15 mm of the edge where there is a zone of compressive stress followed by a zone of tensile stress. In the latter case the magnitude of the axial stress is identical to the hoop stress, (figures 71 and 85). The difference produced by variable 'h' were negligible.

Along the edge the axial stress falls in both cases from a tensile value to zero at the corner. The results obtained are similar with using constant and variable 'h'. However when constant 'h' values are used the hoop stress rises towards the corner, while in the case of the variable 'h' the stress component falls towards the corner, figures 72 and 86. In the case the stresses along the surface (figures 73 and 87), the constant 'h' values produced a change in radial and hoop components until a point within 5 mm of the corner is reached. At this point the radial stress falls to zero while the hoop stress becomes much more tensile. On the other hand where 'h' varies with position (figure 87), both the radial and hoop stresses at the surface rise to a maximum at an intermediate position.

The differences between figures 73 and 87 represent the most obvious differences obtained when 'h' is allowed to vary with position.

The pattern of stress distribution in both cases is determined by certain effects: viz.,

- 1) The temperature distribution in the plate with lowest temperature at the corner.
- 2) The need for zero, normal and shear component at the free edge and surface.
- 3) The need to maintain the continuity of the structure within the plate.

Thus, at the corner the only non-zero component is the hoop stress which has a high tensile value to make the corner region continuous with the rest of the structure. We also find tensile stresses along the surface (figures 72 and 86).

The maximum (figure 87) at the intermediate position is surprising in view of the stress distribution in figure 73.

Maxima will be expected at the corner position at both cases. Unloading of the corner stresses when the temperature falls to a very low value will occur, but 1.0 sec will seem insufficient time for this to occur.

After 7.8 seconds the corner of the plate has cooled sufficiently to reverse the hoop stress (figures 78 and 91). This stress is now compressive. The stress along the surface away from the edge now becomes more compressive as the corner is approached (figures 77 and 90). The pattern of stress has not been greatly affected by the introduction of the variation in surface heat transfer coefficient at different positions on the plate. The most obvious change affects the hoop stress along the edge (figures 77 and 90). This is more tensile when 'h' varies with position.

The similarity of the pattern stress distribution remains unaffected at the end of the quench by the introduction of the variable 'h' values (figures 79-82 and 92-95).

On moving from the corner towards the axis along the surface the stress components became tensile in both cases, although the variable surface condition allowed greater stress levels than did the use of a constant surface heat transfer coefficient. (figures 82 and 95.)

Moving along the edge from the corner region to the centre plane caused the hoop stress to become less and the axial stress to become more compressive

(figures 81 and 94). The magnitudes of these effects were greater when the surface heat transfer coefficient varied around the periphery of the plate.

These residual stress distributions show that the stress pattern was not greatly affected by the use of the more accurate variable surface heat transfer coefficient. However, actual magnitudes did show significant differences so in cases where quantitative data is required the more complex variable surface heat transfer coefficients can be used with benefit. Nevertheless, it should be pointed out that there was evidence of increased instability in this case, so a more refined mesh may be desirable.

5.3.1 HORIZONTAL PLATE

The calculated stresses in the plate quenched in the horizontal position were subject to rather more instability than those obtained from the vertical plate. This arose because the number of elements used to model half the plate section in the symmetrical examples were the maximum that the computer would accept, so the doubling of the section size to include both halves of the section in the horizontal plate was not accompanied by the introduction of additional elements. This effectively halved the density of the elements in the model with a consequent increase in the instability of the results. However, the essential information that was required was obtained with this less dense mesh.

The absolute level of stress at any given point after one second of quenching was higher in the horizontal than the vertical plate. This may be seen from a comparison of the results from the horizontal plate (figures 100-103) with these from the vertical plate (figures 70-73). This is particularly clear along the plate axis (figures 70 and 102) but applies also along the edge (figures 72 and 101).

The calculations involving the horizontal plate used the same boundary conditions on the upper and lower surfaces, so the stress distribution was symmetrical about the central plane. Comparison of figures 34 and 35 show that at a given temperature the surface heat transfer coefficients obtained from the vertical plate were rather higher than was the case with the horizontal plate. It is this effect that is probably responsible for the differences in stress generated after quenching in each position.

The introduction of the variation in the surface heat transfer coefficients on the upper and lower surfaces of the horizontal plate produced a small difference in the corresponding stress levels. Thus figure 110 shows radial and hoop stresses of 26MPa on the upper face and 52MPa on the lower. This compares with 55MPa in the case where both faces have the same cooling conditions (figure 102).

The instabilities make discussion of the stress distribution at the end of the quench difficult, since the differences between the stress levels on the upper and lower surfaces may be badly distorted by instability. Comparison of figures 104 and 112 show an increased level of residual stress on the upper face as a consequence of the variable surface heat transfer coefficient although the corresponding results on the lower face are inconclusive (figures 107 and 115). The results along the edge showed significant differences (figures 105 and 113) but these may have been affected by instability.

In comparison with the experimentally measured stresses obtained from the top half of the plate quenched in the horizontal position the calculated results were significantly lower, although there was agreement as to the sense of the stress.

Thus figure 98 shows a surface hoop and radial stress of 300 MPa compared to 93MPa rising to 140MPa along the top surface (figure 104).

6.0 CONCLUSIONS AND RECOMMENDATIONS FOR FURTHER WORK

1. One of the objectives of this work was to determine the variation of surface heat transfer coefficients 'h' at different positions on the surface of a plate held vertically and horizontally in water. In the case of a horizontal plate the surface heat transfer coefficient during nucleate boiling at a given moment in a quench was higher on the lower face than that obtained on the upper face. In the case of a vertical plate the corresponding surface heat transfer coefficients tended to be greater at the plate corners than at other positions in the plate.

2. The experimental time-temperature relationships were dependent on multi-directional heat flow, while the 'h' values used to calculate the same relationship were based on the possibly incorrect assumption of uni-directional flow. However, this assumption has not produced an error in the subsequent calculations of the temperature/time relationships when the theoretical results were compared with the experimental results.

3. During the present investigation it was found that the temperature distribution that had been obtained by finite element analysis correlated well with selected temperature measurements in quenched plates except that the experimentally determined duration of the vapour blanket was significantly longer than the calculated values.

4. The photographic study of the face of the stainless steel plate during quenching showed the presence of Taylor waves on the surface of the vapour blanket in all cases. It was observed that the last part of the blanket to break down was situated along the upper part of the plate when in a vertical position.
5. The photographic data in the case of the horizontal plate indicated that there are variations between the quenching phenomena on the upper and lower faces. In the case of the lower face evidence of extreme instabilities was observed.
6. After the break down of the vapour blanket the surface heat transfer coefficient rose rapidly to a maximum value. This was associated with the formation of many small bubbles on the vertical face and the upper horizontal face of the plate. These were not observed on the lower horizontal face.
7. As the surface heat transfer coefficient at the lower face of the plate, passed its maximum, a series of almost explosive waves of vapour produced the necessary removal of the steam from underneath the plate.
8. The results have shown that the increased surface heat transfer coefficients obtained towards the edge of the plate increased the temperature gradients in the specimen, which produced overall significantly greater levels of residual stress and strain at the end of the quench.

9. The predicted residual stresses and strains have been shown to be in good agreement with measured values, but there was a small reduction in the level of agreement between experimental and calculated strains.

10. The importance of considering the state of residual stress in the entire cross-section of the specimen has been demonstrated. The finite element method has been shown to be a suitable way of understanding complex and of the surprising phenomena.

To follow on from the results of the present work, additional analysis should be carried out to determine the surface heat transfer coefficients in two dimensional rather than unidirectional heat flow in order to optimise the accuracy in obtaining 'h' values.

Such a model should also include the effect of variable thermal expansion for use in predicting the generation of thermal stress and strain in the case of steel undergoing a martensitic transformation (i.e. unloading action) around the plate which will modify the predicted generation of stress during the quench.

The production of transformation products other than martensite i.e. bainite or pearlite should be included in which the formation of bainite and pearlite are both time and temperature dependent.

7.0 REFERENCES

1. THELNING,K.E, STEEL AND ITS HEAT TREATMENT, 2ND EDI,
PP270-276.
2. MONROE.R.W, BATES,C.E, J HEAT TREATING NO.12, (1983)
PP83-89.
3. BERENSEN,P.J.INT.J.HEAT MASS TRANSFER 5 (1962), 985-999.
4. F.S.ALLEN AND A.J.FLETCHER, MATERIALS SCIENCE AND
TECHNOLOGY 1987, VOL 3, 291.
5. SCOTT,H.SCI PAPERA,BUREAU OF STANDARDS 20 (1925)
PP399.
6. BODSON ET ALIA, TRAIT, THERM, 1976, 104, (83).
7. BECK G., TRAIT. THERM., 1970, 54, (19).
8. METALS HANDBOOK,A.S.M, VOL 2, 1964 (15).8TH EDI.
9. BROMLEY,L.A.,CHEMICAL. ENG. PROGRESS, VOL. 46, 1950,
PP221-227.
10. JORDON,D.P. ADV IN HEAT TRANSFER 5(1968) PP(55-125).
11. BRENSON,P.J., JOURNAL OF HEAT TRANSFER, VOL.83,
1961,PP351-357.
12. TAYLOR, GI, PROC.ROY.SOC., 1950, 201A, 192-196.
13. LEWIS, DJ, PROC.ROY.SOC., 1951, 202A, 81-96.
14. ISHIGAI,S., INOUE,K., KIWAKI,Z., AND INAI,T.,
INTERNATIONAL DEVELOPMENT IN HEAT TRANSFER
CONFERENCE, PAPER, 26,1961, PP224-229.

15. FARAHAT, MM AND MADBOULY, EE, INT.J.HEAT MASS
TRANS., 1977, 20, 269, 277.
16. SEKI, N, FUKUSAKO, S AND TORIKOSHI, K, TRANS, A.S.M.E,
NOV, 1978, 100, 624-628.
17. WINTERTON, RHS, "TRANSITION BOILING", SAFETY AND
ENGINEERING SCIENCE DIVISION, AEE WINFRITH, AUG.1982.
18. "BOILING", LEPPERT, G AND PITTS, CC, ADVANCES IN HEAT
TRANSFER, ED. IRVINE, TF AND HARTRETT, JP, ACADEMIC
PRESS LTD., 1965.
19. MITSUTSUKA, M.I FUKUDA, K. TRANS 151J 1979 19 162.
20. TONG, L.S. NUCLEAR ENG AND DESIGN 21 (1972).
21. WESTWATER, J.W., SANTANGELO, J.G., IND AND CHEM.ENG.
1954, 47 NO.8 1605.
22. MANSION J., TRAIT. THERM, 1976, 104(59).
23. LEMAIRE D, TRAIT. THERM, 1976, 104(71).
24. PASCHKIS V. AND STOLZ G., J.O.M, 1956, 8, (1074).
25. PRICE,R.F,FLETCHER,A.J.METALS TECHNOLOGY 5 (1980)
PP(203-211).
26. MITSUTSUKA.M, FUKUDA K. TRANS.ISIH VOL.21
(1981) PP689-697.
27. PASCHKIS V. AND STOLZ G, FINAL REPORT,
1955-1961 COLUMBIA UNIVERSITY.
28. EDGAR VAUGHAN AND CO, LTD, AQUAQUENCH 1250, TRADE
LIT.

29. STOLZ G, PASCHKIS V, BONILLA C.F. AND ACEVADO
G, J.I.S.I, 1959, 10, (116).
30. BECK G. AND CHEVRIER J.C, INT.J.HEAT MASS TRANSFER,
1971, 14, (1731).
31. LAMBERT N. AND ECONOMOPOULOS M, MATHEMATICAL
MODELS IN METALLURGICAL PROCESS DEVELOPMENT, I.S.I,
1969, 29.
32. BERGLES A. AND THOMPSON W.G, INT.HEAT MASS TRANSFER,
1970, 13, 55.
33. MITSUTSUKA M. AND FUKUDA K, J.I.S.I,
JAPAN, 1977, 5, 636, 673.
34. MITSUTSUKA M. AND FUKUDA K, J.I.S.I, JAPAN, 1978, 6, 4, 70.
35. FRYKENDAHL, B. 2ND JAP-SWE JOINT SYMP ON FERROUS
MET. DEC(1978) PP193-204.
36. HESSLING, S.W MSC THESIS, SHEFF CITY POLY. 1981.
37. JASWA N, M.A. INST. OF METALS LONDON (1956) PP173-185.
38. BODSON ET ALLIA, TRAIT.THER, 1976, 104, 83.
39. MITSUTSUKA M. AND FUKUDA K., J.I.S.I. JAPAN, 1976, 16, 47.
40. F.S.ALLEN, A.J.FLETCHER, A.B.SOOMRO, SHEFFIELD CITY
BY U.K.
41. CARSLAW, H.S, JAEGAR, J.C, CONDUCTION OF HEAT IN SOLIDS
2ND EDI, LONDON 1959.
42. FLETCHER, A.J., METALS TECHNOLOGY 1980, 7, 307.
43. FLETCHER, A.J, PRICE, R.F., METALS TECHNOLOGY 1980, 7,
203.

44. JEANMART,P., BOUVAIST,J., MATERIALS SCIENCE AND TECHNOLOGY 1985, 1, 765.
45. SOOMRO,A.B., PhD THESIS SHEFFIELD CITY POLYTECHNIC 1986.
46. "COMPUTER AIDED HEAT TRANSFER ANALYSIS" ADAMS,J.A., ROGERS,D.F MCGRAW AND HILL N.Y 1973.
47. "NUMERICAL METHODS FOR P.D.E" AMES,W.F, ACADEMIC PRESS AND THOMAS NELSON AND SONS N.Y AND LONDON.
48. WOOLMAN J, AND MOTTRAM R.A, THE MECHANICAL AND PHYSICAL PROPERTIES OF B.S.EN STEEL, LONDON, PERGAMON PRESS, 1966.
49. LEE,J.Y.W ET ALIA, INT.J.HEAT MASS TRANSFER VOL.28, NO.8 (1985) PP1415-1423.
50. DAVIS,W.B.J IRON AND STEEL INST , JUNE (1972) PP437- 441.
51. MAURER E, STAHL UND EISEN, VOL 47, 1927, PP1323- 1327.
52. MAURER E, STAHL UND EISEN, VOL 48, 1928, PP225-228.
53. BUHLER H, 1952, PP224-230.
54. MURA T, MEIJI UNIVERSITY, NO.10, 1957, P2.
55. RUSSELL J.E, SYMPOSIUM ON INTERNAL STRESS, INSTISUTE OF METALS, 1947, 95.
56. TIMOSHENKO S.P AND GOODIER J.N. THEORY OF ELASTICITY, NEWYORK, MCGRAW-HILL, 3RD EDI. 1970.
57. BOLEY B.A, AND WEINER, "THEORY OF THERMAL STRESSES", NEWYORK, WILEY 1960.

58. DONEA, J. INT J NUMERICAL METHODS IN ENG. VOL.8, 1974, PP103-110.
59. BRAUCH, J.C, ZYVOLOSKI, G. INT.J.NUMERICAL METHODS IN ENGG, VOL.8, 1974, PP481-494.
60. BUSBY, H.R, TRUJILLO, D.M. INT.J.NUMERICAL METHODS IN ENGG, VOL.21, 1985, PP349-359.
61. B.NATH, FUNDAMENTAL OF FINITE ELEMENTS FOR ENGINEERS, THE ATHLONE PRESS OF THE UNIVERSITY OF LONDON 1974.
62. ZIENKIWIĆZ O.C.P460-461, THE FINITE ELEMENT METHOD, 3RD EDI-MCGRAW-1983.
63. BENHAN P.P AND HOYLE R.H, THERMAL STRESS, LONDON, PITMAN, 1964.
64. PRICE, R.F. THESIS (PhD) SHEFFIELD CITY POLY 1980.
65. WEINER J., J.APP.MECH., 1956, 23, (395).
66. BOLEY B.A. AND WEINER J., "THEORY OF THERMAL STRESSES", NEW YORK, WILEY, 1960, (543).
67. SPEKTOR A. AND STEPANOVA N., MET.SCIENCE.HEAT TREAT. 1975, 3, 282.
68. FLETCHER, A.J. MET.TECH. NO.6, 1977, PP307-316.
69. PRICE, R.F, FLETCHER, A.J. MET TECH NO.11, 1981, PP427-446.
70. JEANMART P.H. BOUVAIST, J. INT SYMP ON CALC OF INTERNAL STRESSES, SEWDEN, MAY 1984, PP23-42.
71. CHEVRIER J.C, THESIS, C.N.R.S, NANCY, 1973, 95.
72. ARCHAMBAULT P., THESIS, C.N.R.S, NANCY, 1976.

73. R.SCHRODER, MATERIAL SCIENCE AND TECH. OCT 1985,
VOL 1, PP754.
74. BURNETT J.A MATERIAL SCIENCE AND TECH OCT 1985.VOL
1, PP863.
75. HILDENWALL,B. DISSERTATION, LINKOPING UNIV, 1979.
76. SJOSTROM,S. DISSERTATION, LINKOPING UNIV, 1982. THE
CALCULATION OF QUENCH STRESSES IN STEEL.
77. A.J.FLETCHER, C.LEWIS, MATERIAL SCIENCE AND TECH,
OCT 1985, VOL 1, 780.
78. S.DENIS, J.C.CHEVRIER, A.SIMON, G.BECK MEMOIRES
SCIENTIFIGUES, REVUE DE METALLURGEI, APRIL 1989P.221 -
233.
79. G.HORVAY, J.MECH.PHYS.SOLIDS, 1957, 5, 77.
80. FLETCHER A.J, AND R.F.PRICE, MET.TECH, 1981, 8, 427.
81. GOODIER J.N. PHILOS.MAG.1937, 23, 607.
82. CHOI.BI, KOO CH, KIM SY, BULL KOREAN INST MET 1988,
1(2), PP128-138.
83. FLETCHER,A.J., ABBASI,F., MATERIALS SCIENCE AND
TECHNOLOGY 1985 1 830.
84. FLETCHER,A.J, ABBASI,F., MATERIALS SCIENCE AND
TECHNOLOGY 1985 1 770.
85. FLETCHER,A.J., SOOMRO,A.B., MATERIALS SCIENCE AND
ENG. 82 1986 101-105.
86. FLETCHER,A.J., SOOMRO,A.B., METALS TECHNOLOGY 1986 8
402.

87. FLETCHER,A.J., SOOMRO,A.B., MATERIALS SCIENCE AND TECHNOLOGY 1986, 2, 714.
88. ANDREWS,K.W., GEORGE,ALLEN AND UNWIN LTD. "PHYSICAL METALLURGY TECHNIQUES AND APPLICATION" VOL.2, 1971.
89. ABBASI,F. PhD THESIS, SHEFFIELD CITY POLYTECHNIC.
90. BUHLER,G., BUCKHOLZ,H.ARCHIV. FUR DAS ESSEN, 1931 5E 8
413.
91. BUHLER,H., BUCKHOLZ,H.ARCHIV. FUR DAS ESSEN, 1933 5E 7
315.
92. BUHLER,H., ET AL, FUR DAS ESSEN, 1969, 40, 411.
93. FUJIO,H. ET AL. BU;; KS,E VP;.20 NO.146 (1977).
94. S.DENIS, E.GAUTIER, A. SIMON, G.BECK; MATERIALS SCIENCE AND TECHNOLOGY 1, 1985, 805.
95. KRAL,J., HORAK,L., MOIMZER, J., CECH,J., CENTRAL RESEARCH INSTITUTE, SKODA, PLZEN, CSSR STEEL FOUNDRY, SKIDA, PLZEN, CSSR TECHNICAL UNIVERSITY, BRNO, CSSR.
96. INOUE,T., YAMAGUCHI,T., ZHIGANY WANG. MATERIAL SCIENCE AND TECHNOLOGY, 1985, VOL 1, 872.
97. MARK E. TODARO, MARK A. DOXBECK, GEORGE P. CAPSIMALIS APR. 1987, ASM INTERNATIONAL METAL PARK.
98. DISCUSSION ON THE ROLE OF TRANSFORMATION PLASTICITY IN THE CALCULATION OF QUENCH STRESS IN STEELS.
S.DENIS, A.SIMON ECOLE DES MINES, RESIDUAL STRESSES IN SCIENCE AND TECHNOLOGY VOL 2, 1986, NANCY (FRANCE)
565-572.

99. F.G.RAMMERSTORFER ET ALIA; IN PROC. SYMP, 'EIGEN SPANNUNGEN- ENTSTCHUNG-BERECHUNG-MESSUNG-BEWERTUNG', KERLSRUHE, 1983.
100. F.G.RAMMERSTORFER ET AL; COMPUT, STRUCT, 1981, 13, 771-779.
101. D.F.FISCHER ET AL; IN NUMERICAL METHODS IN THERMAL PROBLEMS; 1981, SWANSEA, PINERIDGE PRESS LTD.
102. DENIS-JUDLIN, THESE, INST.NAT POLYTECHNIQUE DE LORRAINE, NANCY (1980).
103. S.DENIS, A.SIMON AND G.BECK, ANALYSIS OF THE THERMOMECHANICAL BEHAVIOUR OF STEEL DURING MARTENSITIC QUENCHING AND CALCULATION OF INTERNAL STRESSES, C.N.R.S ECOLE DES MINES,INSTITUTE NATIONAL POLY.DE LORRAINE, PARC DE SAURUP-54042-NANCY-CEDEX(FRANCE).
104. I.Y.Y., AND CHEN.Y., TRANSACTIONS OF THE ASME, JOURNAL OF ENG.MATERIALS AND TECHNOLOGY, VOL.110, OCT 1988, PP372-379.
105. TODARO,M.E, DOXBECK,M.A., AND CAPSIMALIS,G.P., "RESIDUAL STRESS IN QUENCHED STEEL CYLINDERS", ASM CONF. ON RESIDUAL STRESS APRIL 27-29, 1987, P.59.
106. HUANG,D.J., MAYO,W.E., AND CHEN,Y., "RESIDUAL STRESS MEASUREMENTS IN TIME-CONTROLLED QUENCHED AUSTENITIC STAINLESS STEEL", TO APPEAR IN JOURNAL OF EXPERIMENTAL MECHANICS, 1988.

107. GREENWOOD,G.W., JOHNSON,R.M., PROC.ROY.SOC. 1965,
283 APP 403.
108. SATTLER,H.P., WASSERMAN,G.J.LESS COM MET 1972, 28,
APP 119.
- 109.R.SCHRODER. MATERIALS SCIENCE AND
TEC.OCT 1985, VOL 1, 754-764.
110. R.SCHRODER AND B.SCHOLTES. AHRTEREI-TECH.
MITT.BEIHEFT, 1982, 64-72 AND 1982, 39 280-292.
111. H.J.YU, U. WOLFSTIEG AND E.MACHERAUCH,
ARCH.EISENHUTTEW., 51:195(1980).
112. S.DENIS, J.C.CHEWIER, A.SIMON AND G.BECH,
MEM.SCIENT.REV.MET 76:221(1979).
113. ABEL.J.F,ANDDEALIC.S, INTRODUCTION TO THE FINITE
ELEMENT METHOD, P117-118, 147-148, VAN NOSTRAND
REINHOLD,1972.
114. PAFEC, PAFEC 75 THEORY AND RESULTS MANUAL,
P2.89,1985.
115. ZIENKIEWICZ,O.C, THE FINITE ELEMENT METHOD, 1977.
116. PAFEC, PAFEC 75 THEORY AND RESULTS MANUAL 1975 HILL
BOOK COMPANY(UK)LTD.
- 117.ZEINKIEWIĆZ O.C, THE FINITE ELEMENT METHOD IN
ENGINEERING SCIENCE, NEWYORK.MCGRAW-HILL.1971.
118. DESAI C.S., AND ABLE J.F., INTRODUCTION TO THE FINITE
ELEMENT METHOD, PRINCETON, N.J, VAN NOSTRAND
REINBOLD, 1972.

119. J.N.REDDY, AN INTRODUCTION TO THE FINITE ELEMENT METHOD 1984.
120. LEWIS,C., FLETCHER,A.J., "INT SYMP ON CALC OF INTERNAL STRESSES", SWEDEN. MAY 1984, PP80-97.
121. TREUTING,RG AND READ,WT, J.APPL.PHYSICS, FEB., 1951, (22), 2, 130-134.
122. ALLEN,FS,PhD THESIS, SHEFFIELD CITY POLY, 1981.

Table 1

The chemical composition and physical properties of grade 316 stainless steel.

Table 2

The physical properties of grade 316 stainless steels as used in finite element programme.

(Thermal and stress analysis).

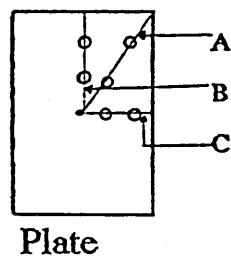
C	Mn	P	S	Si	Cr	Ni	Mo
0.08(%)	2.0(%)	0.045(%)	0.03(%)	1.0(%)	16-18(%)	10-14(%)	2-3(%)
Thermal Conductivity			$14.5744 + 0.0164T (W \cdot m^{-2} \cdot K^{-1})$				
Thermal Diffusivity			$3.912 \cdot 10^{-6} + 2.6255 \cdot 10^{-9}T (m^2 \cdot s^{-1})$				
Specific Heat Capacity			$458.25 + 0.2488 T - 1.3773 \cdot 10^{-4} T^2 (J \cdot Kg^{-1} \cdot K^{-1})$				

Poissons ratio; ν	0.3
Youngs Modulus; E N/mm^2	193000
Density; ρ Kg/mm^3	0.000008
Specific heat capacity; C_p $J/Kg^{\circ}C$	500
Thermal conductivity; λ $W/mm^{\circ}C$	0.0215
Coefficient of Expansion; α C^{-1}	$16.5 \cdot 10^{-6}$
Yield Stress; Y N/mm^2	$T > 850$ 51.0 $T > 549$ 40.0 $T < 400$ 155 $T > 20$ 244
Work Hardening Coefficients nts; Wl MPa	$T > 600$ C 2400 $T < 600$ C 4300

Table 3

Extrapolated cooling curves and surface heat transfer coefficient data obtained during a water quench from thermocouples placed at the top of the plate in a vertical quench.

- (A) Position along upper half of the diagonal face of the plate.
- (B) Upper half of a vertical section through face centre.
- (C) One half of a horizontal section through face centre.



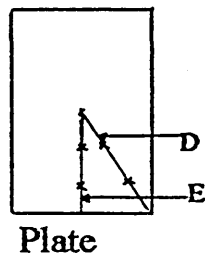
<i>Thermocouple Orientation</i>	<i>Time until end of Vapour blanket (Sec)</i>			<i>Temperature at end of Vapour blanket (°C)</i>			<i>Maximum value of S.h.t.c (W/m² °C)</i>			<i>Surface temperature at which max S.h.t.c occurs (°C)</i>		
<i>Thermocouple positions</i>	<i>A</i>	<i>B</i>	<i>C</i>	<i>A</i>	<i>B</i>	<i>C</i>	<i>A</i>	<i>B</i>	<i>C</i>	<i>A</i>	<i>B</i>	<i>C</i>
<i>1-Centre</i>	<i>8.0</i>	<i>5.0</i>	<i>6.0</i>	<i>760</i>	<i>780</i>	<i>775</i>	<i>6900</i>	<i>6400</i>	<i>5361</i>	<i>315</i>	<i>377</i>	<i>362</i>
<i>2-Intermediate</i>	<i>5.5</i>	<i>7.0</i>	<i>7.2</i>	<i>780</i>	<i>780</i>	<i>780</i>	<i>6500</i>	<i>6690</i>	<i>9007</i>	<i>354</i>	<i>305</i>	<i>312</i>
<i>3-Intermediate</i>	<i>3.0</i>	<i>8.0</i>	<i>4.0</i>	<i>800</i>	<i>770</i>	<i>790</i>	<i>8200</i>	<i>8100</i>	<i>7305</i>	<i>306</i>	<i>303</i>	<i>366</i>
<i>4-Corner edge</i>	<i>1.0</i>	<i>4.5</i>	<i>1.5</i>	<i>820</i>	<i>790</i>	<i>825</i>	<i>13000</i>	<i>6315</i>	<i>7250</i>	<i>180</i>	<i>294</i>	<i>256</i>

Table 4

Extrapolated cooling curves and surface heat transfer coefficient data obtained during a water quench from thermocouples placed at the bottom of the plate in a vertical quench.

(D) Position along lower half of the diagonal face of the plate.

(E) Position along lower half of the vertical section through face centre.



Thermocouple Orientation	Time until end of Vapour blanket (Sec)		Temperature at end of Vapour blanket (°C)		Maximum value of S.h.t.c (W/m ² °C)		Surface temperature at which max S.h.t.c occurs (°C)	
	D	E	D	E	D	E	D	E
Thermocouple positions								
1-Centre	8.3	8.0	780	780	6500	6582	334	320
2-Intermediate	4.5	7.15	800	770	5300	8000	390	270
3-Intermediate	2.6	4.3	795	790	5660	8750	264	358
4-Corner edge	1.25	1.5	830	830	12500	8000	180	316

Table 5

Extrapolated cooling curves and surface heat transfer coefficient data obtained during a water quench from thermocouples placed at the top of the plate in a horizontal quench.

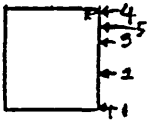
Thermocouple Orientation 	Time until end of Vapour bla- nket (Sec)	Temperature at end of Vapour blanket ($^{\circ}\text{C}$)	Maximum value of S.h.t.c ($\text{W}/\text{m}^2\text{ }^{\circ}\text{C}$)	Surface tempera- ture at which max S.h.t.c occurs ($\text{W}/\text{m}^2\text{ }^{\circ}\text{C}$)
1-Centre	9	790	4968	276
2-Interme- diate	4.5	790	6102	293
3-Interme- diate	3	800	5273	322
4-Corner edge	0.6	800	10823	217
5-Top edge	1.2	800	5999	366

Table 6

Extrapolated cooling curves and surface heat transfer coefficient data obtained during a water quench from thermocouples placed at the bottom of the plate in a horizontal quench.

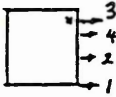
Thermocouple Orientation 	Time until end of Vapour blanket (Sec)	Temperature at end of Vapour blanket ($^{\circ}\text{C}$)	Maximum value of S.h.t.c ($\text{W/m}^2\text{ }^{\circ}\text{C}$)	Surface temperature at which max S.h.t.c occurs ($\text{W/m}^2\text{ }^{\circ}\text{C}$)
1-Centre	16.5	760	9920	171
2-Intermediate	4.5	810	6439	268
3-Corner edge	0.8	820	13183	213
4-Top edge edge	1.5	825	8751	378

TABLE 7

Extrapolated cooling curves for the 2D heat flow case using constant and variable surface heat transfer coefficient in a vertical and horizontal quench.

Thermocouple Positions	Temperature of vapour blanket (°C)					Temperatures (°C) at time 93 secs					Temperatures (°C) at time 134 secs				
	Centre	Intermediate	Corner edge	Top edge	---	Centre	Intermediate	Corner edge	Top edge	---	Centre	Intermediate	Corner edge	Top edge	
Vertical plate with constant 'h'	850	850	850	880	---	420	420	420	250	---	295	295	295	180	
Vertical plate with variable 'h'	800	800	850	880	---	300	300	130	190	---	300	300	100	150	
Horizontal plate with constant 'h'	800	800	800	---	---	650	650	650	---	---	450	450	450	---	
Horizontal plate with variable 'h'	Lower surface	790	800	840	---	700	575	420	---	---	350	290	260	---	
	Upper surface	810	800	840	---	575	530	420	---	---	400	350	260	---	

Figure 1

Variation of surface heat flux with surface temperature obtained from Ni cylinders of various diameters by

Beck & Chevrier³⁰

(a) 10mm diameter

(b) 15mm diameter

(c) 30mm diameter

Figure 2

Schematic representation of the movement of the nucleate boiling front Ni cylinders when quenched vertically in water. (After Beck & Chevrier³⁰)

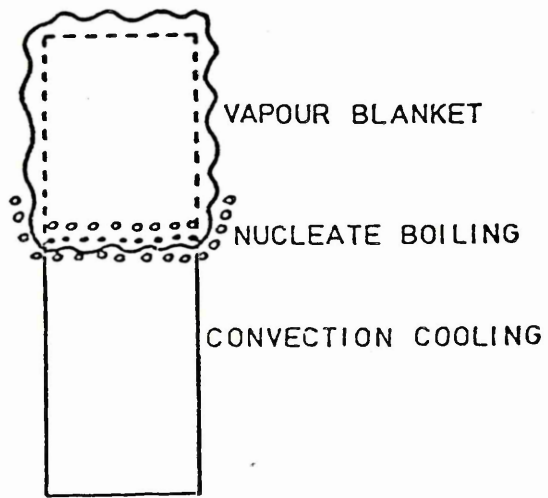
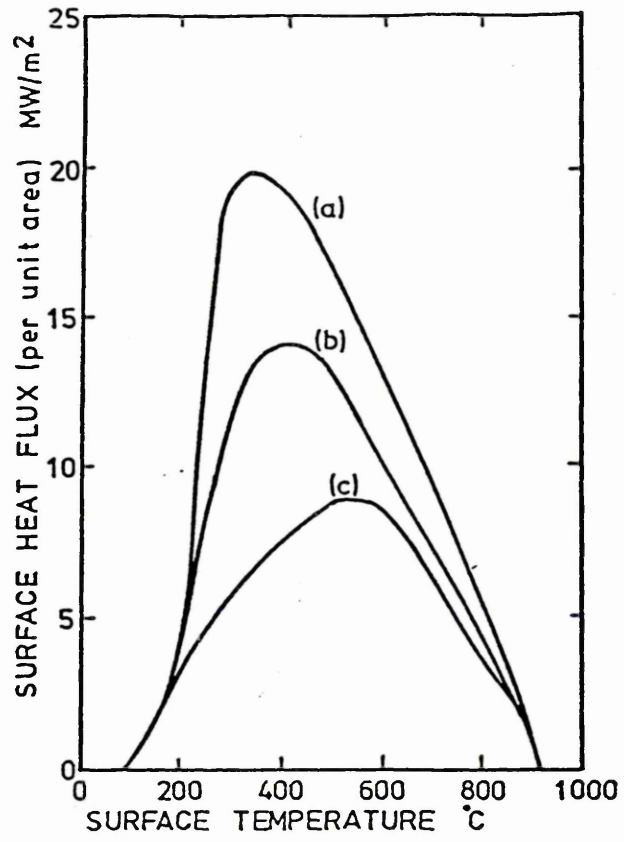


Figure 3

Effects of water temperature on surface heat transfer coefficients. (26)

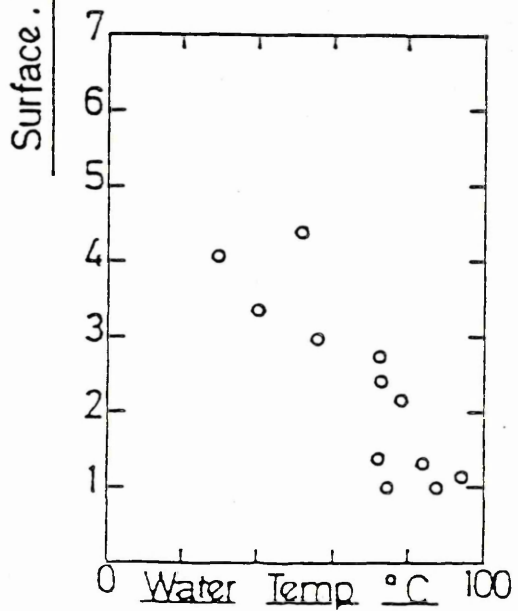
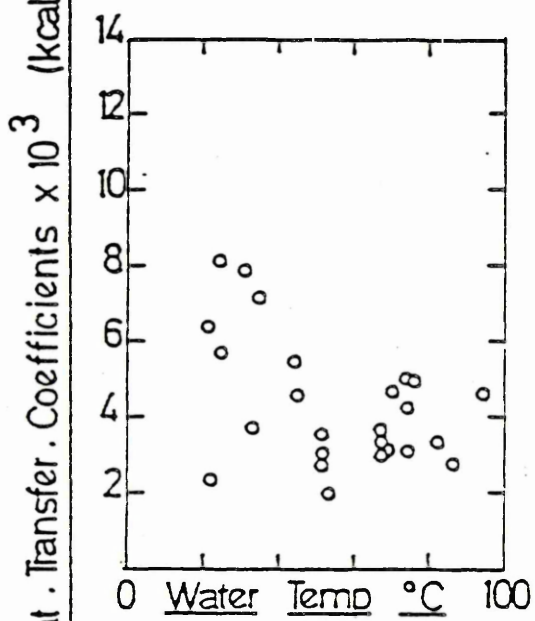
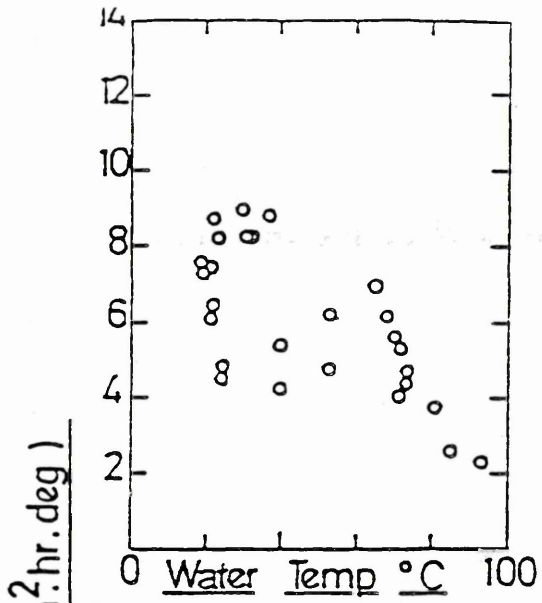
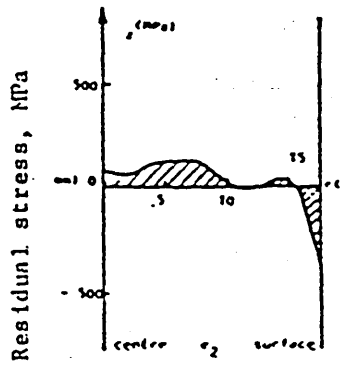
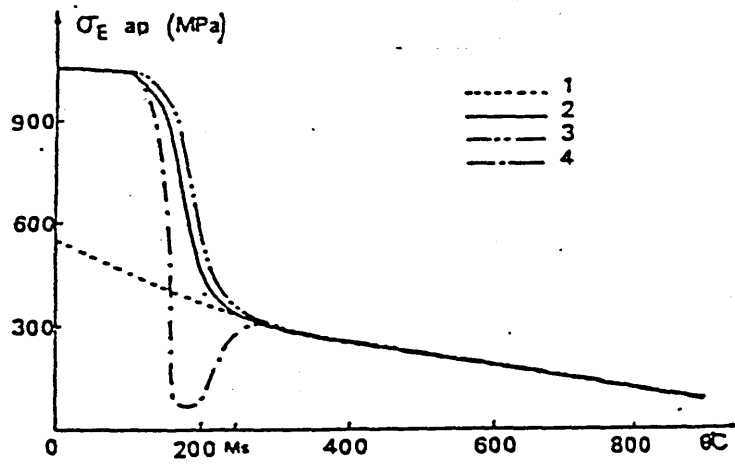


Figure 4

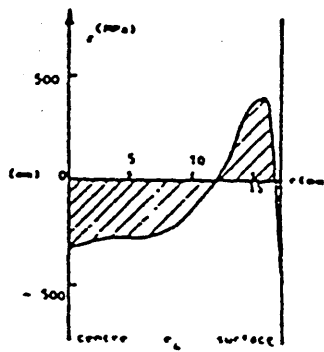
Elastic limit as function of temperature. Curve 1 for no transformation and curve 4 is an attempt to take account of transformation plasticity¹⁰² .

Figure 5

The effect of transformation plasticity. Left figure calculated by curve 2 in figure 4 and right figure by curve 4^{102,112} .



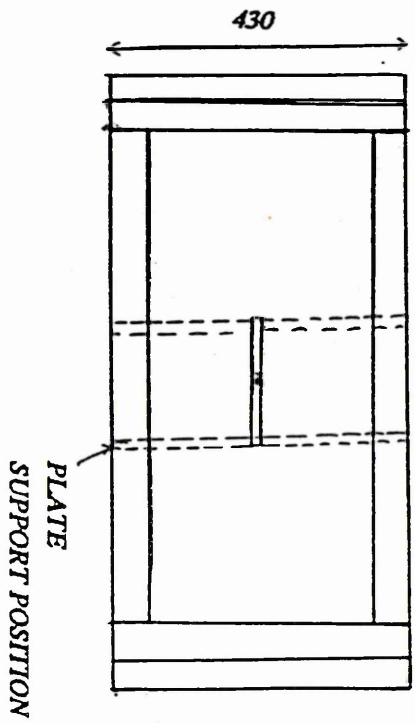
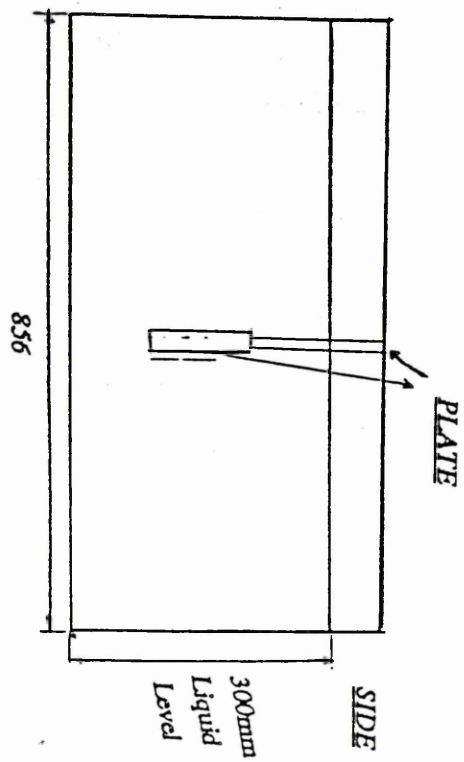
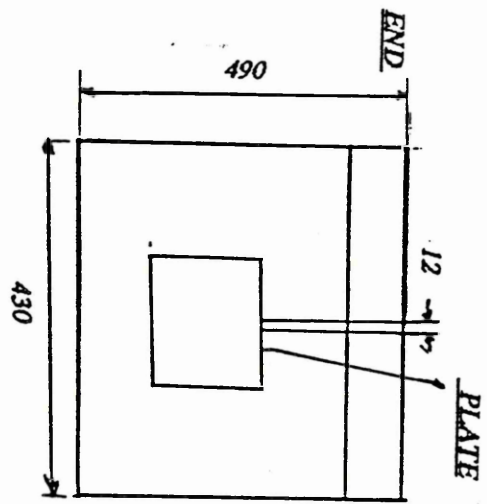
without transformation plasticity



with transformation plasticity

Figure 6

Quench tanks dimensions (mm) vertical quench.



PLAN

Figure 7

Shows five positions which were considered in each experiment and involved one of the following in vertical quench;

- (a) positions along upper half of the diagonal face of the plate.
- (b) corresponding positions along lower half of the same diagonal.
- (c) upper half of a vertical section through the face centre.
- (d) corresponding positions along lower half of the same vertical face.
- (e) one half of a horizontal section through the face centre.

Figure 8

Shows the plate quenched horizontally with positions of the thermocouples at the upper face of the plate.

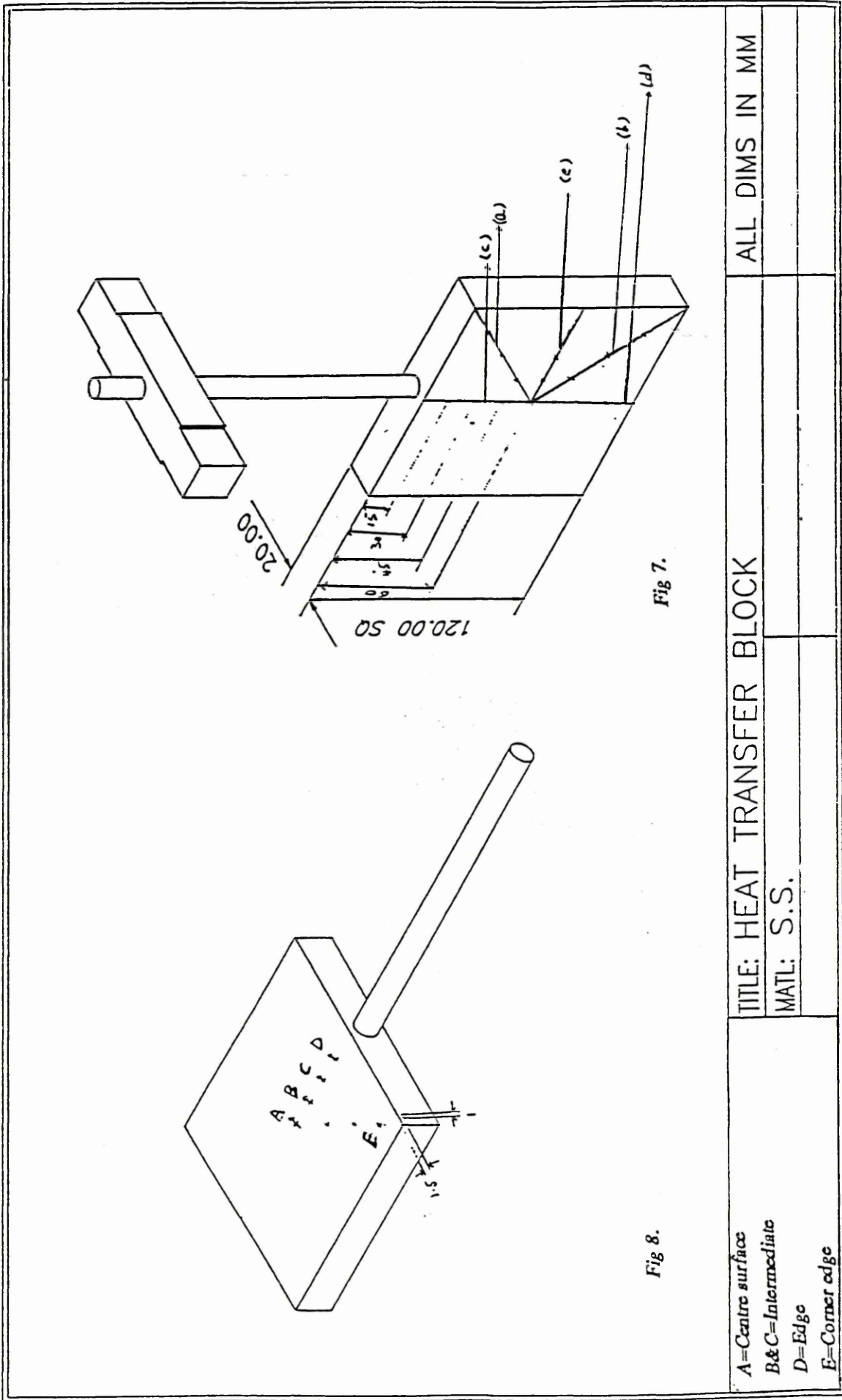


Fig 8.

Fig 7.

<p>A=Centre surface B&C=Intermedialto D=Edge E=Corner edge</p>	<p>TITLE: HEAT TRANSFER BLOCK MATL: S.S.</p>	<p>ALL DIMS IN MM</p>
---	---	-----------------------

Figure 9

Shows the plate quenched horizontally with positions of the thermocouples at the lowerer face of the plate and at top as well.

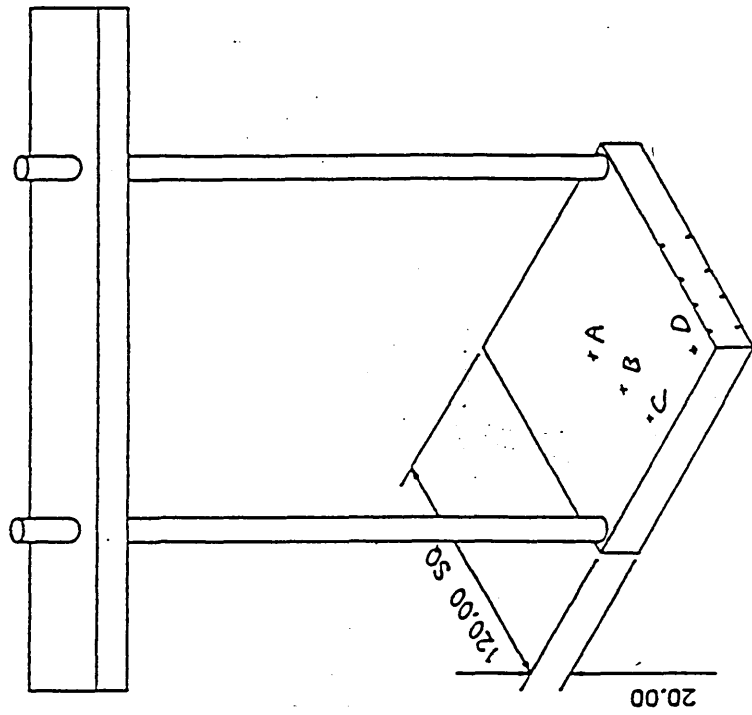


Fig 9.

A=Centre surface
 B=Intermediate
 C=Edge
 D=Corner edge

TITLE: HEAT TRANSFER BLOCK

MATL: S.S.

ALL DIMS IN MM

Figure 10a & 10b

Represent the horizontal quench with position of thermocouples at the lower face of the plate.

Figure 11a & 11b

Represent the horizontal quench with position of thermocouples at the upper face of the plate.

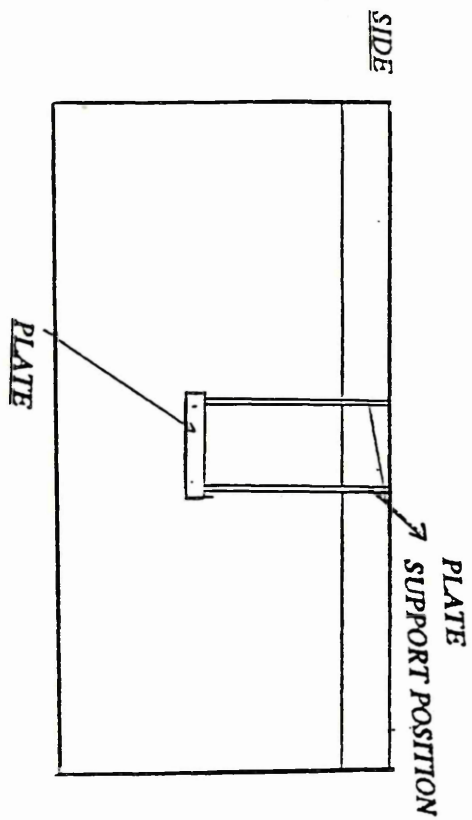


Fig. 10a.

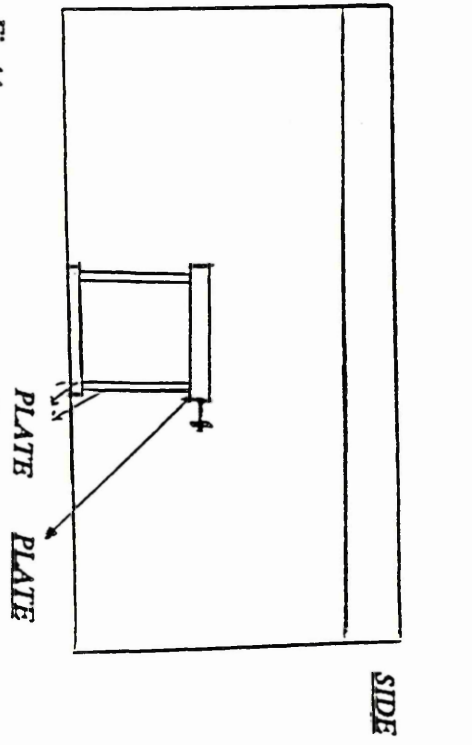


Fig. 11a.

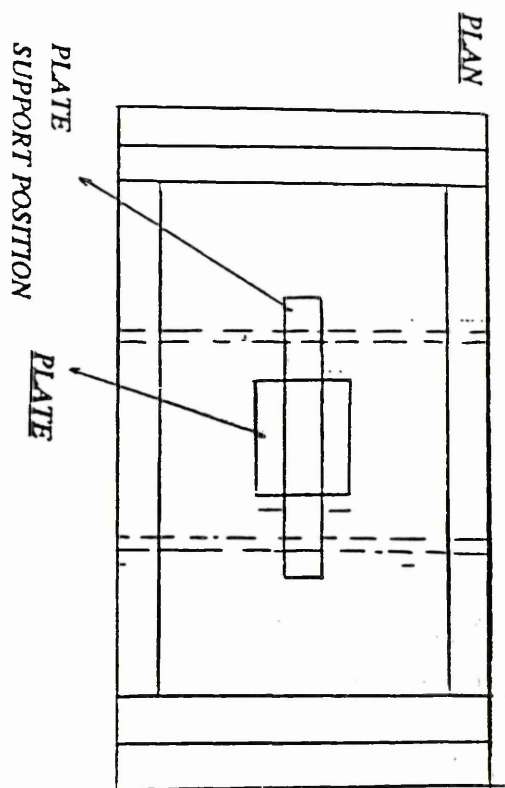


Fig. 10b.

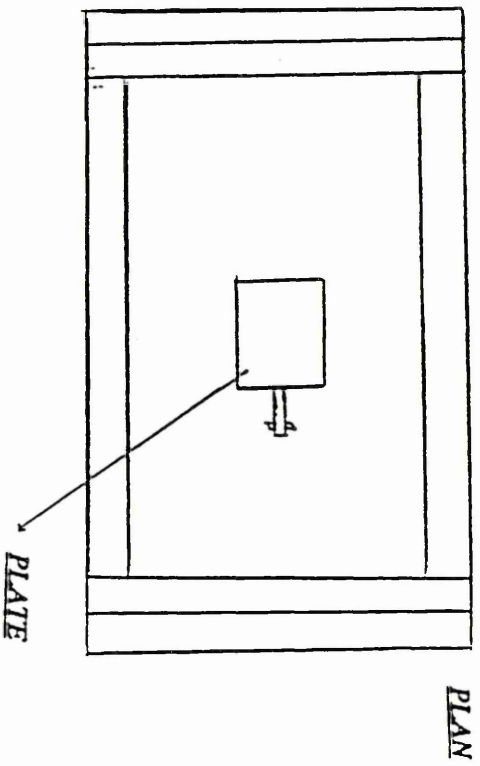
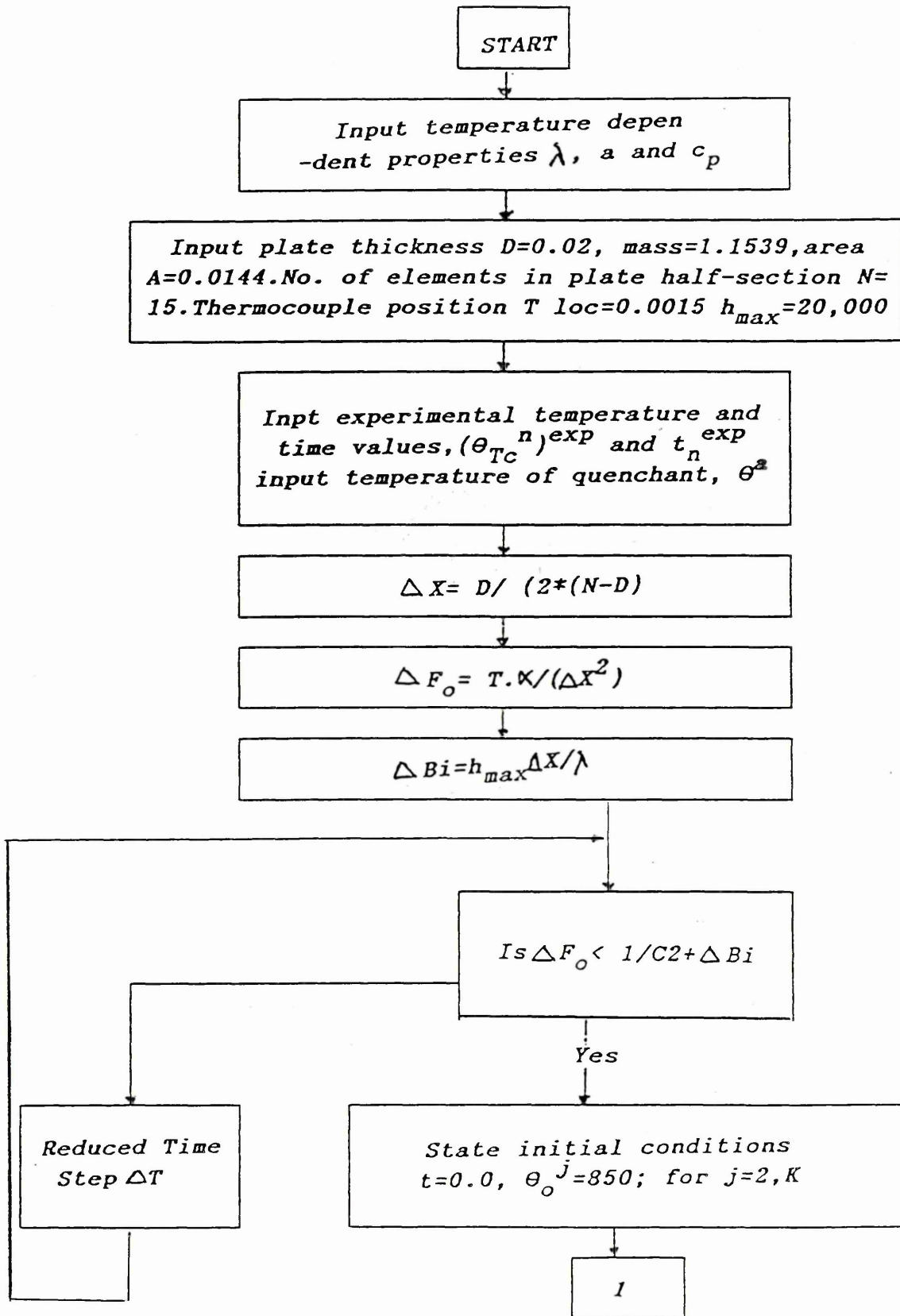
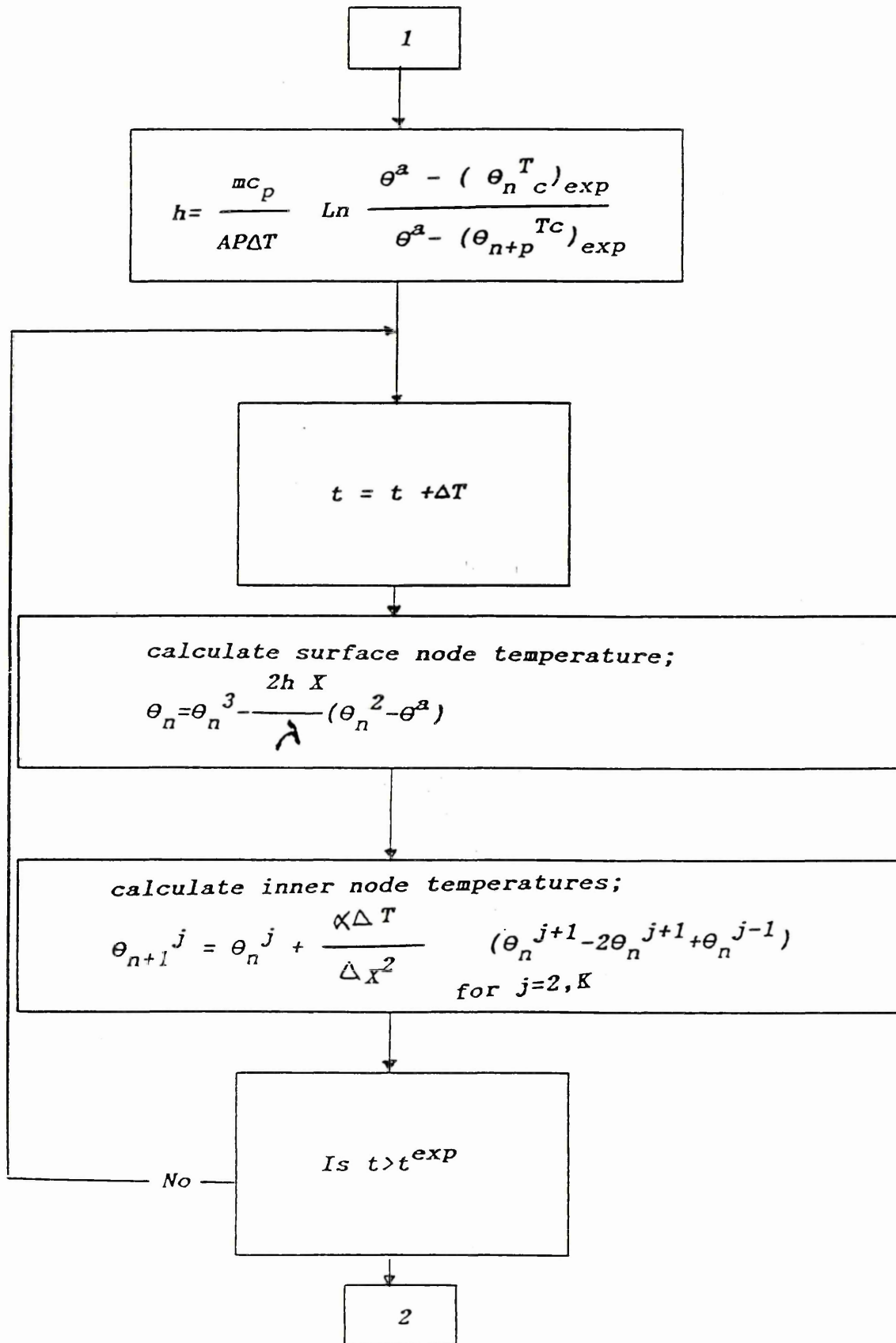


Fig. 11b.

Figure 12

Flow diagram of the procedure for the calculation of the surface heat transfer coefficient during quenching.





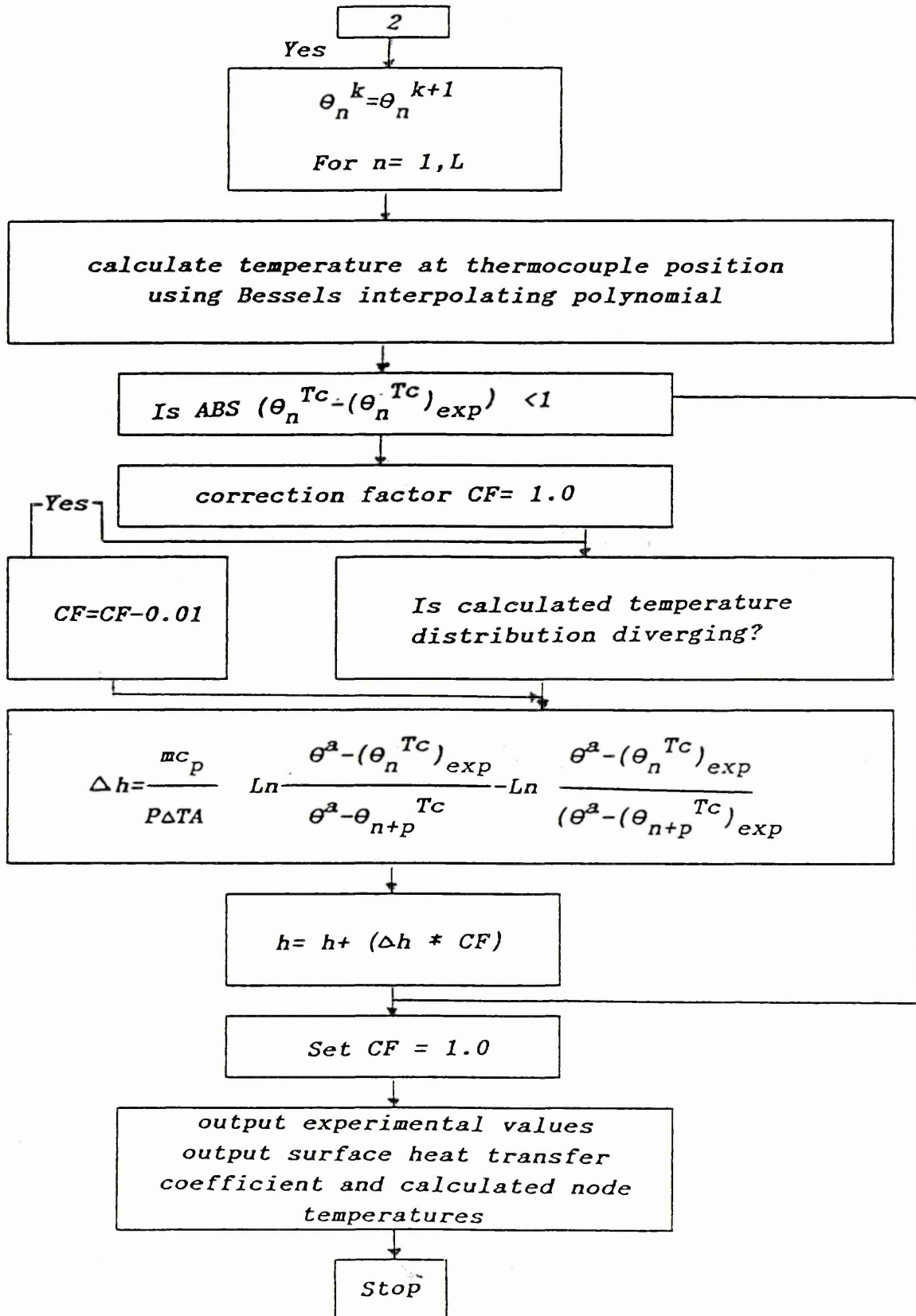


Figure 13

Shows the relationships between stress and strain.

Figure 14

Variation in the strain-hardening coefficient with temperature for 835M30 specimens cooled from 850°C; -.- -.-, $\dot{\epsilon} = 0.33 \cdot 10^{-3} \text{ s}^{-1}$; $\dot{\epsilon} = 0.65 \cdot 10^{-3} \text{ s}^{-1}$; —•—, $\dot{\epsilon} = 5.8 \cdot 10^{-3} \text{ s}^{-1}$; ———, relationship used in calculations.

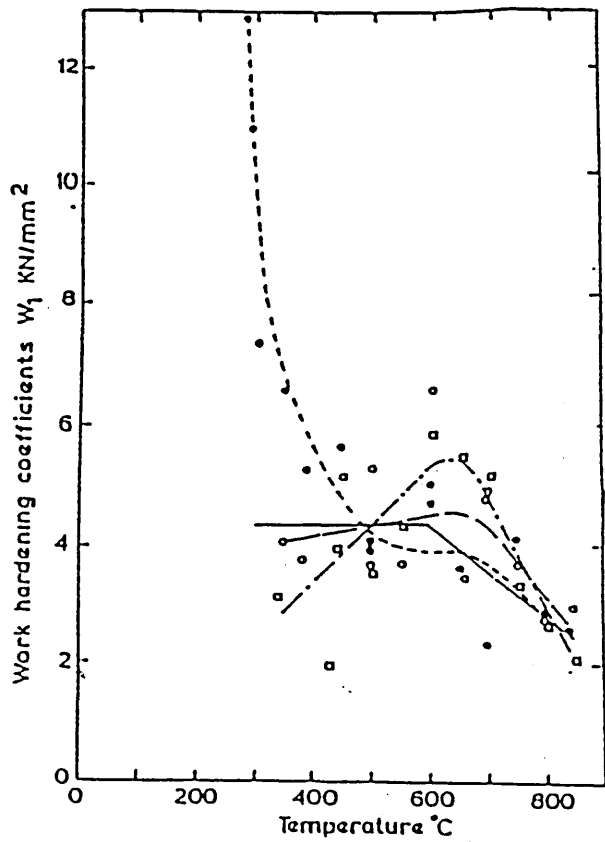
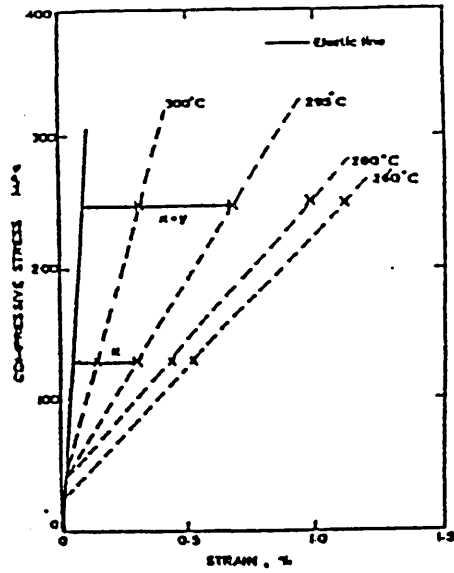


Figure 15

The measurement points on the stainless steel plate from which the residual strain was determined.

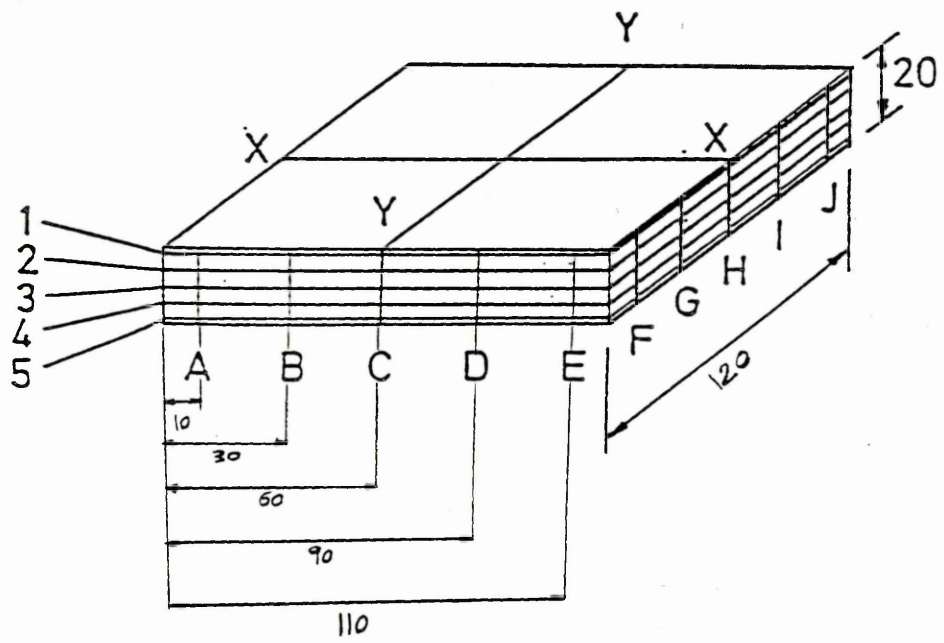


Figure 16

Illustrates the location of measurements made across the plate thickness used to determine distortion without edge effects.

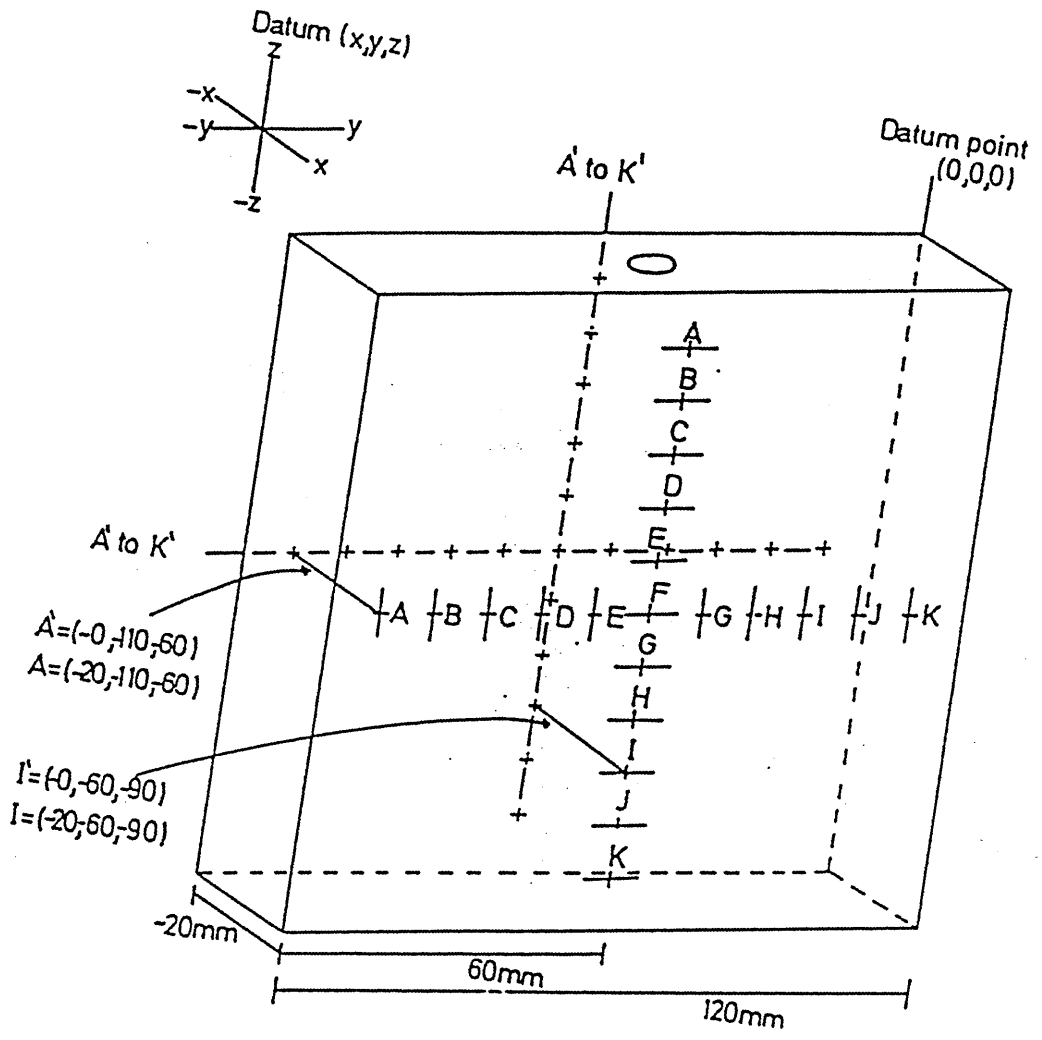


Figure 17

Shows the effect of edge of the plate on the strain produced during quenching .

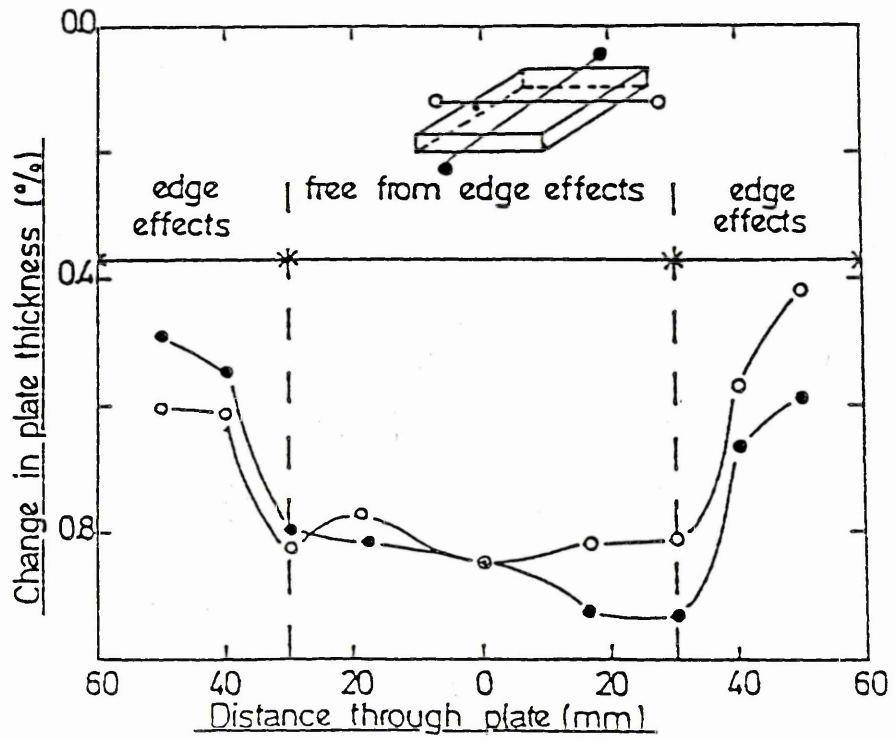


Figure 18

Arrangement of the quenched stainless steel and the cast iron supporting plate during the measurement of residual stresses.

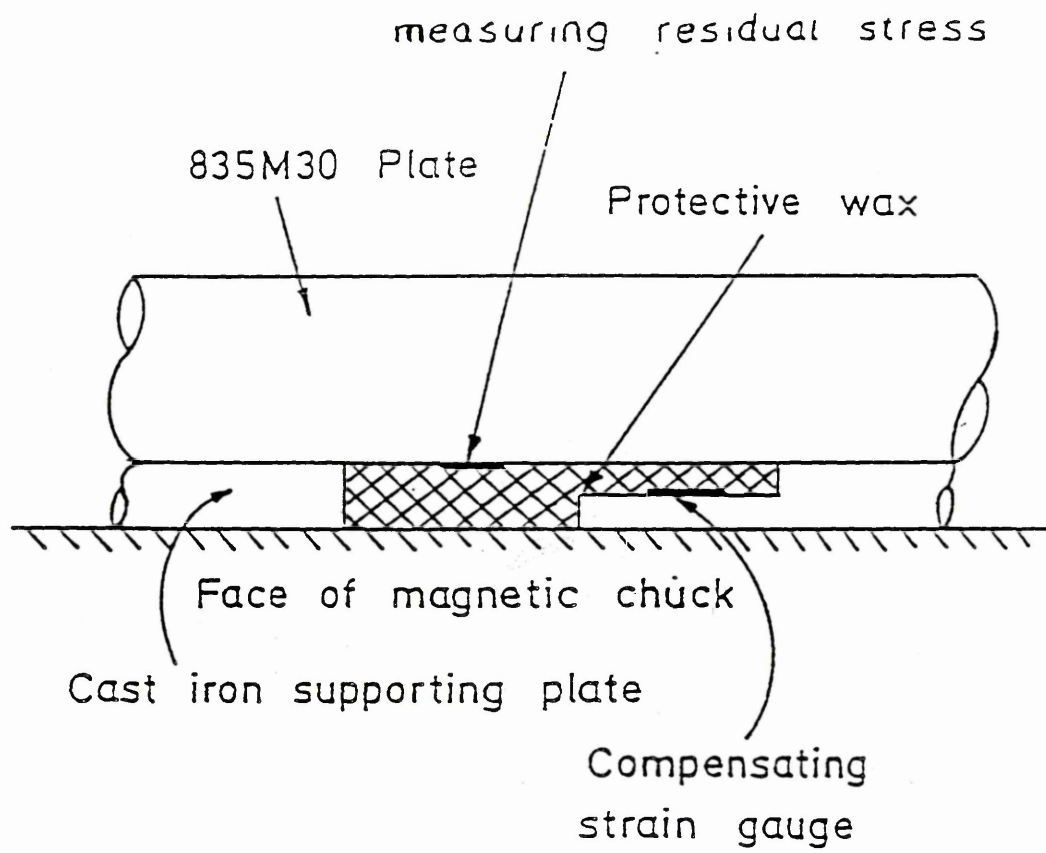


Figure 19

Illustrates position of strain gauges on;

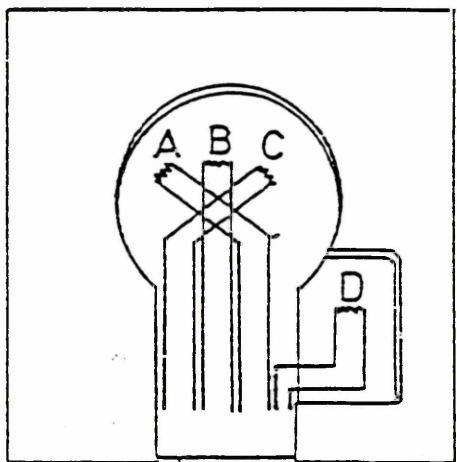
(a) work plate and supporting plate

(b) compensating plate.

Figure 20

Simplified diagram showing connection of strain gauges to Data Logger.

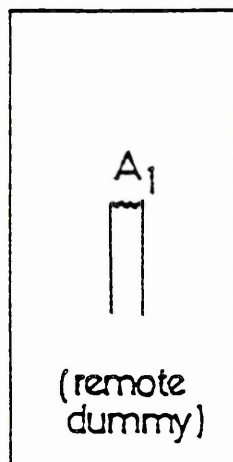
.a.



Work
plate

supporting
plate

.b.



Compensating
plate

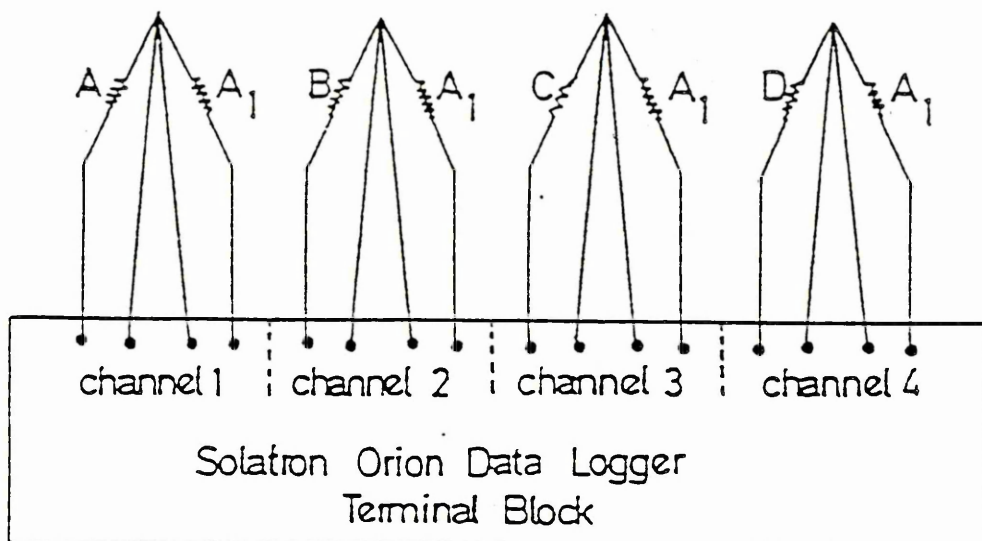
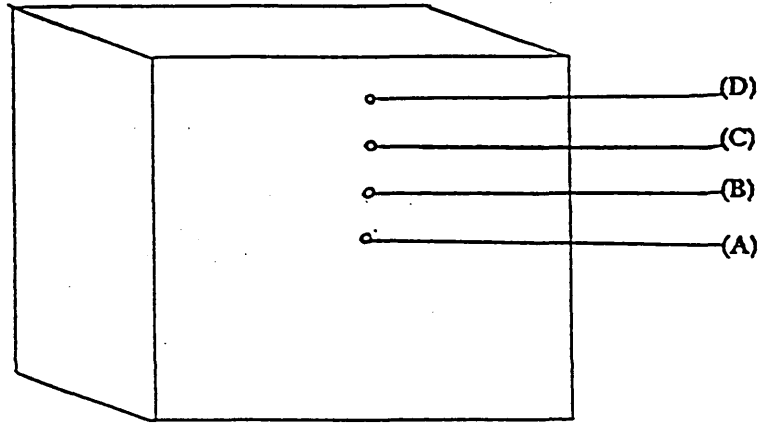


Figure 21

Average cooling curve of 3 experiments of thermocouple positions along upper half of a vertical section through the face centre of the plate quenched vertically in water, where \ddagger , \times , \diamond and $+$ represent the centre (A), two intermediates (B,C), and top edge (D) respectively.

Schematic representation of the plate.



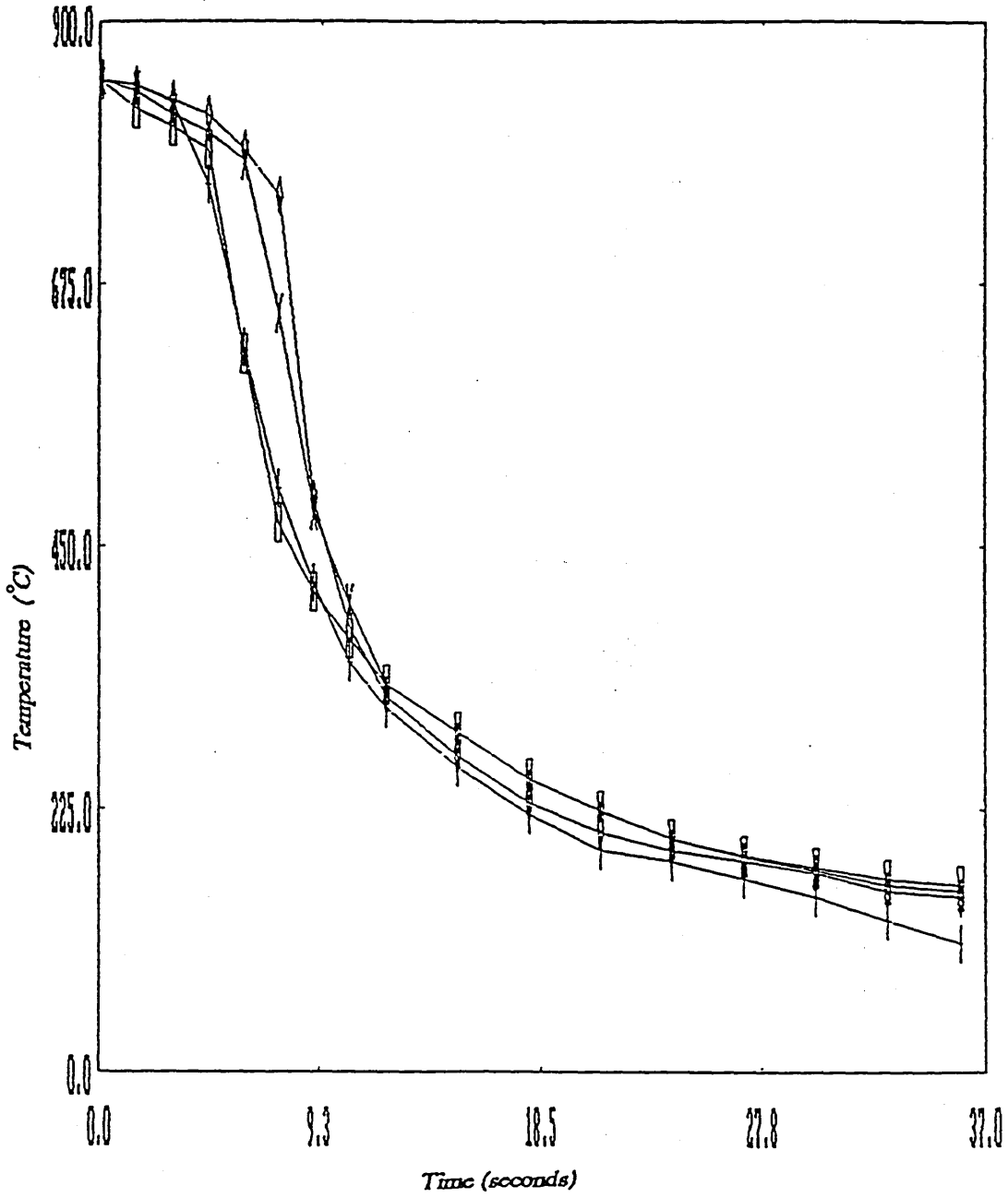
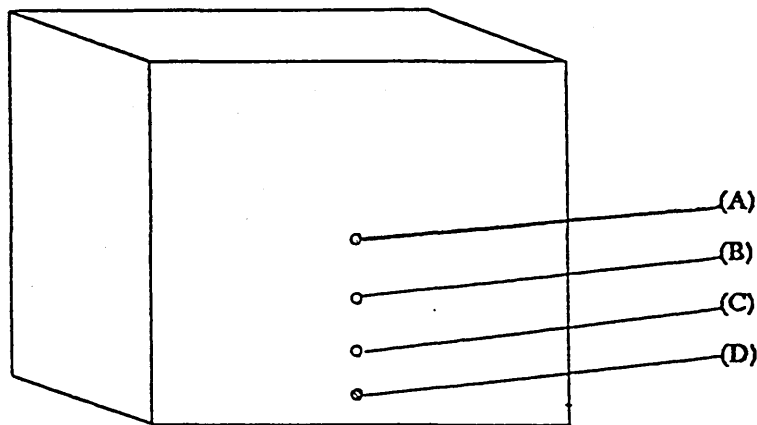


Figure 22

Average cooling curve of 3 experiments of thermocouple positions along lower half of a vertical section through the face centre of the plate quenched vertically in water, where ϕ , \times , \diamond and $+$ represent the centre (A), two intermediates (B,C), and lower edge (D) respectively.

Schematic representation of the plate.



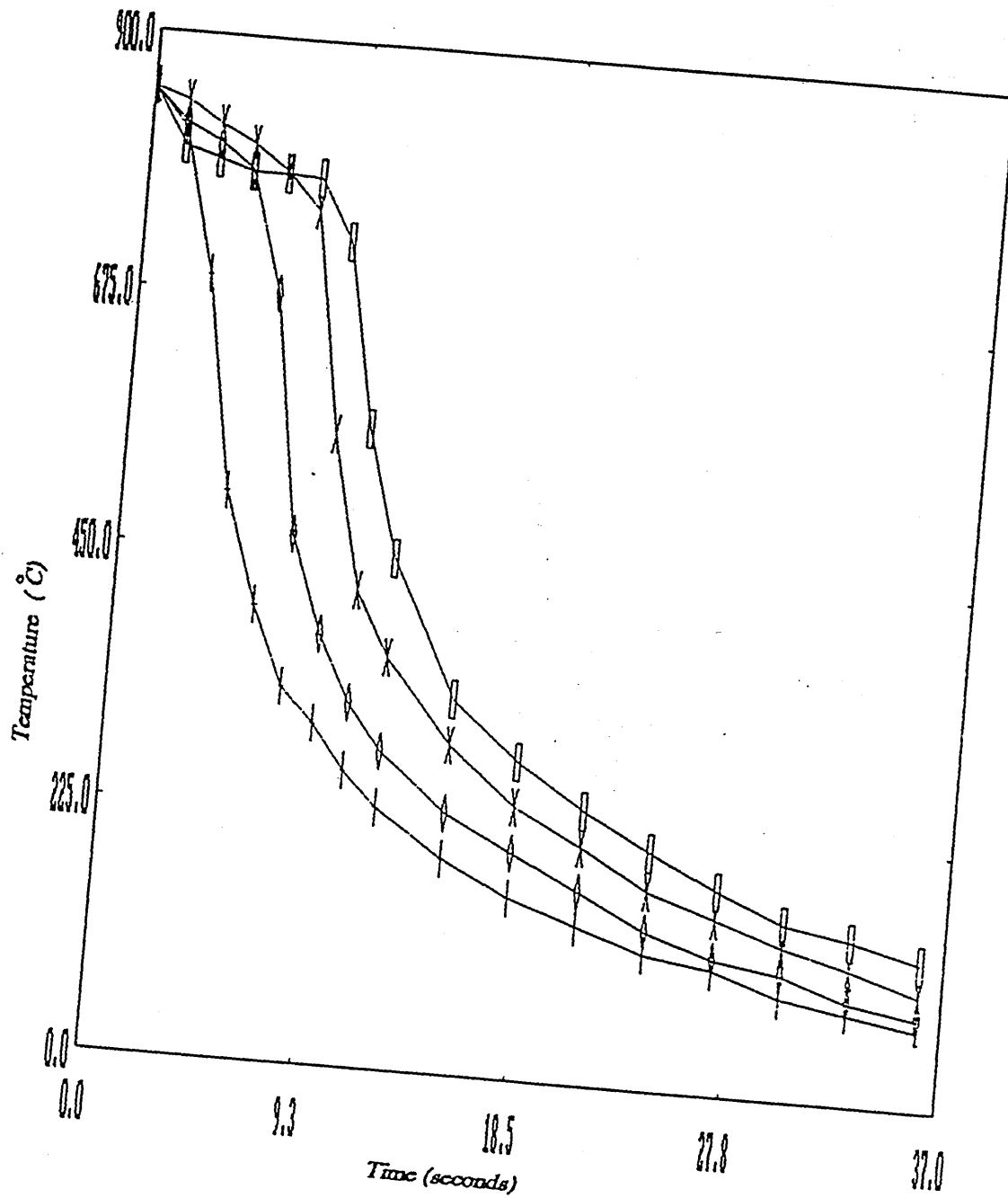
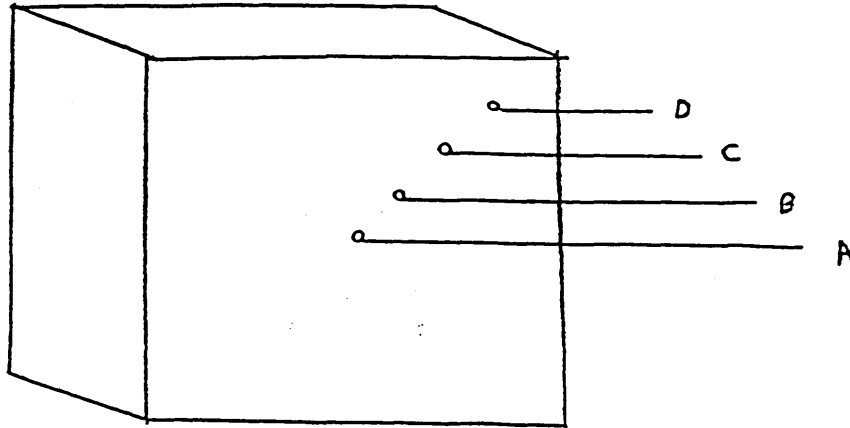


Fig (23)

Average cooling curve of 3 experiments of thermocouple positions along upper half of the diagonal face of the plate quenched vertically in water, where θ , t_1 , t_2 & t_3 represent the centre (A), two intermediates (B,C), and corner edge (D) respectively.

Schematic representation of the plate.



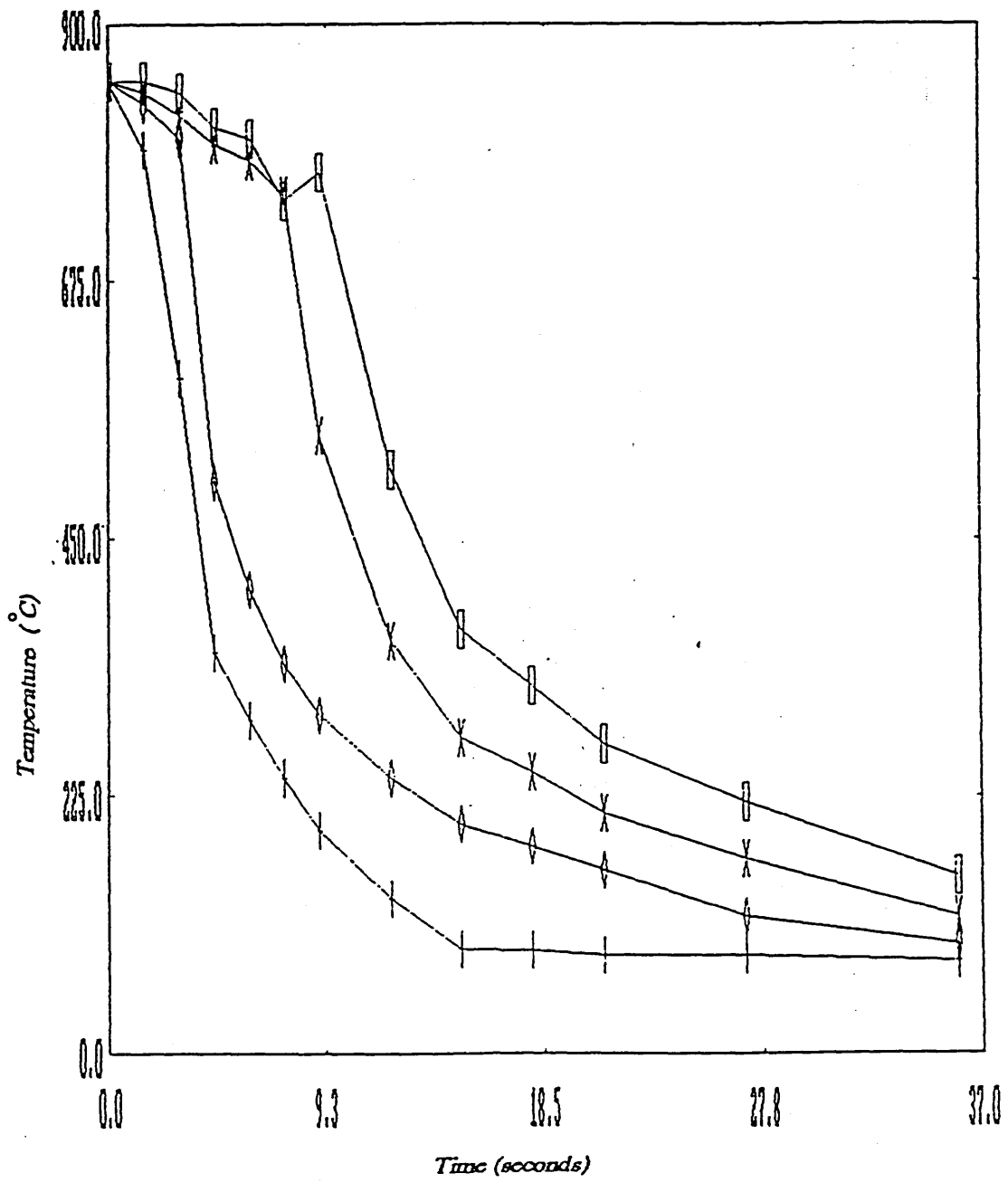
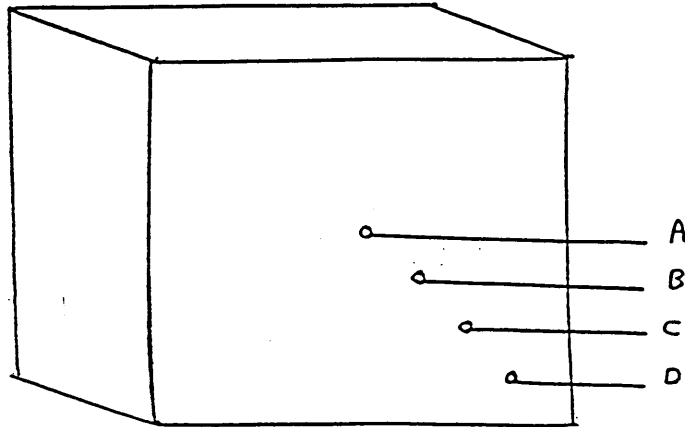


Fig (24)

Average cooling curve of 3 experiments of thermocouple positions along lower half of the diagonal face of the plate quenched vertically in water, where \oplus , \times , \diamond & \dagger represent the centre (A), two intermediates (B,C), and corner edge (D) respectively.

Schematic representation of the plate.



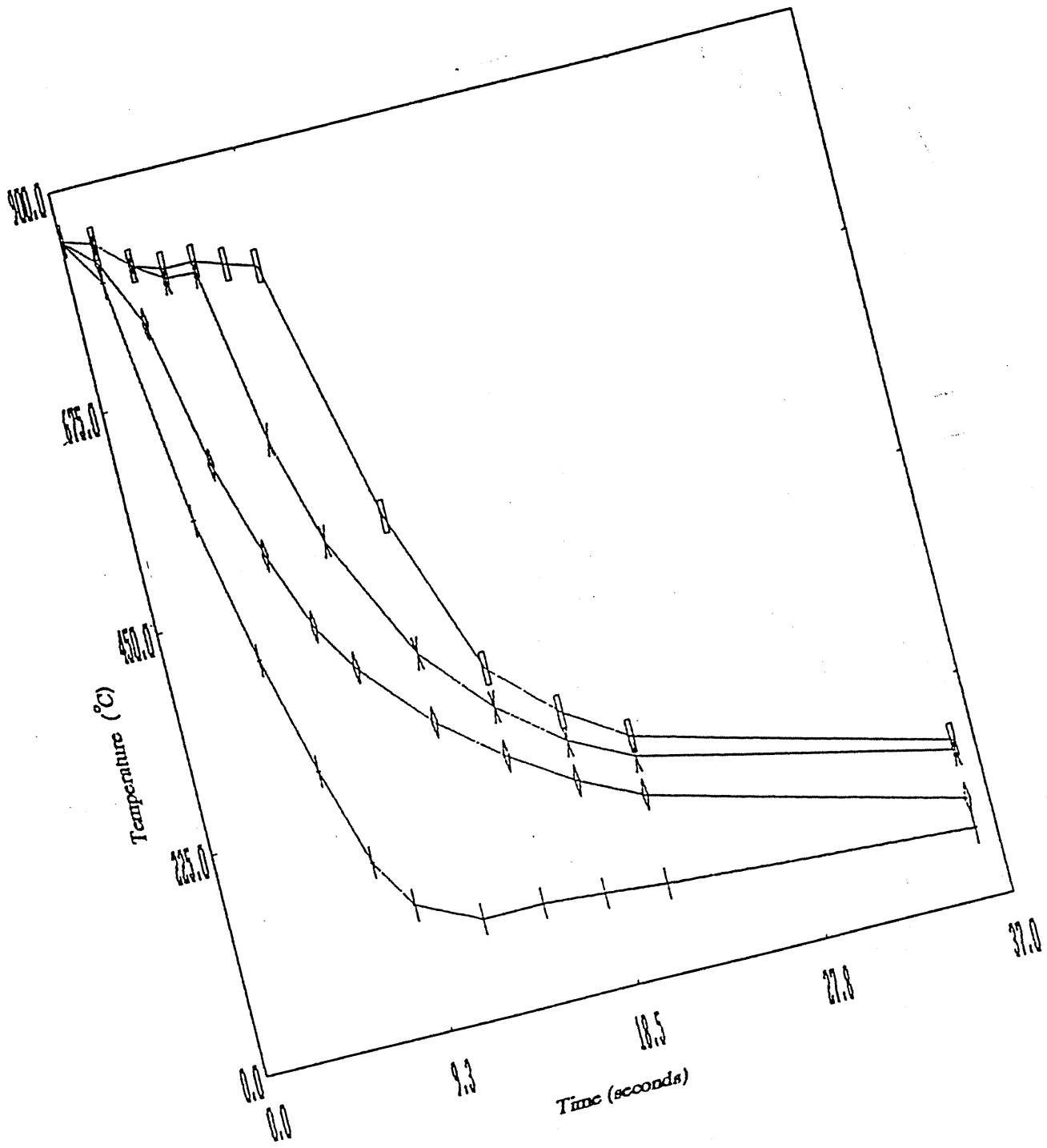
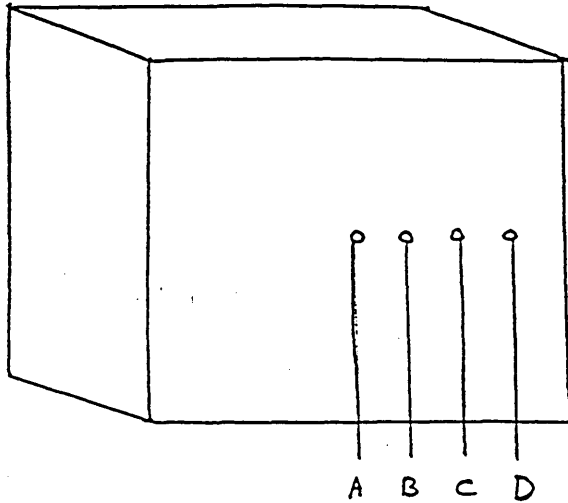
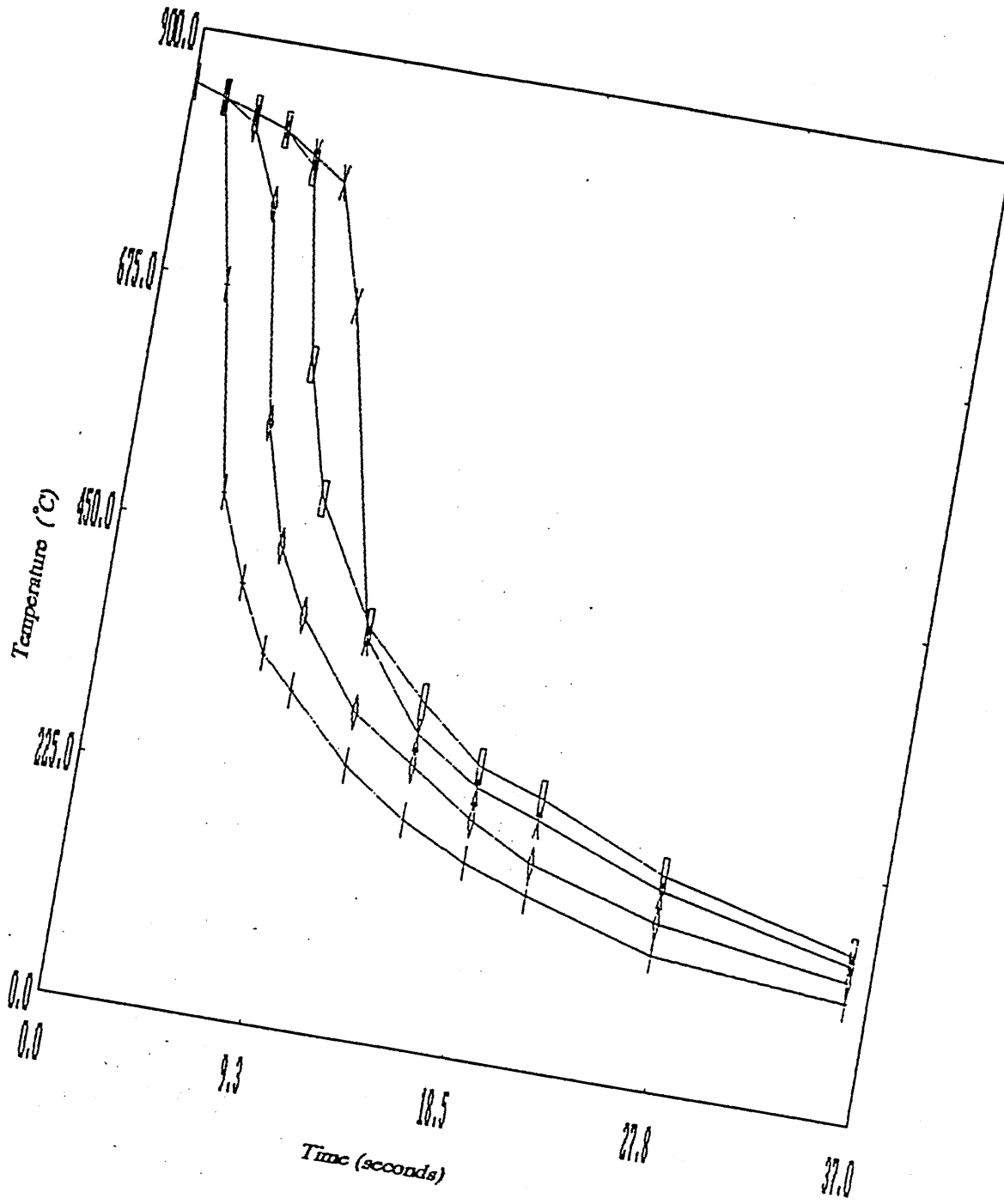


Fig (25)

Average cooling curve of 3 experiments of thermocouple positions along mid section through the face centre of the plate quenched vertically in water, where ϕ , $*$, ϕ & $+$ represent the centre (A), two intermediates (B,C), and side edge (D) respectively.

Schematic representation of the plate.





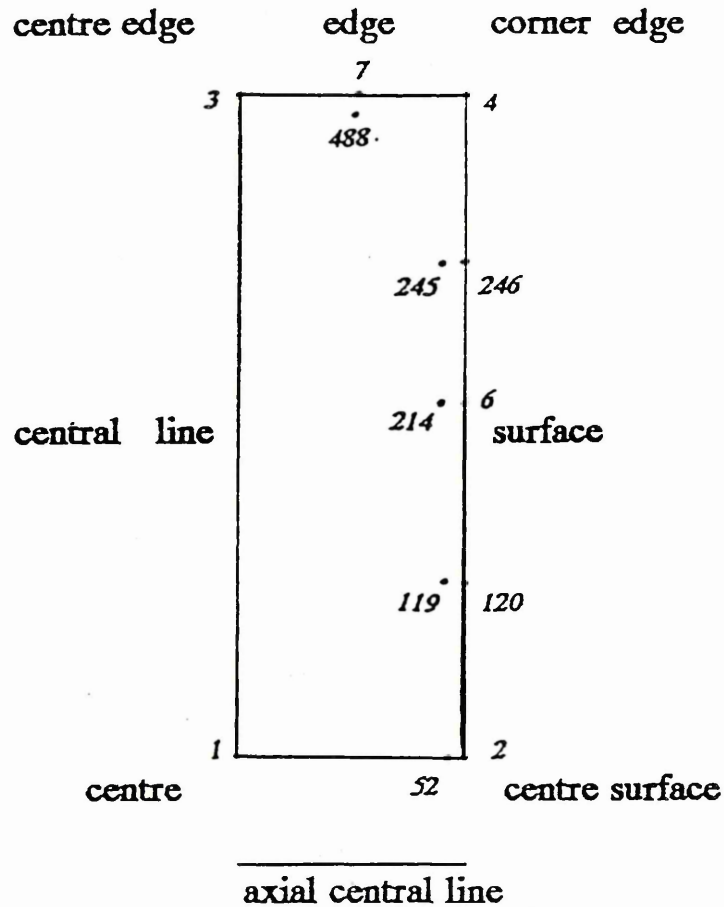


Fig 26

Shows thermocouple position relative to the specific nodal positions used in the finite element calculations.

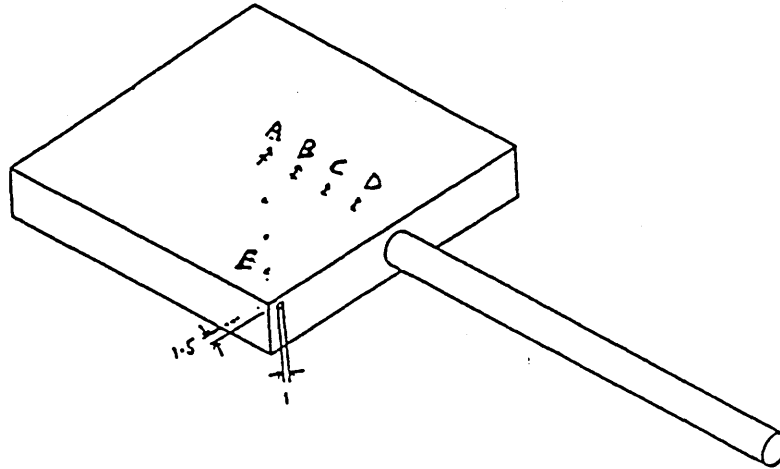
Nodes; 2,120,6,246,4,7 and 3 are placed around the face surface of the plate.

Nodes; 52,119,214,245 and 488 are placed at a points 1.5mm below the subsurface.

This latter group represents the points of the hot junction of the thermocouple.

Figure 27

Average cooling curve of 3 experiments of thermocouple positions along top face of the plate quenched horizontally in water, where A,B,C,D,& E represent the centre-surface (A), two intermediates (B&C), top edge (D) and corner edge (E) respectively.



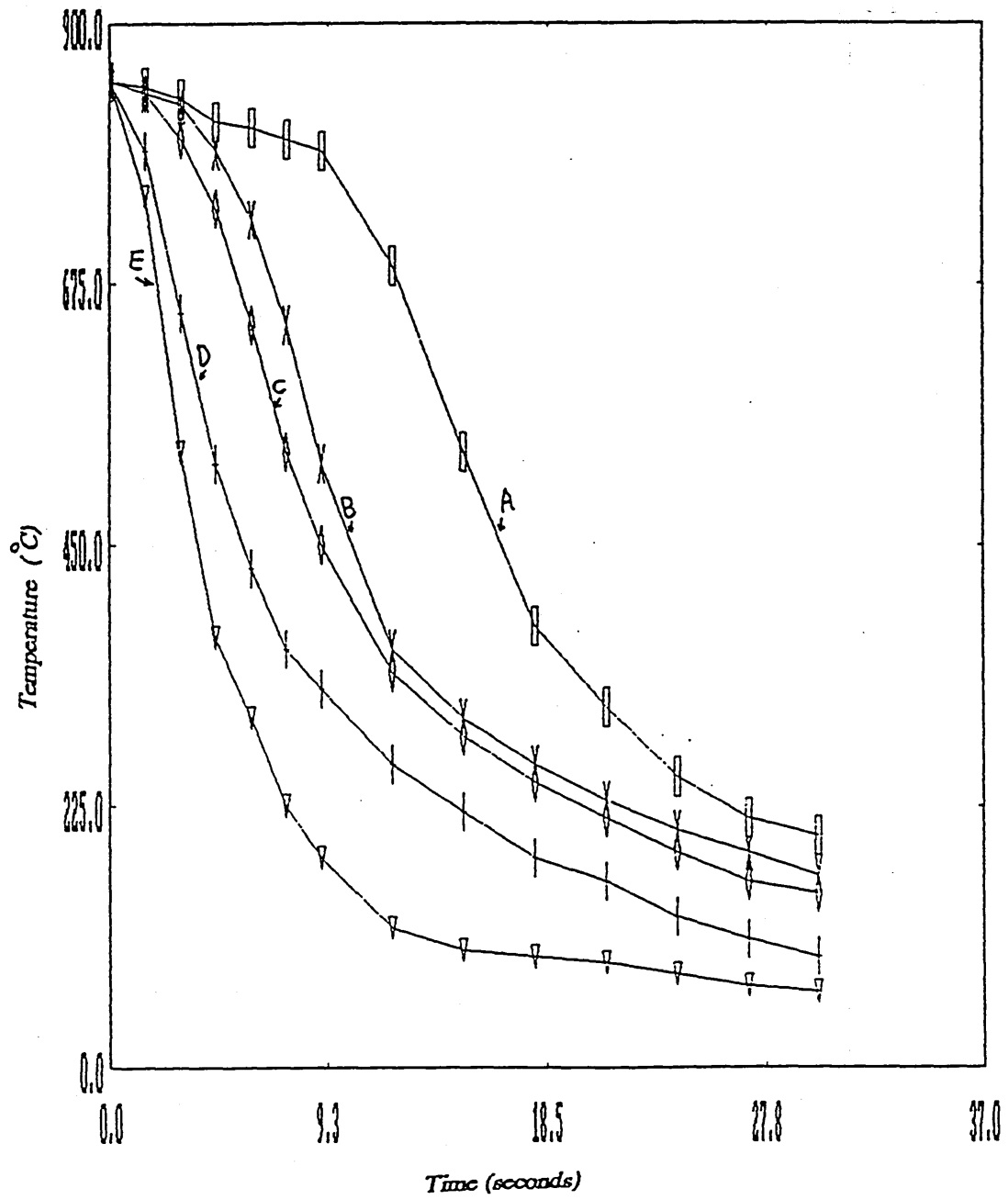
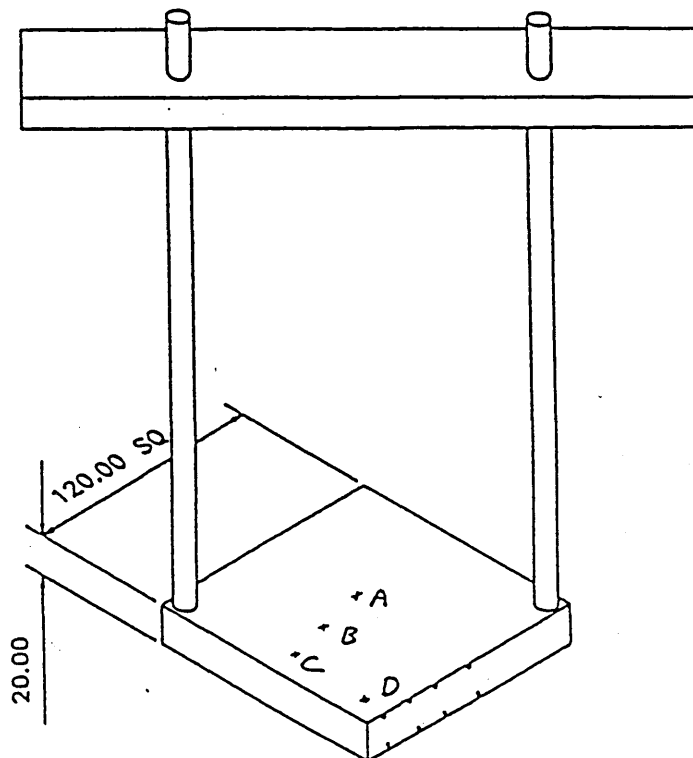


Figure 28

Average cooling curve of 3 experiments of thermocouple positions along bottom face the plate quenched horizontally in water, where A,B,C,D represent the centre-surface (A), intermediate (B), top edge (C) and corner edge (D) respectively.



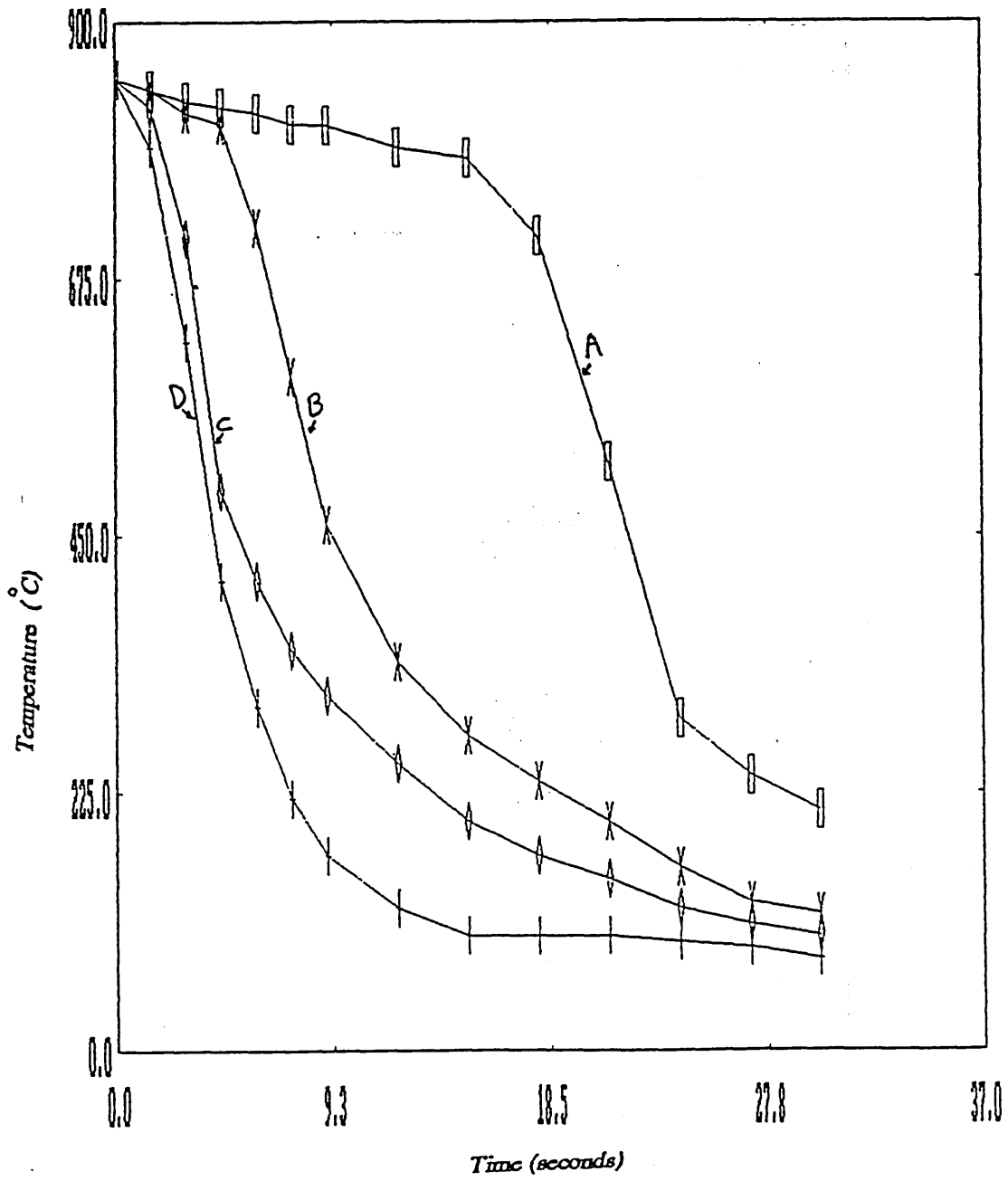


Fig 29

Surface heat transfer coefficient (WmK^{-2-1}) against surface temperature $^{\circ}C$, where $\square, \times, \diamond$ and $+$ represent the centre A, two intermediates (B,C) and top edge D respectively along the upper half of a vertical section through the centre of the face of the plate in a vertical quench.
Ref to schematic representation of fig 21.

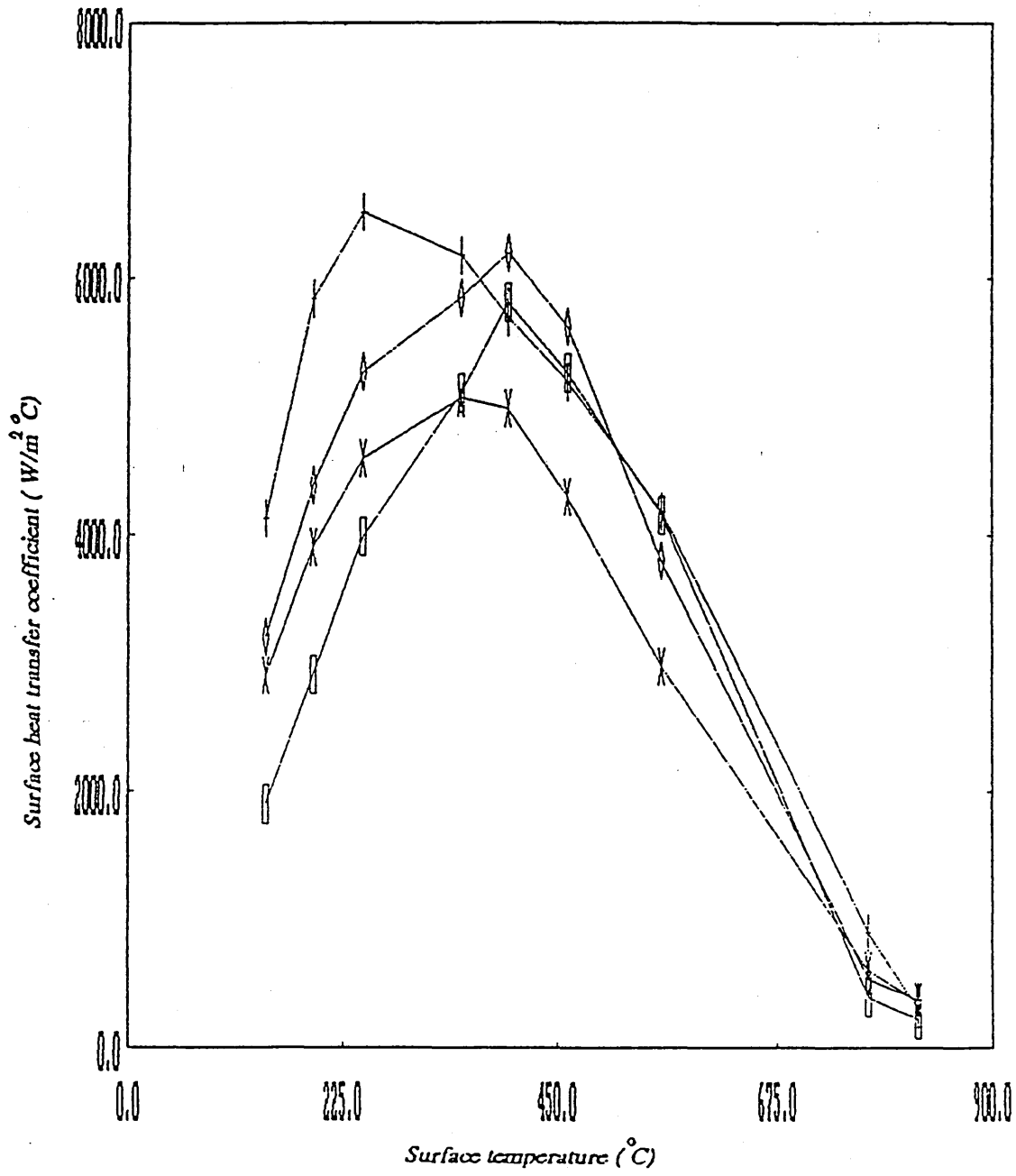


Fig 30

Surface heat transfer coefficient (WmK^{-2-1}) against surface temperature $^{\circ}C$, where $\square, \times, \diamond$ and $+$ represent the centre A, two intermediates B & C and lower edge D respectively along the lower half of a vertical section through the face of the plate in a vertical quench.

Ref to schematic representation of fig 22.

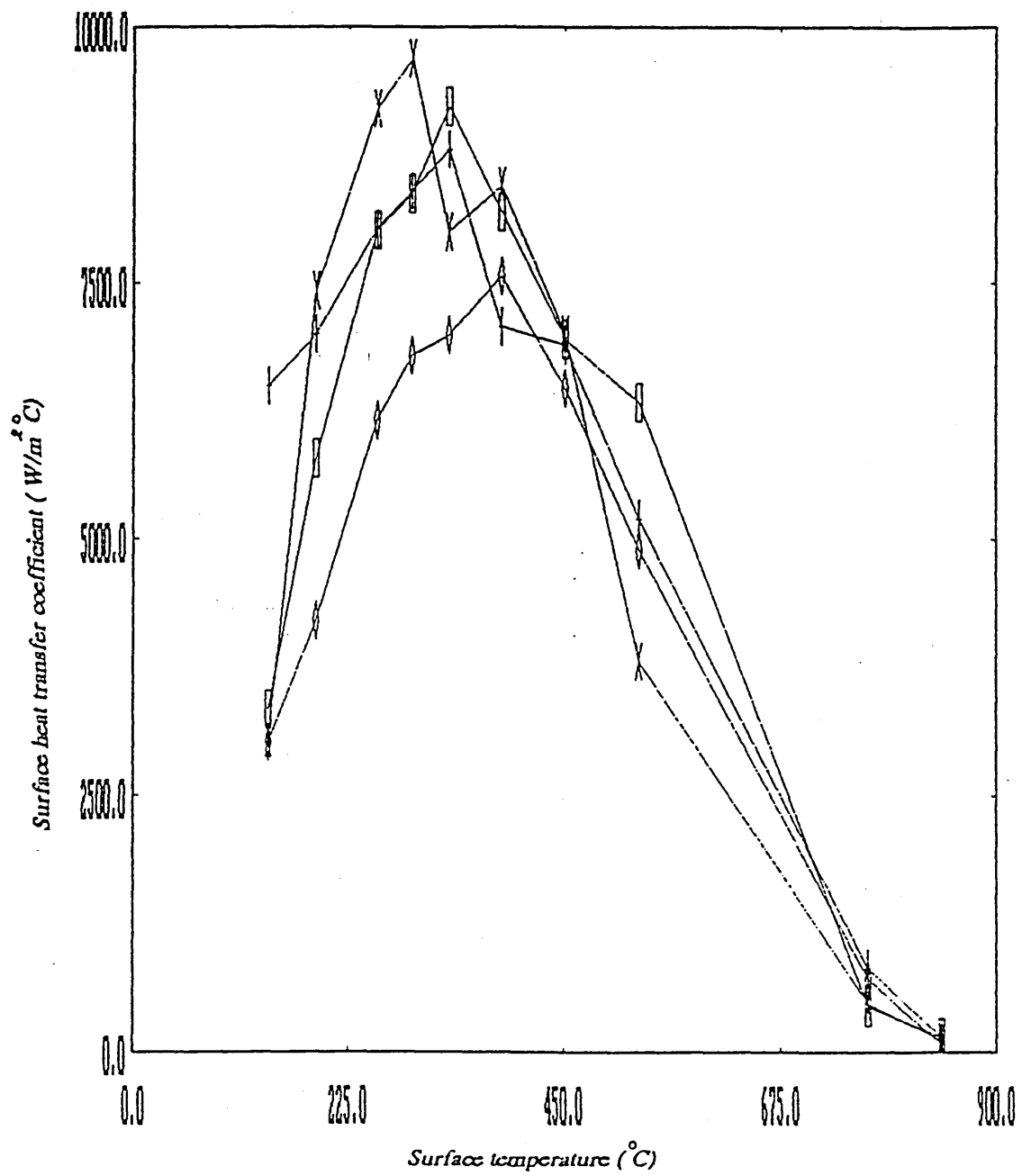


Fig 31

Surface heat transfer coefficient ($\text{Wm}^{-2}\text{K}^{-1}$) against surface temperature $^{\circ}\text{C}$, where \ddagger, \ast, \oplus and \dagger represent the centre A, two intermediates B & C and corner edge D respectively along the upper half of the diagonal face of the plate in vertical quench.

Ref to schematic representation of fig 23.

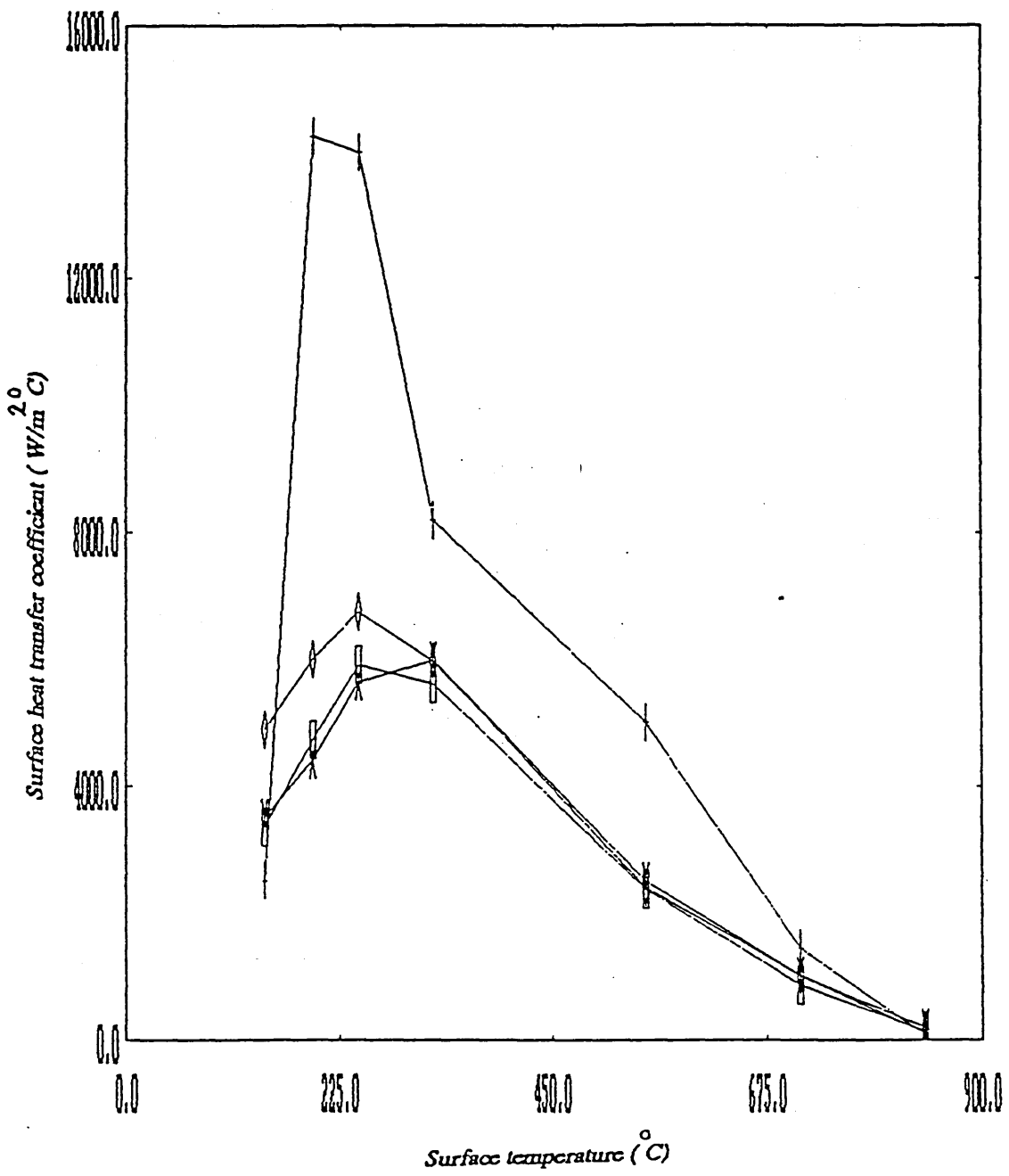


Fig 32

Surface heat transfer coefficient ($\text{Wm}^{-2}\text{K}^{-1}$) against surface temperature $^{\circ}\text{C}$, where \oplus , \times , \diamond and \dagger represent the centre A, two intermediates B & C and corner edge D respectively along lower half of the diagonal face of the plate quenched vertically in water.

Ref to schematic representation of fig 24.

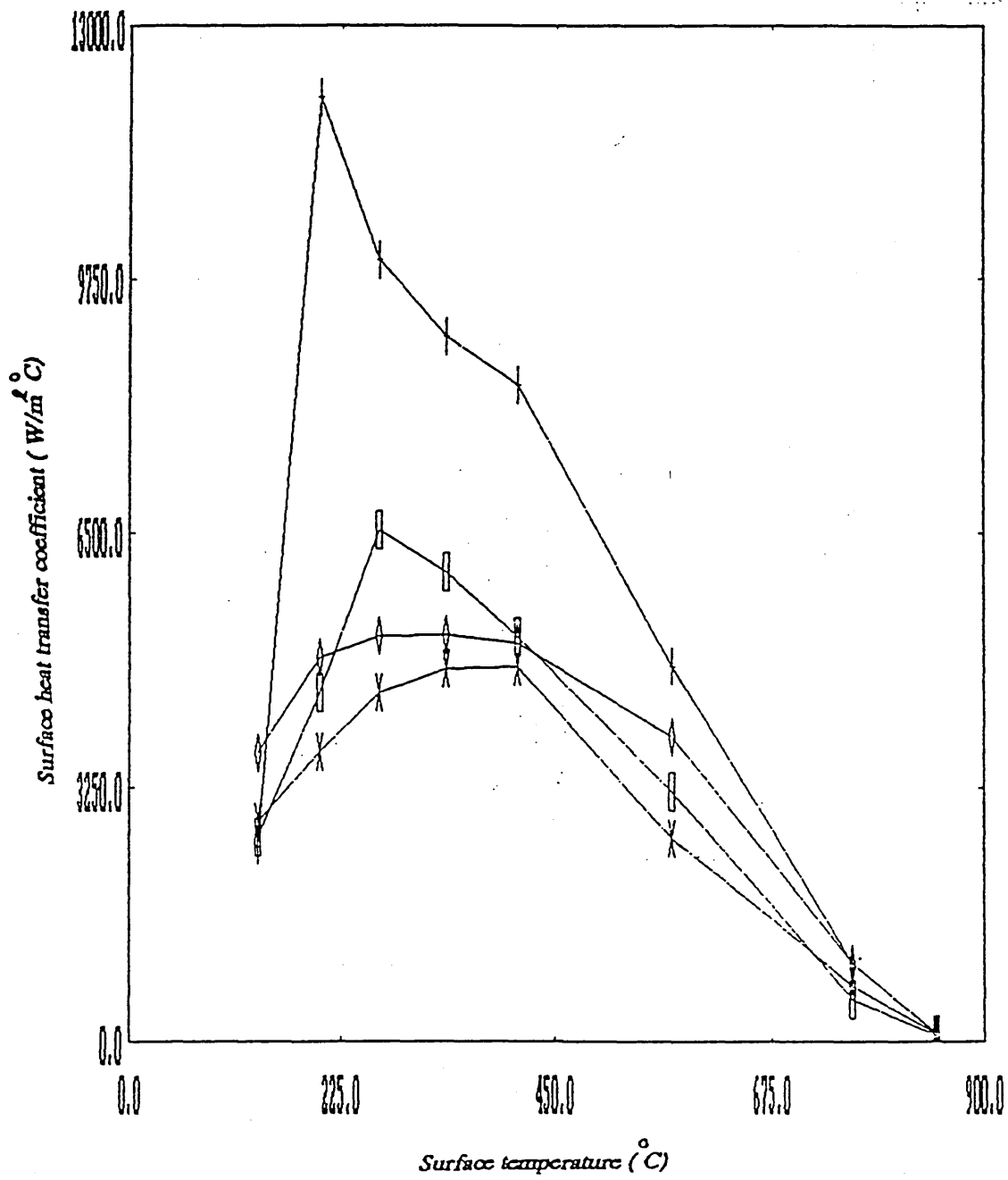


Fig 33

Surface heat transfer coefficient (WmK^{-2-1}) against surface temperature $^{\circ}C$, where \square , \times , \diamond and \dagger represent the centre A, two intermediates B & C and side edge D respectively along the horizontal mid section through the face centre of the plate quenched vertically in water.

Ref to schematic representation of fig 25.

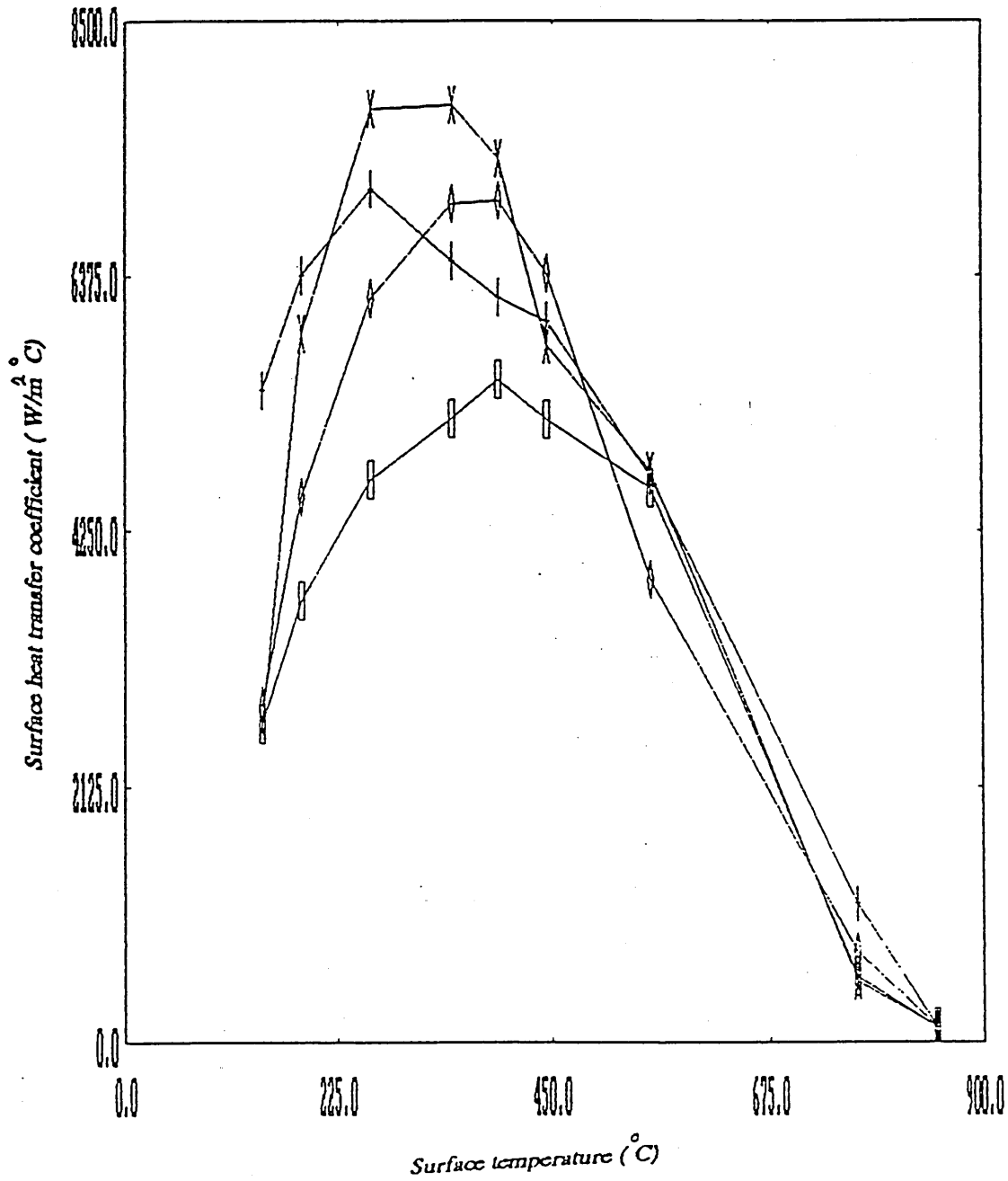
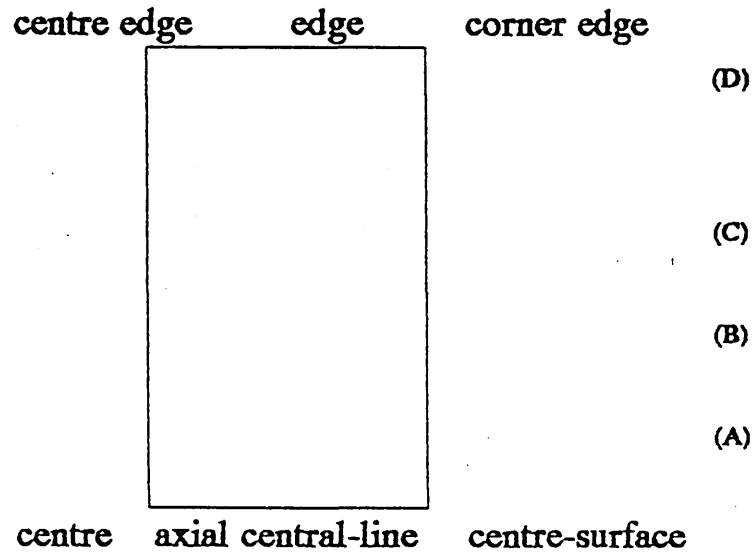
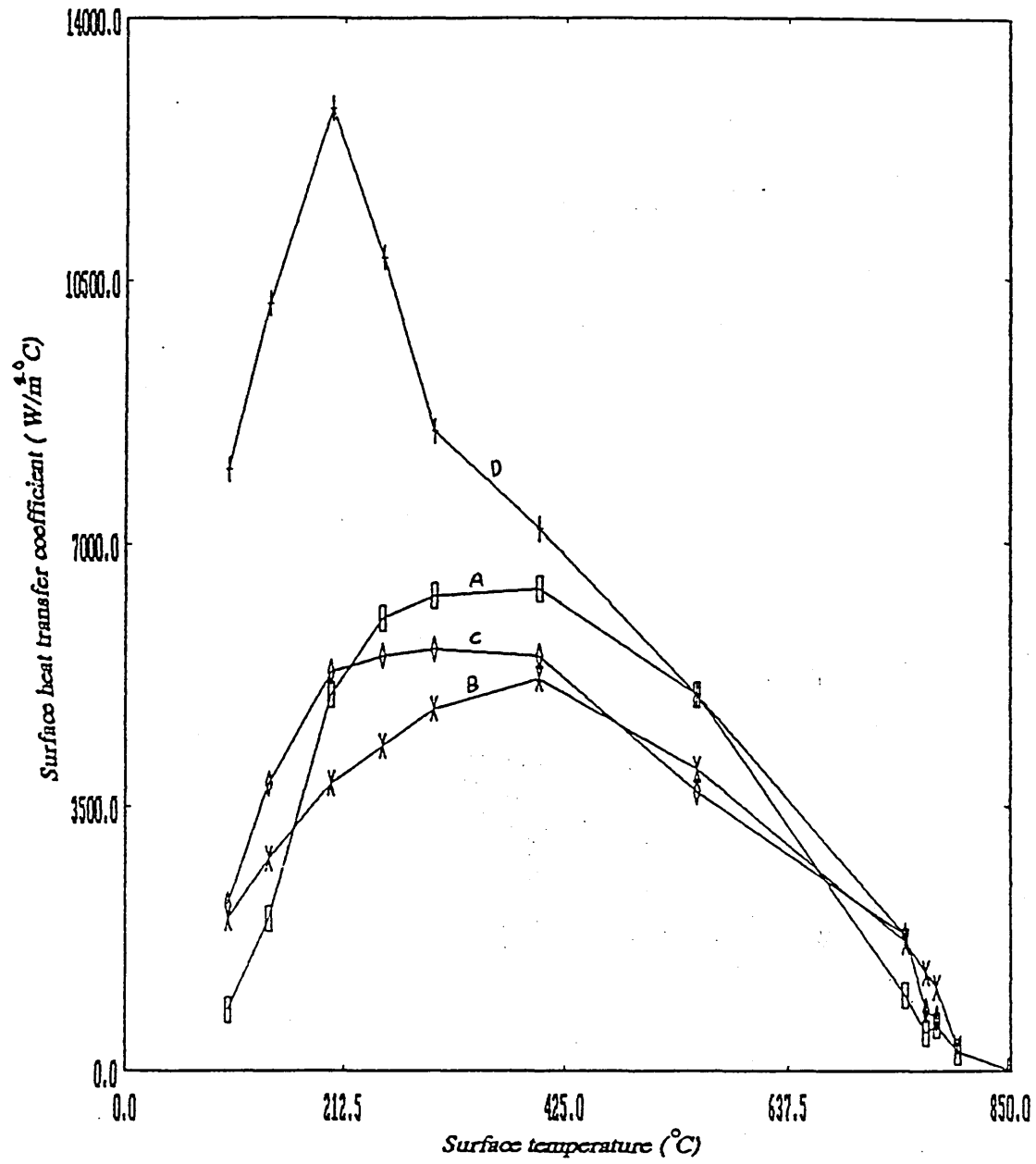


Figure 34

Average of surface heat transfer coefficient ($W m^{-2} K^{-1}$) against surface temperature $^{\circ}C$, where A,B,C and D represent the centre surface (A), two intermediates (B&C) and corner edge (D) respectively through the thickness of the plate in a vertical quench.

Schematic representation of the section through the thickness of the plate.





⊕ A

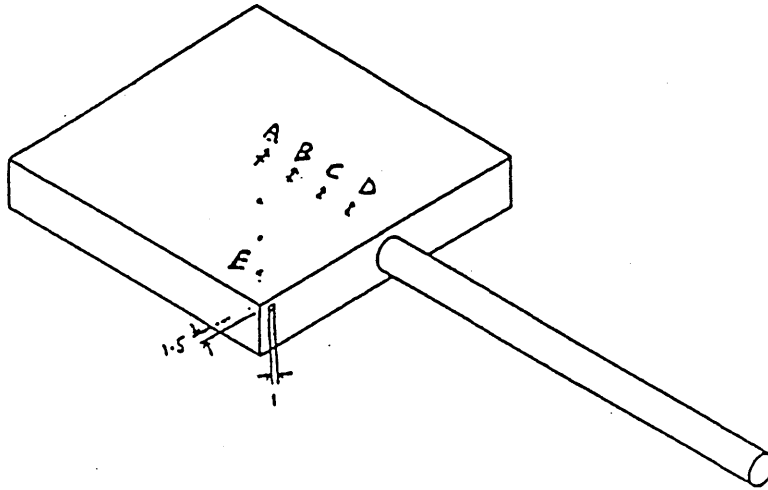
× B

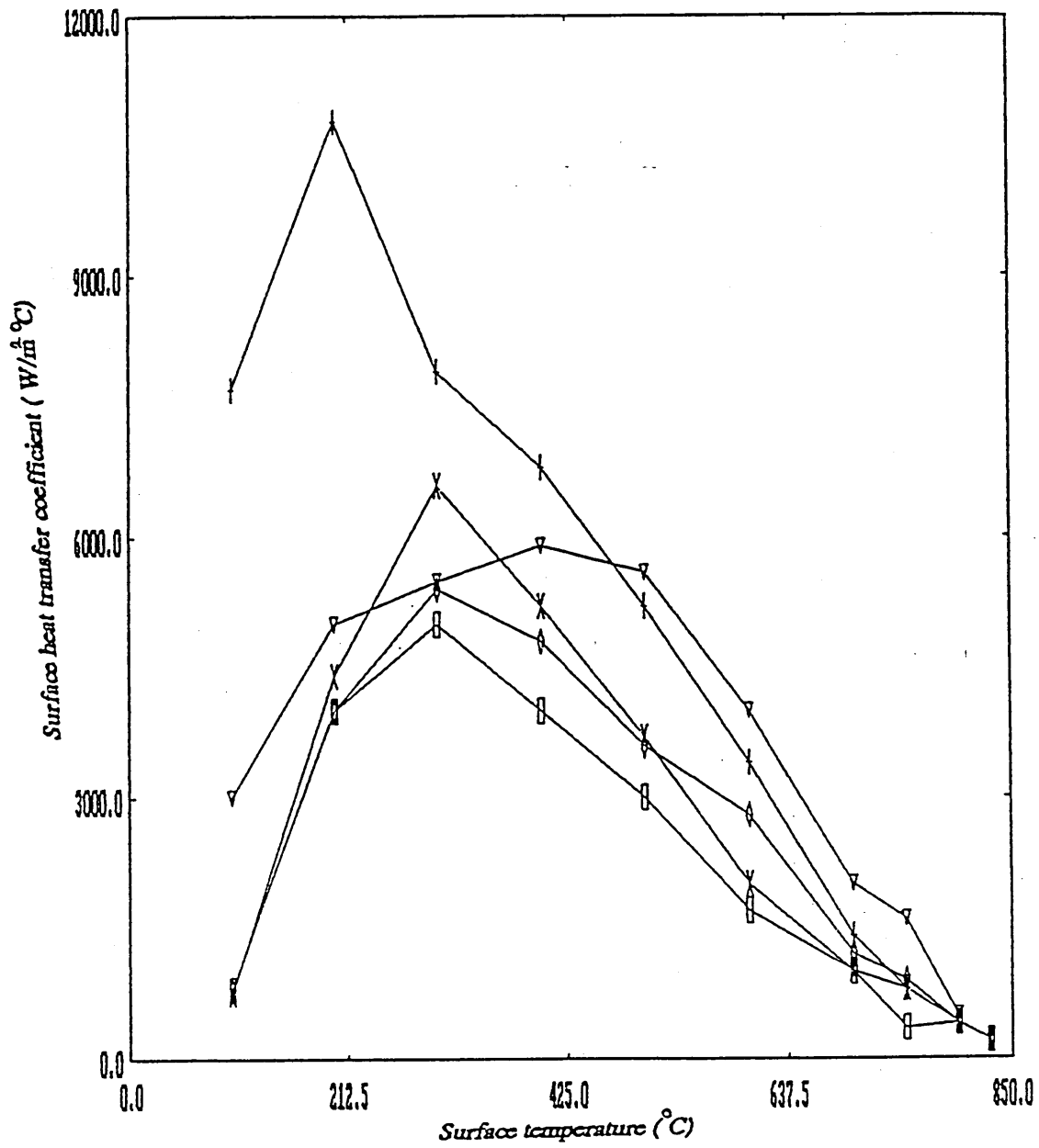
⊕ C

+ D

Figure 35

Average of surface heat transfer coefficient ($W m^{-2} K^{-1}$) against surface temperature $^{\circ}C$, where \ddagger , \ast , \diamond , ∇ & \dagger represent the centre surface (A), two intermediates (B&C) and top edge (D) & corner edge (E) respectively through the thickness of the plate by considering the top face of the plate in horizontal quench.





⊕ A

⊗ B

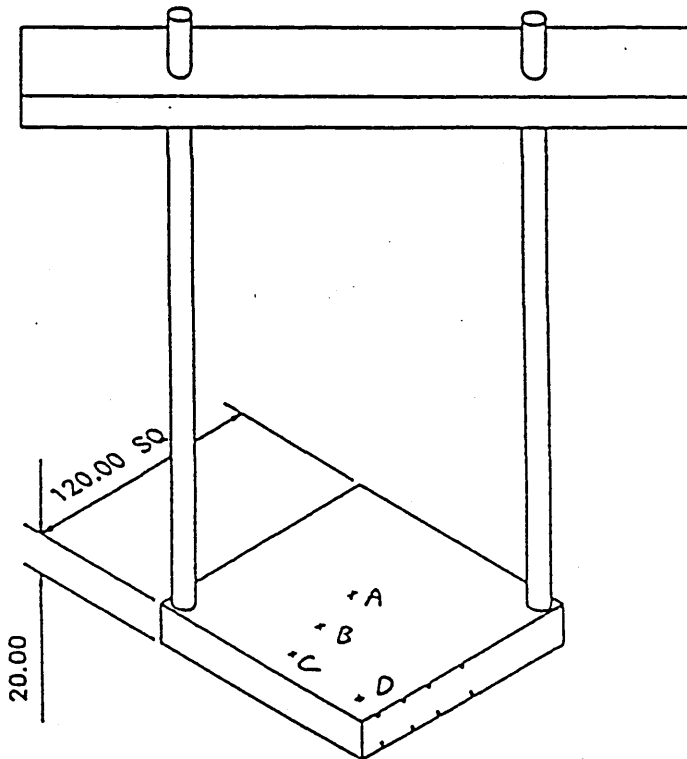
⊕ C

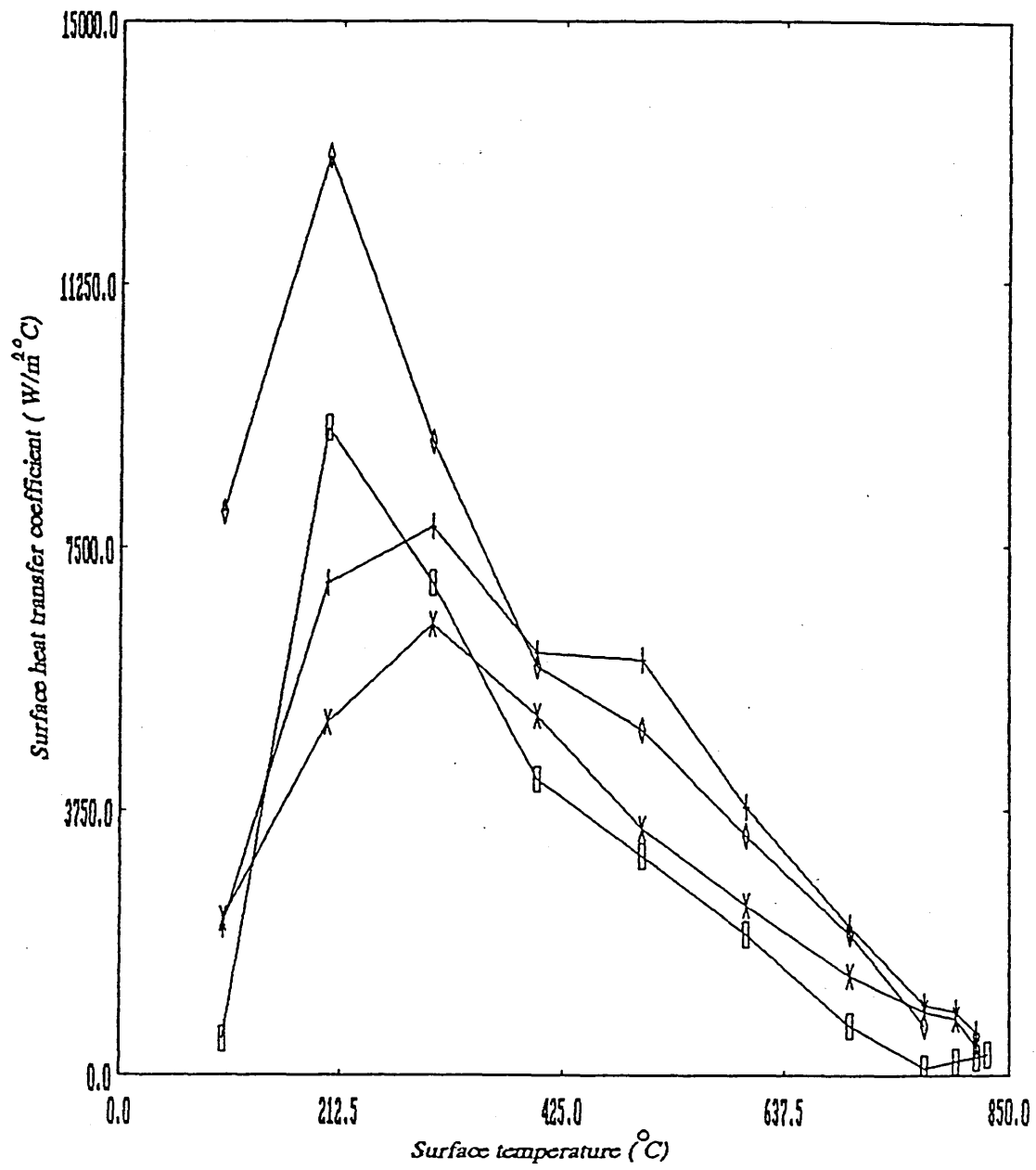
⊗ D

⊕ E

Figure 36

Average of surface heat transfer coefficient ($W m^{-2} K^{-1}$) against surface temperature $^{\circ}C$, where \oplus , \otimes , \dagger & \diamond represent the centre surface (A), intermediate (B), top edge (C) and corner edge (D) respectively through the thickness of the plate by considering the bottom face of the plate in horizontal quench.





A

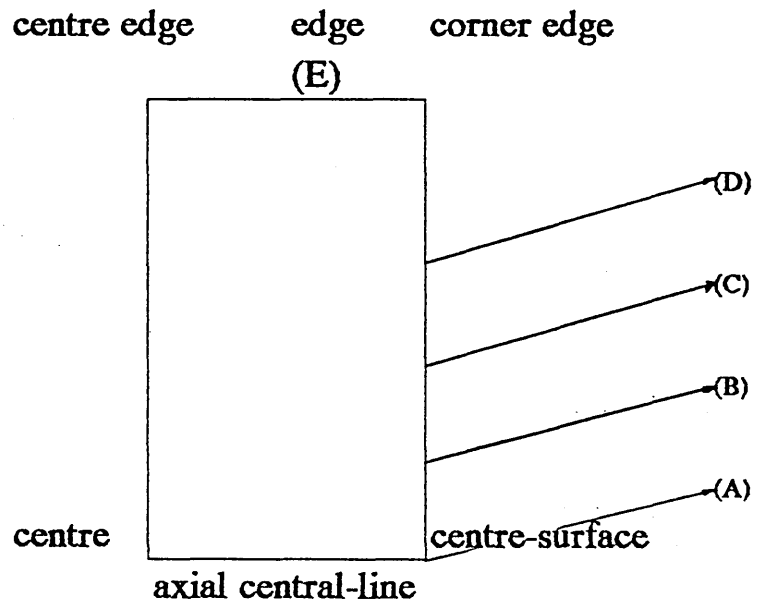
x B

+ C

+ D

Figure 37

Predicted relationships between time & temperature for the two dimensional heat flow case using constant surface heat transfer coefficient in a vertical quench, where \square , \times , \diamond , \dagger and ∇ represent the centre-surface (A), two intermediate (B&C), corner edge (D) and (E) top edge respectively. Calculation using the Finite Element Technique.



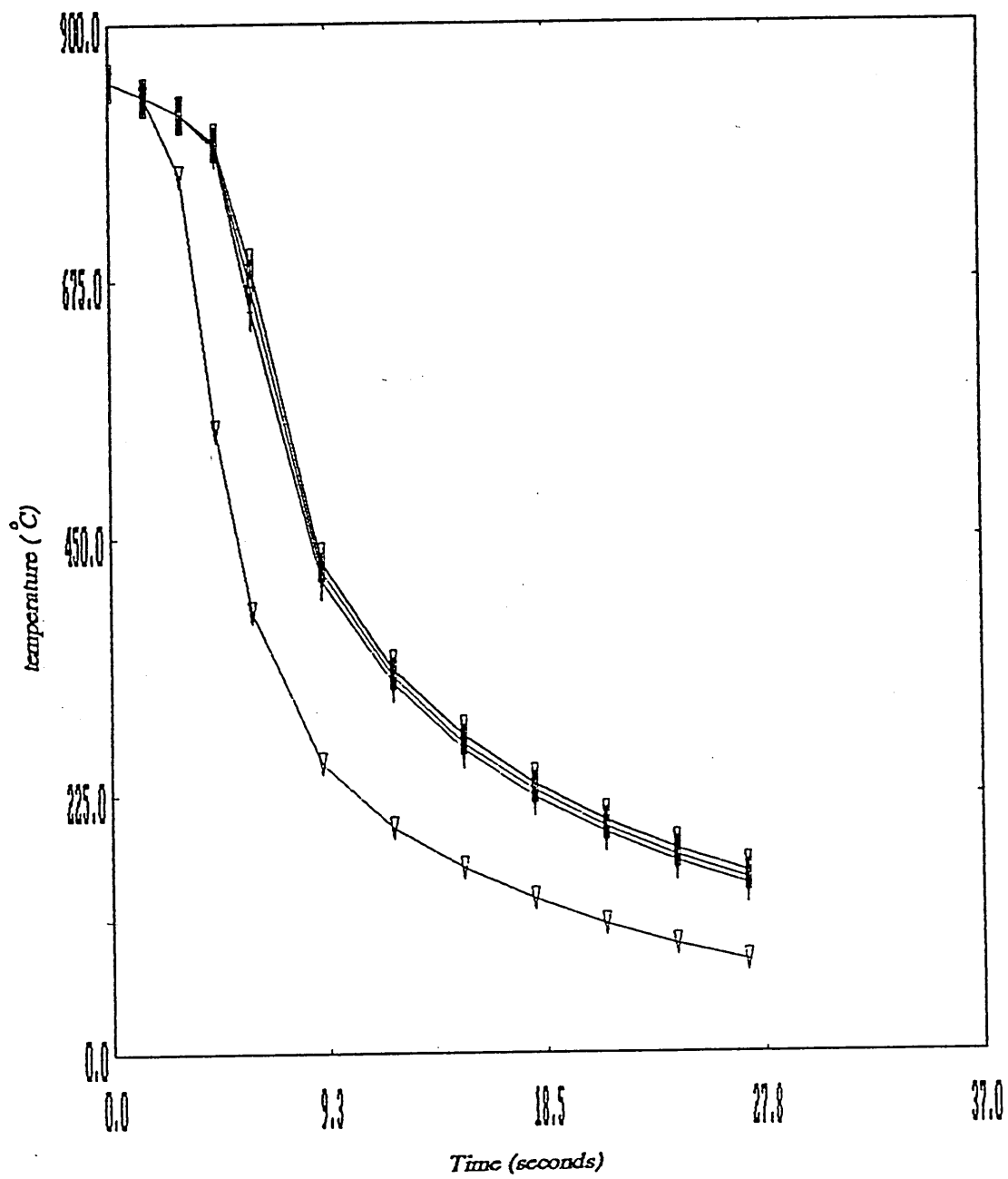
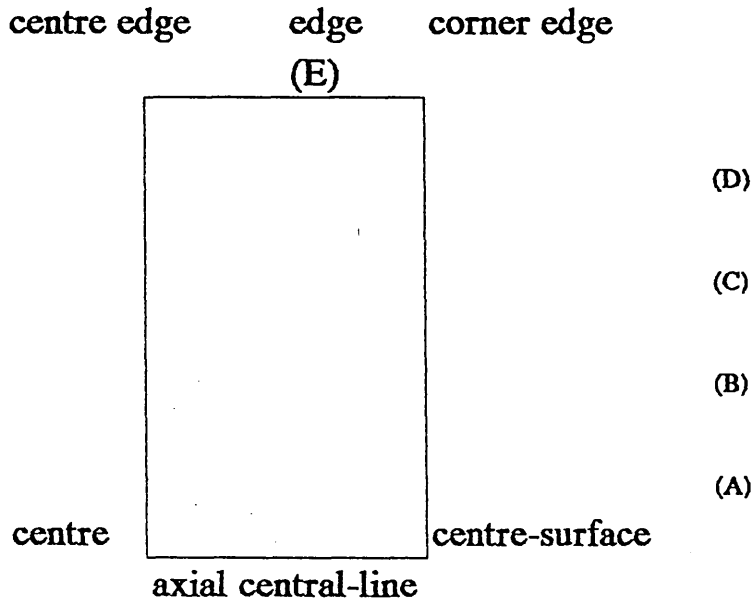


Figure 38

Predicted relationships between time & temperature for the two dimensional heat flow case of a water using variable surface heat transfer coefficient in a vertical quench, where \square , \times , \diamond , $+$, \triangle represent the centre-surface (A), two intermediate (B&C), corner edge (D) and (E) top edge respectively. Calculation using the Finite Element Technique.



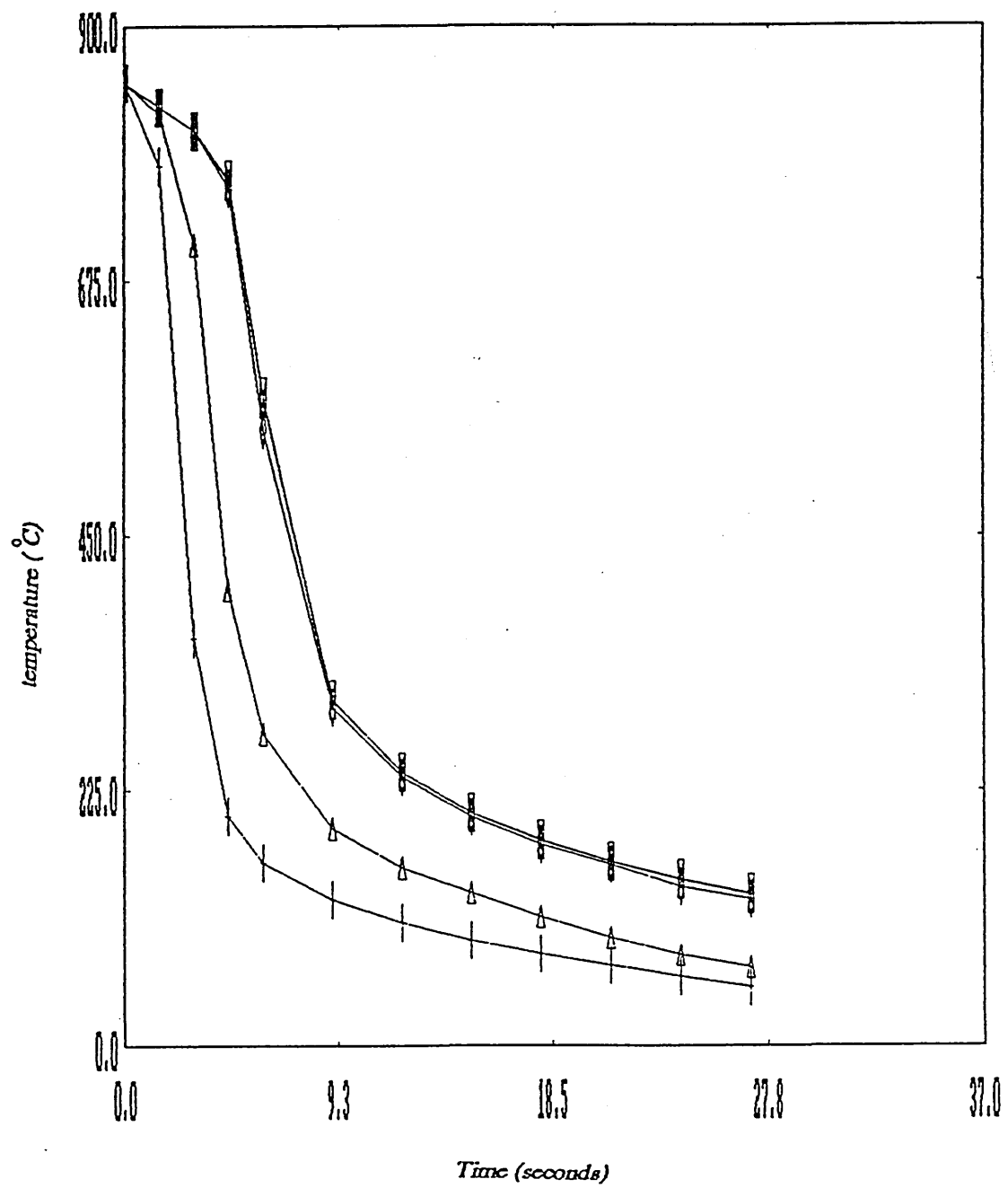
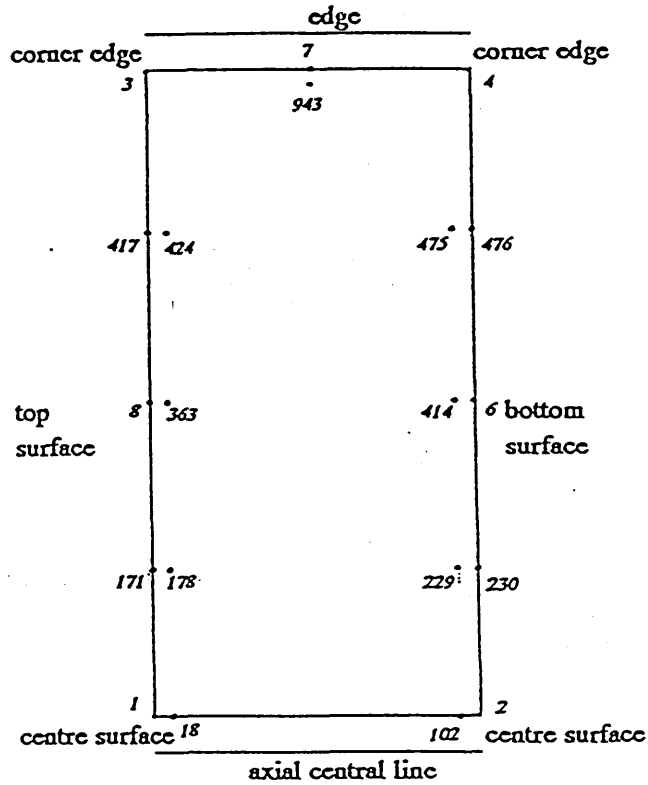


Figure 39

Predicted temperature profiles for the 2-D heat flow case of a horizontal quenched plate by finite element programme using constant 'h', where \square , \times , \diamond , $+$, ∇ & \triangle are the representative of nodes 102 centre, 229 intermediate, 475 corner edge, at bottom surface, 424 corner edge, 178 intermediate and 18 centre at top surface of the plate.



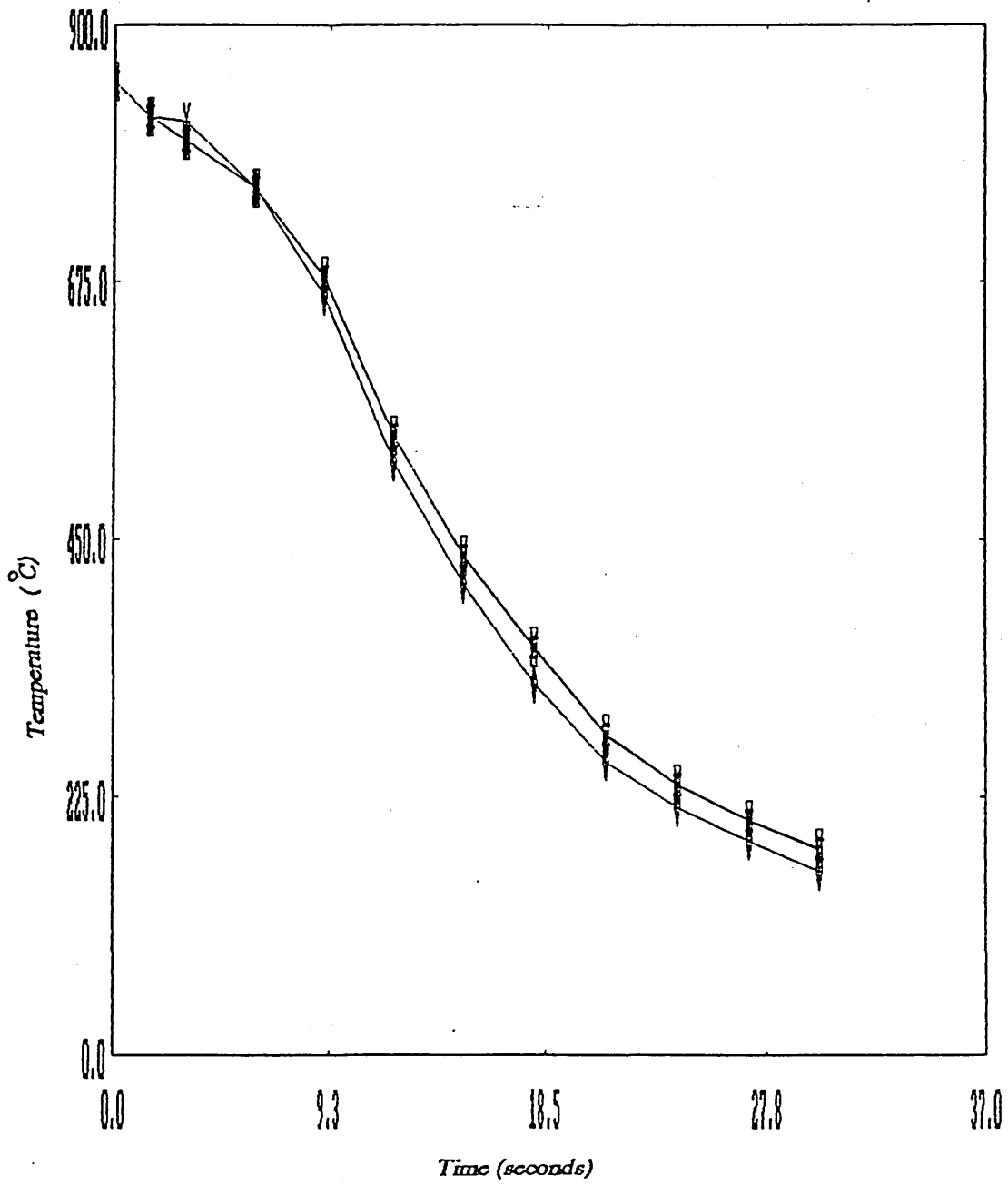
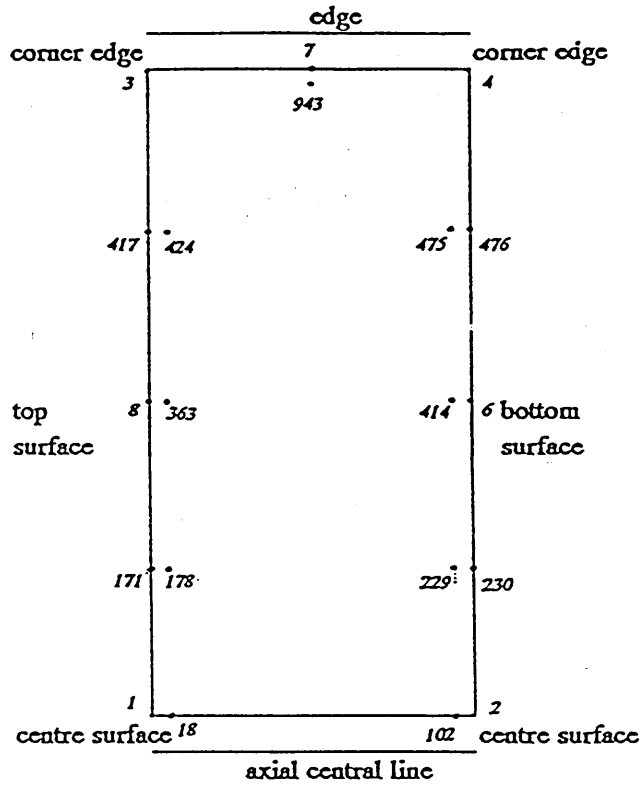


Figure 40

Predicted temperature profiles for the 2-D heat flow case of a horizontal quenched plate by finite element programme using variable 'h', where \square \times \diamond $+$ \triangle & \triangle are the representative of nodes 102 centre, 229 intermediate, 475 corner edge, 424 corner edge, 178 intermediate and 18 centre at both surface sides of the plate.



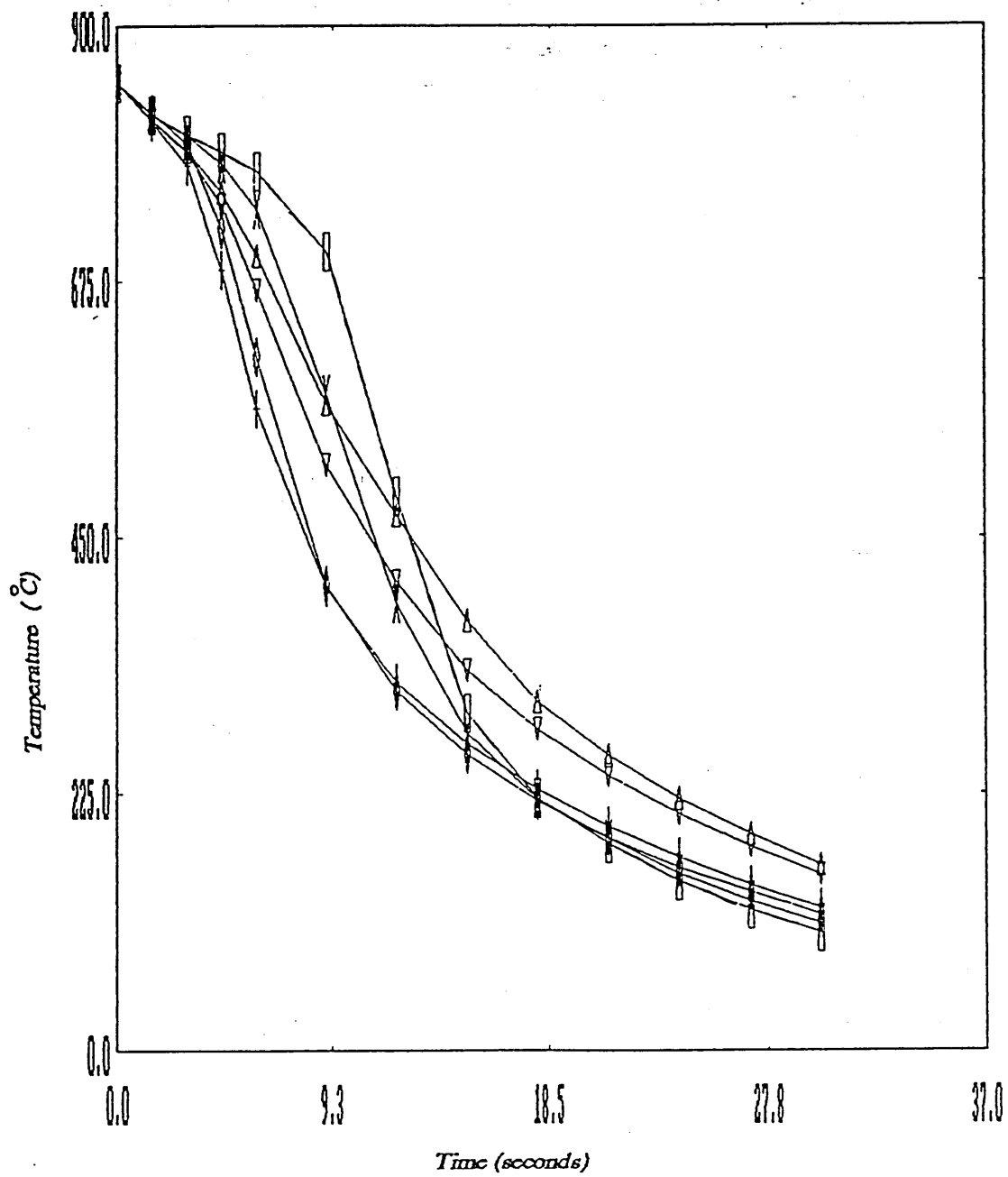


Fig 41

Face of a plate quenched vertically in water showing the vapour blanket stage.

Time = $1/3$ second.

Fig 42

Face of a plate quenched vertically in water showing the vapour blanket stage and evidence of Taylor waves in the vapour blanket.

Time = $2/3$ second.

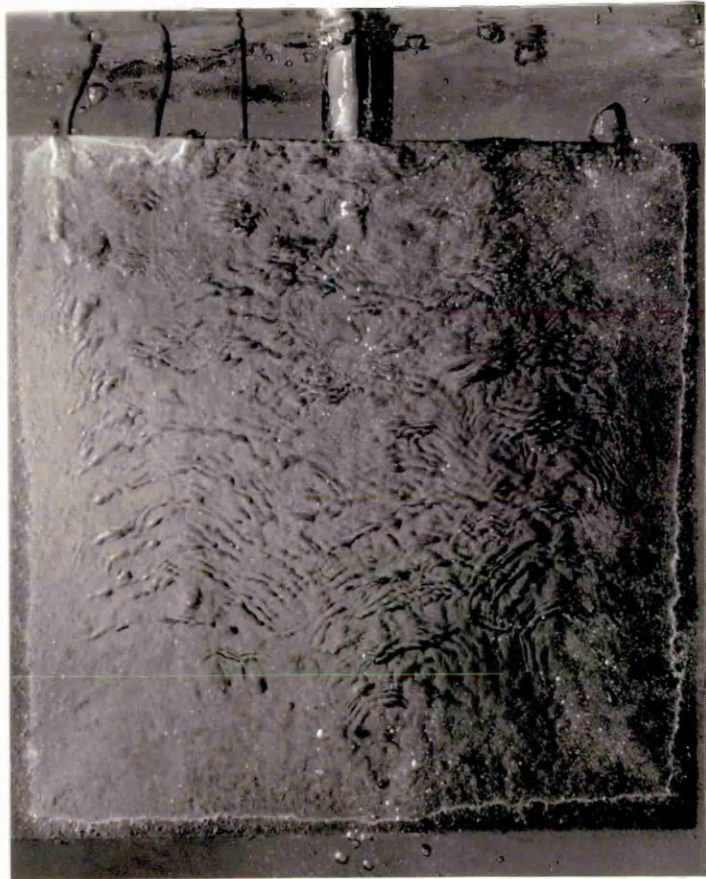
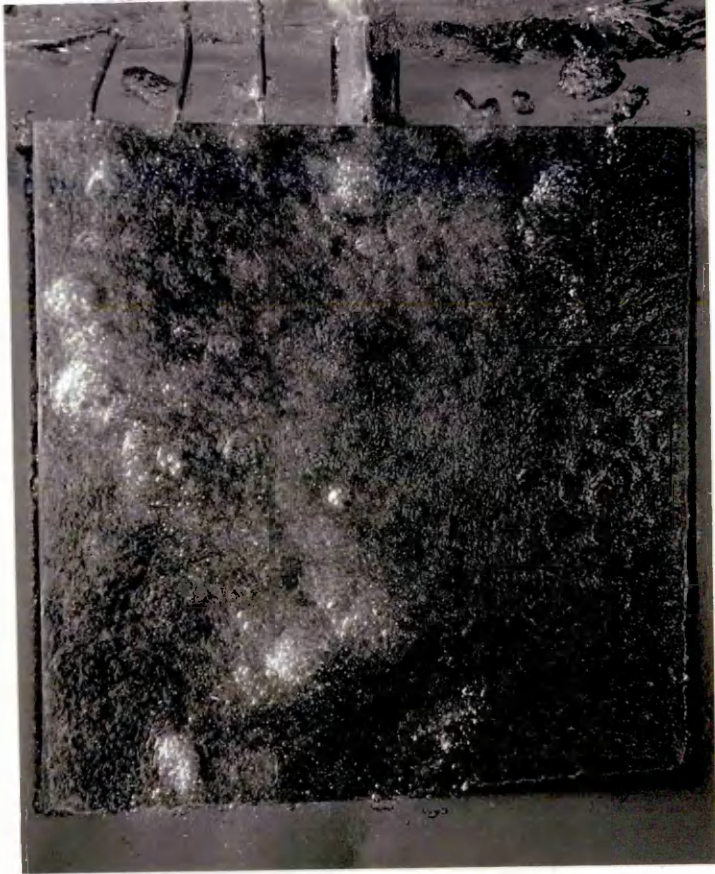


Fig 43

Face of a plate quenched vertically in water showing the appearance of the vapour blanket stage. Evidence of reappearing of Taylor waves which move towards top edge of the plate.

Time = $1\frac{1}{3}$ seconds.

Fig 44

Face of a plate quenched vertically in water showing the appearance of vapour blanket and nucleate boiling stages at corners representing the surface at about the period of the maximum surface heat transfer coefficient.

Time = 2 seconds.

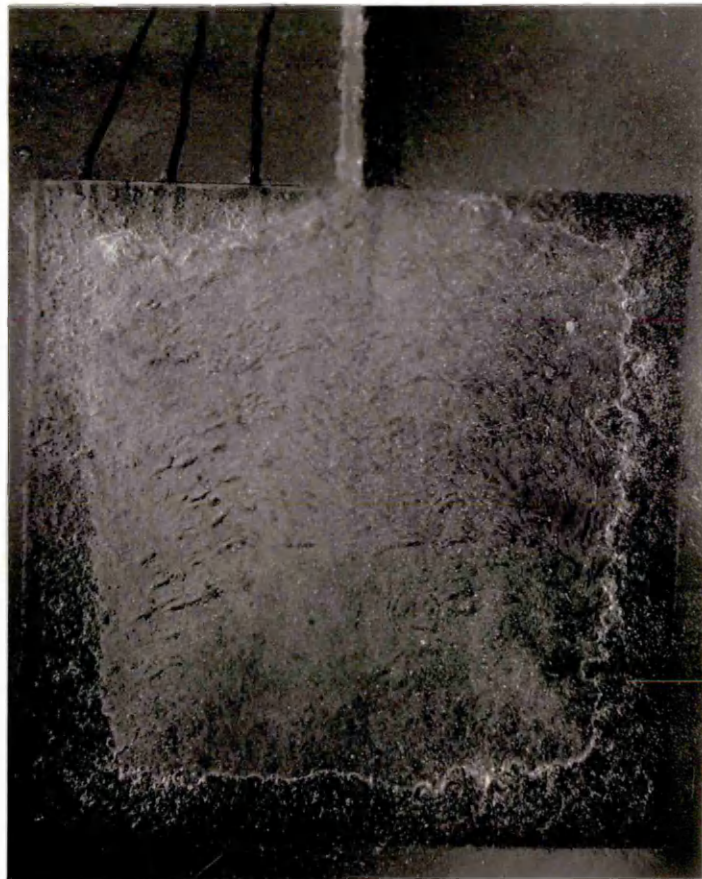


Fig 45

Face of a plate quenched vertically in water showing the reduction in vapour blanket and nucleate boiling stages at the surface of the plate.

Time = 7 seconds

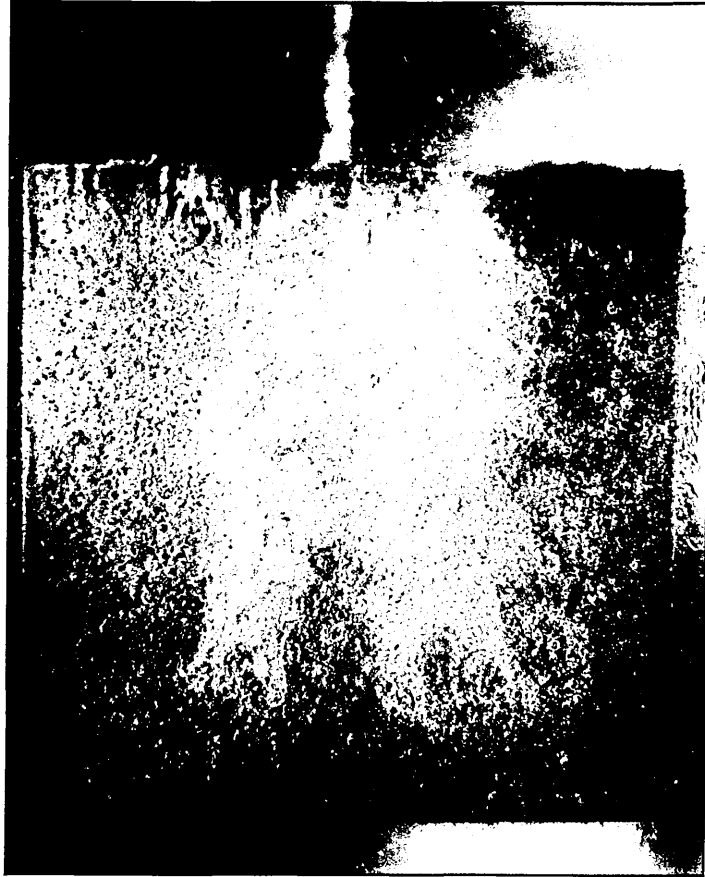


Fig 46

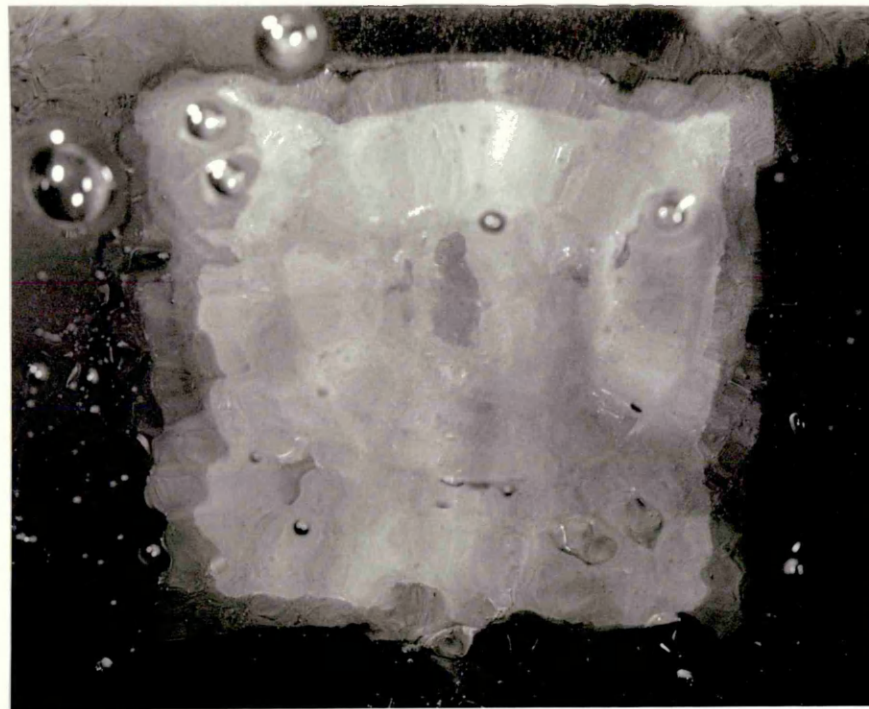
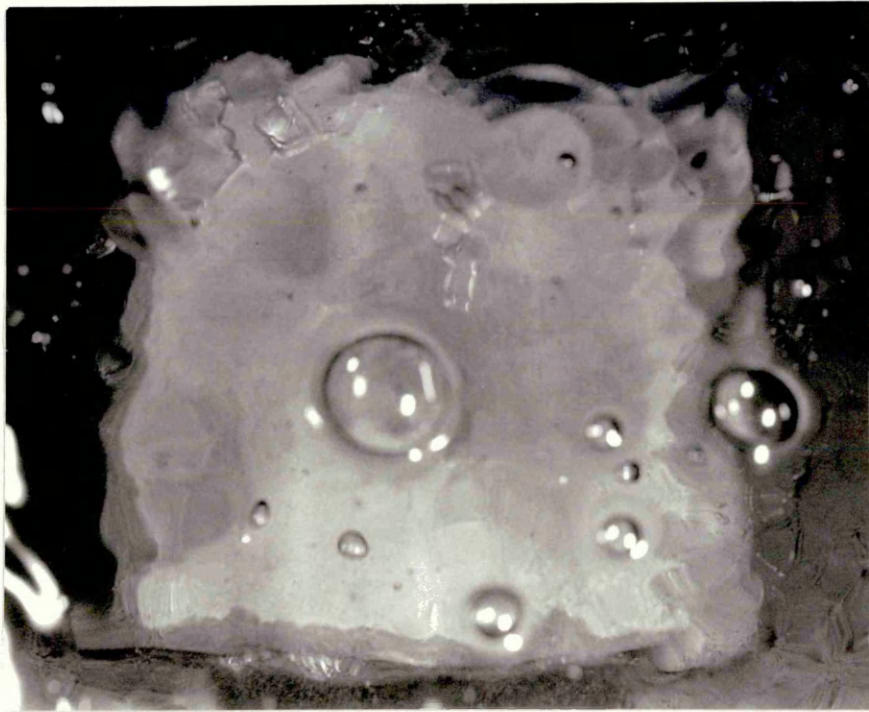
Face of a plate quenched vertically in water showing the appearance of Newtonian cooling stage.

Time=11 seconds

Figs (47-48)

Upper face of the plates quenched horizontally in water
showing the vapour blanket stage.

Time = $1\frac{1}{3}$ and 2 seconds



Figs (49-50)

Upper face of the plates quenched horizontally in water
showing the reduction in the vapour blanket stage.

Time=4.5 and 8.5 seconds

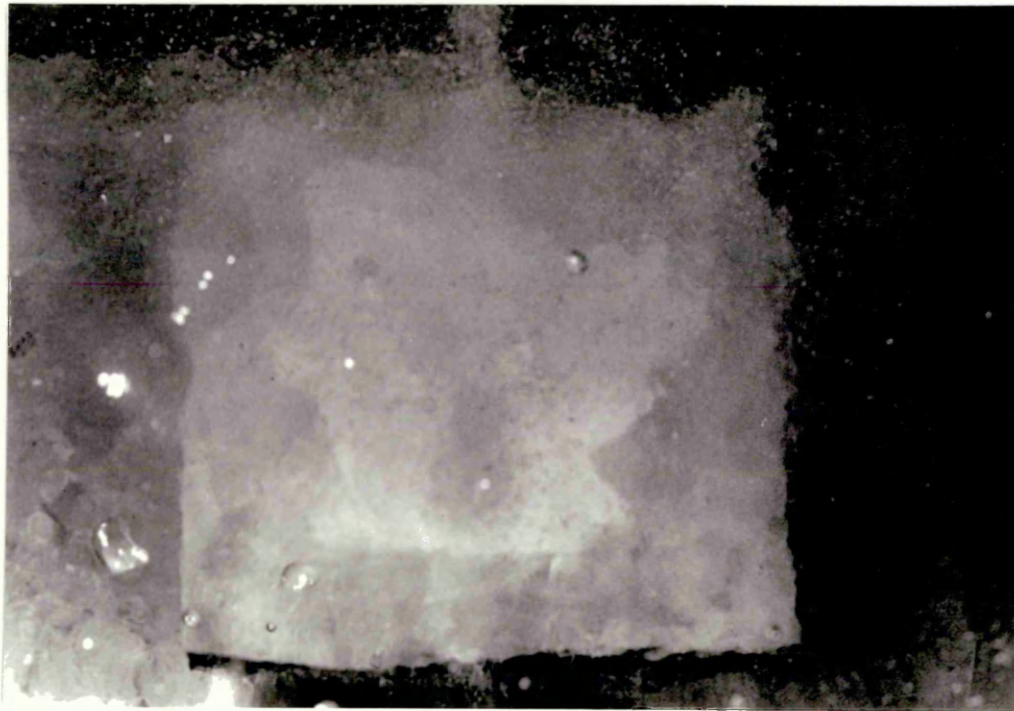
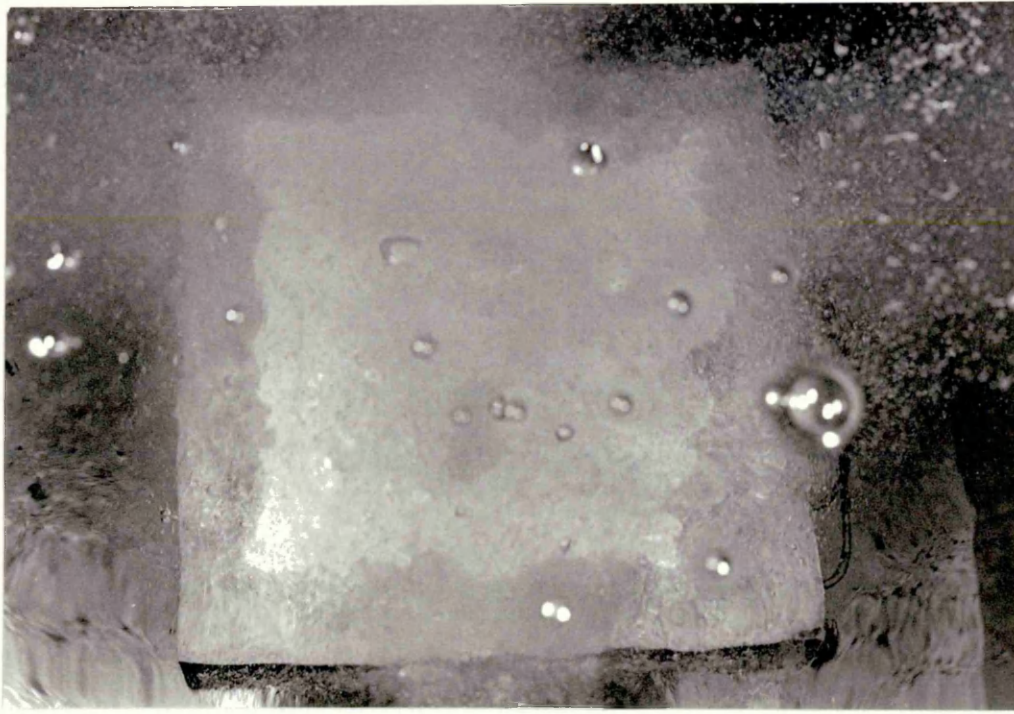


Fig 51

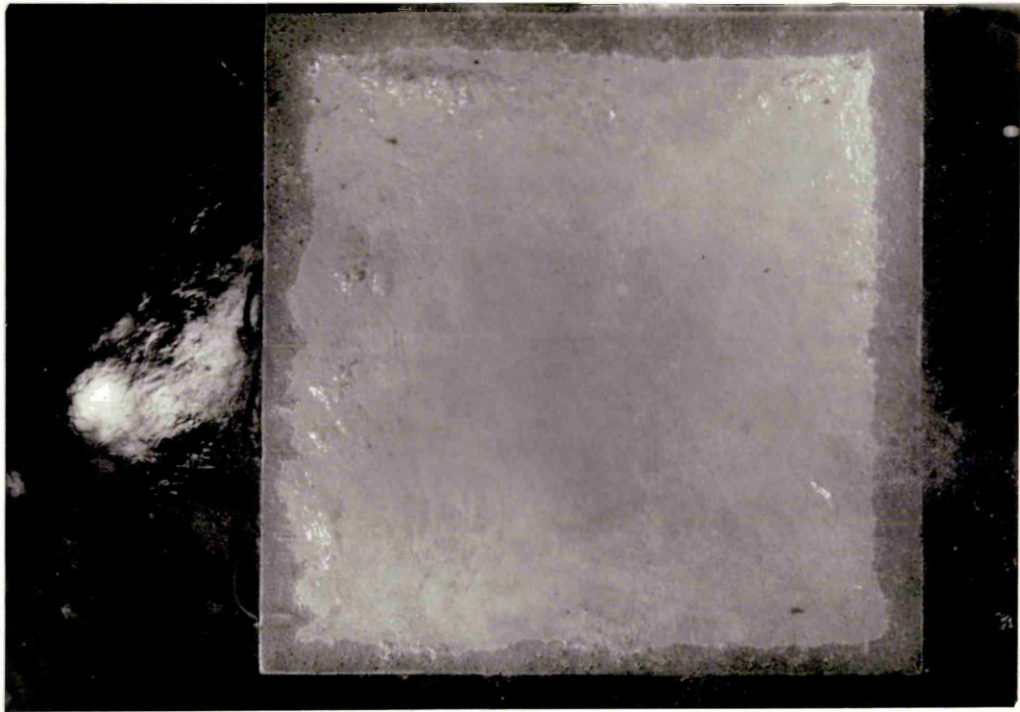
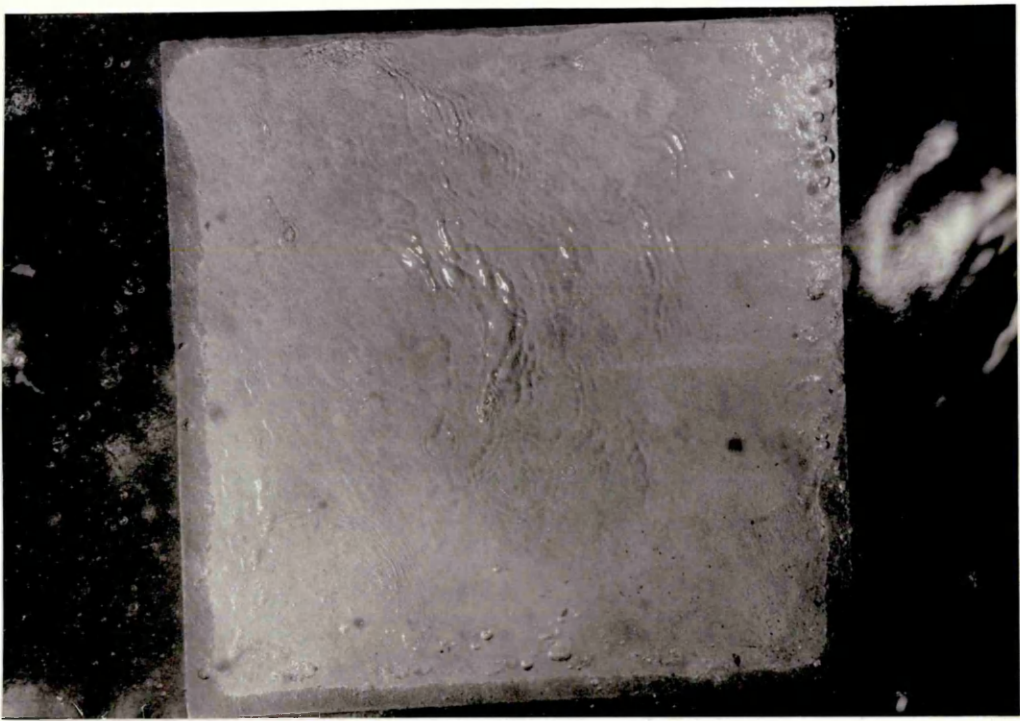
Upper face of the plate quenched horizontally in water.

Time=10 seconds

Figs (52-53)

Underneath of the plates quenched horizontally in water
showing the Taylor waves in the vapour blanket stage.

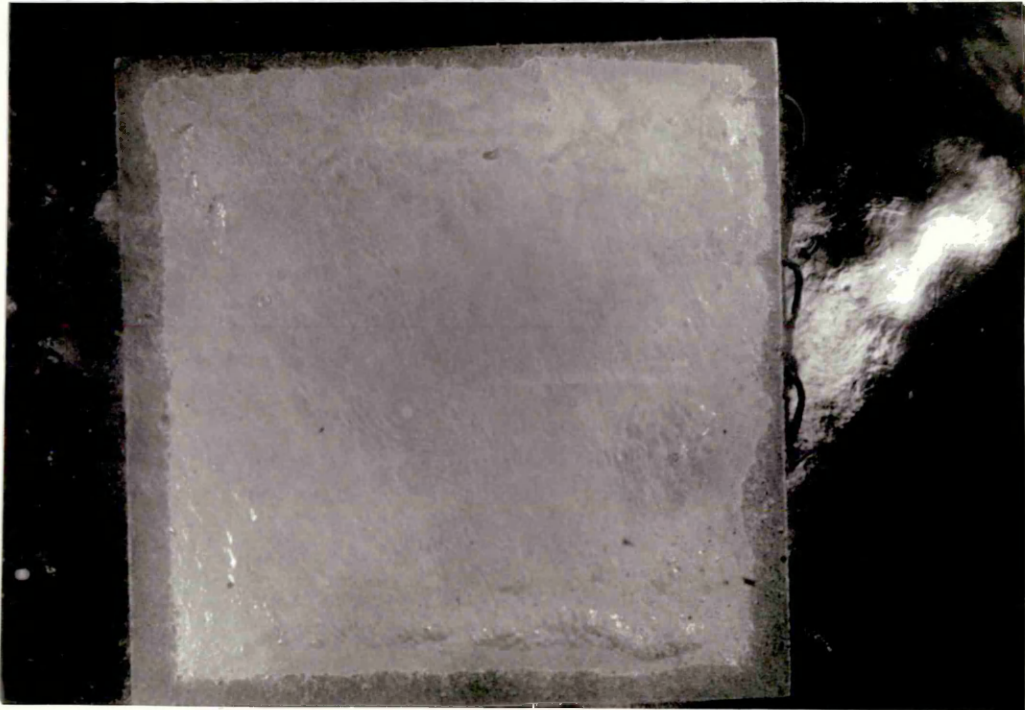
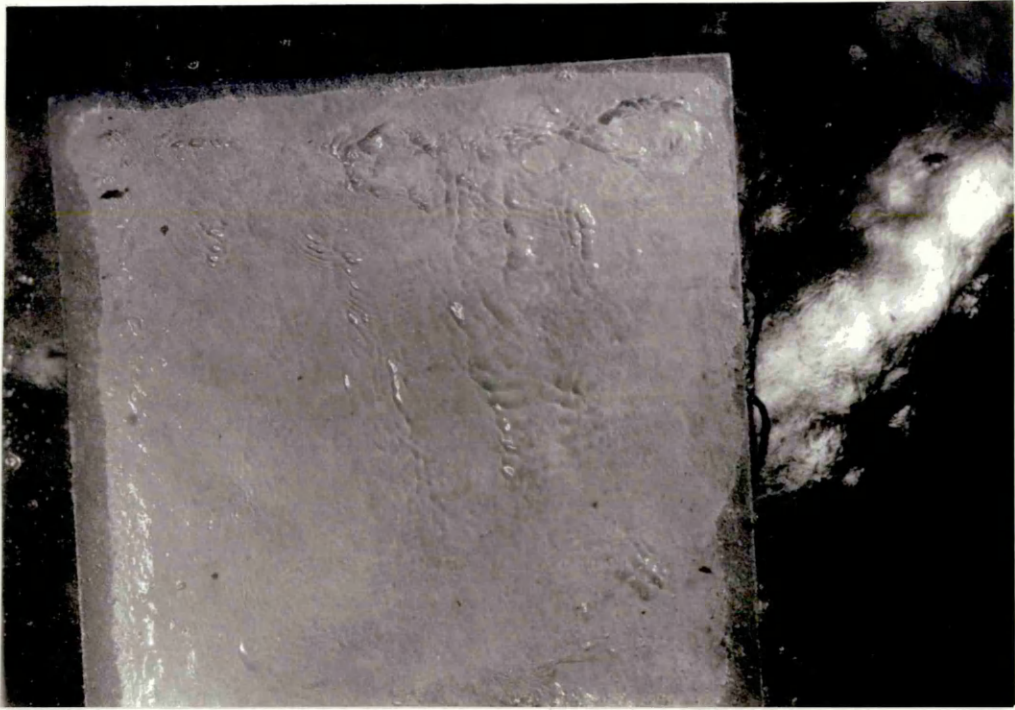
Time = 1.0 and 1.5 seconds



Figs (54-55)

Underneath of the plates quenched horizontally in water.

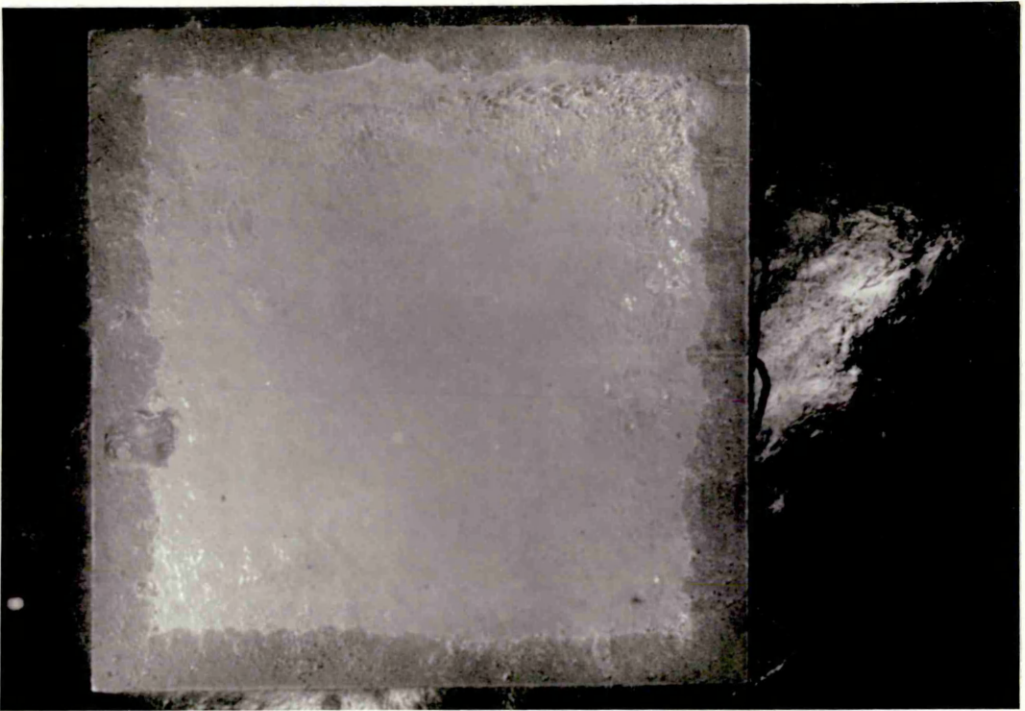
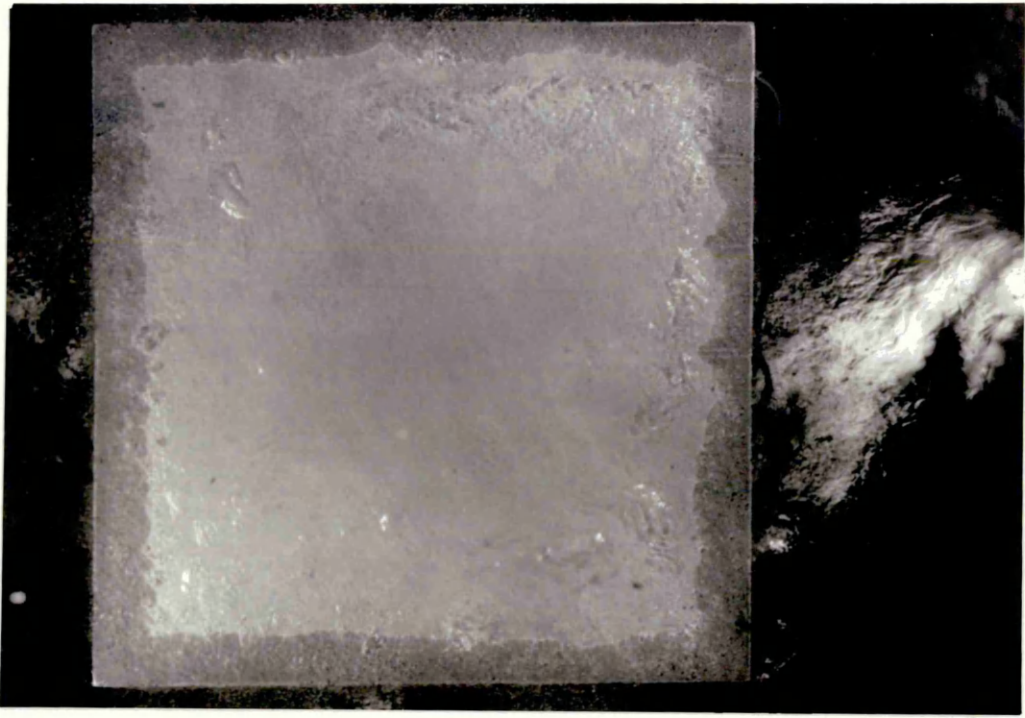
Time = $1\frac{1}{2}$ and $1\frac{2}{3}$ seconds



Figs (56-57)

Underneath of the plates quenched horizontally in water showing the appearance of the nucleate boiling stage.

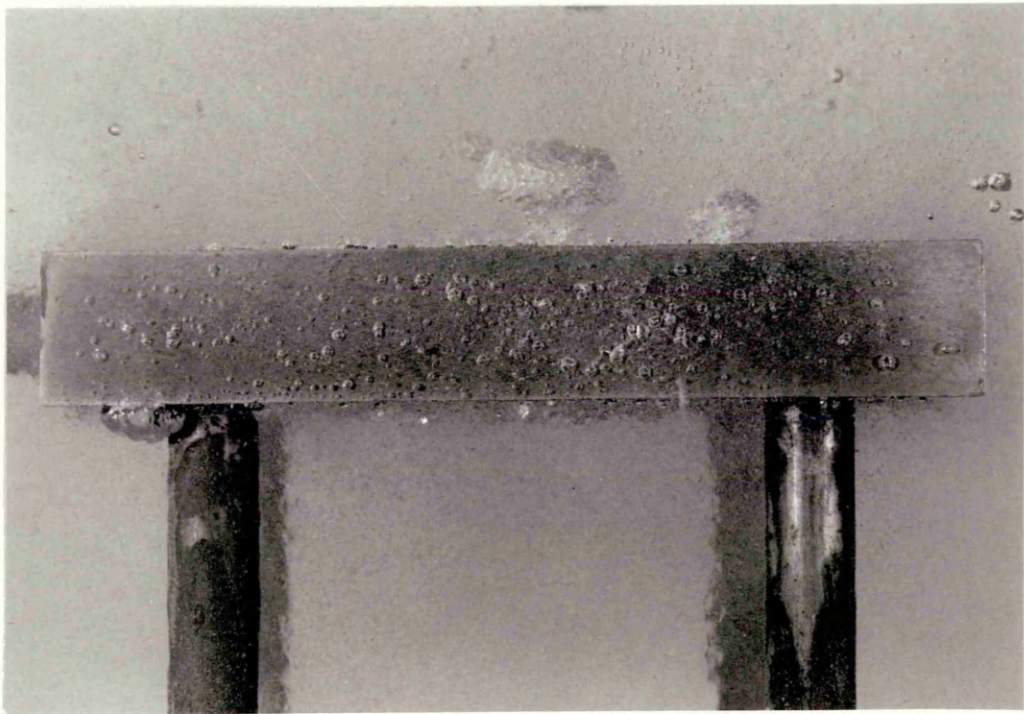
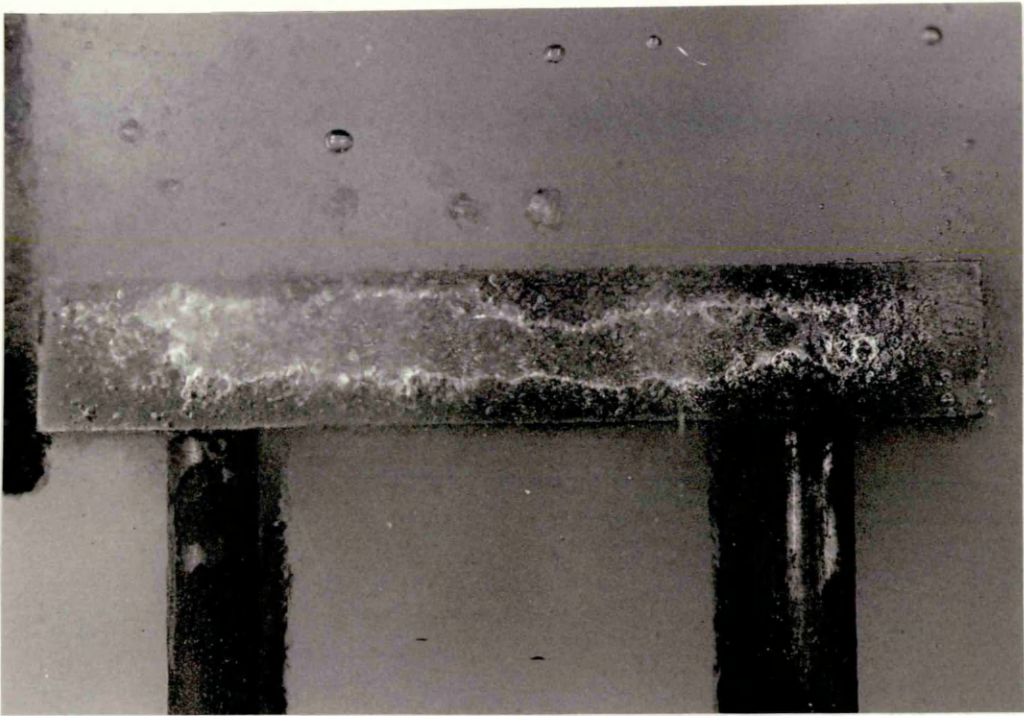
Time= $2\frac{1}{3}$ and 2.5 seconds



Figs (58-59)

Edge of the plate quenched horizontally in water.

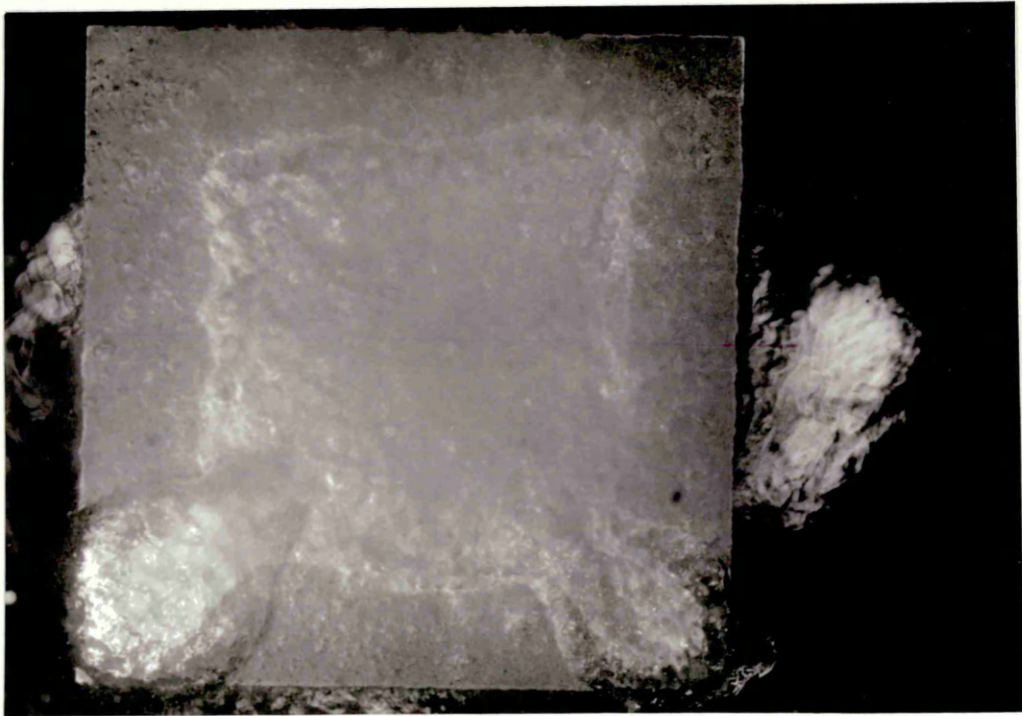
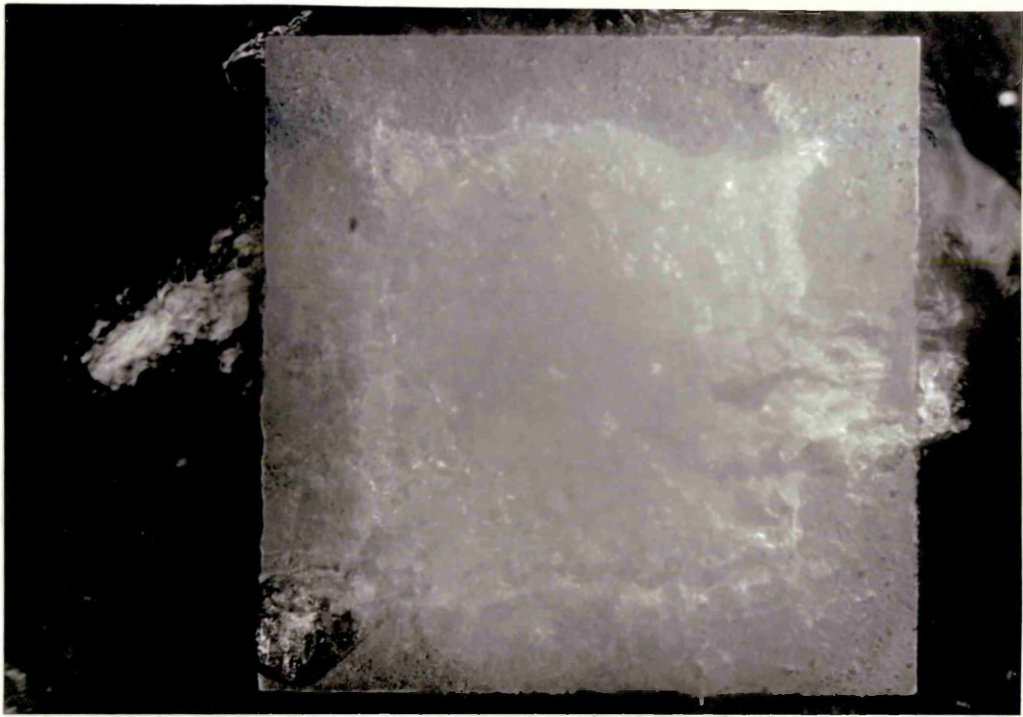
Time=2 and $5\frac{2}{3}$ seconds



Figs (60-61)

Underneath of the plates quenched horizontally in water
showing the appearance of the nucleate boiling stage.

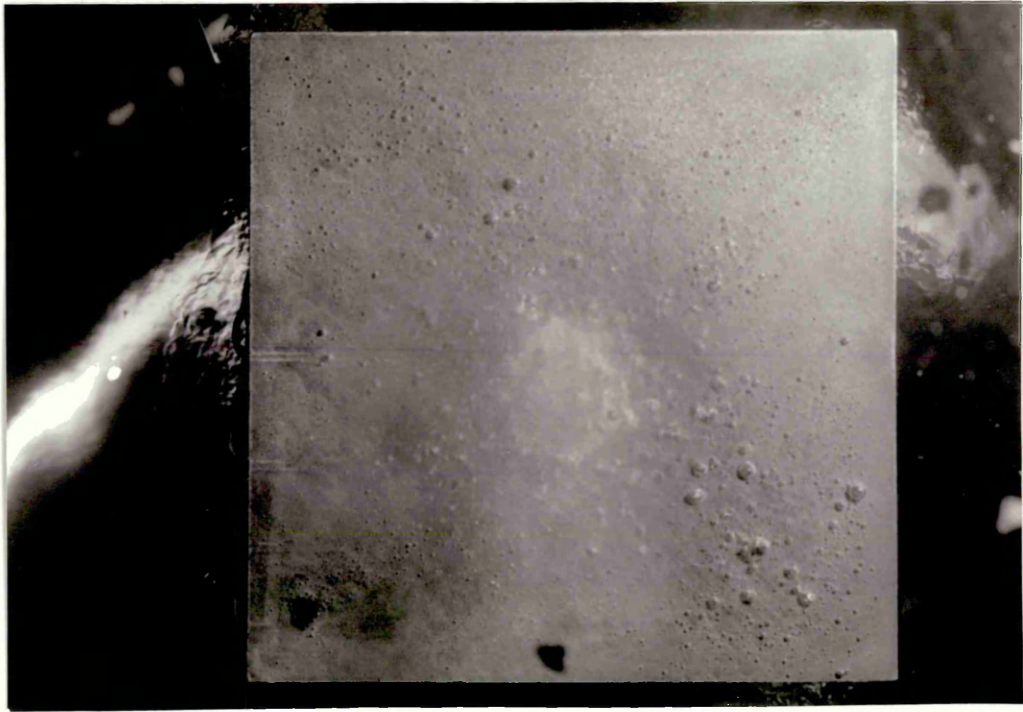
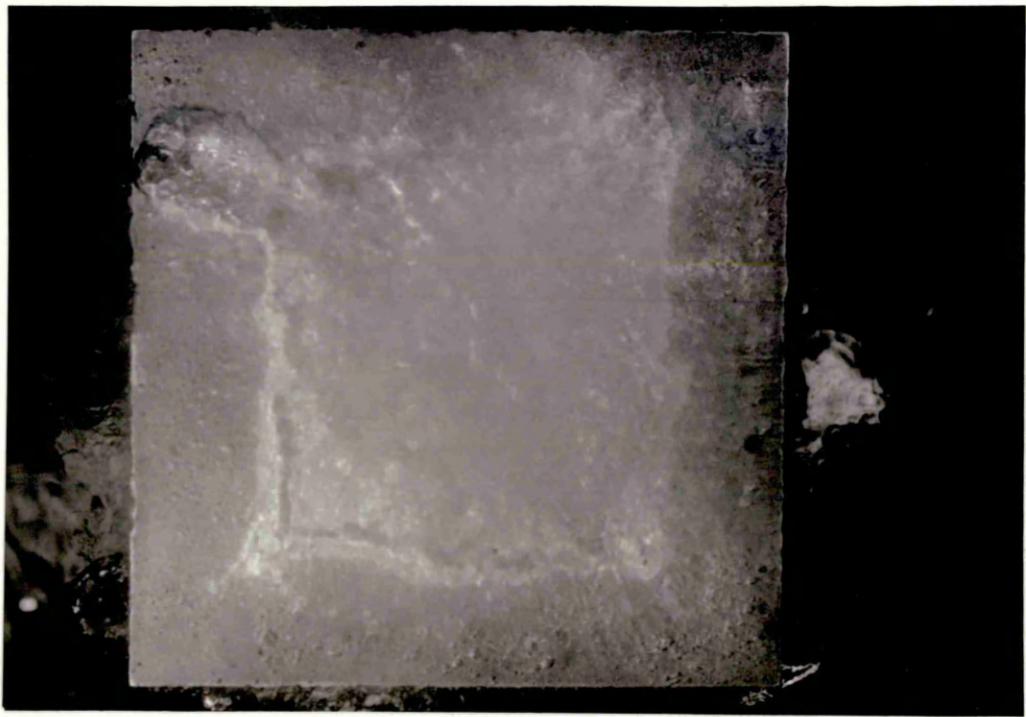
Time = 5.5 and $6\frac{1}{3}$ seconds



Figs (62-63)

Underneath of the plates quenched horizontally in water

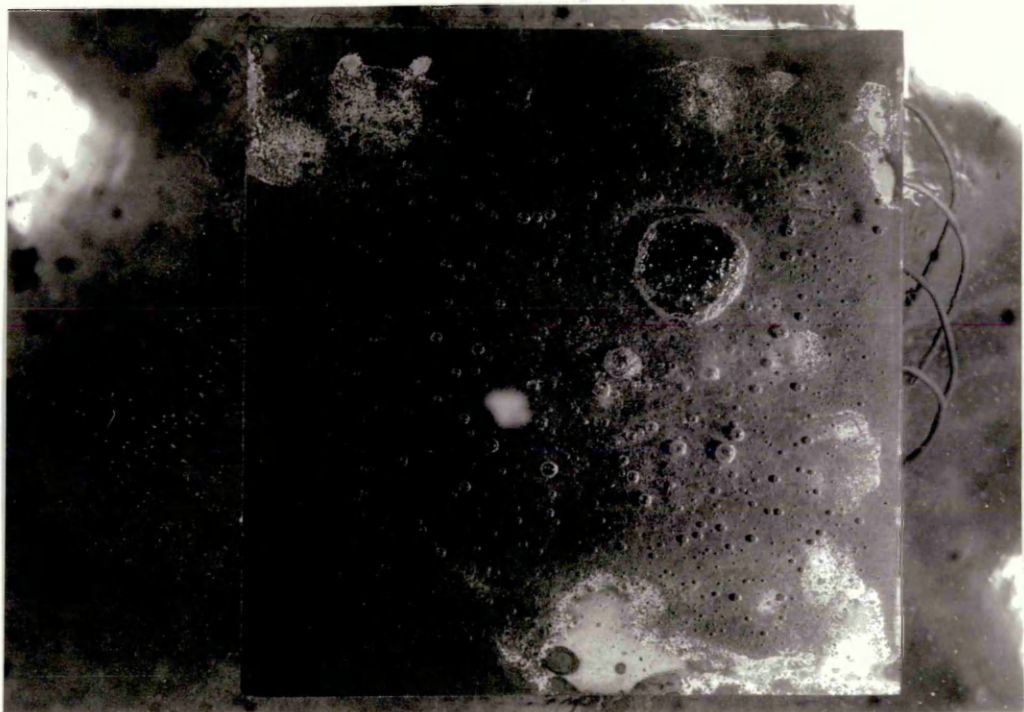
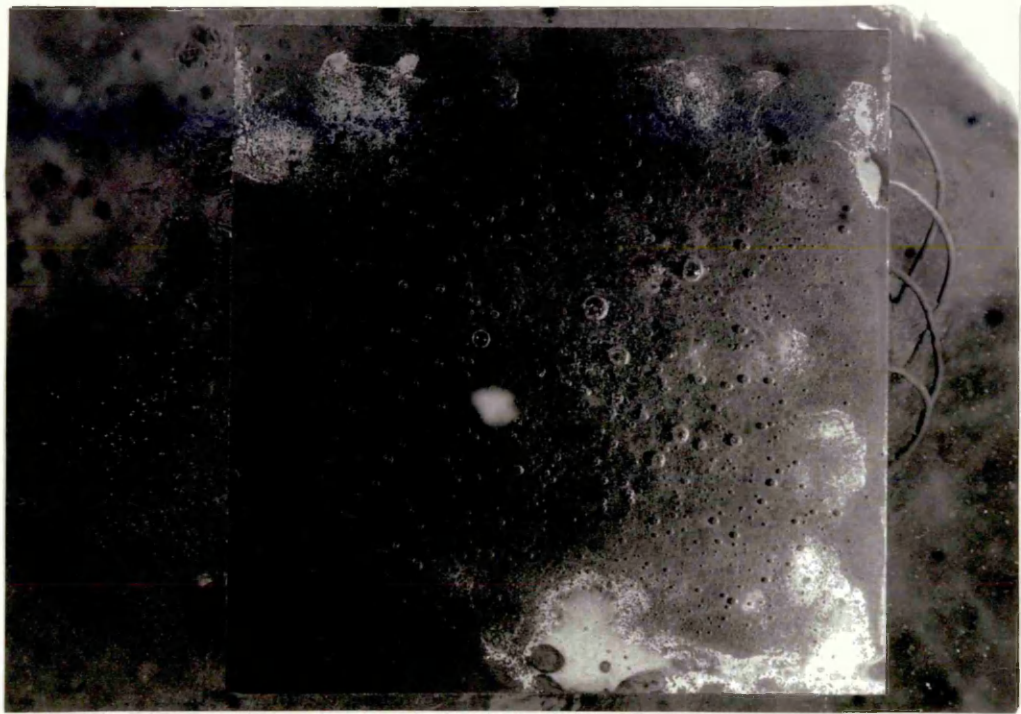
Time = $6\frac{2}{3}$ and $19\frac{1}{3}$ seconds



Figs (64-65)

Underneath of the plates quenched horizontally in water
showing the appearance of bubbles.

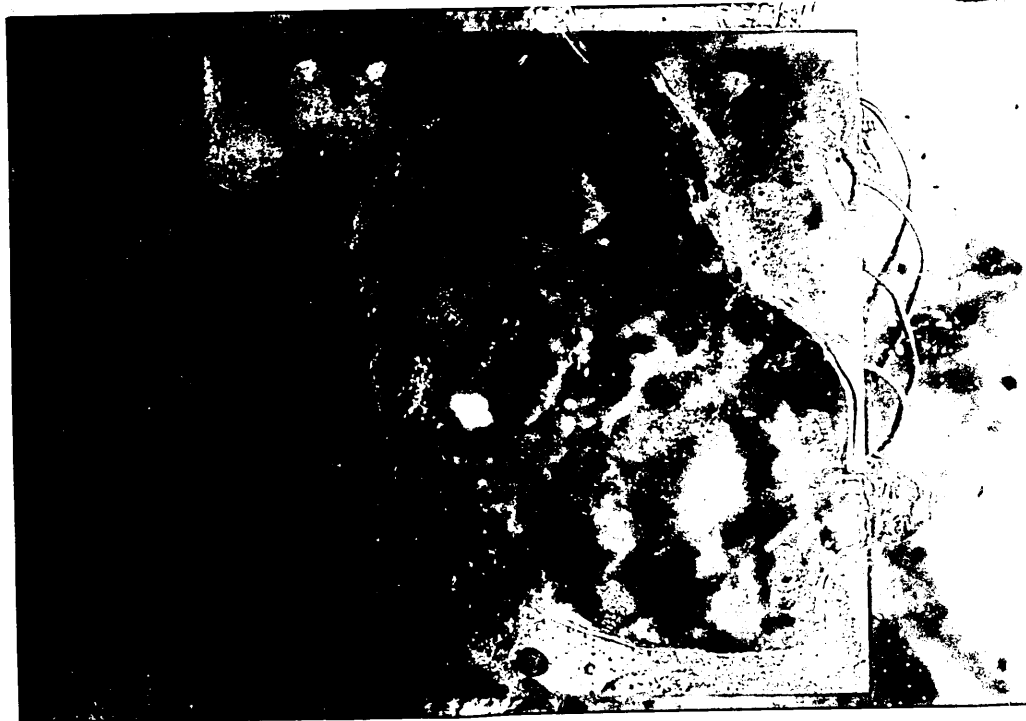
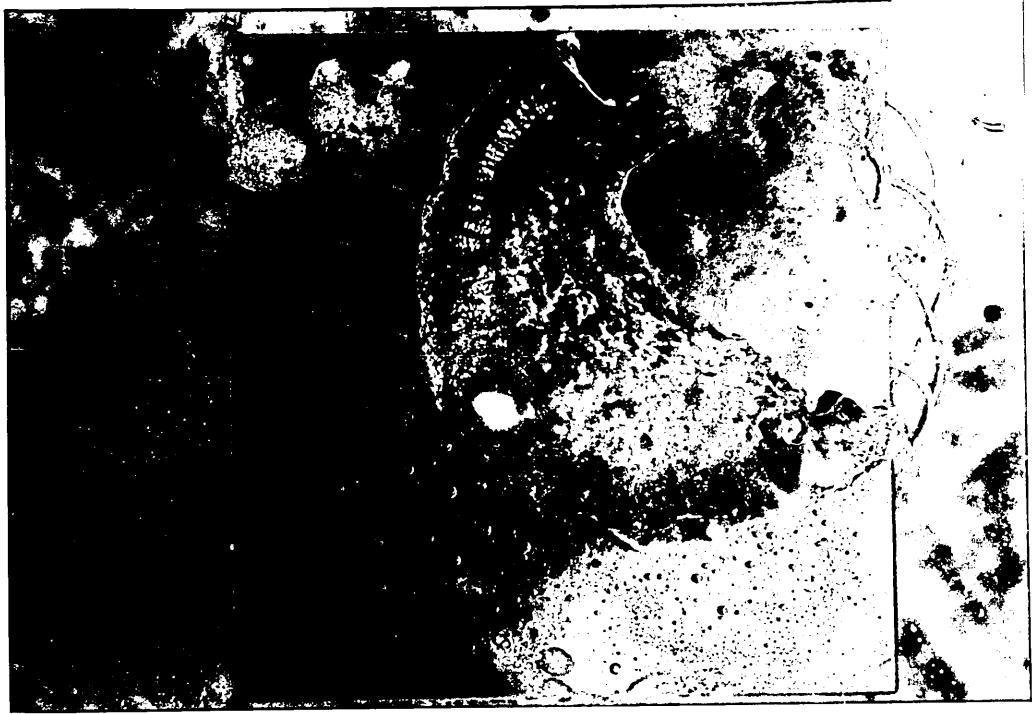
Time= 24 and $24\frac{1}{3}$ seconds



Figs (66-67)

Underneath of the plates quenched horizontally in water
showing the appearance of a big bubble.

Time= 24.5 and 24(2/3) seconds



Figs (68-69)

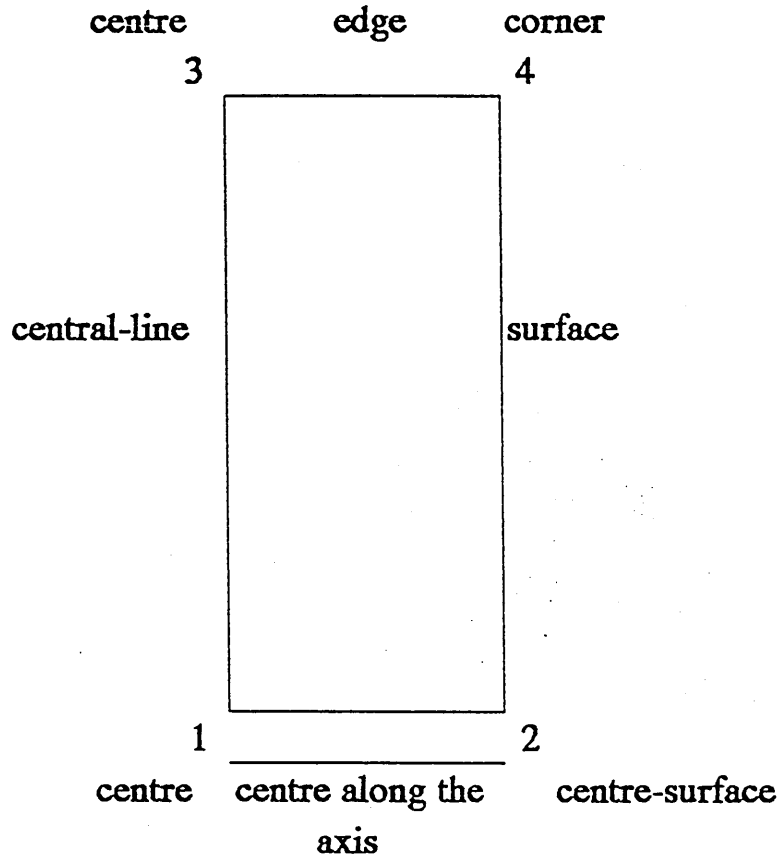
Underneath of the plates quenched horizontally in water
showing sudden disappearance of the big bubble.

Time = 25 and $25\frac{1}{3}$ seconds



Figures (70-73)

Distribution of stresses along the axis of the plate;
distances from axial central line, central line, centre edge
and surface (mm) at 1.0 second into 2-D water quench analysis
by using constant heat transfer coefficients around the surface.



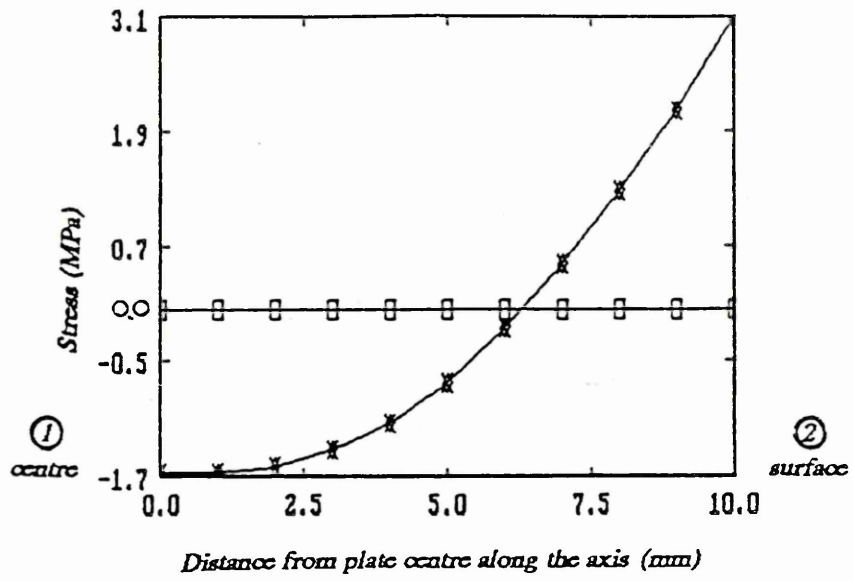


Fig. 70

- Axial
- * Radial
- ◇ Hoop

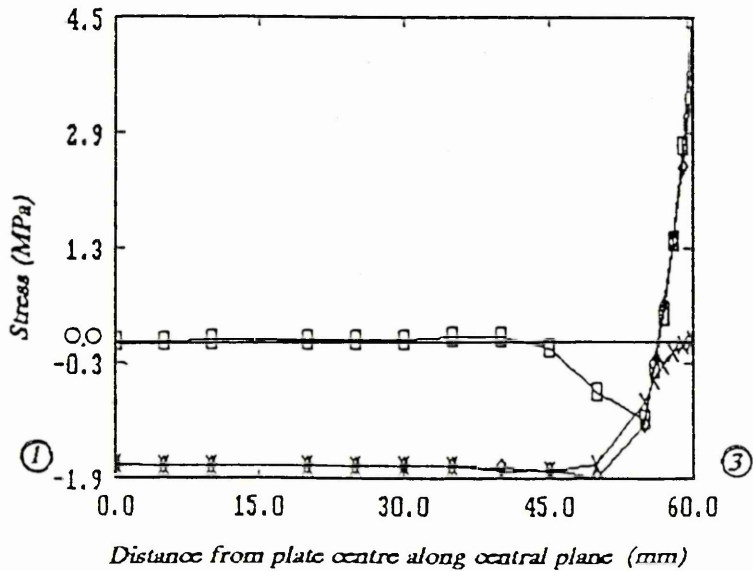
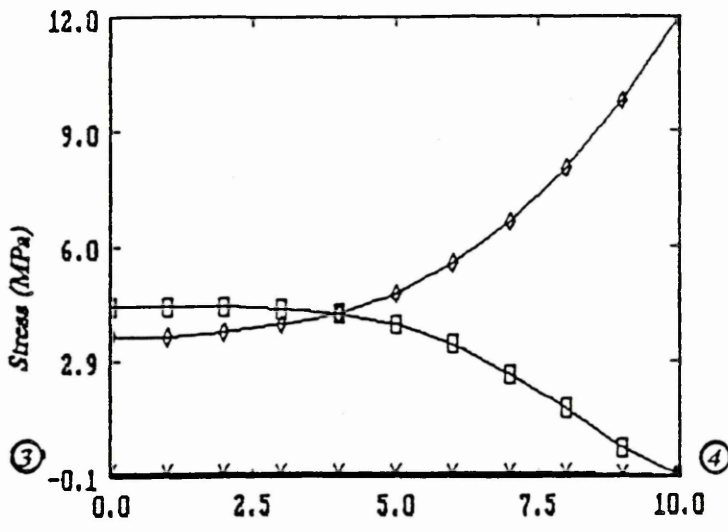
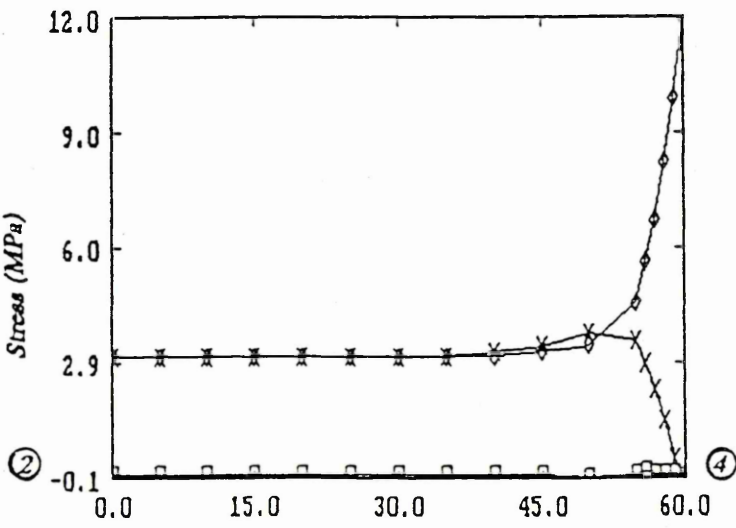


Fig. 71



Distance from plate centre along the edge (mm)
Fig.72

- ⊕ Axial
- × Radial
- ◇ Hoop

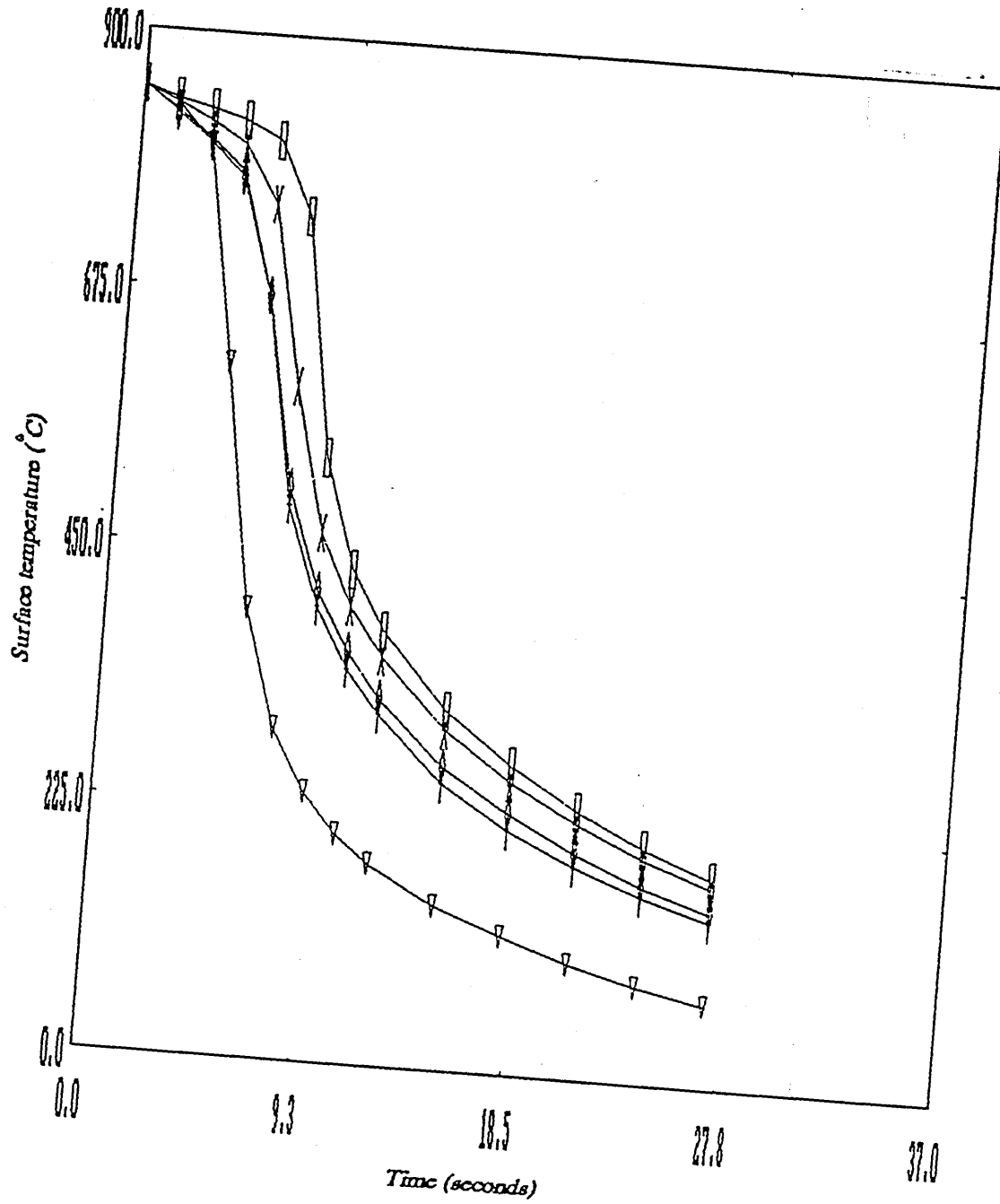


Distance along surface from axis (mm)
Fig.73

Figure 74

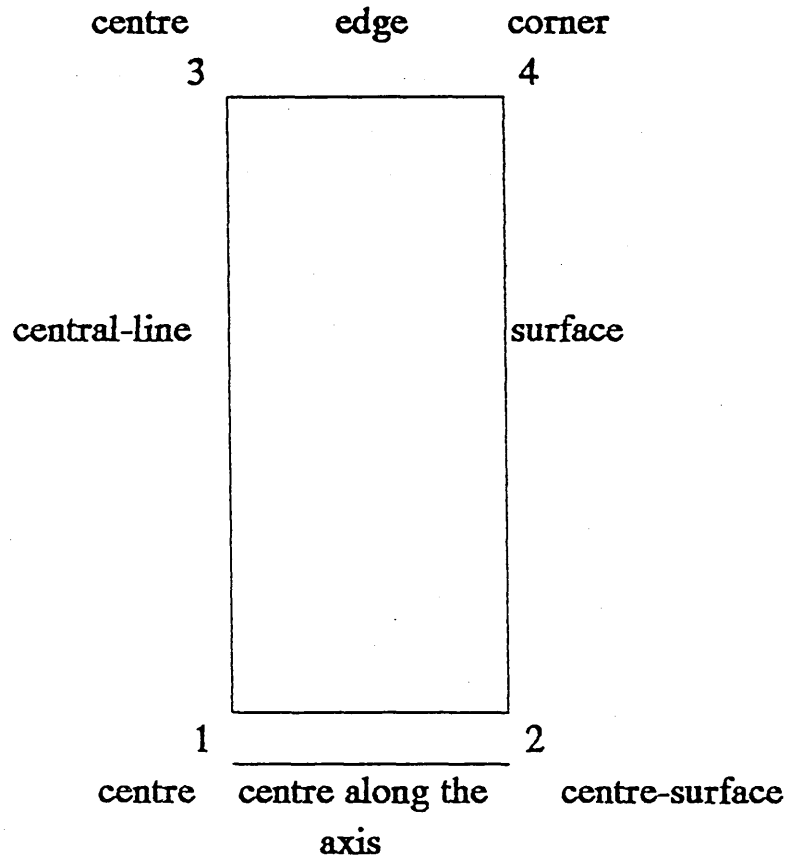
Predicted temperature profiles for the 2-D heat flow case of a vertical quench using constant surface heat transfer coefficient by finite element programme.

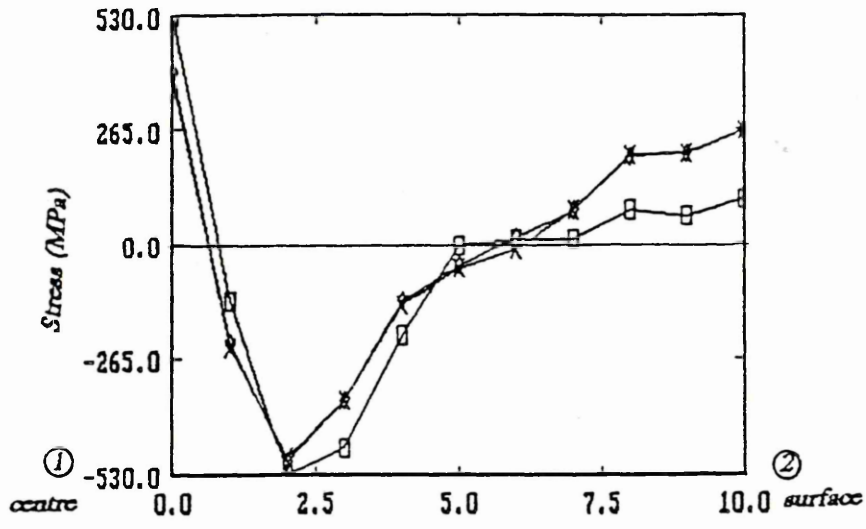
Surface temperature Vs time (sec) where \oplus , \ast , \diamond , \dagger & ∇ represent the centre node 2, 2 intermediates nodes (120, 6, 246), corner node 4 and top edge node 7 respectively. See key fig 26.



Figures (75-78)&(79-82)

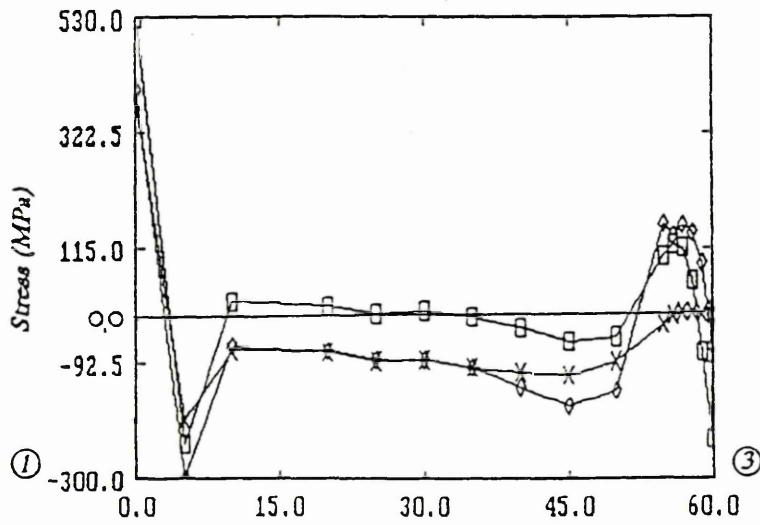
Distribution of stresses along the axis of the plate;
distances from axial central line, central line, centre edge
and surface (mm) at 7.8 and 40 seconds into the 2-D water
quench analysis by using constant heat transfer coefficients
around the surface.



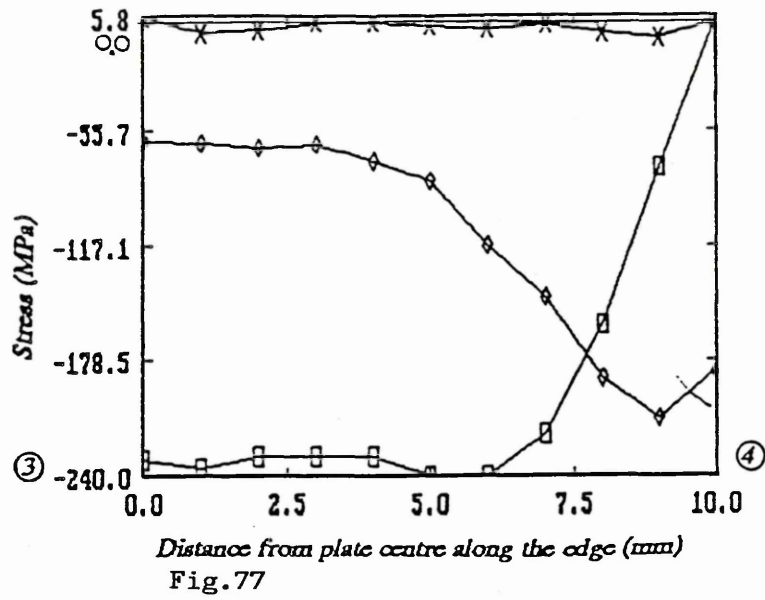


Distance from plate centre along the axis (mm)
Fig. 75

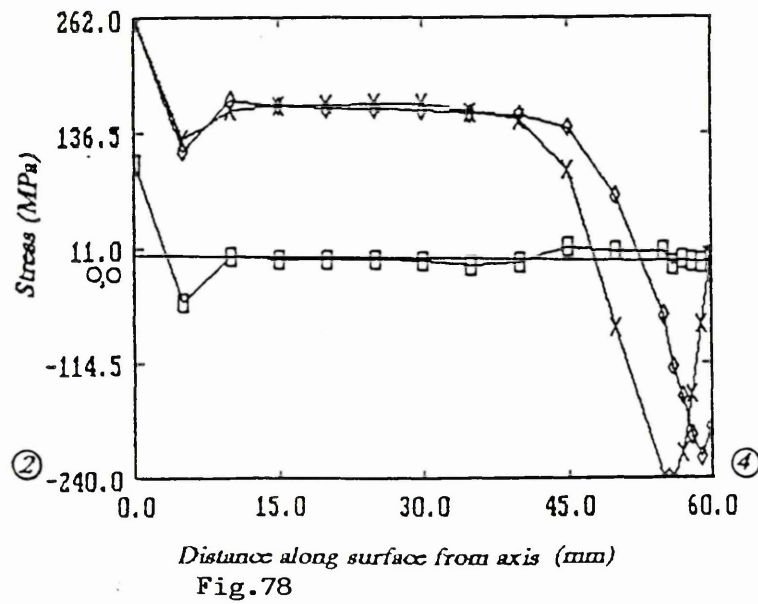
- Axial
- * Radial
- ◇ Hoop



Distance from plate centre along central plane (mm)
Fig. 76



⊕ Axial
 * Radial
 ◇ Hoop



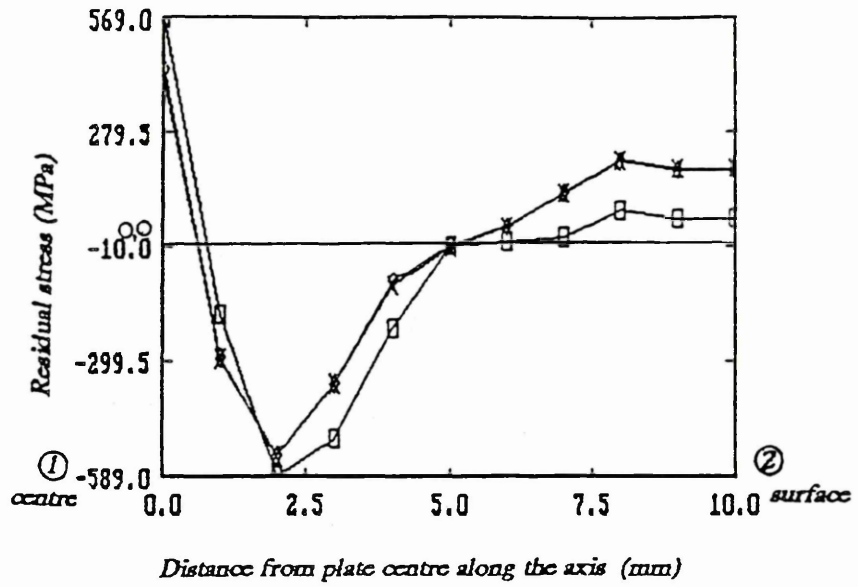


Fig.79

- Axial
- × Radial
- ◇ Hoop

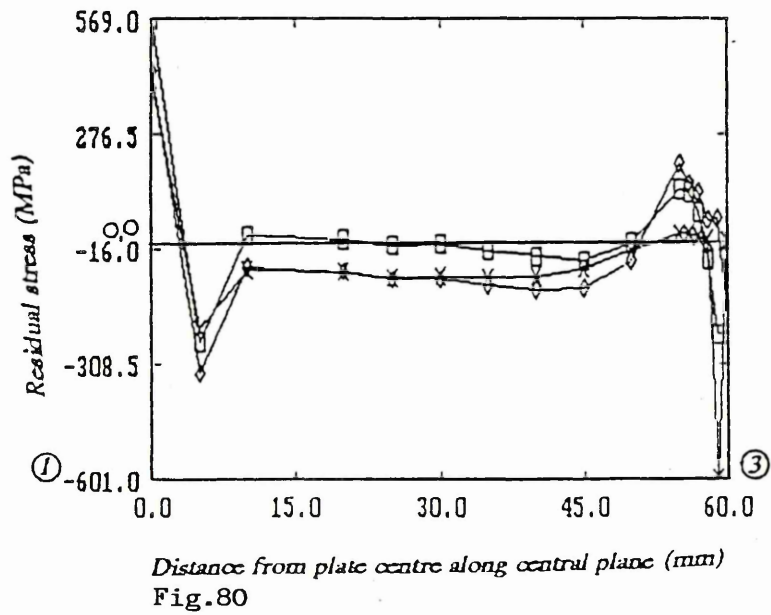


Fig.80

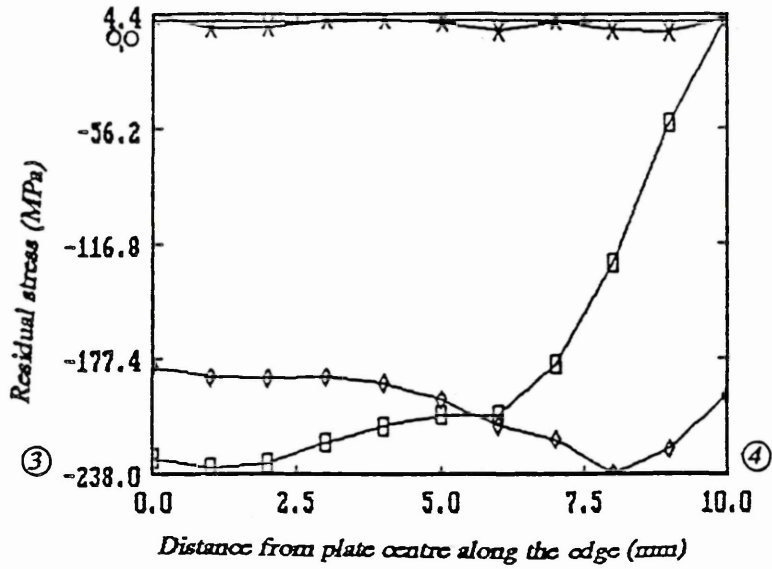


Fig.81

□ Axial
 * Radial
 ◇ Hoop

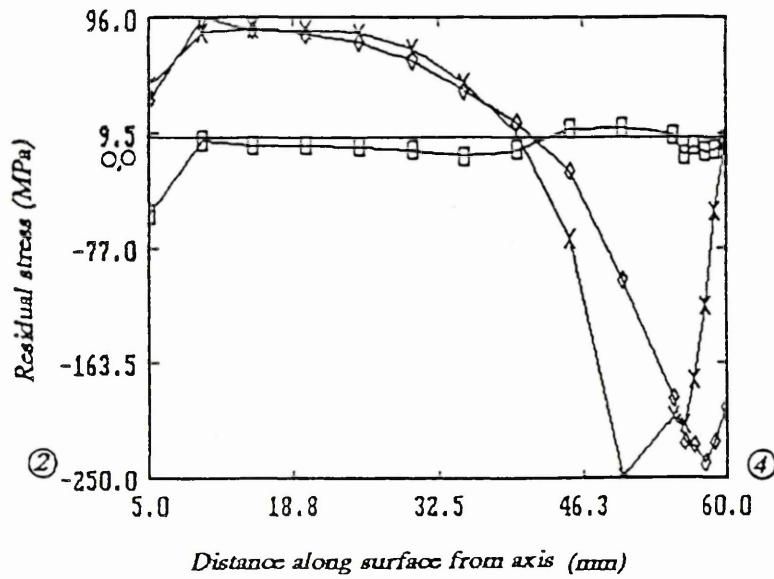
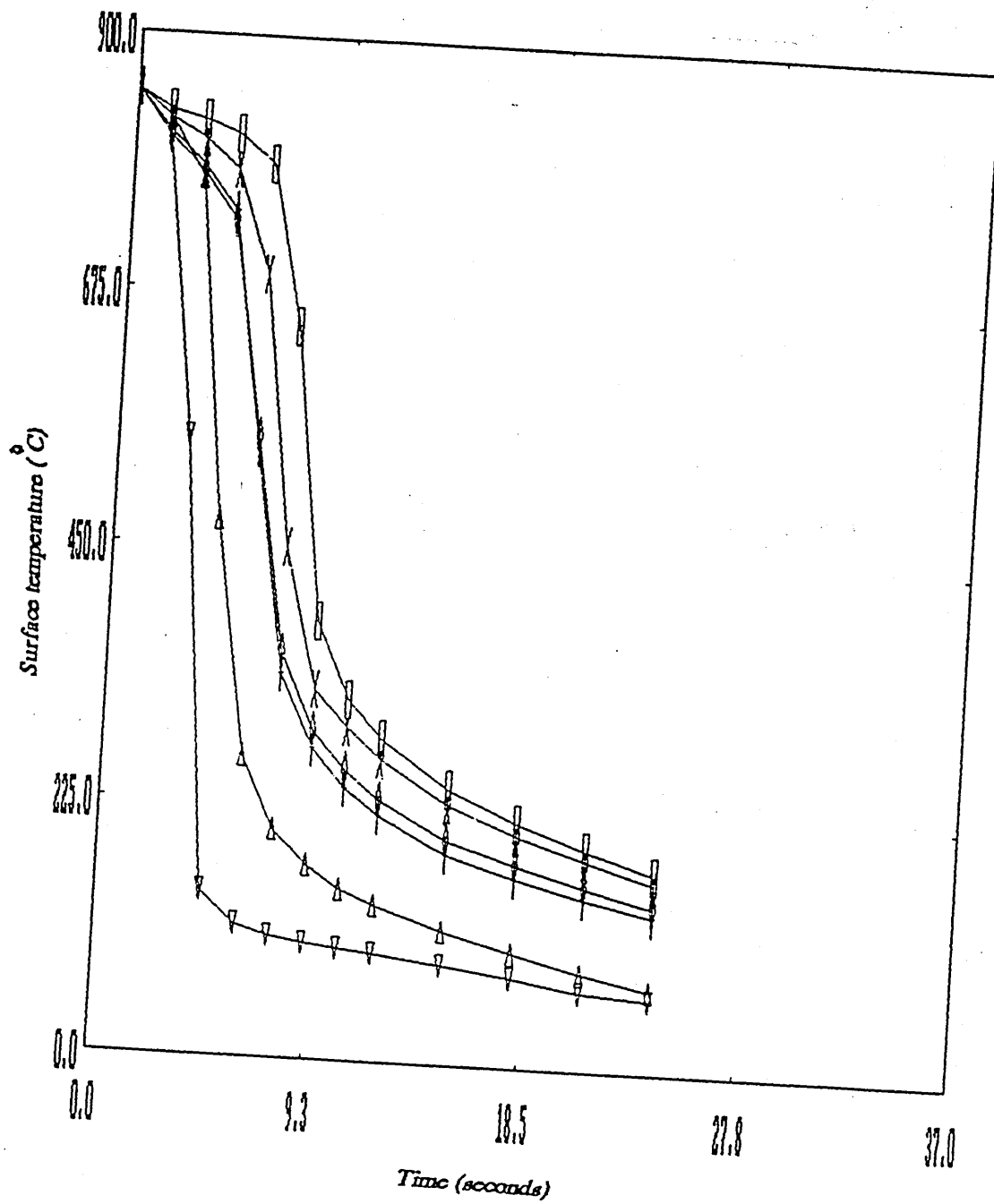


Fig.82

Figure 83

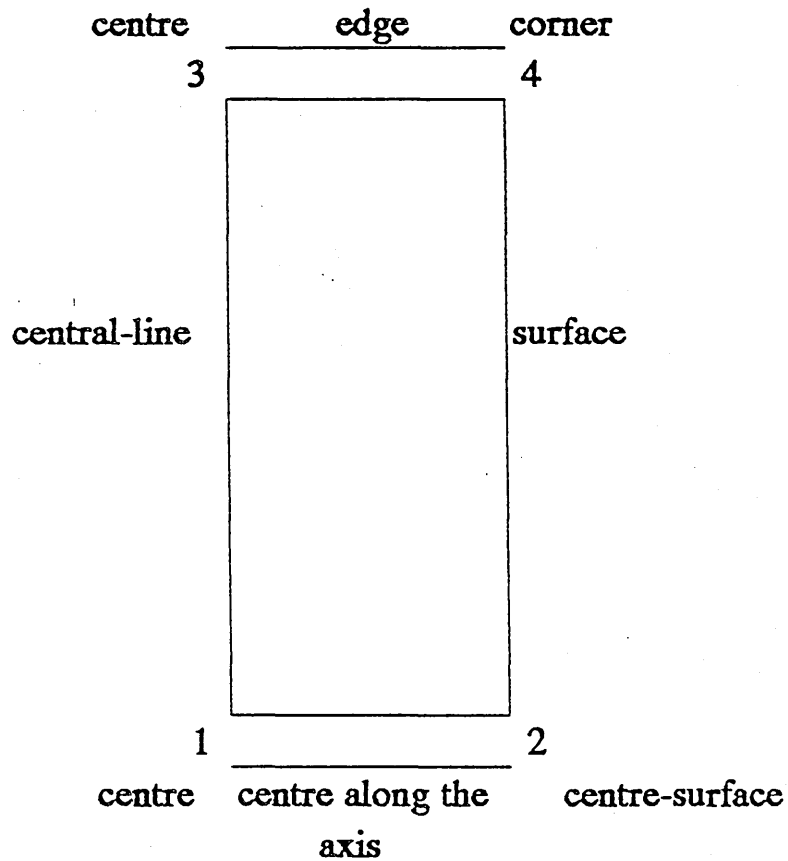
Predicted temperature profiles for the 2-D heat flow case of a vertical quench using variable surface heat transfer coefficient by finite element programme.

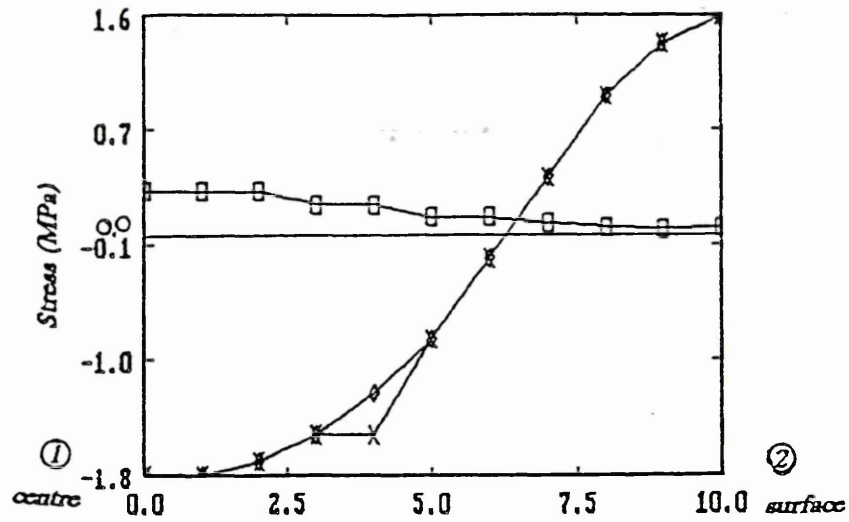
Surface temperature Vs time (sec) where \square \times \diamond $+$ \triangle & ∇ represent the centre node 2, 3 intermediates nodes (120,6,246), corner node 4 and top edge node 7 respectively. See key fig 26.



Figures (84-87)

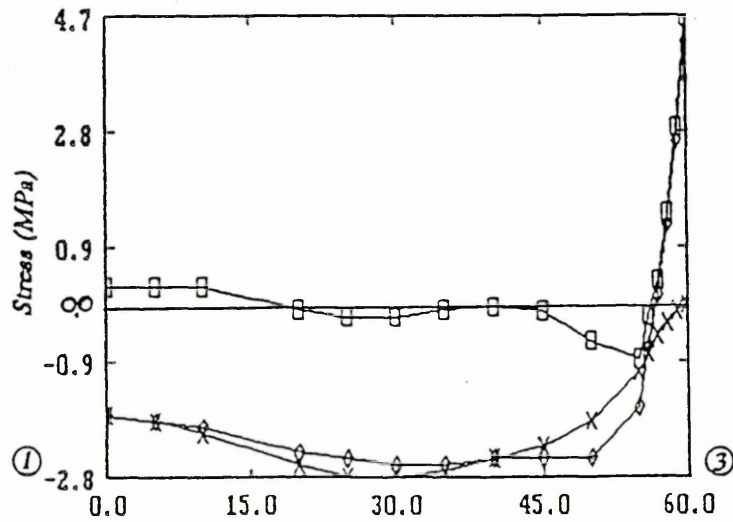
Distribution of stresses along the axis of the plate;
distances from axial central line, central line, centre edge
and surface (mm) at 1.0 second into 2-D water quench analysis
by using variable heat transfer coefficients around the surface.



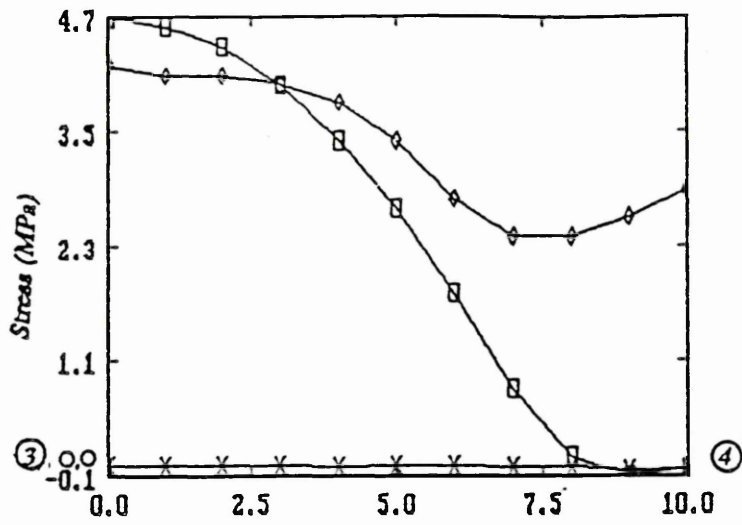


Distance from plate centre along the axis (mm)
Fig. 84

⊕ Axial
× Radial
◇ Hoop

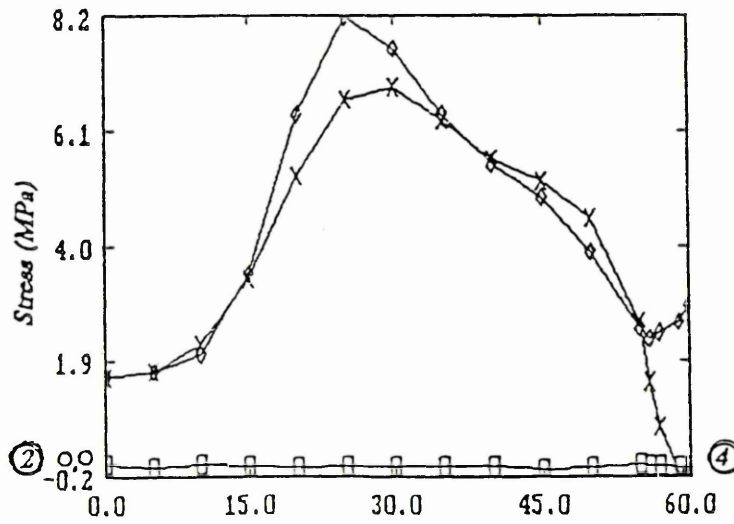


Distance from plate centre along central plane (mm)
Fig. 85



Distance from plate centre along the edge (mm)
 Fig.86

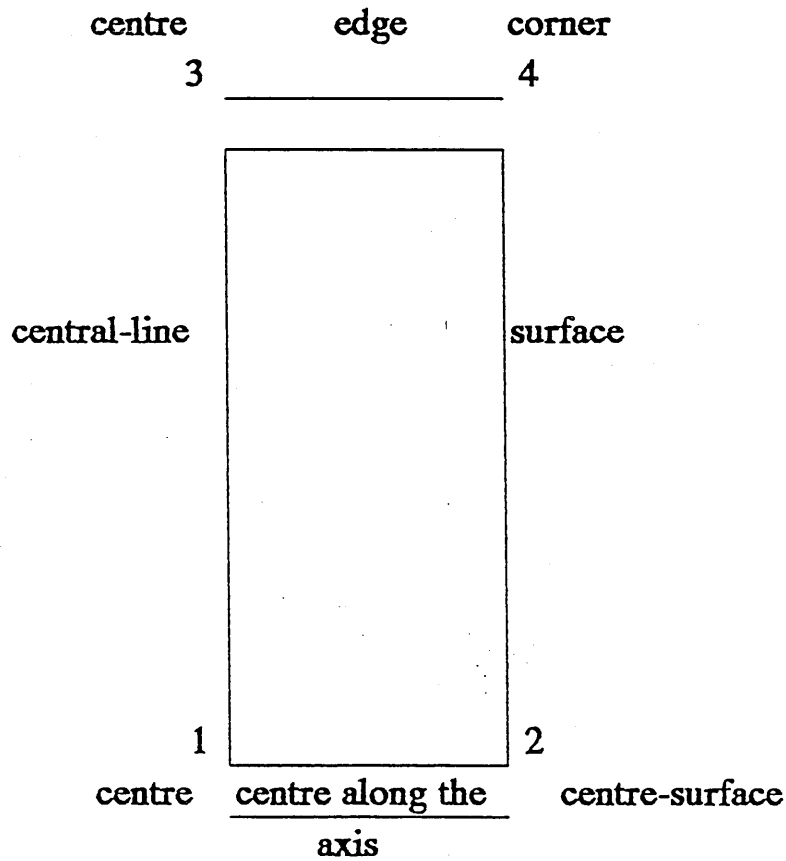
- Axial
- * Radial
- ◇ Hoop

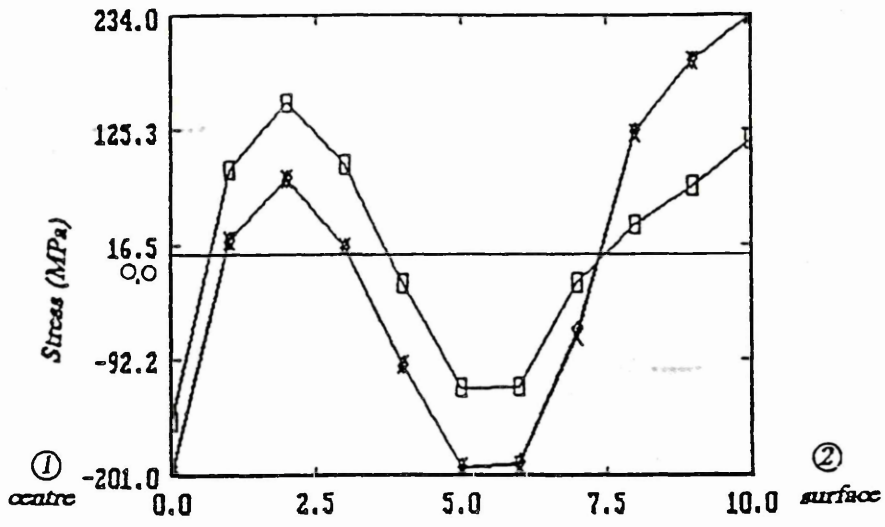


Distance along surface from axis (mm)
 Fig.87

Figures (88-91)&(92-95)

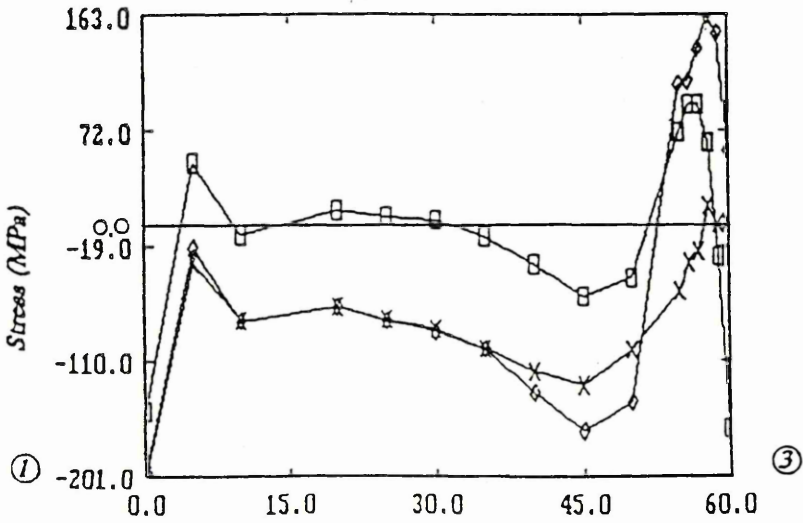
Distribution of stresses along the axis of the plate;
distances from axial central line, central line, centre edge
and surface (mm) at 7.8 and 40 seconds into the 2-D water
quench analysis by using variable heat transfer coefficients
around the surface.





Distance from plate centre along the axis (mm)
Fig.88

⊕ Axial
* Radial
⊖ Hoop



Distance from plate centre along central plane (mm)
Fig.89

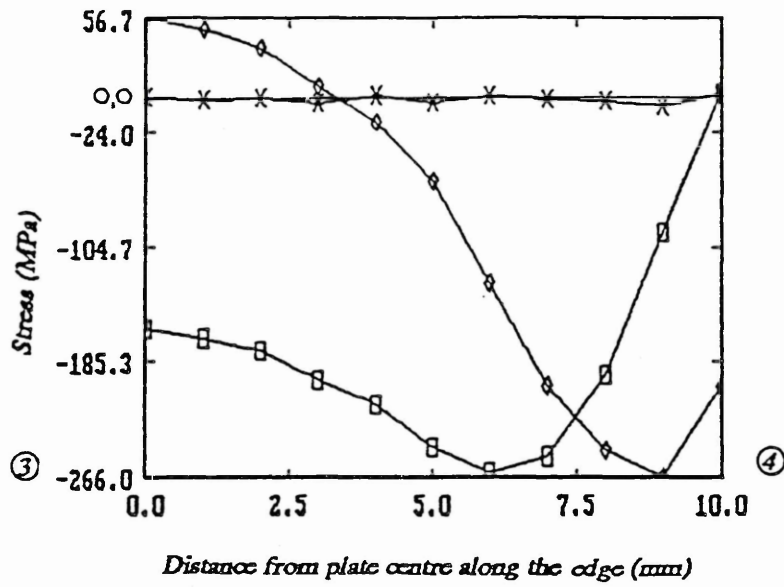


Fig.90

⊕ Axial
 × Radial
 ⊕ Hoop

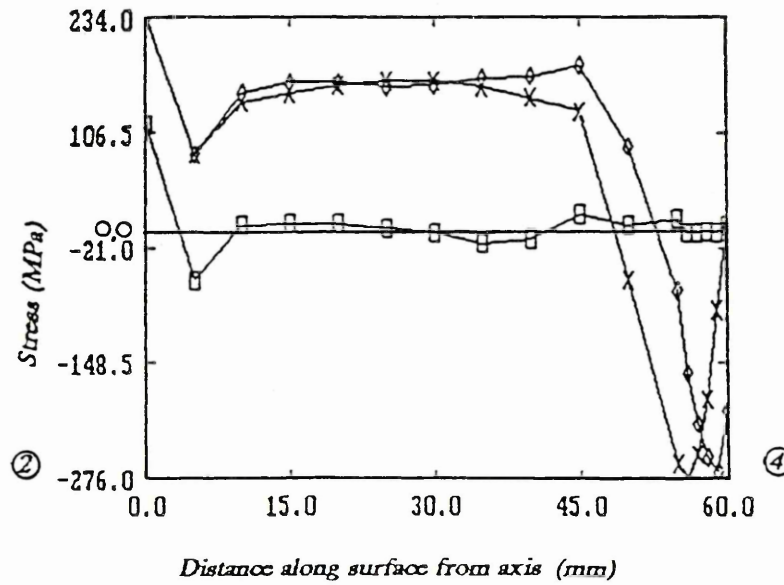


Fig.91

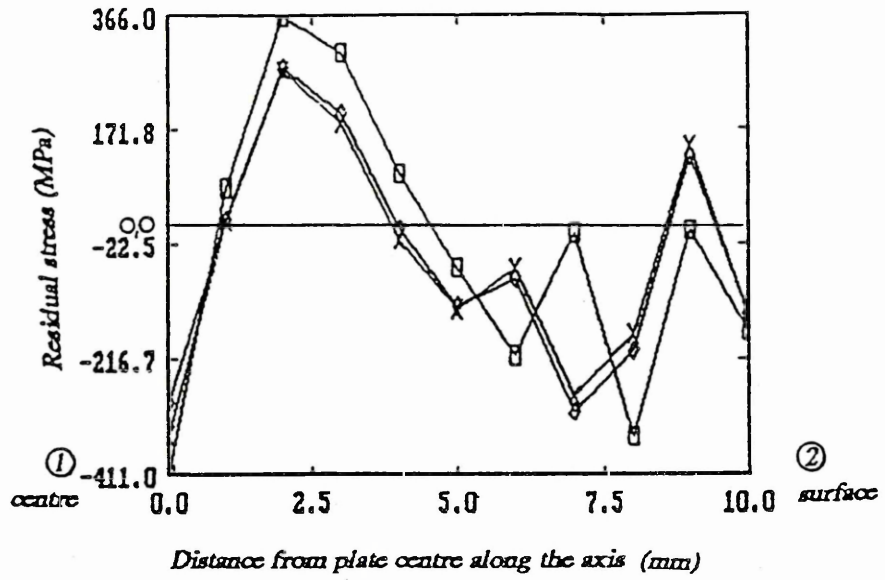


Fig.92

- Axial
- × Radial
- ◇ Hoop

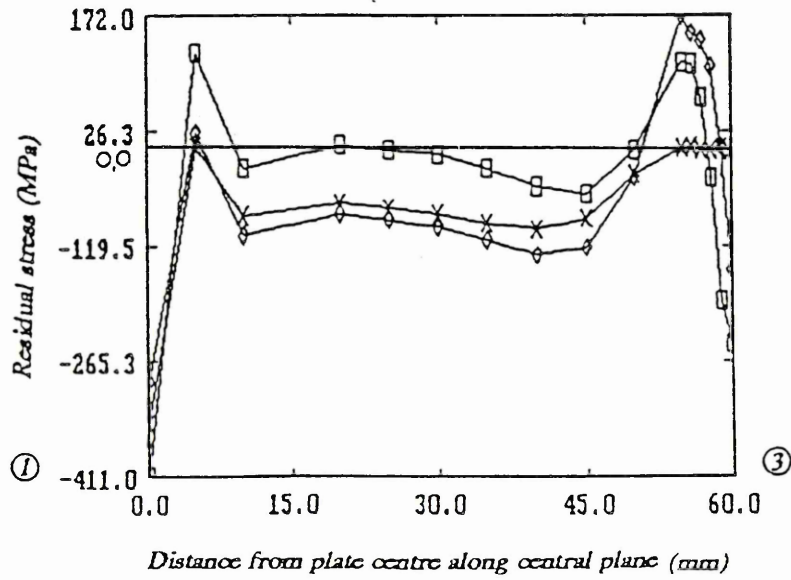


Fig.93

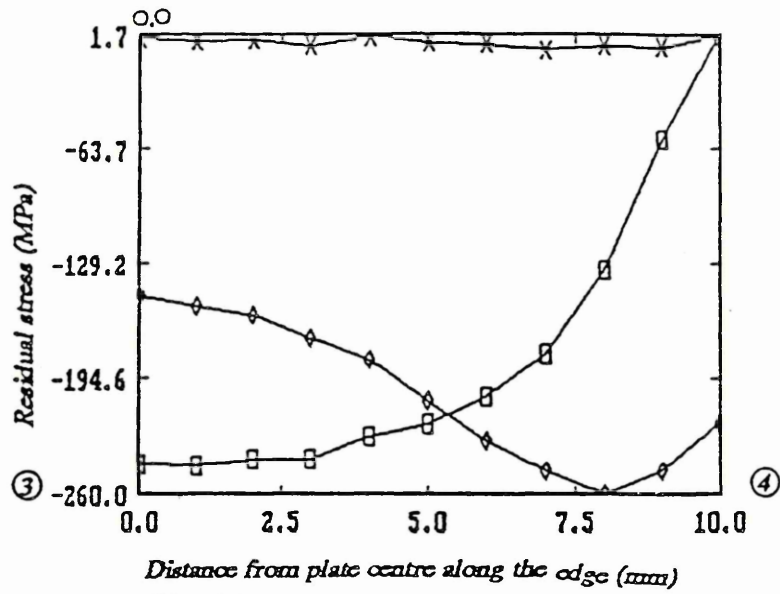


Fig.94

- Axial
- * Radial
- ◇ Hoop

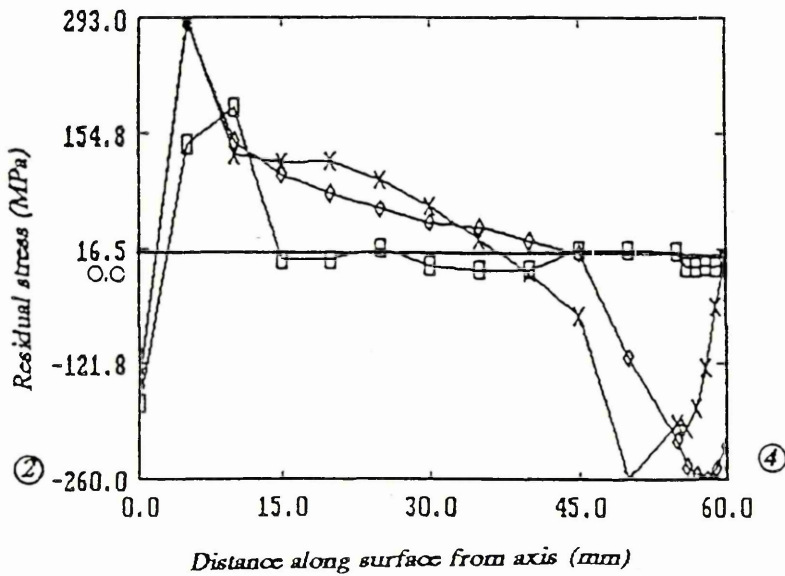


Fig.95

Fig 96

Comparison of calculated and experimentally measured residual strains in stainless steel plate quenched vertically in water.

$\square, \dagger, \diamond, \Delta, \phi, \times$ represent the depth beneath the surface with 10, 30, 60, 90 & 110 mm respectively.

Ref. Figure 15.

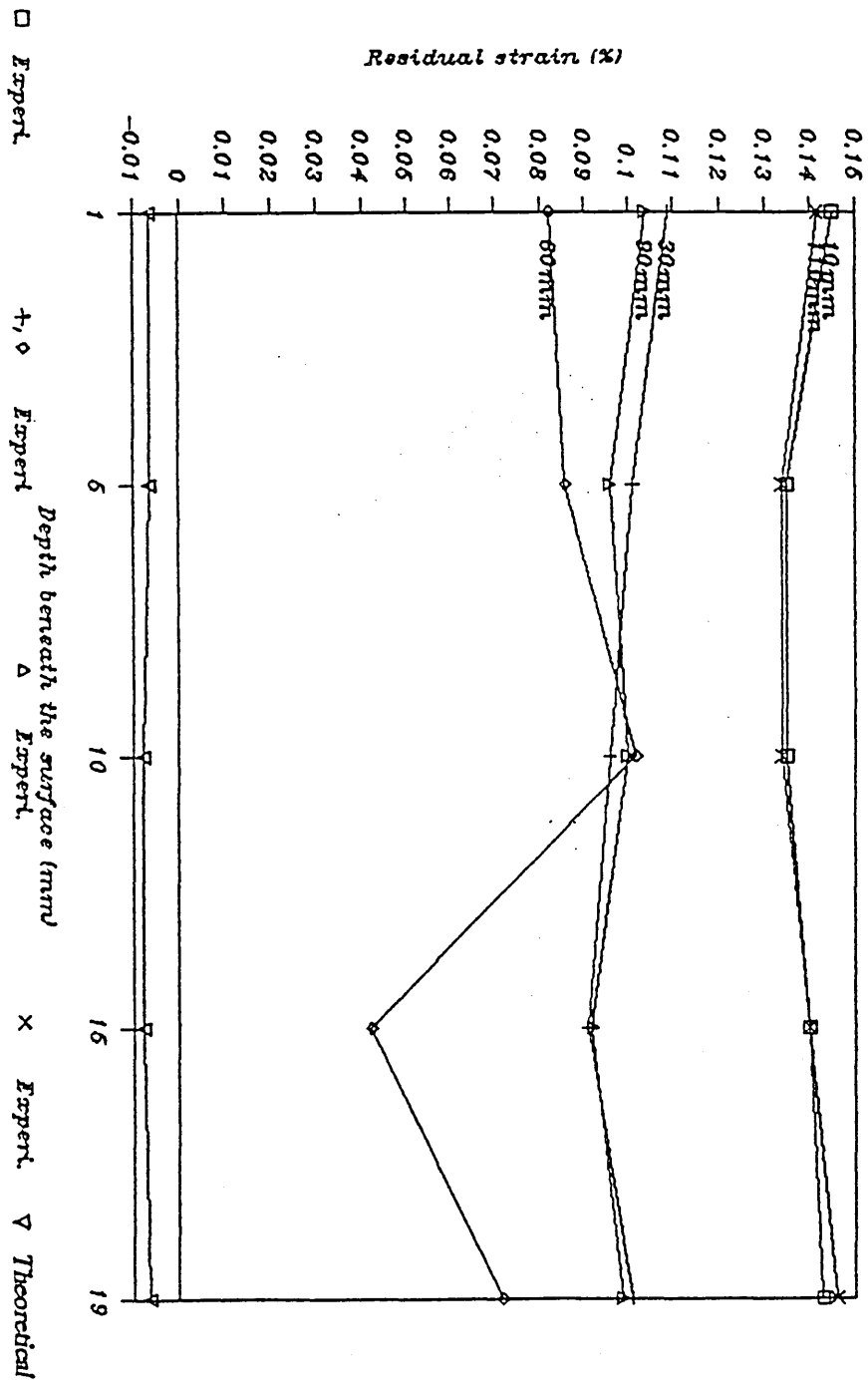


Fig 97

Comparison of calculated and experimentally measured residual strains in stainless steel plate quenched horizontally in water.

□, +, ◇, △, φ, × represent the depth beneath the surface with 10, 30, 60, 90 & 110 mm respectively.

Ref. Figure 15.

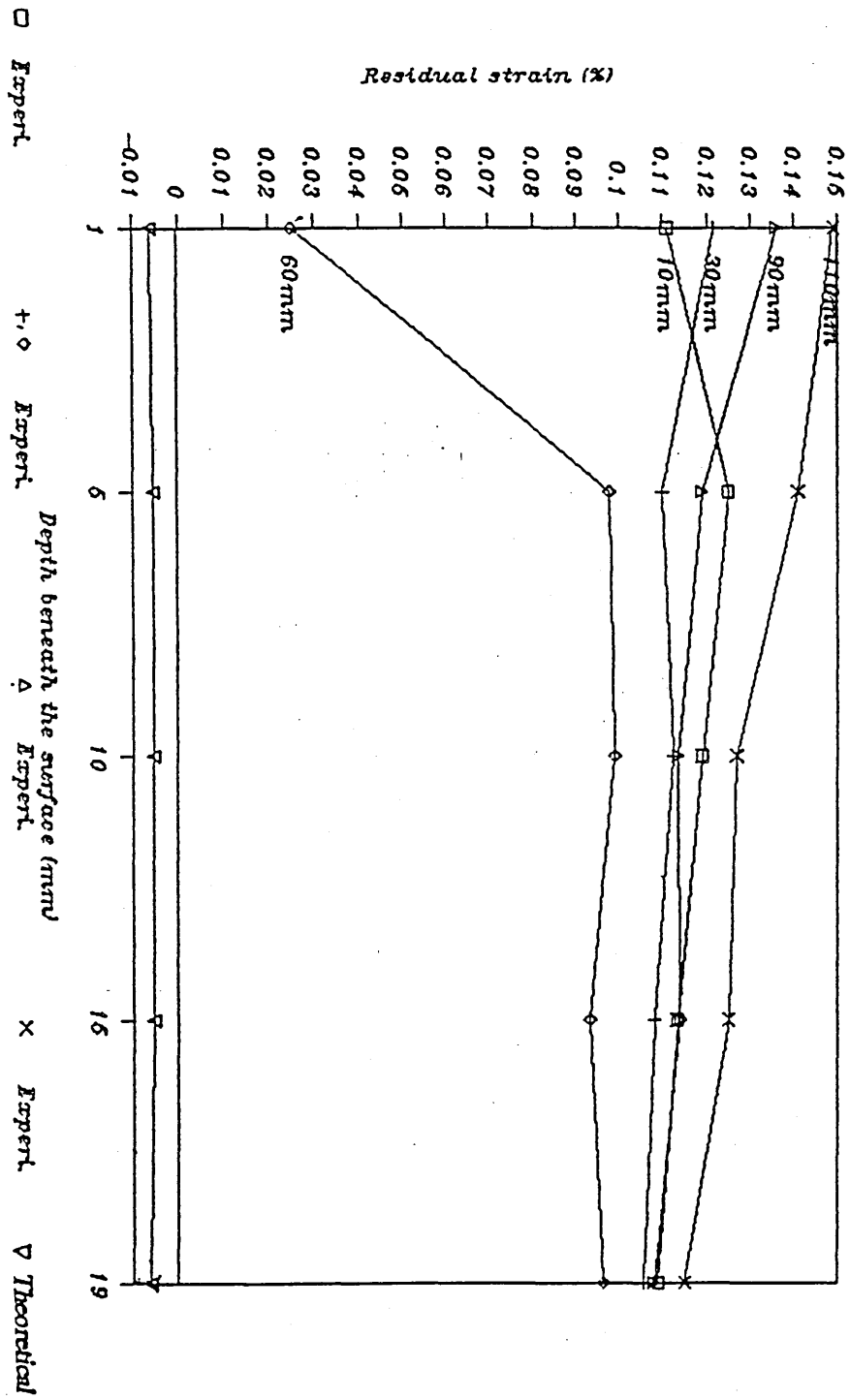
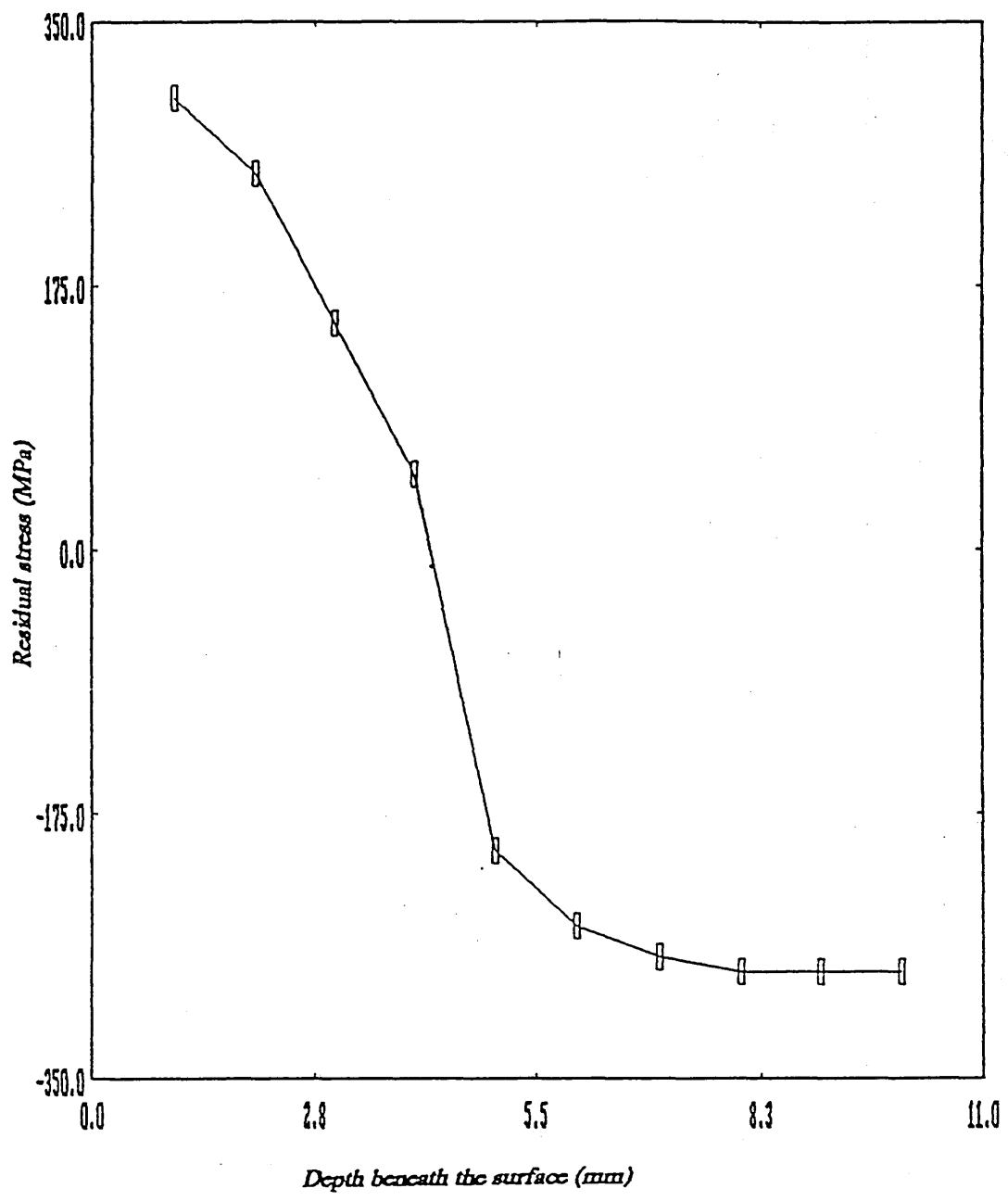


Fig 98

Measured residual stress in stainless steel plate quenched horizontally in water.



⊠ Experimental

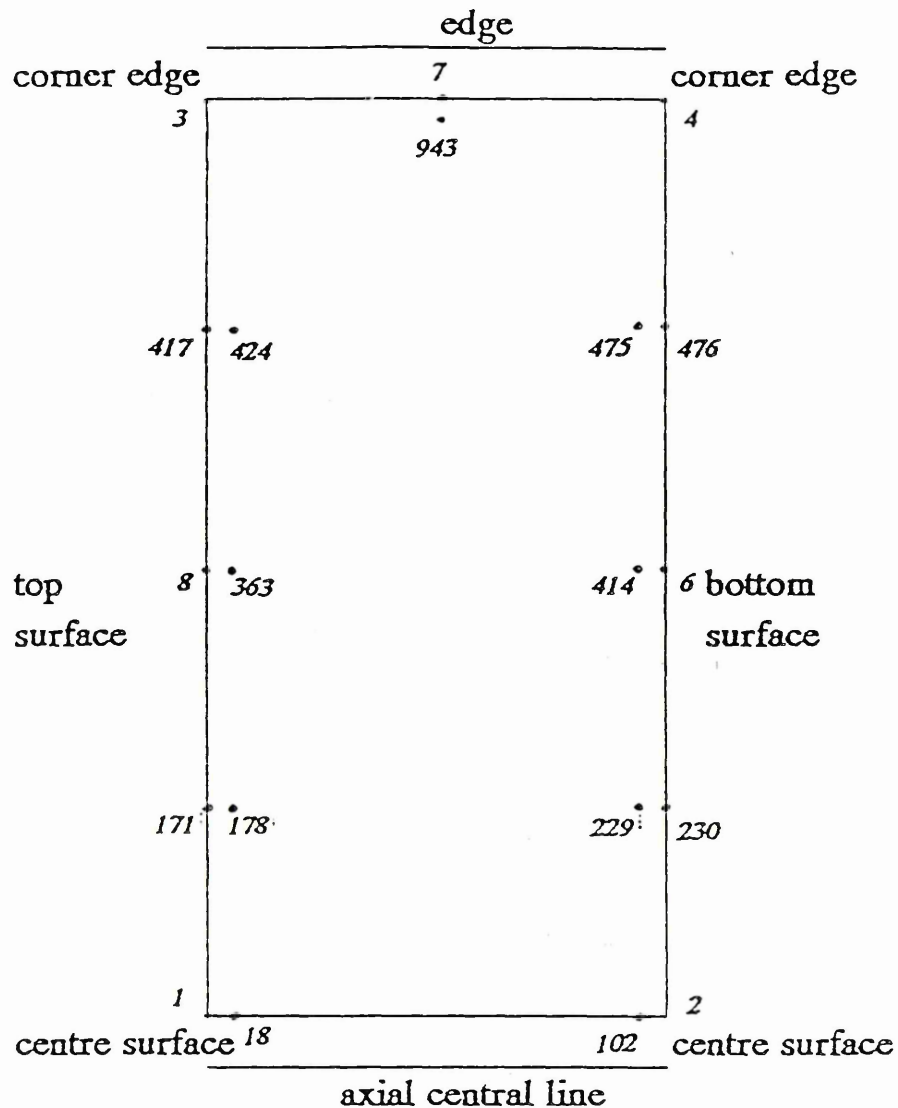


Fig 99

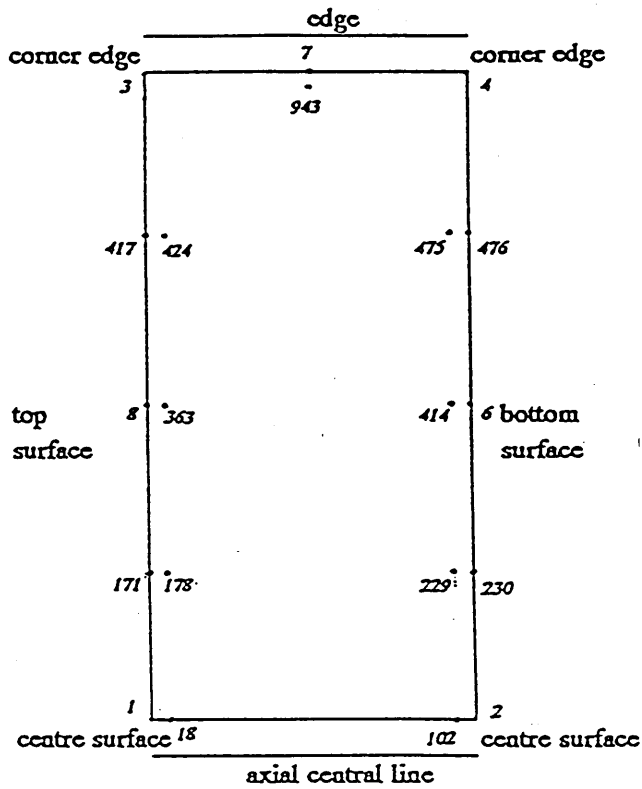
Shows thermocouple positions relative to the specific nodal positions used in finite element calculations through the whole thickness covering from top to bottom surface of the plate.

Nodes; 2, 230, 6, 476, 4, 7, 3, 417, 8, 171 and 1 are placed around the face surface of the plate.

Nodes; 102, 229, 414, 475, 943, 424, 363, 178 and 18 are placed at a points 1.5mm below the surface.

Figs (100-101)

Distributions of stress along the surface and edge of the plate (NODE 1 to 3) & (NODE 3 to 4) at 1.0 second into the 2-D horizontal quench analysis by using constant 'h'.



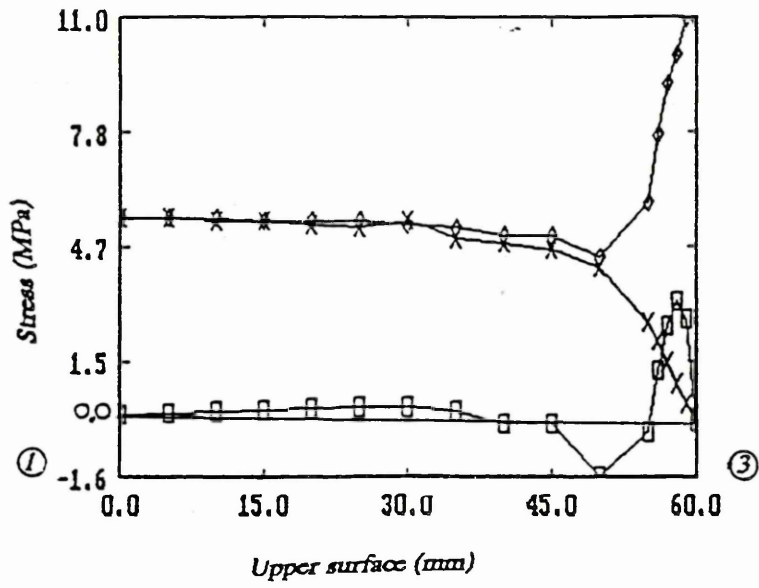


Fig.100

□ Axial
 × Radial
 ◇ Hoop

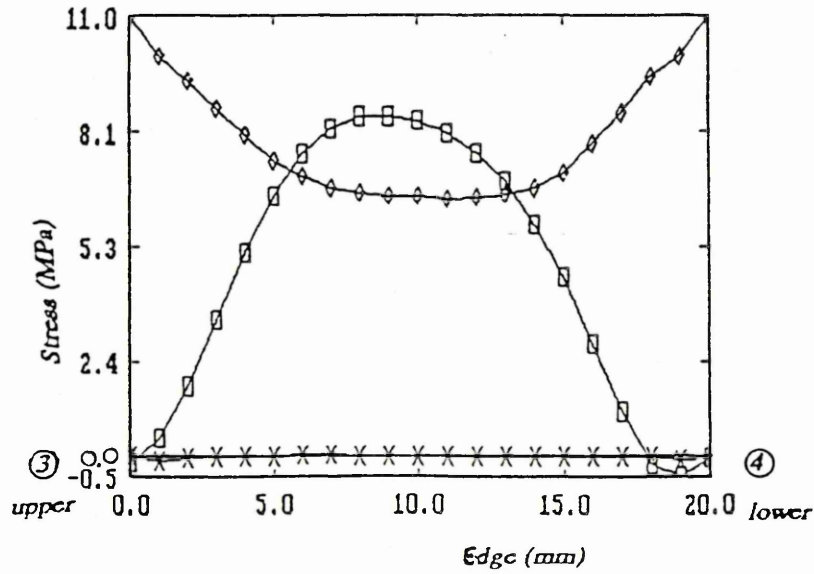
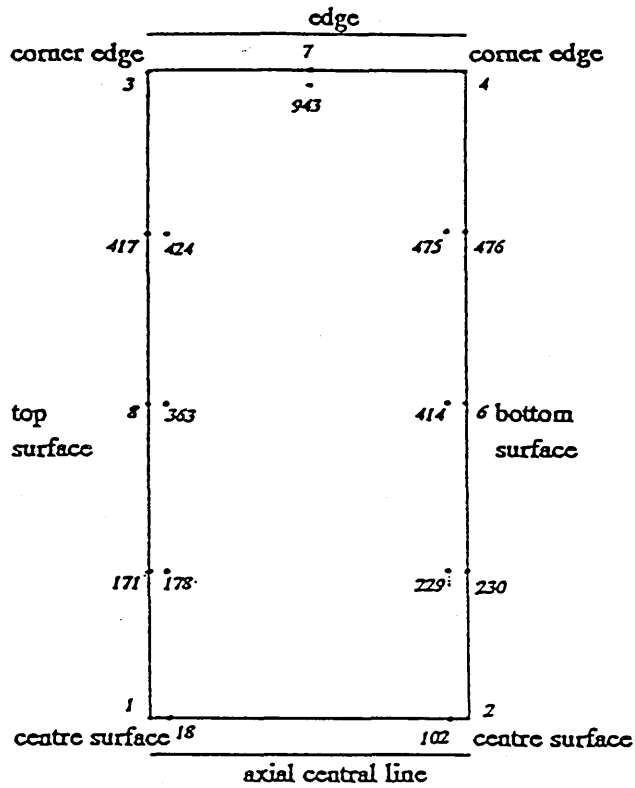


Fig.101

Figs (102-103)

Distributions of stress along the axial and surface of the plate (NODE 1 to 2) & (NODE 2 to 4) at 1.0 second into the 2-D horizontal quench analysis by using constant 'h'.



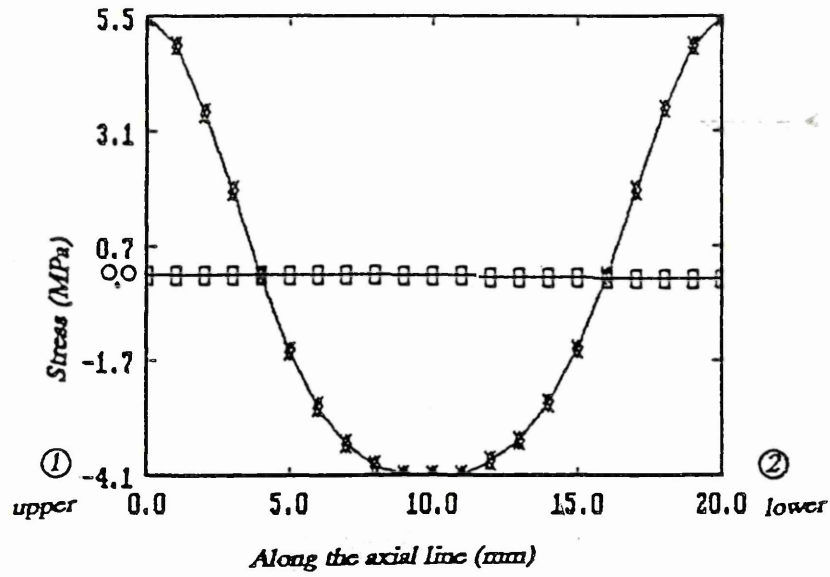


Fig.102

⊕ Axial
 × Radial
 ◇ Hoop

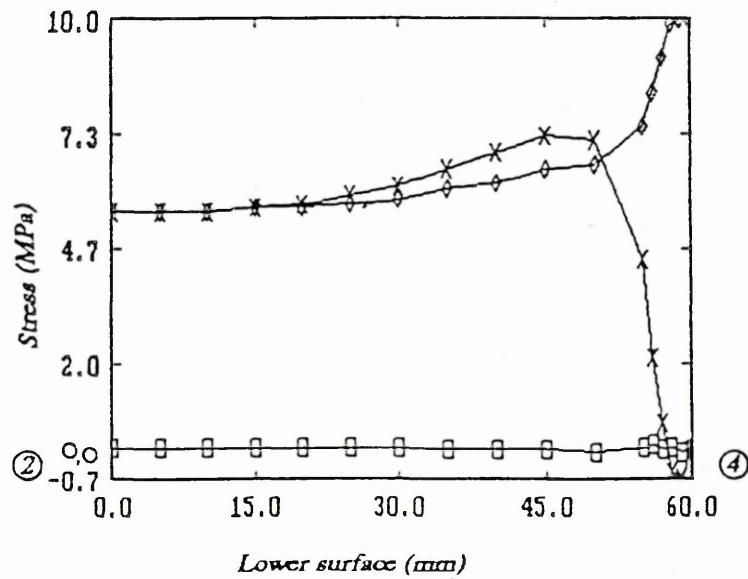
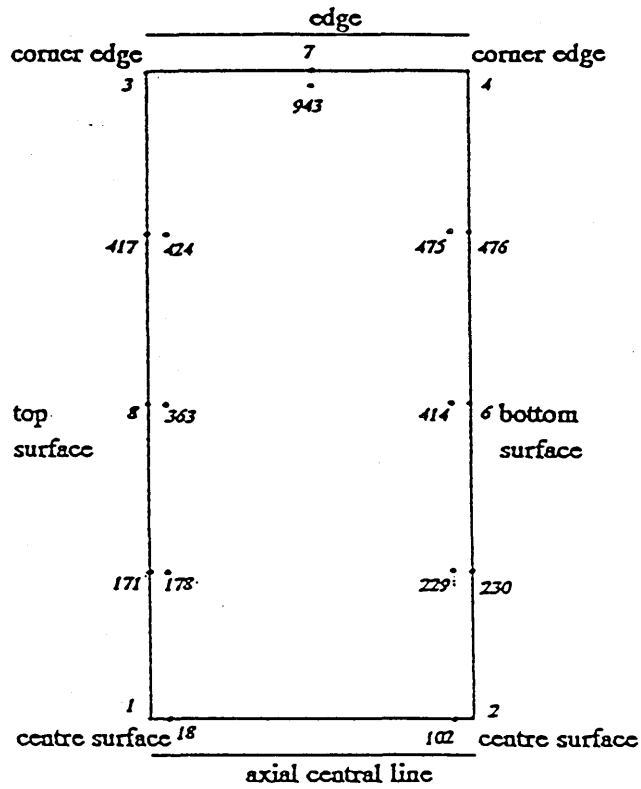


Fig.103

Figs (104-105)

Distributions of stress along the surface and edge of the plate (NODE 1 to 3) & (NODE 3 to 4) at 40.0 seconds into the 2-D horizontal quench analysis by using constant 'h'.



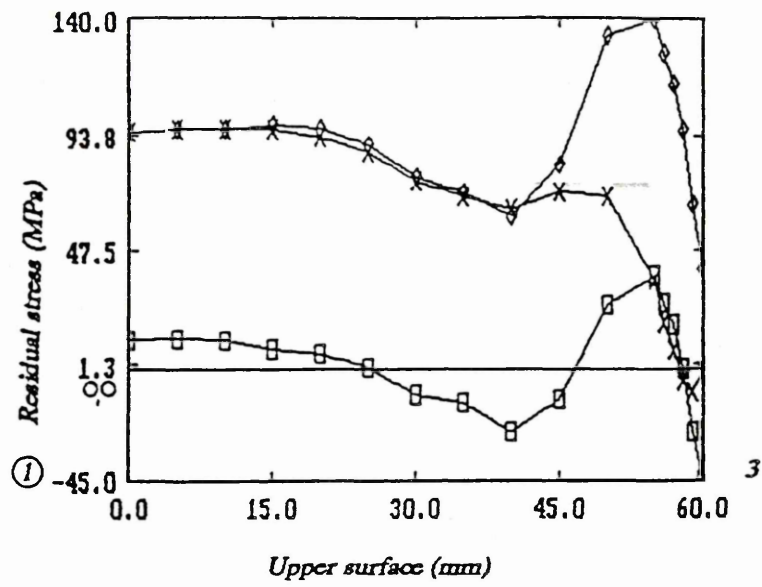


Fig.104

□ Axial
 × Radial
 ◇ Hoop

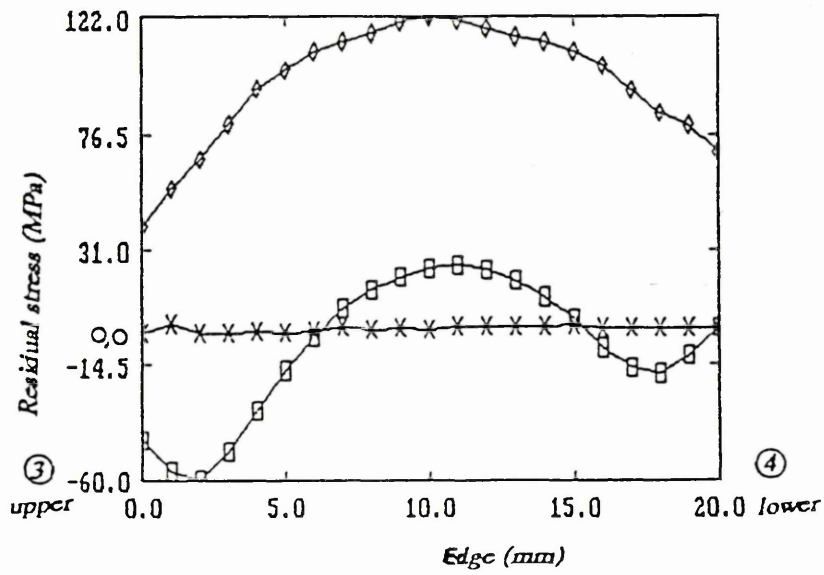
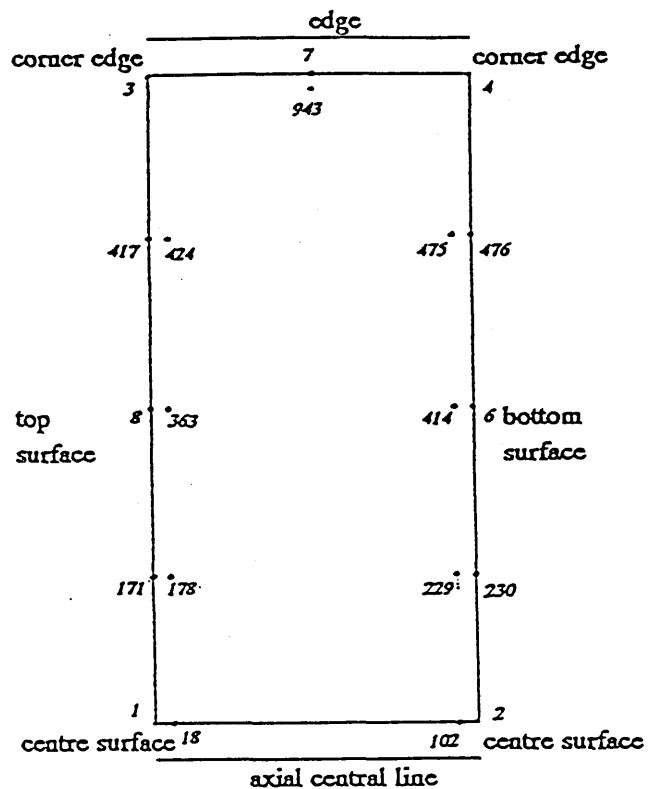


Fig.105

Figs (106-107)

Distributions of stress along the axial and surface of the plate (NODE 1 to 2) & (NODE 2 to 4) at 40.0 seconds into the 2-D horizontal quench analysis by using constant 'h'.



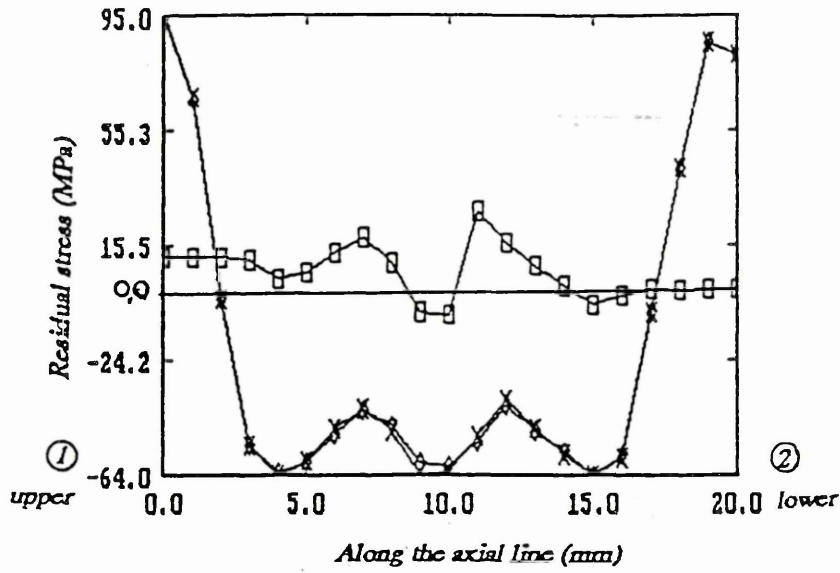


Fig.106

□ Axial
 × Radial
 ◇ Hoop

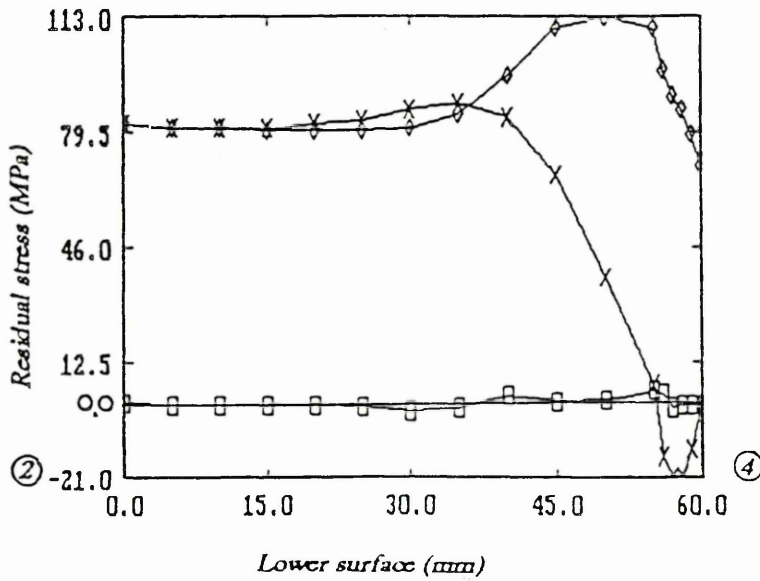
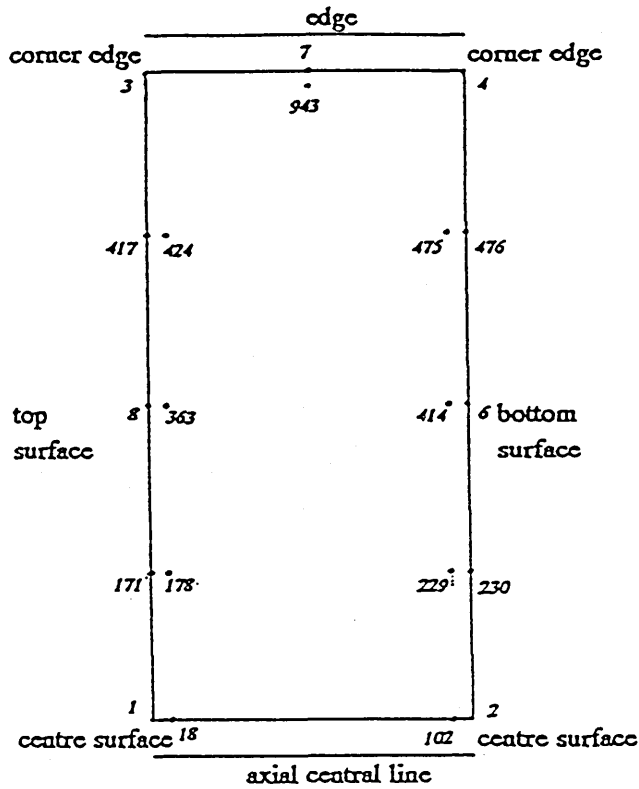


Fig.107

Figs (108-109)

Distributions of stress along the surface and edge of the plate (NODE 1 to 3) & (NODE 3 to 4) at 1.0 second into the 2-D horizontal quench analysis by using variable 'h'.



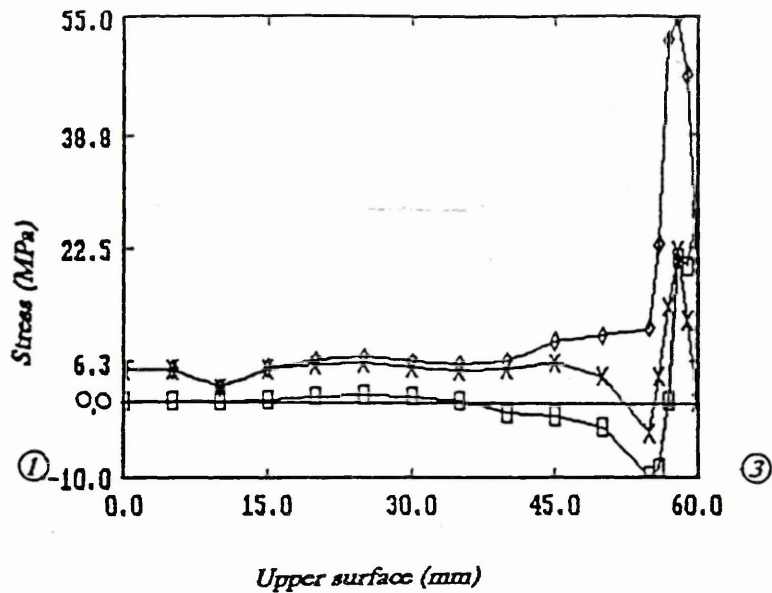


Fig.108

- Axial
- × Radial
- ◇ Hoop

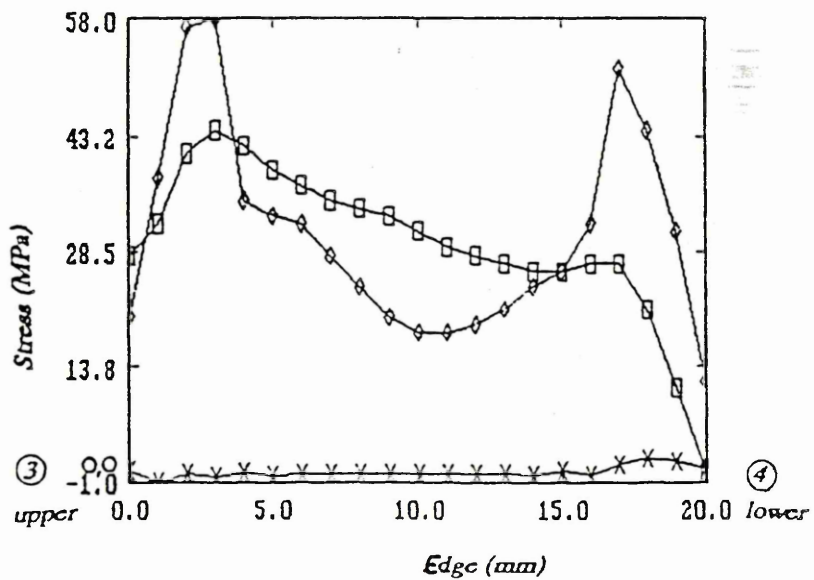
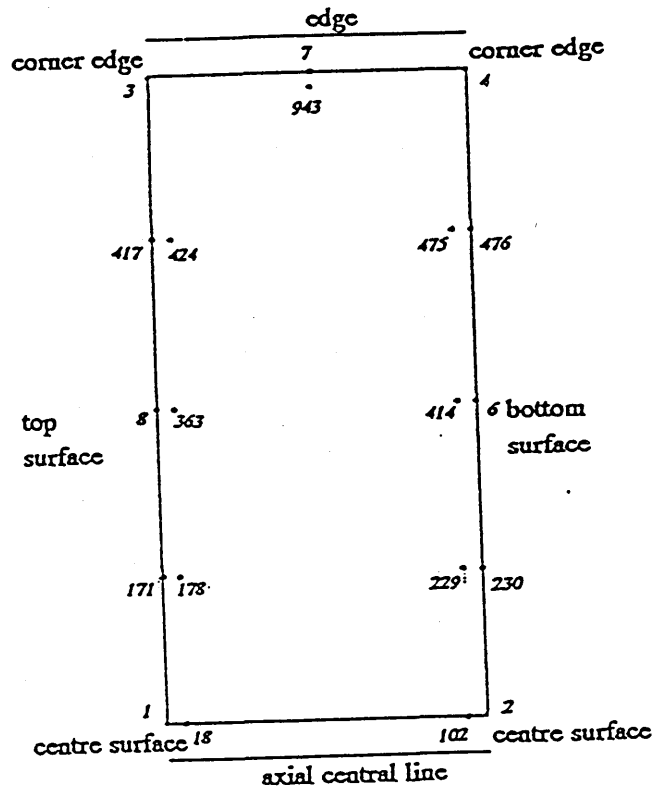


Fig.109

Figs (110-111)

Distributions of stress along the axial and surface of the plate (NODE 1 to 2) & (NODE 2 to 4) at 1.0 second into the 2-D horizontal quench analysis by using variable 'h'.



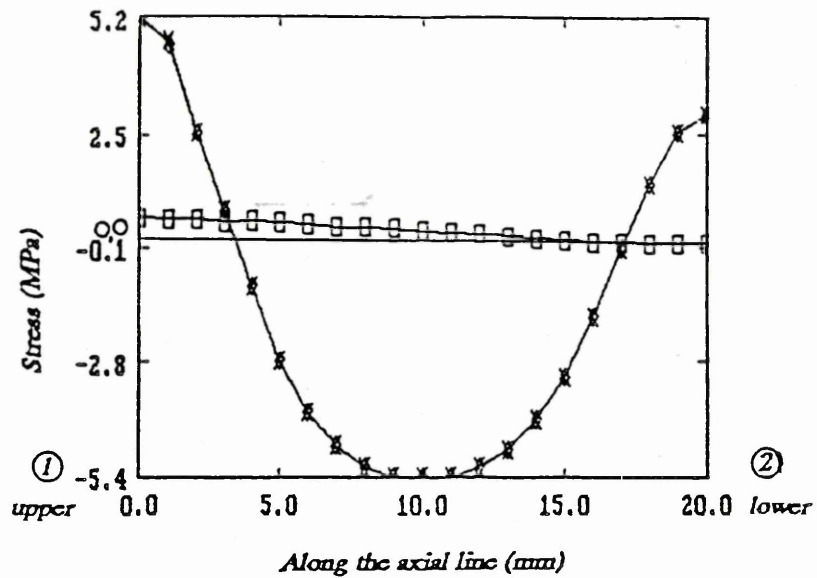


Fig.110

⊕ Axial
 * Radial
 † Hoop

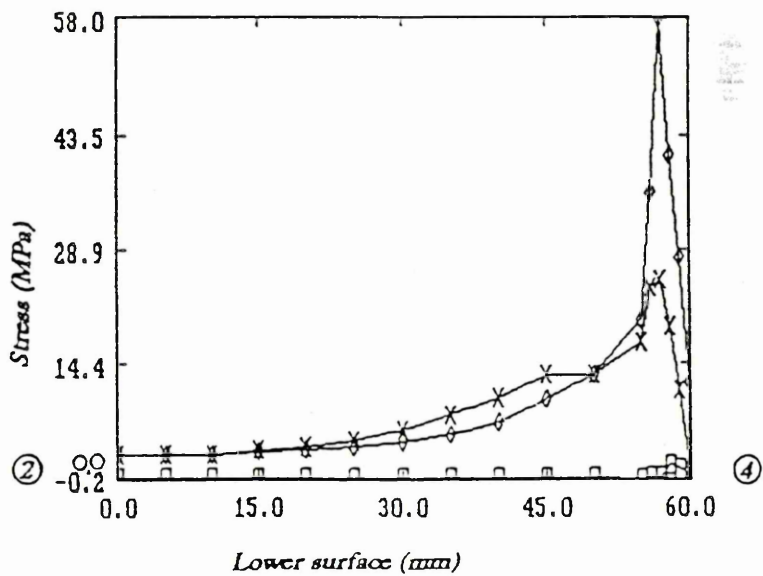
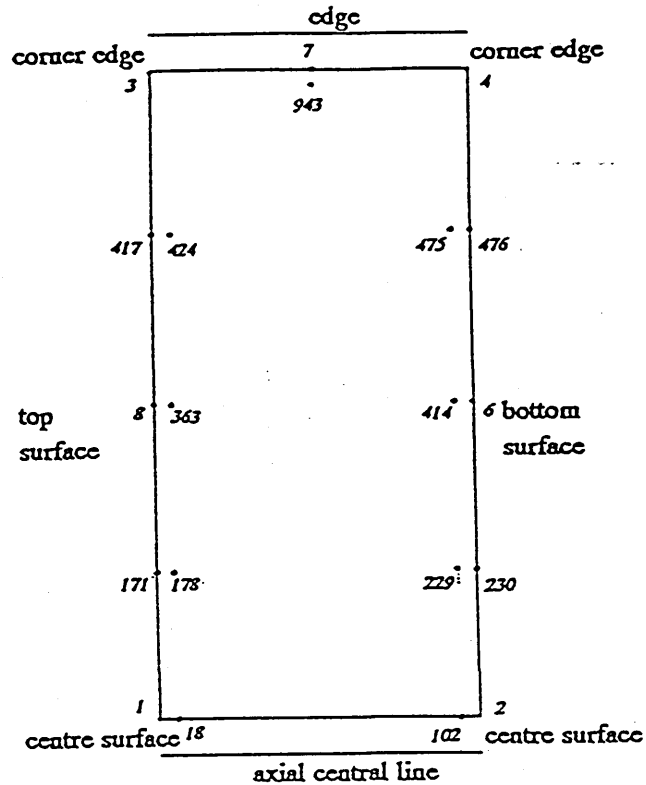


Fig.111

Figs (112-113)

Distributions of stress along the surface and edge of the plate (NODE 1 to 3) & (NODE 3 to 4) at 40.0 seconds into the 2-D horizontal quench analysis by using variable 'h'.



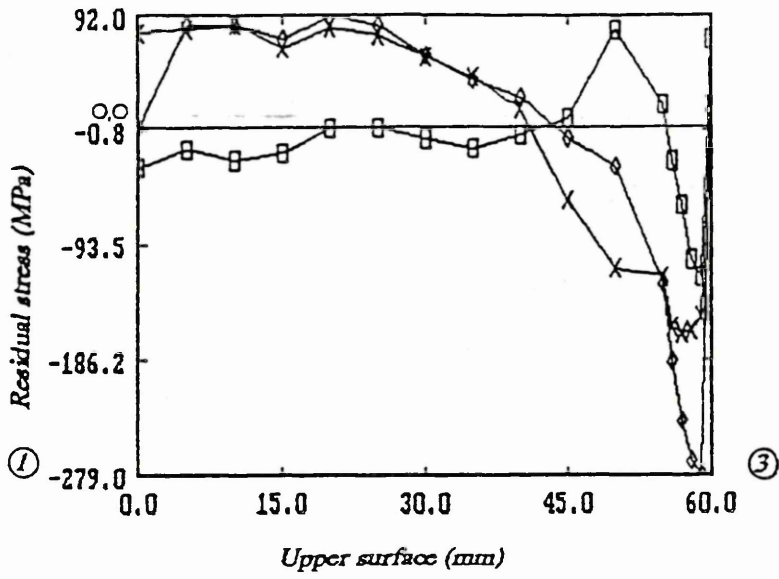


Fig.112

- ⊕ Axial
- * Radial
- ◇ Hoop

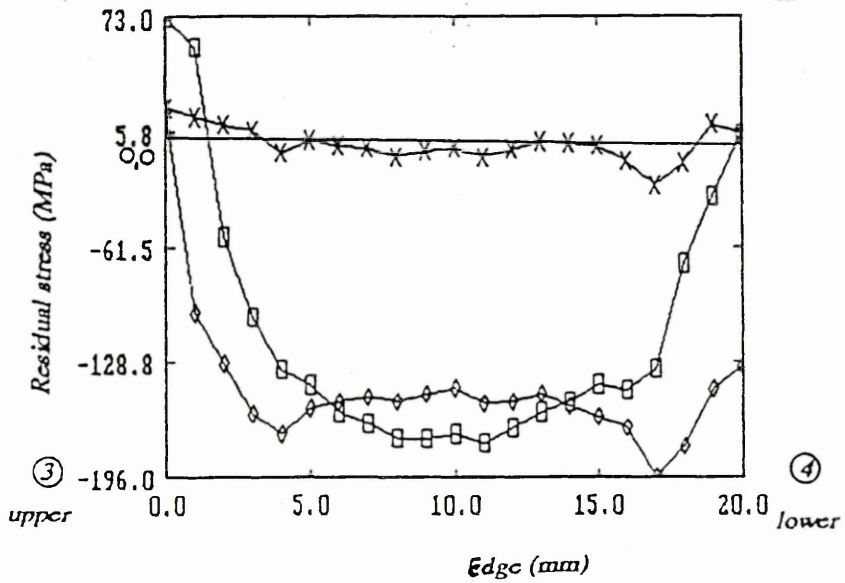
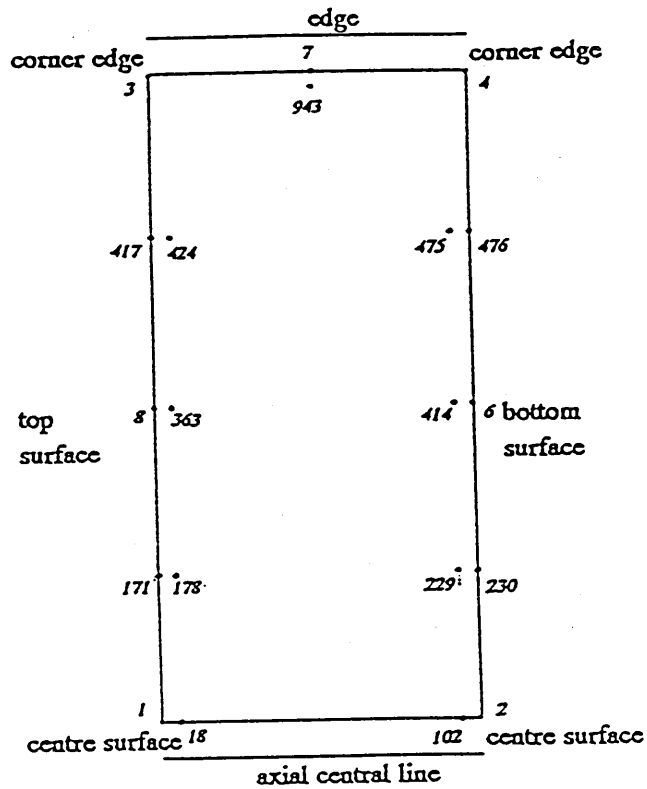


Fig.113

Figs (114-115)

Distributions of stress along the axial and surface of the plate (NODE 1 to 2) & (NODE 2 to 4) at 40.0 seconds into the 2-D horizontal quench analysis by using variable 'h'.



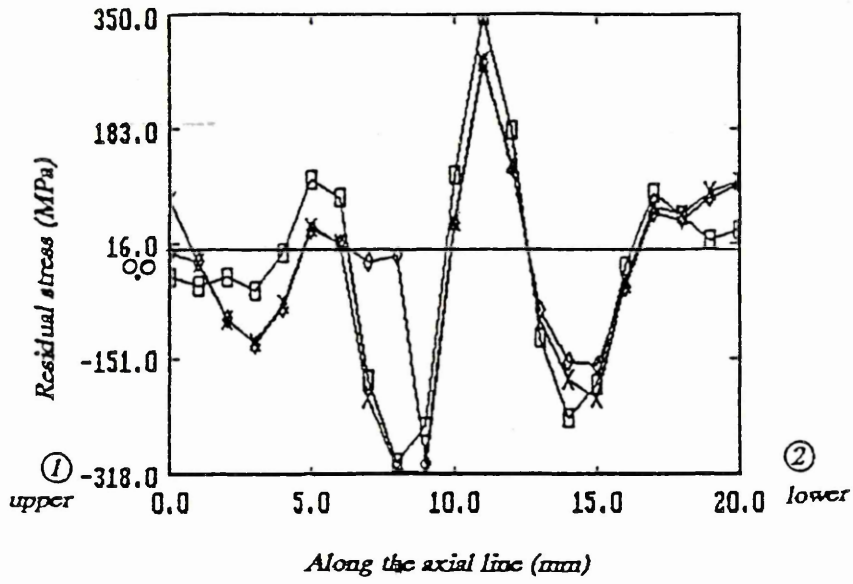


Fig.114

- Axial
- × Radial
- ◇ Hoop

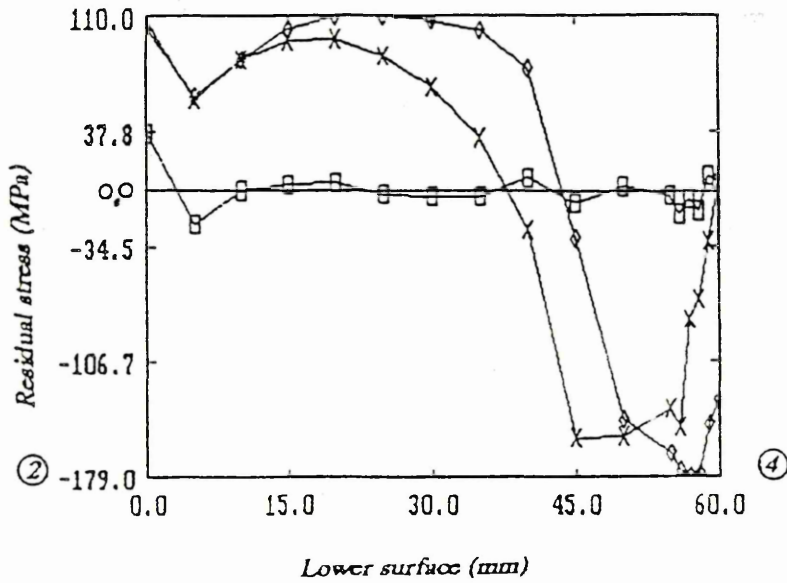


Fig.115

APPENDIX A

The following PAFEC 75 finite element analysis was carried out to enable the residual stresses to be determined by using the results of the thermal analysis in a vertical and horizontal quenched plates, and also gives introduction to the package which was used in the calculation.

The PAFEC 75 finite element package

The finite element package PAFEC is typical of the commercially available finite element systems. The package consists of ten definite phases, each carrying out a specific task towards a solution. The ten phases are;

1.READ

Data modules are read in, default values are inserted and the modules are placed on to backing store.

2.PAF BLOCKS

Any paf block data is replaced by the full nodal co-ordinate and topological description of the complete mesh of elements.

3.ELEMENTS

The system equations are solved for the primary unknowns in the problem being tackled.

4.STRESS

The stresses are found.

These phases may be requested even if the activities they refer to have not been mentioned in the modules. In such cases default modules are taken. The PAFEC 75 package is modular and due to its flexibility requires solution type.

Each module within the data file is started by its heading.

The termination of a module is performed by the next module header, with the exception of the control module. The control file may be separated from the main data file - hence, the reason for control file termination.

The termination of all data is identical by END.OF.DATA.

PAFEC MODULES

Each module begins with a header which identifies it. The PAFEC system recognises the first four letters as the header, except for the control module which must be specified in full following the header is the contents line which identifies the properties.

THE CONTROL MODULE

The control module starts with control and ends with control.end. In between these a number of command statements can be entered. This informs the computer what will be required in the subsequent analysis.

All commands must be specified in full. Depending on what analysis was carried out, determined the required phases. For the thermal analysis phases 1,4,6,7 were needed. The thermal stress analysis required an extra phase9.

CONTROL

CALC.TRANS.TEMPS

SAVE.TEMPS.TO.AAAA

AXISYMMETRIC SKIP.AUTO.FRONT

PHASE=1,4,6,7

CONTROL.END

Each of the modules will be briefly described.

CALC.TRANS.TEMPS

This stated that a transient temperature calculation was required. The data file produced by PIGS, did not contain enough information for a PAFEC computer run to take place. Additional information modules had to be inputted into each data file, which where the thermal analysis and thermal stress analysis modules. For the thermal data file, to run completely the following modules were edited into the programme;

CONTROL MODULE

TEMPERATURE MODULE

UNSTEADY.THERMAL.TIMES MODULE

MATERIAL MODULE

PLATES.ANS.SHELLS MODULE

HEAT.TRANSFER MODULE

TABLES MODULE

ITERATION MODULE

For the thermal stress data file, to run the following modules were edited into the programme,

CONTROL MODULE

MATERIAL MODULE

PLATES.AND.SHELLS MODULE

RESTRAINTS MODULE

INCREMENTAL MODULE

YIELDING.ELEMENTS MODULE

SLOPE.AND.YIELD.TABLES MODULE TABLES MODULE

TIMES.FOR.THERMAL.STRESS.CALCULATIONS MODULE

SAVE.TEMPS.TO.AAAA

This option saved the calculated temperatures into a file name AAAA. The file name could be any list of up to nine letters. This file was used to calculate the thermal stresses, and was used in conjunction with the option READ.TEMPS.FROM.AAAA in the CONTROL module of the thermal stress data file.

The CONTROL modules, which edited the thermal stress data file, was very similar to that of the temperature data file.

The following lines had to be inserted.

CONTROL

AXISYMMETRIC

PHASE=1,4,6,7

READ.TEMPS.FROM.AAAA

STRESS

PLASTIC

UNSTEADY THERMAL TIMES MODULE

This was edited only into the thermal data file. The full module to be inserted was,

UNSTEADY.THERMAL.TIMES

TIME.STEP MAX.TIME NUMBER

0.05 20 2

HEAT.TRANSFER MODULE

This allowed the variation in the ambient temperature with time and the variation in the film coefficient with either time or temperature. It enabled the heat transfer parameters to be specified for a fluid-solid interface defined by a line, or plane, or list of nodes.

GENERALISED CONSTRAINTS MODULE

This module was used only in the thermal stress data file. In figure 22 all points along the axial central line and central line had to be restrained to move equidistantly in the X & Y direction. This module controlled the movement of all points along both directions. The form of the module which was edited into the data file is shown below;

RESTRAINTS

NODE.NUMBER PLANE DIRECTION

```
1      1  1
1      2  2
```

The number of nodes to be restrained was listed under the node heading. The directions 1 & 2 indicated that the restraint occurred in the X & Y direction respectively.

TIMES.FOR.THERMAL.STRESS.CALCULATIONS

This module was only edited into the thermal stress data file. The full module is shown below;

TIMES.FOR.THERMAL.STRESS.CALCULATIONS

TIME LOAD.CASE CHANNEL.NUMBER

```
1  1      1
```

The time column indicated the time during which a transient stress calculation

was performed. The load.case was an arbitrary number which corresponded to the load module. Such a load.case could be formed from any load module, eg. pressure, load, temperature. The load.case in this analysis came from the temperature module. Temperature values were extracted from the thermal analysis at the specified times.

The channel.number was associated with the read.temps.from.aaaa option in the control module. Only one file was needed and so the channel.number was assigned the value one. If two files were required then the channel.number was assigned one and two respectively.

All the modules which were edited into the data files had to be saved. This was accomplished by simply typing in file, when it is in the edit mode. The computer automatically saved all new edits under the same file name.

PERFORMING A PAFEC CALCULATION ON THE COMPUTER

All information relating to the section mesh of the plate was stored in both data files. Both data files had to be run separately. The thermal analysis data file was run first. The thermal stress data file would only run with additional information was made available after the thermal analysis calculation had been completed.

To initiate the calculate, the following command was typed in;

PAFRUN FILE NAME -Q SMALL.

If the PAFEC job was large it will be saved and run during the night time. The PAFEC job would run even after the user had logged out.

AXISYMMETRIC, The structure is assumed to be axisymmetric about the global X-axis, Y being radial coordinate. The idealisation models just one generator plane.

TOLERANCE, The tolerance used in establishing whether nodes are coincident is to be changed to the value given. The value must be of the form $10E_j$, the notation means 10 to the power j which can be a positive or negative integer.

END, The job is to end after the completion of the current phase. All system files produced by the job are deleted.

FULL.CONTROL, Only these phases present in the control module are to be executed.

RESTART, The job is to continue from the beginning of the phase given.

SAVE, The results from the current phase are to be saved.

NODES MODULE

This is used to define the co-ordinates of the structure to be analysed. Each node can be defined using either global or a user defined local axis set.

ELEMENT MODULE

This module is used to connect the nodes to form a two or three dimensional structure. The elements are isoparametric hence, structures with curved surfaces can be modelled by specifying the mid-side nodes.

PLATES AND SHELL MODULE

This module is used for two-dimensional stress analysis calculation. It consists of plate or shell.number, material.number and thickness. This module is used to specify the thickness of the two-dimensional structures.

MATERIAL MODULE

The PAFEC system contains a library of ten preprogrammed materials. However, the user may also define material properties can also be used. For two dimensional stress analysis this module must be used in conjunction with plate.and.shell module.

PAFBLOCK MODULE

This module is used to divide the structure to a number of pre-defined blocks. These blocks are then subdivided to accommodate as many elements as is thought suitable, by using the mesh module.

MESH MODULE

This is used in conjunction with pafblock module, it defines the spacing of the elements within a pafblock.

RESTRAINTS MODULE

The restraints module enables specific degrees of freedom to be restrained. This can be done for individual, nodes, line or planes.

The restraints module is essential when an analysis is required which involved loading, failure to use this module results in a failure phase 4. This module is also very important when only a part of a symmetrical structure is modelled, as it used to simulate the behaviour of the rest of the structure.

ERROR NOTIFICATION WITHIN PAFEC

During each PAFEC job run a considerable number of ifles are created, a summary of these files are;

- .001 output file for phase 1 (data read out)
- output file for a 2 (data replacement)

.BS data backing store file
.004 output for a 4 (constraints)
(stiffness matrices)
.007 output for a 7 (displacement)
.009 9 stresses
.PS P.I.G.S graphical output file
.PS P.I.G.S. generated stress file
.SS stress file
.FS frontal solution scratch file
.ES elemental stiffness file
data file name alpha/numeric data file name.

Thus, if an error occurs within the run, the user is faced with a daunting task of locating the error, before he can make any attempt to correct it. For this reason, PAFEC user error locating routines in each phase, and the results are via phase output file.

PIGS

PIGS is a powerful aid for production of models and data files. The system contains several menus which are accessed via the root menu.

USING PIGS FOR POST PROCESSING

To obtain the data and print outs of various phases of PAFEC containing the relevant data, the phase seven stores the temperatures of all the nodes of thermal analysis, while the results for the thermal stress analysis was stored in phase nine.

For the thermal stress analysis PIGS displayed contour lines of varying stresses on the section of the plate mesh at any chosen load case which corresponded directly to the chosen times step.

Using PIGS the types of stresses required could be varied and these stresses were;

- (1) MAXIMUM STRESS
- (2) MINIMUM STRESS
- (3) HOOP STRESS
- (4) VON MISES STRESSES

At any time the stress contour displays could be printed out. Examples of such are shown in the results section. The numerical results for a PAFEC heat transfer and thermal stress analysis were filled in phases seven and nine. The print out was obtained during phase seven and nine respectively. This indicated the temperatures and stresses at individual node points at various transient times. The above print outs were used to plot the relationships between temperatures and stresses.

ANALYSIS

This option allows this user to display the stress contours, displaced shape and the model shape interactively on the terminal screen. In order to select this option backing store must be post phase 9.

B.S. RETRIEVE

This option is used to access the backing store created during the processing of data files.

D_i SAVE

This allows the user to save the data created. Once used, it can be recalled by using D_i retrieve command for further developments or modification of the data file.

FILE

This is used to file the data created to produce a 'DAT' file for analysis using PAFEC.